

---

# IMPACT OF WAVE PROPAGATION IN COMPOSITE ELASTIC MEDIA

---

A THESIS SUBMITTED IN FULFILMENT OF THE  
REQUIREMENTS  
FOR THE DEGREE OF DOCTOR OF PHILOSOPHY  
(SCIENCE)

by

SOMASHRI KARAN



DEPARTMENT OF MATHEMATICS  
JADAVPUR UNIVERSITY, INDIA


## CERTIFICATE FROM THE SUPERVISORS

This is to certify that the thesis entitled “ **IMPACT OF WAVE PROPAGATION IN COMPOSITE ELASTIC MEDIA**” submitted by Mrs. SOMASHRI KARAN, who got her name registered (Index No. – 256/15/Maths./24) on November 6, 2015 for the award of Ph.D. (Science) degree of JADAVPUR UNIVERSITY, is absolutely based upon her own work under the joint supervision of Prof. Subhas Chandra Mandal, Department of Mathematics, Jadavpur University, Kolkata-700032 and Dr. Sanjoy Basu, Assistant Professor, Department of Mathematics, Arignar Anna Government Arts and Science College, Karaikal-609605, Puducherry, India, and that neither this thesis nor any part of it has been submitted for either any degree/diploma or any other academic award anywhere before.

Date: 20/12/2022  
Place: Jadavpur, Kolkata

  
Subhas Chandra Mandal

Professor  
DEPARTMENT OF MATHEMATICS  
Jadavpur University  
Kolkata – 700 032, West Bengal

  
Sanjoy Basu

**Dr. SANJOY BASU, M.Sc.(UJ), Ph.D.(UJ)**  
Assistant Professor  
(General Central Service - Group A-Secreted)  
Department of Mathematics  
Arignar Anna Government Arts & Science College  
Nehru Nagar, Karaikal, Puducherry - 609 605  
Employee Code : AAG343

---

## *Acknowledgements*

I would extend my sincerest gratitude and indebtedness to **Dr. Subhas Chandra Mandal**, Professor, Department of Mathematics, Jadavpur University and **Dr. Sanjoy Basu**, Assistant Professor, Department of Mathematics, Arignar Anna Government Arts and Science College, Karaikal, Puducherry for guiding me throughout the whole tenure of my doctoral program. Without their continuous support, words of motivation, and a helping hand in all phases it would not have been possible to complete my work.

I also take this very opportunity to acknowledge the support of the Head of the Department of Mathematics, Jadavpur University, and other teachers and staffs for their encouragement. I would also like to thank the Department for providing me with all the facilities required to complete my work.

I am grateful to my colleagues Sourav Kumar Panja, Subhadeep Naskar, Palas Mandal, Ujjal Dhabal, Pintu Baidya, Sanim Alam at the Department of Mathematics, Jadavpur University for all their kind assistance and co-operation and sharing knowledge that helped me to continue my work.

Lastly, I appreciate the efforts of my three sisters (Manjushri karan, Tanushri Karan, Madhushree Karan) and brother-in-law Pallab Kumar Sau in taking the family responsibilities during the crucial time while my work was in progress. I feel emotional to express my sincere gratitude to my parents. Also my niece (Rishika Sau and Ritwika Sau) helped me to keep my mind full of happiness so that I can work with full concentration. Without their encouragement, inspiration, and ceaseless help, it was not possible for me to accomplish my work.

Date : 20/12/2022

Place : Jadavpur, Kolkata

*Somashri Karan*  
Somashri Karan 20/12/2022

*This thesis is dedicated to my Mathematics  
teacher, Sumit Kumar Pradhan who gave me  
the love of Mathematics,  
&  
my parents Tapan Kumar Karan & Sudipta  
Karan for their love, endless support and  
encouragement.*

# Contents

<b>Contents</b>	<b>iii</b>
<b>1 Introduction</b>	<b>1</b>
<b>2 Methodology</b>	<b>35</b>
2.1 Dual Integral Equation Method . . . . .	36
2.2 Abel's Integral Equation Solution . . . . .	38
2.3 Integral Equation Solution following the Hankel Transform approach	39
2.4 Linear non-singular Integral Equations numerical solution by Fox and Goodwin Method . . . . .	40
2.5 Numerical Inversion of Laplace Transform . . . . .	44
2.6 Gaussian Integration . . . . .	46
2.7 Wiener-Hopf Method . . . . .	49
<b>3 Interaction of Shear Wave with Cracks</b>	<b>55</b>
3.1 Edge crack subject to anti-plane shear wave in an orthotropic strip .	55
3.2 Interaction of shear waves with semi-infinite moving crack inside of a orthotropic media . . . . .	72
<b>4 Impact of a torsional load on a penny-shaped crack sandwiched   between two elastic layers embedded in an elastic medium</b>	<b>97</b>
<b>5 Torsional wave propagation on a penny-shaped crack in an or-   thotropic layer sandwiched between two rigid discs bonded by an   orthotropic elastic half-space</b>	<b>116</b>
<b>Bibliography</b>	<b>135</b>
<b>List of Publications and Communicated Papers</b>	<b>159</b>

*Chapter-1*  
*Introduction*

# Chapter 1

## Introduction

- **Historical sketch**

The theory of elasticity is dependent on the fact that an elastic body responds when a force is applied to it. In a body that is elastic, the original shape is recovered after the forces causing deformation (not too large) are removed. All materials share the elastic property determined by substances as long as the deformation does not exceed specific limitations defined by the fundamental properties of the body.

A strained body is one in which the relative positions of points are altered. In the analysis of strain, deformations are the changes in the relative positions of points. The distance between 2 points of a rigid body remains constant throughout its history. Within a rigid body, rotations and translations may occur as displacements.

A number of milestones have been made in the development of this theory since Galileo's time (1638), including Hooke's law discovery in 1678 and Navier's formulation of the general equations in 1821.

Some specific correlation between forces and deformations describes the nature of elastic solids. A linear law derived from Hooke's law generalization is fundamental to such relationships. As per Hooke's law (1678), the extensions of spring-like bodies are proportional to the tensile forces. Later in (1980), Mariotte explored a similar type of law to study the stability of cantilever beams. According to Mariotte, cantilever beams resist flexure because some longitudinal fibers extend, while others

contract. It is true that Mariotte's assumption about the force distribution in fibers was accurate, but his study did not examine the form that the beam's axis assumed. Jacob Bernoulli (1705) considered the elastic nature of a solid by deriving the equation of a curve presumed by a deformed beam's axis. According to his equation, the bending moment across the point determines the elastic's curvature at every point.

Navier first derived the general equations for equilibrium & vibration related to elastic solid material in 1821. Navier derived three macroscopic differential equations for the components of displacement within an isotropic elastic material using a description of molecular interaction in which forces act along the lines linking two particles and are proportional to the change in distance between them. The form of these equations is accurate; however, the Navier equations include just one elastic constant due to an oversimplification of molecular interaction. Navier was also able to determine the equilibrium equations on the solid surface (the boundary conditions) taking the assistance concerning Lagrange's virtual work concept.

Cauchy (1823), who started from distinct assumptions and was drawn to Navier's work, developed the linear theory of elasticity, which is essentially unaltered today. Later on, a revolutionary principle about energy conservation of elastic solid was presented by George Green. Contributions from Navier, Cauchy, and Green weren't as important. Much is involved in developing foundations and broad ideas as it is in solving a particular sort of boundary-value problem.

The development throughout the 20th century was mainly focused on the issues of the presence of solutions along with the integration of numerous wide categories of boundary value problems. Significant research was conducted on the shell theory and the development of non-linear elasticity theories, and the basic issues in plane elasticity were addressed in detail.

The research about waves and vibration phenomena also become a significant history from hundred years ago. Next to the findings of Galileo, the name of a few famous researchers in the wave propagation field are Navier, Poisson, Ostrogradsky, Lamé, Stokes, Clebsch, and Christoffel. G. Kirchhoff (1824-1887) made significant advancements in the kinematic theory of thin rods and the investigation of plate deflection.



Discussions about different wave propagation in solids have been made in the books written by Yoffe (1951), Kolsky (1963), Brekhovskikh (1960), Graff (1973), and Hudson (1980), Broberg (1999), Zhang and Gross (1999), T. Kundu (2008), J. Achenbach (2012), R.C. Payton (2012).

A rigid body will deform in direct proportion to the applied force, and it would return to its original shape once an applied force is withdrawn. Finding is applicable to the majority of construction materials due to working loads even if certain bodies flow and others break. Strain, denoted by

$$e = (\Delta l/l),$$

is expressed as a ratio of rate of change in a dimension ( $(\Delta l)$ ) to the original dimension ( $l$ ), whereas stress is described as the ratio of force to the area over which it operates. When done correctly, the amount of stress to strain depends only on the material and not on the material's form or size. This could only be handled in basic situations, but from simple situations, it is always possible to calculate the outcome in more complex situations, like torsion or bending. The constant, which has the same dimensions as the stress, is known as the modulus.

Things become easier if we just think about a little portion of the subject, like a tiny cube that we mentally mark off in a distant part of the body. Any tiny surface, like one of the cube's faces, experiences a force that may be broken down into 3 mutually perpendicular components: a normal compression or tension, and 2 shearing forces parallel to the surface. We get the equivalent stresses by dividing them by the area of the surface. Each of the cube's six faces is affected by these stresses. There should be relationships between the stresses since the cube cannot physically rotate or move. Only 3 elongations and 3 shears, or six total, may be individually defined. Six strains were found in the strained state of the cube, which may be resolved in stretches parallel to the faces and distortions of the faces into rhombuses. There might be as many as 36 possible elastic constants since every one of the 6 strains is dependent on each of the 6 stresses. For the least symmetric types of crystals, there are still twenty-one elastic constants.

Fortunately, the characteristics of most materials exhibit some degree of symmetry, and this symmetry may be utilized to lower the number of independent elastic

constants. Only materials that are isotropic, or identical in all directions, will be taken into consideration since they are the most symmetric. This is common in substances that are uniformly composed and either polycrystalline or amorphous. Other situations are tensor analysis tasks that we won't cover here. A matrix with 3 rows and 3 columns that relate to the 3 coordinate directions in space may be used to represent both the stress and the strain. These matrices have the feature of being decreased to a diagonal of three elements by making an appropriate decision for the axes' orientation since they are symmetric (may be mirrored in the main diagonal). We now only have three normal strains that are dependent on three normal stresses (the shears have disappeared in the diagonalization) since the stress and strain are diagonalized along the same axes. These are referred to as the primary stresses and strains. Since each of the axes should be relatively similar, we may have a maximum of nine elastic constants.

- **Types of Elastic Body**

With reference to properties of elastic materials, classification of solids may be done in two categories as follows:

- 1) homogeneous and non-homogeneous solid.
- 2) isotropic, orthotropic and anisotropic solid.

In an elastic solid, if the elastic properties seems to be exactly equal throughout all of its points, the solid body is named as homogeneous; otherwise, the body is said to be non-homogeneous. Within an elastically homogeneous solids, relations of stress-strain become independent with respect to the position, while in non-homogeneous solids, they become functions of a position, i.e., when the medium has non-homogeneous elastic characteristics, the modules of rigidity  $\mu$  and Poisson's ratio  $\nu$  are not remaining constants and should be anticipated with change from point to point inside solid material. They might differ either regularly, as in the case of differential functions of spatial coordinates, or discretely, as in the instance of artificial laminated materials.

An isotropic body has elastic qualities that are consistent in all directions drawn through a particular location, while an anisotropic body often has variable elastic

properties for each direction. Elastically equivalent directions are those for which the elastic characteristics are the same. All paths traced through a specific point in an isotropic body are elastically comparable, but only some of them are in an anisotropic body. Materials that are orthotropic vary in their physical characteristics along three rotating axes that are mutually orthogonal. They became subsets of anisotropic solids as their characteristics vary depending on the direction from which measurements are taken.

## • Stress

A mechanical structure absorbs external forces that the body experiences as surface forces (such as when bending a stick) as well as body forces (vertical telephone pole standing weight on its own). Internal forces develop within the body as a consequence of these pressures. Understanding internal forces is crucial because they must be less than the strength of the material used to construct the body at all places. This information is determined by stress, which is understood to represent the load per unit area intensity since the material strengths are recognized in terms of stress inherently.

Consider a body (Fig.1.1) that is in equilibrium with varied loads. If a body is divided into cross-sections, forces must be applied to its “cross-sectional” area for it to remain in equilibrium like the original body. A force  $\Delta P$  is operating on a portion of area  $\Delta A$  at any cross-section. This force vector has a component normal to the surface,  $\Delta P_n$ , as well as another parallel to the surface,  $\Delta P_s$ . The description of stress then provides

$$\sigma_n = \lim_{\Delta A \rightarrow 0} \frac{\Delta P_n}{\Delta A}, \quad \tau_s = \lim_{\Delta A \rightarrow 0} \frac{\Delta P_s}{\Delta A}.$$

The stress components perpendicular with the surface,  $\sigma_n$ , is known as “normal stress”, and the stress parallel to the surface,  $\tau_s$ , is known as the “shear stress”. The stress is unchanged if a new cross-section is taken through the same point, but its two components, normal stress  $\sigma_n$ , and shear stress  $\tau_s$ , will vary. Nevertheless, it was shown that any 3 mutually orthogonal coordinate systems ( $x$ ,  $y$ ,  $z$ ) including a Cartesian coordinate system, are sufficient to define stress at a location.

Now, we have considered a cross-section of the body that is parallel to the  $yz$ -plane as illustrated in Fig.1.2. An area  $\Delta A$  is subject to the force vector  $\Delta P$ .  $\Delta P_x$  is normal to a surface as the component. The force vector  $\Delta P$  being parallel with the surface may be further factorised into components with respect to  $y$  and  $z$  axes as  $\Delta P_y$  and  $\Delta P_z$ .

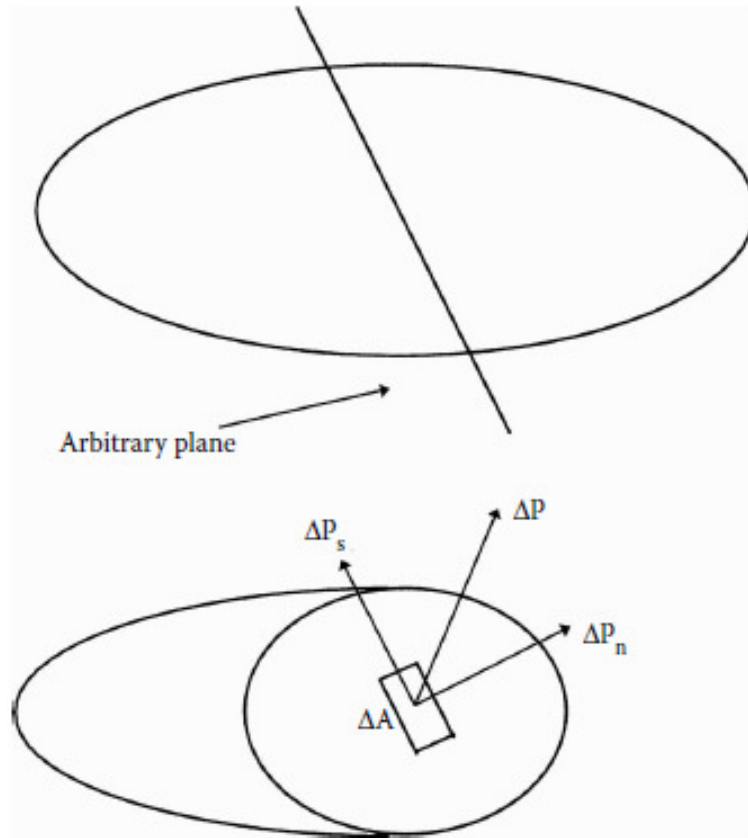


**Fig.1.1** Stresses on an infinitesimal area on an arbitrary plane.

The different stress's definitions are as follows:

$$\sigma_x = \lim_{\Delta A \rightarrow 0} \frac{\Delta P_x}{\Delta A}, \quad \tau_{xy} = \lim_{\Delta A \rightarrow 0} \frac{\Delta P_y}{\Delta A}, \quad \tau_{xz} = \lim_{\Delta A \rightarrow 0} \frac{\Delta P_z}{\Delta A}.$$

For cross-sections that are perpendicular to the  $xy$  and  $xz$  planes, stresses may also be determined. The typical method for determining all of these stresses is to

take an infinitesimal cuboid inside "right-hand coordinate system" and calculate the stresses on every of its faces. The six shear stresses are related as

$$\tau_{xy} = \tau_{yx}, \quad \tau_{yz} = \tau_{zy}, \quad \tau_{zx} = \tau_{xz}.$$

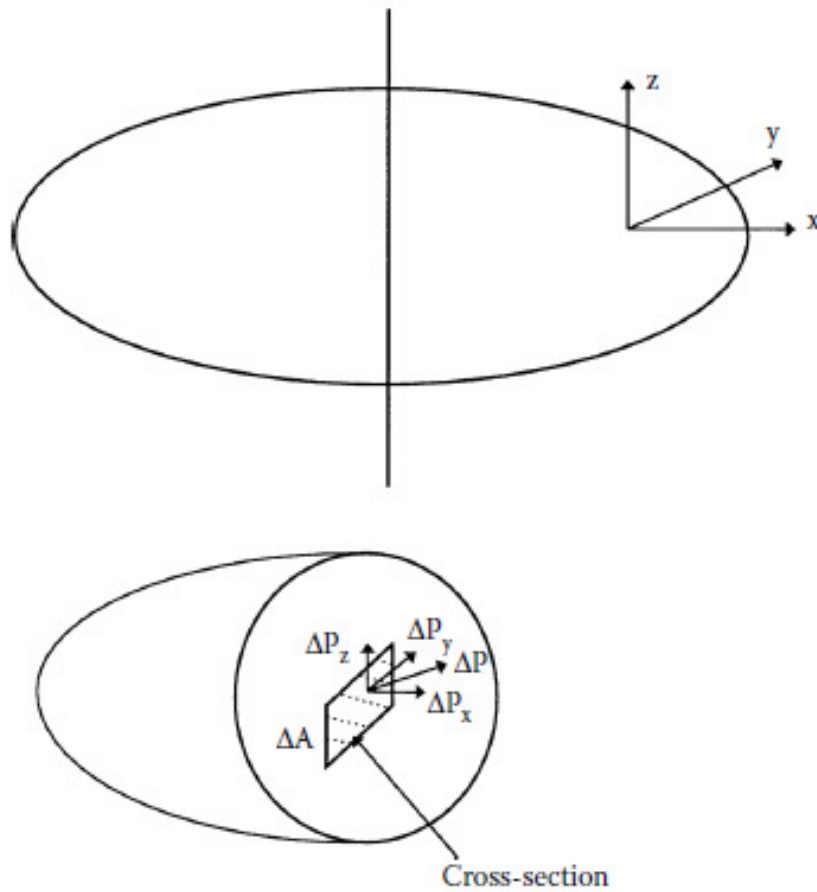


**Fig.1.2** Forces on an infinitesimal area on the y-z plane.

Therefore, there are six stresses independent with each other. The stresses  $\sigma_y$ ,  $\sigma_z$  are normal to the cuboid's surfaces, and the stresses  $\tau_{yz}$ ,  $\tau_{zx}$ ,  $\tau_{xy}$  are along the cuboid's surfaces.

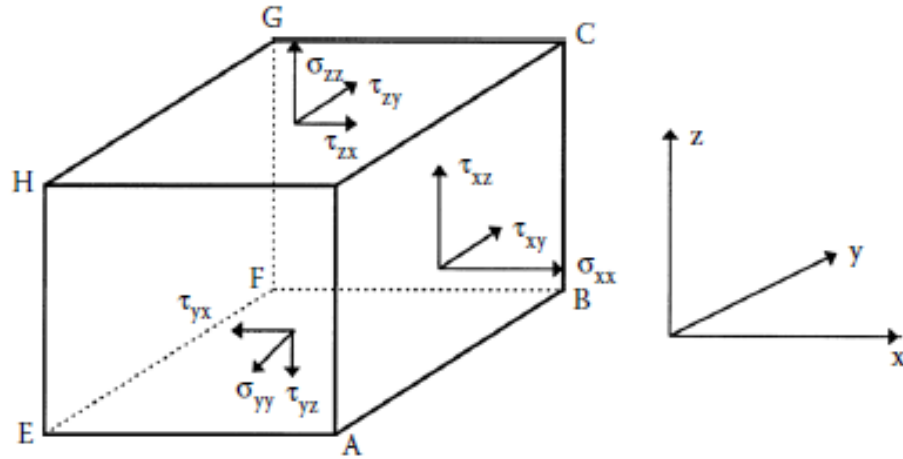


**Fig.1.3** Stresses on an infinitesimal cuboid.

We can write the nine different stresses in a  $3 \times 3$  matrix as :

$$\underline{\sigma} = \begin{pmatrix} \sigma_x & \tau_{xy} & \tau_{xz} \\ \tau_{yx} & \sigma_y & \tau_{yz} \\ \tau_{zx} & \tau_{zy} & \sigma_z \end{pmatrix}$$

Normal compressive stress is negative, but normal tensile stress is positive. The shear stress is positive or negative depending on whether the normal to the face it is acting on and the direction of the shear stress are both negative or positive.

- **Strain**

Similar to the necessity of understanding internal forces, understanding deformations brought on by external pressures is crucial. Additionally, discovering stresses in a body often necessitates discovering deformations.

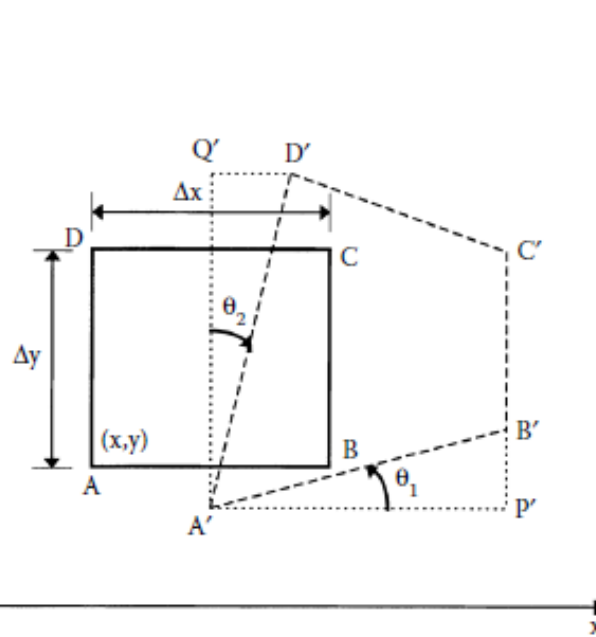


**Fig.1.4 Normal and shearing strains on an infinitesimal area in the x-y plane.**

Deformations are defined in terms of strains, or the relative alteration in the body's shape and size. Additionally, a general definition of the strain at a point is given on an infinitesimal cuboid inside a right-hand coordinate system. The sides of the infinitesimal cuboid's lengths vary under loads. The cube's faces also become deformed. A normal strain is represented by the length change, while a shearing strain is represented by the distortion. The strain on the cuboid's ABCD face is seen in Fig.1.4.

- **P-waves and S-waves**

P - waves are longitudinal and resemble sound waves. In P - waves, particle motion either moves in the same direction as or in the opposite direction from how waves move. These waves go through a medium at the quickest speed and are connected to volume changes.

S - waves also termed transverse or shear waves, are waves in which the direction of the particles motion is perpendicular to the direction in which the wave is propagating. They can seed pure rotation inside the medium with no change of volume.

Shear modulus and density both affect S wave velocity. Because fluids have no shear resistance, they cannot spread across fluids like air or water.

## • Hooke's Law and Stress-strain Relations

According to "Hooke's Law", the correlation between strain and stress is the same for a force acting in either direction, and the strain created due to many forces equals the total of the strains which can be created from every force acting alone.

The simplest relation is a linear one, referred to as Hooke's Law. If we stretch a sample in the x direction - i.e., apply normal stress  $\sigma_x$  then we can write  $e_x = \frac{\sigma_x}{E}$ , where E denotes the modulus of elasticity related to tension. Now stretching a sample in one direction will usually have the effect of changing its shape in others - usually decreasing it. The effect here is to produce strains

$$e_y = -\nu \frac{\sigma_x}{E}, \quad e_z = -\nu \frac{\sigma_x}{E},$$

where  $\nu$  is a property of the material called Poisson's ratio. It usually takes values in the range of 0.25 - 0.3.

These statements are accurate for the case where the stresses become lower than the material's elastic limit. It is possible for a solid body to have no elastic area at all. Every stress component is a linear function of each of the 6 strain components in the general situation of anisotropy. The Hooke's law's generalized form is

$$\sigma_{ij} = C_{ijkl} e_{kl}, \quad (i, j, k, l = 1, 2, 3). \quad (1.1)$$

Here where  $\sigma_{ij}$  indicates the stress components,  $e_{kl}$  denotes the strain components. The coefficients  $C_{ijkl}$  represent symmetric with relation to the first 2 and the last 2 indices.

We may use the notation to avoid dealing with a double sum.

$$\begin{aligned} \sigma_{11} = \sigma_1, \quad \sigma_{22} = \sigma_2, \quad \sigma_{33} = \sigma_3, \quad \sigma_{23} = \sigma_4, \quad \sigma_{31} = \sigma_5, \quad \sigma_{12} = \sigma_6, \\ e_{11} = e_1, \quad e_{22} = e_2, \quad e_{33} = e_3, \quad e_{23} = e_4, \quad e_{31} = e_5, \quad e_{12} = e_6. \end{aligned}$$



Equation (1.1) reduces to

$$\sigma_i = C_{ij}e_j, \quad (i, j = 1, 2, 3, 4, 5, 6).$$

So, the general stress-strain law may be expressed using a highest of 36 independent constants.

With the presence of strain energy density function  $W$ , the coefficient matrix takes symmetric form, i.e.

$$\sigma_i = C_{ij}e_j, \quad (i, j = 1, 2, 3, 4, 5, 6).$$

with

$$C_{ij} = C_{ji},$$

and the number of elastic constants concerning a general anisotropic material diminishes to 21.

The significant types of symmetry about elastic material are as follows:

1. **One plane of elastic symmetry:**

Consider a material that is elastically symmetric in terms of  $x_1x_2$ -plane (also described by  $x_3$ -plane). Thus, in the  $x_1$  direction, there is a normal to the  $x_2x_3$ -plane, which is the plane of symmetry. Material with one symmetry plane is also called monoclinic material (for example, Gypsum, Borax, Ice etc.). Here, the number of elastic constants diminishes to 13. The coefficient matrix appears as

$$\begin{bmatrix} C_{11} & C_{12} & C_{13} & 0 & 0 & C_{16} \\ C_{12} & C_{22} & C_{23} & 0 & 0 & C_{26} \\ C_{13} & C_{23} & C_{33} & 0 & 0 & C_{36} \\ 0 & 0 & 0 & C_{44} & C_{45} & 0 \\ 0 & 0 & 0 & C_{45} & C_{55} & 0 \\ C_{16} & C_{26} & C_{36} & 0 & 0 & C_{66} \end{bmatrix}$$

The stress-strain relation becomes

$$\begin{bmatrix} \sigma_1 \\ \sigma_2 \\ \sigma_3 \\ \sigma_4 \\ \sigma_5 \\ \sigma_6 \end{bmatrix} = \begin{bmatrix} C_{11} & C_{12} & C_{13} & 0 & 0 & C_{16} \\ C_{12} & C_{22} & C_{23} & 0 & 0 & C_{26} \\ C_{13} & C_{23} & C_{33} & 0 & 0 & C_{36} \\ 0 & 0 & 0 & C_{44} & C_{45} & 0 \\ 0 & 0 & 0 & C_{45} & C_{55} & 0 \\ C_{16} & C_{26} & C_{36} & 0 & 0 & C_{66} \end{bmatrix} \begin{bmatrix} e_1 \\ e_2 \\ e_3 \\ e_4 \\ e_5 \\ e_6 \end{bmatrix}$$

## 2. Three plane of elastic symmetry (Orthotropic bodies):

A material that displays symmetry with reference to elastic properties regarding two orthogonal planes is termed as orthotropic (for example, Prepeg, Carbon fiber, Graphite-epoxy Composite, Glass-epoxy Composite etc.). Two planes of symmetry imply three planes of symmetry. Here, we get total 9 elastic constants. We get the coefficient matrix in transformed form as

$$\begin{bmatrix} C_{11} & C_{12} & C_{13} & 0 & 0 & 0 \\ C_{12} & C_{22} & C_{23} & 0 & 0 & 0 \\ C_{13} & C_{23} & C_{33} & 0 & 0 & 0 \\ 0 & 0 & 0 & C_{44} & 0 & 0 \\ 0 & 0 & 0 & 0 & C_{55} & 0 \\ 0 & 0 & 0 & 0 & 0 & C_{66} \end{bmatrix}$$

The stress-strain relations are

$$\begin{bmatrix} \sigma_1 \\ \sigma_2 \\ \sigma_3 \\ \sigma_4 \\ \sigma_5 \\ \sigma_6 \end{bmatrix} = \begin{bmatrix} C_{11} & C_{12} & C_{13} & 0 & 0 & 0 \\ C_{12} & C_{22} & C_{23} & 0 & 0 & 0 \\ C_{13} & C_{23} & C_{33} & 0 & 0 & 0 \\ 0 & 0 & 0 & C_{44} & 0 & 0 \\ 0 & 0 & 0 & 0 & C_{55} & 0 \\ 0 & 0 & 0 & 0 & 0 & C_{66} \end{bmatrix} \begin{bmatrix} e_1 \\ e_2 \\ e_3 \\ e_4 \\ e_5 \\ e_6 \end{bmatrix}$$

### 3. Plane of isotropy (Transversely isotropic body):

Assume a solid as described below:

Parallel planes of elastic symmetry passing through each point have elastic equivalent (planes of isotropy) in all directions. In other terms, a material is considered as transversely isotropic when it admits an axis of symmetry such that all rays pointing in its direction are equal (for example, Boron-Epoxy Composite). Therefore, the independent elastic constants reduced to 5. When the axis of symmetry is  $x_3$ -axis, the coefficient matrix appears as

$$\begin{bmatrix} C_{11} & C_{12} & C_{13} & 0 & 0 & 0 \\ C_{12} & C_{11} & C_{13} & 0 & 0 & 0 \\ C_{13} & C_{13} & C_{33} & 0 & 0 & 0 \\ 0 & 0 & 0 & C_{44} & 0 & 0 \\ 0 & 0 & 0 & 0 & C_{44} & 0 \\ 0 & 0 & 0 & 0 & 0 & (C_{11} - C_{12}) \end{bmatrix}$$

The stress-strain relation becomes

$$\begin{bmatrix} \sigma_1 \\ \sigma_2 \\ \sigma_3 \\ \sigma_4 \\ \sigma_5 \\ \sigma_6 \end{bmatrix} = \begin{bmatrix} C_{11} & C_{12} & C_{13} & 0 & 0 & 0 \\ C_{12} & C_{11} & C_{13} & 0 & 0 & 0 \\ C_{13} & C_{13} & C_{33} & 0 & 0 & 0 \\ 0 & 0 & 0 & C_{44} & 0 & 0 \\ 0 & 0 & 0 & 0 & C_{44} & 0 \\ 0 & 0 & 0 & 0 & 0 & (C_{11} - C_{12}) \end{bmatrix} \begin{bmatrix} e_1 \\ e_2 \\ e_3 \\ e_4 \\ e_5 \\ e_6 \end{bmatrix}$$

#### 4. Isotropic body:

In isotropic material, elastic properties are same in all directions (for example, Aluminum alloy, Brass, Nickel alloy etc.). Here, we get 2 elastic constants which are independent, and the matrix concerning coefficient takes the form

$$\begin{bmatrix} C_{11} & C_{12} & C_{12} & 0 & 0 & 0 \\ C_{12} & C_{11} & C_{12} & 0 & 0 & 0 \\ C_{12} & C_{12} & C_{11} & 0 & 0 & 0 \\ 0 & 0 & 0 & (C_{11} - C_{12}) & 0 & 0 \\ 0 & 0 & 0 & 0 & (C_{11} - C_{12}) & 0 \\ 0 & 0 & 0 & 0 & 0 & (C_{11} - C_{12}) \end{bmatrix}$$

i.e.,

$$\begin{bmatrix} \lambda + 2\mu & \lambda & \lambda & 0 & 0 & 0 \\ \lambda & \lambda + 2\mu & \lambda & 0 & 0 & 0 \\ \lambda & \lambda & \lambda + 2\mu & 0 & 0 & 0 \\ 0 & 0 & 0 & \mu & 0 & 0 \\ 0 & 0 & 0 & 0 & \mu & 0 \\ 0 & 0 & 0 & 0 & 0 & \mu \end{bmatrix}$$

where  $C_{12} = \lambda$ ,  $C_{11} - C_{12} = 2\mu$ ,  $C_{11} = \lambda + 2\mu$ .

The stress-strain relation becomes

$$\sigma_{ij} = \lambda \delta_{ij} e_{nn} + 2\mu e_{ij}, \quad (i, j, n = 1, 2, 3).$$

### Relations between Stress-strain in anisotropic body:

Orthotropic solid( plane stress):

$$\sigma_{xx}/\mu_{12} = C_{11}e_{xx} + C_{12}e_{xy},$$

$$\sigma_{yy}/\mu_{12} = C_{12}e_{xy} + C_{22}e_{yy},$$

$$\sigma_{xy}/\mu_{12} = e_{xy}.$$

$C_{ij}$  ( $i, j = 1, 2$ ) indicates dimensionless parameters connected with the elastic constants of the material as stated below [Lekhiniskii (1963)]

$$C_{11} = E_1/\mu_{12}(1 - \nu_{12}^2 E_2/E_1),$$

$$C_{22} = E_2/\mu_{12}(1 - \nu_{12}^2 E_2/E_1) = C_{11} E_2/E_1,$$

$$C_{12} = \nu_{12} E_2/\mu_{12}(1 - \nu_{12}^2 E_2/E_1) = \nu_{12} C_{22} = \nu_{21} C_{11},$$

related to generalized plane stress, and with

$$C_{11} = (E_1/\Delta\mu_{12})(1 - \nu_{23}\nu_{32}),$$

$$C_{22} = (E_2/\Delta\mu_{12})(1 - \nu_{13}\nu_{31}),$$

$$\begin{aligned} C_{12} &= E_1(\nu_{21} + \nu_{13}\nu_{32}E_2/E_1)/\Delta\mu_{12} \\ &= E_2(\nu_{12} + \nu_{23}\nu_{31}E_1/E_2)/\Delta\mu_{12}, \end{aligned}$$

$$\Delta = 1 - \nu_{12}\nu_{21} - \nu_{23}\nu_{32} - \nu_{31}\nu_{13} - \nu_{12}\nu_{23}\nu_{31} - \nu_{13}\nu_{21}\nu_{32},$$

related to plane strain. The material's engineering elastic constants are represented in the aforementioned equations by  $E_i$ ,  $\mu_{ij}$  as well as  $\nu_{ij}$  ( $i, j = 1, 2, 3$ ), where the subscripts 1, 2, and 3 correspond to the axes of the material's orthotropy in the

$x$ ,  $y$  and  $z$  directions, respectively and  $E_i$  and  $\nu_{ij}$  also fulfill Maxwell's relation.

$$\nu_{ij}/E_i = \nu_{ji}/E_j.$$

Transversely isotropic body:

Letting the  $z$ -axis perpendicular with isotropic plane, where the  $x$ -axis and  $y$ -axis are taken arbitrarily in this plane, the relations between stress and strain in terms of the five independent elastic constants are prescribed as follows:

$$e_{xx} = C_{11}\sigma_{xx} + C_{12}\sigma_{yy} + C_{13}\sigma_{zz},$$

$$e_{yy} = C_{12}\sigma_{xx} + C_{11}\sigma_{yy} + C_{13}\sigma_{zz},$$

$$e_{zz} = C_{13}(\sigma_{xx} + \sigma_{yy}) + C_{33}\sigma_{zz},$$

$$e_{xy} = 2(C_{11} - C_{12})\sigma_{xy},$$

$$e_{yz} = C_{44}\sigma_{yz},$$

$$e_{zx} = C_{44}\sigma_{zx},$$

where  $C_{ij}$  ( $i, j = 1, 2, 3$ ) denotes dimensionless parameters connected with the elastic constants of the material as follows [Lekhiniskii (1963)].

$$C_{11} = \frac{E_1}{\Delta \mu_{13}} \left(1 - \frac{E_1}{E_3} \nu_{31}^2\right),$$

$$C_{33} = \frac{E_3}{\Delta \mu_{13}} (1 - \nu_{12}^2),$$

$$C_{12} = \frac{E_1}{\Delta \mu_{13}} (\nu_{12} + \frac{E_1}{E_3} \nu_{31}^2),$$

$$C_{13} = \frac{E_1}{\Delta \mu_{13}} \nu_{31} (1 + \nu_{12}),$$

$$\Delta = 1 - \nu_{12}^2 - 2 \frac{E_1}{E_3} \nu_{31}^2 (1 + \nu_{12}).$$

In the twentieth century, the field of fracture mechanics was established and matured. Its literature is currently quite vast. Fatigue is perhaps the most effective application of fracture mechanics. It is essential to take a step back and examine the advancement of fracture mechanics at the beginning of the new century. The first example is a stone hand-axe from the Paleolithic period. Nevertheless, when it was created, man and his hominid predecessors had been shaping stone for more than a million years. One man had to make sure that the massive, costly constructions he was building wouldn't break and fall apart.

Scaling is a major component of fracture mechanics. At first, Leonardo da Vinci (1452–1519) reported an understanding of the scaling of fracture, and the 2nd explanation can be understood from one of his note-books, which shows his strength experiments on iron wires. The exact scaling rules for bars under tension and bending were originally provided by Galileo Galilei in his “Dialogues Concerning Two New Sciences” in 1638. He used it to illustrate a topic on beam fracture. It was difficult to construct ships, palaces, or temples of immense scale such that all of their oars, yards, beams, iron bolts, etc., would keep together, and Galileo observed that this effect imposed a limit on the size of buildings, both man-made and natural. Due to the fact that their branches would collapse under their weight, nature grows very large trees. The discipline, which combines the mechanics of cracked mediums with mechanical characteristics, is known as “fracture mechanics”. As suggested by the name fracture mechanics focuses on the occurrences and phenomena associated with fractures. Some well-known catastrophes in recent history have a dense connection to the development of fracture mechanics. Several hundred Liberty ships suffered significant damage during World War II. The failures were mostly caused by the transition from riveted to welded construction, and the main reason was the

combination of poor weld characteristics with stress concentrations, as well as the construction's poor use of fragile materials.

According to a collection of ideas known as fracture mechanics, solids or structures that have a geometric discontinuity at the scale of the structure behave differently. Discontinuity properties could take the form of line discontinuities in 2D medium (like shells and plates) or surface discontinuities inside 3D medium. Our knowledge of the behavior of engineered materials has been fundamentally altered by the development of fracture mechanics into a mature scientific and technical field.

Some fundamental works and concepts dealing with fracture mechanics have been described in the books by Kassir and Sih (1975), Murakami and Keer (1993), G.C. Sih (1991, 2008), L.B. Freund (1998), L. S. Sokolnikoff (2008), A.E.H. Love (2013), M.Kuna (2013), T.L. Anderson (2017). The adoption of a new design philosophy is one of the key effects of fracture mechanics: The damage tolerance design technique is widely accepted as the industry standard for designing airplanes. At the University of Dorpat (now Tartu), in Estonia, Kolosov (1909) developed fundamental mathematical tools for his Ph.D. dissertation. Inglis (1913) addressed a fundamental crack model independently, and Hopkinson (1913) recommended that nonlinear events at the crack edge must be taken into consideration in his discussion of Inglis' article. Griffith (1920) eventually accomplished this, but by applying surface energy and energy considerations idea, he prevented the examination of the crack edge neighborhood. Weibull (1939 a, b) developed a statistical theory of fracture in response to Griffith's studies with thin glass rods. Orowan (1952) expanded Griffith's technique with all situations related to small-scale yielding (where plastic flow is restricted to a tiny area along the edge of the crack) including all dissipative energy, namely plastic work and surface energy. New and practical ideas like the SIF: stress intensity factor and energy release rate were first proposed by Irwin in 1957. The notions that formed the basis of LEFM (Linear Elastic Fracture Mechanics) were the critical SIF or the fracture toughness. Barenblatt (1959 a, b) proposed the notion of field autonomy at the crack edge, and his concept of cohesion modulus was derived from a linearized model of the neighborhood of the fracture edge. In reality, all the various LEFM ideas are constructed directly or implicitly based on the notion of autonomy, which therefore serves as the core foundation of LEFM.



In a brief, autonomy denotes that, given specific general parameters, the processes along a fractured edge are always identical in any material, independent of body & loading geometry, and followed by some predetermined general conditions. Both mathematically and qualitatively, the advancement in the domains of fracture and crack mechanics was fairly significant since the 1950s. In this somewhat limited area, it is impossible to adequately explain the evolution, although a few people will be named. The first person that comes to recognise is J. R. Rice, who developed exceptional contributions in almost every domains of fracture and crack analysis. Starting in the mid-1960s, he introduced a path-independent integral, J-integral concept, for crack analysis [Rice (1968)], which served as the basis for nonlinear fracture mechanics, and more recently, he has made contributions to 3D dynamic crack propagation [ Rice and Geubelle (1995), Rice and Cochard (1997), Rice and Morrissey (1998)].

The important and innovative contributions made in the dynamic sector by L. B. Freund and B. V. Kostrov deserve special recognition. Kostrov found solutions to many challenging issues for the study of earthquake source physics as well as dynamic propagation of crack. He was the 1st to find a solution to the nonconstant crack expansion model [Kostrov, 1966]. A 4 publications series on crack propagation with nonconstant velocity along with other dynamic issues, like stress wave interaction with cracks, may be listed among Freund's many contributions [Freund (1972*a*, 1972*b*, 1973, 1974)].

A comprehension about fracture mechanics become essential to establish profound design methodologies to ensure the structural integrity of solid body. The mechanics of dynamic fracture may be roughly defined as the solid mechanics having stationary or moving cracks, where material inertia and stress wave interaction have a major effect. Dynamic fracture problems can be classified as following:

- (i) Solids with stationary cracks under dynamic loading.
- (ii) Solids with dynamic and moving crack subject to quasi-static loading.
- (iii) Solids with dynamic and moving crack subject to dynamic loading.

It may be challenging for designers and mechanical engineers to create technical structures that are suitable for their intended purpose and to accurately determine how safe they are against failure.

There are essentially three considerations that must be made to tackle this issue.:

- How may the nature of a certain material be characterized ?
- What mechanisms of failure does the taken material demonstrate, and what is corresponding quantitative failure conditions ?
- How could stresses and strains in each location within the material be accurately calculated while considering the recognized behavior of the material and the external load, and how could the behaviour of the concerning failure be acquired ?

The employment of elastic waves in seismology and geophysics has made difficulties with the diffraction of these waves of major relevance in current times. These categories of problems may be divided into 2 types. Primarily, the waves diffraction due to semi-infinite plane barriers or cracks located within the medium, and secondly, the diffraction influenced by inclusions such as a wedge, circular disc, rigid strips, cones, or barrier of several random shapes. Due to the presence of entrapped imperfections, it is frequently impossible to acquire a homogeneous perfect bond between 2 materials with various mechanical elastic properties, as is the case, for instance, in the joints of various reinforced composites, ceramics, and metals utilized in the production of electronic devices. Layered composites are also common in nature, such as Earth's stratification. In reality, faults appear at the interface of geophysical stratifications, while during the manufacture process, defects occur at the interface between two bonded layers.

Problems related to mechanics of solids may be divided into two types: exact analytical solutions and approximate solutions employing several numerical techniques where it is not possible to solve analytically. In real situation, it seems tough to find exact analytical solution. For this reason, several techniques have been derived to handle the solution regarding solid mechanics. The complex variable technique is a numerical method to solve mixed boundary value problems in 2 - dimension. The other well-known recent technique to solve these models in solid mechanics is the approach to solve by of an integral equation. When we consider The other technique

is the integral equation technique where components of displacement are expressed in terms of potential function to reduce mathematical computation.

There are essentially three categories that may be used to categorize wave propagation in solids. The first kind of wave is elastic, where the stresses within the substance adhere to Hooke's law. The two other major kinds are visco-elastic waves, in which both elastic and viscous stresses are present, and plastic waves, in which the material's yield stress is surpassed.

Next, we turn our attention to a fascinating research aspect in electrostatics, the diffraction of elastic waves with cracks. Almost all structural materials have cracks, whether as a consequence of inherent flaws or production techniques. Many times, the cracks are negligibly tiny, meaning that they have little effect on the material's strength. However, in other cases, the cracks are significant enough or could grow to be large enough to cause fatigue, stress, corrosion cracking, etc., necessitating their consideration when determining the strength. Due to its use in seismology and geophysics, crack models involving the diffraction of elastic waves have gained significant attention in recent years. In reality, faults are found at the interfaces of geophysical stratifications, whereas imperfections are found at the junctions of adjacent layers in manufactured laminates. This stress singularity at the bi-material interface, which is close to the vicinity of the finite fracture, is significant due to its potential practical use. There are many engineering fields that are susceptible to rapid crack propagation. In Earth science, a study of the elastic field close to the moving fracture has become crucial from the perspective of earthquake engineering.

The traditional analytical inspection of fracture mechanics entails computing the stress and deformation fields near the rim of the crack while also applying a fracture criterion inside the context of a continuum model, like the homogeneous, isotropic linearly elastic continuum. The analytical effort is quasi-static in traditional analysis since inertia (or dynamic) effects are disregarded.

Fracture mechanics analysis must be handled as dynamic problems and can be classified into two major categories as:

1. Cracked bodies exposed to quickly changing loads.
2. Bodies with cracks that are moving quickly.

The crack tip is an environment that is disrupted by wave motions in both classes.

The first class of dynamic difficulties are concerns with impact and vibration. In the study of such problems, it is discovered that the dynamic stresses at in homogeneity in a body are larger than the stresses calculated from the equivalent static equilibrium problem. This happens when a mechanical disturbance with propagating waves hits a cavity. When cavity has a sharp edge, the overshoot related to dynamic stress will be more noticeable. When a crack opens, the stress field close to the fracture tip may be considerably modified by dynamic processes. Because of dynamic amplification, there may be situations in which a crack does not propagate when subjected to a applied system of loads, but does so when subjected to a quickly applied system of loads, generating waves that impact rim of the crack.

The second type of problems is also equivalently significant. In fact, there exists various forms of big engineering structures where crack expansion occurs quickly. Some specimens can be stated like ship hulls, gas transmission pipelines, aircraft fuselages, as well as nuclear reactor components. Earthquake analysis is another field where moving cracks can be observed.

### • Modes and Shapes of Crack

Crack propagation within engineering solids often involves the separation of crack surfaces. Mainly crack opening is observed in the following 3 types:

Mode I:

Mode I takes place when the crack surface proceeds to open due to the normal stress ( $\sigma$ ). That is why, Mode I is also named as the opening mode.

Mode II:

Mode II occurs when the crack surfaces slide over one another. For this reason, Mode II is also known as Sliding Mode or the In-Plane Shear Mode.

Mode III:

In the case of Mode-III, crack surfaces have a movement parallel to the leading edge and tear apart because they move relative to each other. Mode - III occurs when

the crack surfaces move, that is why, another name of Mode-III is Tearing Mode or the Out-of-Plane Mode.

So far, the following shapes have been observed in cracks:

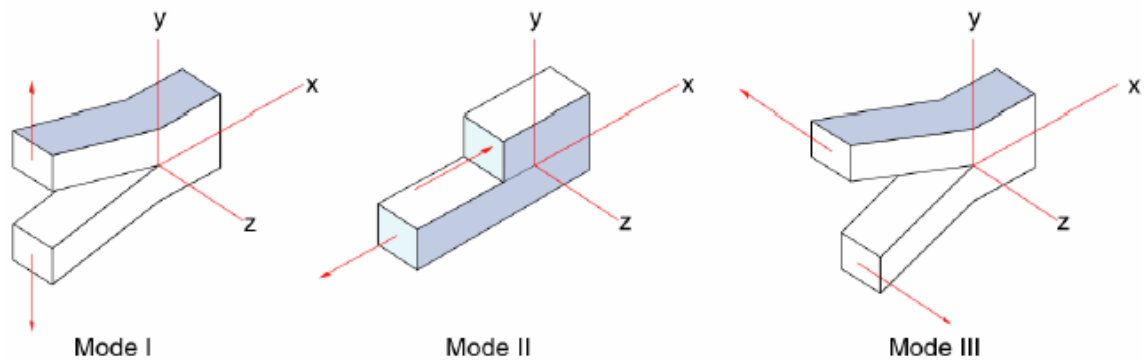


**Fig.1.5 Different modes of crack.**

As of now, several crack shapes can be revealed as stated below: follows:

1. Semi-infinite crack.
2. Finite Griffith crack.
3. Penny shaped crack.
4. Non-planar crack.
5. Edge crack.

### • Boundary Value Problem

Mixed boundary value problems are linked to the wave propagation and diffraction problems. Numerous types related to boundary value problems concerning the elasticity theory have been illustrated in the book by Knops and Payne (1971).

In general, classification of boundary value problems may be done in the following major three categories:

A. Traction boundary value problems.

On the boundary surface, the components of stress are specified.

B. Displacement boundary value problems.

The components of displacement are described on the boundary surface.

C. Mixed boundary value problems.

In this case, several forms of mixed boundary conditions can be described upon the surface or different parts of the surface.

## • Stress Intensity Factor

It is used to forecast the stress state created by an applied force at the crack tip in fracture mechanics. This stress state is defined as stress intensity factor (SIF) and generally denoted by  $K$ . It is a significant method in the domain of damage tolerance and is a theoretical construct that is typically used for a homogeneous, linear elastic material. It is essential for developing a failure criteria for brittle materials. Materials with small-scale yielding at a crack tip may also benefit from the method. The position and size of the fracture, the distribution of the stresses on the components, and the geometry of the material all affect magnitude of  $K$ .

The stress distributions ( $\tau_{ij}$ ) at the crack rim, in polar coordinate ( $r, \theta$ ) considering origin at the rim of the crack, are estimated by the linear elastic theory and appears in as following:

$$\tau_{ij}(r, \theta) = \frac{K}{\sqrt{2\pi r}} f_{ij}(\theta) + \text{higher order terms.}$$

Here,  $K$  indicates the SIF and  $f_{ij}(\theta)$  signifies dimensionless quantity based on the applied load and the geometry of the material. The stress becomes unbounded

as  $r$  tends to zero, which causes this relation to break extremely near the crack tip. The linear elastic solution is no longer valid close to the fracture tip where plastic distortion generally occurs at high loads. However, it may be argued that the aforementioned relation still describes the stress distribution around the crack if the plastic zone is modest.

The SIF for each of the three modes is denoted by a distinct subscript. The SIF concerning mode-I is denoted as  $K_I$  and is used as the mode to open cracks. The SIF concerning mode-II denoted by  $K_{II}$  is employed in the sliding mode of cracks, and the SIF concerning mode-III denoted by  $K_{III}$  is used in the tearing mode. Formally, these factors are expressed in the following form

$$\begin{aligned} K_I &= \lim_{r \rightarrow 0} \sqrt{2\pi r} \tau_{yy}(r, 0), \\ K_{II} &= \lim_{r \rightarrow 0} \sqrt{2\pi r} \tau_{xy}(r, 0), \\ K_{III} &= \lim_{r \rightarrow 0} \sqrt{2\pi r} \tau_{yz}(r, 0). \end{aligned}$$

Several articles reviewing the field of elastodynamic fracture mechanics have been published. Example of such articles are Achenbach (1972), Freund (1975), Achenbach (1976), Freund (1976), and Kanninen (1978).

Current dynamic fracture mechanics solutions are mostly limited to valid situations of linear elastic fracture mechanics (LEFM). These became acceptable when the fracture tip's plastic deformation was minimal enough to be overpowered with the elastic field around it. Using dynamically calculated fields of stress and deformation, LEFM may be used to address issues with crack growth initiation under imposed loads as well as quickly unstable crack propagation and arrest. Nevertheless, engineering structures that need to be protected against the danger of catastrophic large-scale fracture propagation are often made of ductile, strong materials. For such materials, LEFM techniques can only provide roughly accurate forecasts for the start of fracture propagation. Even under static settings, the elastic-plastic procedures needed to get exact results have not yet been fully realized. The employment of elastic waves in seismology and geophysics has made difficulties with their diffraction by cracks or strips of major relevance in recent years. Almost all

structural materials include cracks or inclusions, either naturally or as a consequence of production methods. The branch of mechanics known as "fracture mechanics" focuses on the investigation of the growth of inclusions or cracks within materials.

It employs experimental solid mechanics approaches to determine the resistance of the material to fracture and analytical solid mechanics techniques to examine the driving force upon a crack. Failures have happened for a variety of causes, such as unpredictability in the environment or loads, material flaws, inadequate design, and shortcomings in construction or maintenance. There is a technique for design against fracture, and this is a highly active field of the current study. Due to the limited use of the previously stated stress analysis techniques, without a grasp of fracture, this study will serve as an introduction to a crucial area of this discipline. We shall concentrate on fractures brought on by straightforward tensile over stress, although the designer is once again advised to take into account as many potential failure reasons as feasible. The investigation of elastic wave diffraction by inclusions or cracks in composite materials has grown significantly relevant. If the inclusions or cracks are found near the interface of the stacked medium, the study's relevance increases.

The investigation about propagation of wave and diffraction problems is concerned with mixed boundary value problems. The stress singularity close to the finite crack's edge is significant due to its potential practical use. If the cracks or inclusions have been observed within finite or infinite elastic strips, the investigations seems to be difficult. Also, crack problems situated in composite elastic media are more relevant in the present day.

One of the key issues in light of the manufacturing process and construction technology is the dynamic problem subject to impact of torsional load. The crack is mainly generated by the impact of torsional load. The study of the sudden impact by torsional load in half-space is investigated by M. L. Ghosh (1964), G. Eason (1966) and R. Shail (1970). T. Shibuya (1975) analyzed the problem of the torsional impact of a thick elastic plate. Hadi Hafezi et al. (2012) investigated elastic-plastic stress-strain relationships at the crack tip area and strain-life damage in the research of fatigue crack development models. In this research, the UniGrow model performance is evaluated on the basis of existing experimental constant amplitude



crack propagation data gathered from Portuguese riveted metallic bridges for numerous metallic materials. Recently, a number of new developments on the basis of the elasticity theory, fatigue crack growth models, stress intensity factors for some practical crack geometries and their numerical analysis are discussed in the book of T. Kundu (2008). The solution for obtaining the transient stress intensity factor of an elliptical crack within a thick plate, one side of which is subjected to a sudden temperature change under arbitrary normal loading, was analyzed by Shah and Kabayashi (1971). An elliptical crack in a large beam in pure bending is also described in this paper. Transient dynamic of SIF concerning a crack located within a non-homogeneous interfacial layer between 2 distinct half-planes have been considered by S. Itou (2001).

Matysiak and Pauk (2003) looked at the model based of edge cracks inside an elastic layer lying on the Winkler foundation. Berinci and Erdol (2004) conducted an analysis of the issue of a layered composite with a crack at the bottom layer loaded with a hard stamp. The dynamic behaviour regarding a crack located at the edge of a orthotropic strip which is functionally graded was examined by Guo et al. (2005). Kadioglu (2005) investigated response concerning an edge crack located within a hollow cylinder made of transversely isotropic material. Li (2005) analyzed two fully bonded distinct strips (orthotropic) containing a crack which is located at the interface of the strips and perpendicular to the boundaries of the strips.

Matbuly (2008) analyzed the mode-III crack perpendicular to the interface between two distinct strips. Mode I conducting crack under generally applied loads in piezo-electromagnetic-elastic-layer was investigated by Rogowski (2014). Ding and Li (2014) considered analysis of the crack which are collinear in nature and located within a functionally graded coating-substrate model made of orthotropic media. Hu and Chen (2015) have explored a magneto-electroelastic layer bonded between 2 half-planes that contains a mode-I crack.

The BEM (boundary element method) is used to analyze the stress intensity factors (SIF) of interface cracks between dissimilarly adjoined anisotropic materials by Shiah et al. (2019). Fakoor and Farid (2019) addressed a crack problem (combination of mode-I and mode-II) to study crack propagation in orthotropic media where cracks follow fibers. Singh et al. (2019) calculated the SIF and COD around the rim of a crack (semi-infinite) which is propagating within a linear orthotropic media

inserted between 2 similar type of half-planes. Adopting the Fourier transform technique, Basak and Mandal (2019) deduced fracture analysis for a crack (semi-infinite) located at the interface of two distinct strips made of isotropic material using the Wiener-Hopf equation. P. Mandal (2020) derived equations regarding SIF and COD near a crack (semi-infinite) moving within a semi-infinite and isotropic half-space under the influence of SH-wave. Influence of the elastic wave dispersion caused by 2 parallel cracks (semi-infinite) within mechanical metamaterials based on the discrete Wiener-Hopf method by Huang et al. (2021). Numerous solutions to the issue of orthotropic media with a semi-infinite and moving crack were extensively studied. Among these is the behaviour of a semi-infinite moving crack between two bonded distinct orthotropic strips by Naskar and Mandal (2022); scattering phenomena of longitudinal shear loads of a semi-infinite crack in a homogeneous, elastic orthotropic material by Emenogu et al. (2022); Applying systematic 2D FEA (“Two-Dimensional Finite Element Analysis”) in orthotropic SENB (“Single-Edge Notched Bend”) specimens, SIF and COD was determined by Huang and Wang et al. (2022).

The SIF of a 3D interface crack in dissimilar anisotropic materials was analyzed by Nagai et al. (2007). Yosibash (2007) discovered the functions of edge stress intensity in three-dimensional anisotropic composites. Fo-tuhi and Fariborz (2007) investigated the in-plane stress analysis of an orthotropic plane with several flaws. Itou (2012) has explored the SIF for two parallel interface fractures between two distinct orthotropic half-planes under strain and a nonhomogeneous bonding layer. Monfared and Ayatollahi (2013) have explored the dynamic stress intensity characteristics of many fractures in an orthotropic strip having FGM covering. Tavangari and Salehzadeh (2014) discovered the SIF using the Ritz approach in a media with a penny-shaped crack. Munshi and Mandal (2006) addressed the P-wave diffraction problem caused by an edge crack inside an infinitely long elastic strip. The issue of a flexible plate experiencing vertical vibration with a stiff core on the ground (saturated) was examined by Chen et al. (2007). Crack front waves inside an anisotropic material have been discussed by Willis and Movchan (2007) and the problem of stability of an intersonic crack to a perturbation of its edge was solved by Obrezanova and Willis (2008). Morteza (2011) found a solution to the rigid circular disc’s rocking vibration issue in a transversely isotropic full-space, while Morteza

et al. (2010) examined the rigid circular disc's forced vertical vibration within a transversely isotropic half-space.

The technology of layered composites has experienced significant development in the field of structural design, process engineering, macromechanics, material characterization, and optimization. The influence of torsional waves can not be avoided to prevent damage to solids by an earthquake and many more real situations. Torsion is one kind of wave disturbance originating pressure on the crack surface and disc surfaces leading to the onset of crack propagation and stress field around the circular discs within engineering solids. Propagation of torsional waves takes place in turbines, drillings, etc. Also, in the field of engineering foundations, various shapes of inclusion as circular, strip, rectangular, and other types, have been used to make the desired foundation. The orthotropic materials are themselves a composite medium made up of a stack of layers (called plies/ lamina) to formulate a laminate [Nayfeh (2006)]. These orthotropic materials, such as graphite, epoxy, aluminium composite, carbon-fiber offers a remarkable advantage compared to conventional isotropic materials as they provide a high strength ratio, long fatigue life, high stiffness, corrosion-resistance, etc. In commercial industries such as the airline market, these composite materials are used for profit by reducing the mass of aircraft to save fuel costs [A.K. kaw (2005), Ahmad et al. (2019)]. To get a high level of mechanical performance like high-stiffness, lightweight phenomena, flexibility, durability, etc, orthotropic materials are designed as multi-directional laminates by combining two or more materials. In fracture analysis, the response of layered composites having cracks and inclusions is highly influenced by the orthotropic anisotropy.

Some books related to composite materials providing rigorous applications in the fields of aircraft, automotive, infrastructure, recreational (sports) industries, geomechanics etc., are written by Sih and Chen (1981), D. Roylance (1995), Nayfeh (2006), Vasiliev (2008). Within engineering solids, generally, it is observed that the set of cracks starts when the numerical values of SIFs exceed a certain limit (depending on material anisotropy), named as critical SIFs. In structural engineering, our main aim is to prevent crack propagation to avoid damage of solid structure by controlling the values of SIFs within a certain range, called critical SIFs. Among the problems related to multilayered anisotropic media, Sih and Chen (1972) gave a solution to a penny-shaped crack problem situated inside a four-layered composite

laminate of isotropic elastic media subject to torsion. Stress analysis was investigated by Rabieifar et al. (2018) of functionally graded orthotropic medium with several axisymmetric cracks by the impact of torsional load, by Wu et al. (2021) for multiple penny-shaped crack in an infinite transversely isotropic magneto-electro-elastic space. The solution to an impact caused by torsion around a crack shaped like a penny has been derived for an orthotropic FGM by Li et al. (1999). Craciun and Barbu (2015) carried out a solution in compact closed form for a prestressed orthotropic composite with an elliptical hole due to uniform tensile and uniform tangential shear loads using a conformal mapping technique. Selvadurai and Samea (2021) represented the axisymmetric problem of a penny-shaped crack in a poroelastic half-space based on Biot poroelasticity. He et al. (2021) proposed the simulation model for penny-shaped cracks with the help of Lagrange interpolation polynomials and the boundary element method (BEM).

The problem of torsional elastic wave diffraction using a rigid annular disk at a bi-material interface was solved by Ghosh and Mandal (1993). Wang et al. (1999) studied the crack model of functionally graded penny-shaped crack subject to dynamic loads. Wang et al. (2000) investigated the fracture mechanics for multilayers with penny-shaped crack influenced by dynamic load due to torsion. A.P.S. Selvadurai (2002) investigated the mechanics of an elastic half-space that is cracked and attached to a rigid circular disk. Manna et al. (2003) investigated the model of a rigid disc oscillating due to torsion within an infinite cylinder. Huang et al. (2005) investigated the stress analysis regarding a crack shaped like a penny within a non-homogeneous solid media influenced by torsion. Menshykov et al. (2008) discussed the contact problem for an open crack shaped like a penny during a tension-compression wave incident perpendicularly. Mykhaskiv and Khay (2009) investigated fracture analysis regarding an inserted rigid-disc and a penny-shaped crack due to incidence of wave, which is time-harmonic by nature. The stress analysis for a crack in the form of a penny interacting with inclusions and voids was taken into investigation by Lee and Tran (2010). Li et al. (2011) analyzed the crack model involving coulomb traction on a crack in the form of a penny inside a 3D piezoelectric body. Dovzhik (2012) has studied the half-space fracture compressed across crack shaped like a penny that is close to the surface. The analysis of a crack in the form of a penny inside a plate with finite thickness due to homogeneous shearing stress was examined by D.-S. Lee (2013). The penny-shaped crack model within transversely

isotropic media exposed to uniform symmetric as well as anti-symmetric heat flow was examined by Yang et al. (2014). Aizikovich et al. (2015) have established a semi-analytical explanation for a crack shaped like a penny within a soft inhomogeneous layer. Gilbert and Lee (2015) further considered the crack model involving Penny-Shaped Crack in a Poroelastic Plate. I.A. Abbas (2016) discussed the finite element analysis of an internal penny-shaped crack in an unbounded thermoelastic medium.

A penny-shaped crack problem in thermo-magneto-electro-elasticity has been solved by Li et al. (2017). Propagation of time-harmonic elastic waves through a double-periodic array of penny-shaped cracks was investigated by Mykhaskiv et al. (2019). Dynamic stress factor due to the penny-shaped crack in a three-component elastic solid consisting of two dissimilar half-spaces and an intermediate layer have been analyzed by Mykhaskiv and Stankevych (2019). An infinite homogeneous isotropic elastic medium with surface elasticity on the crack boundary is studied for a nanosized penny-shaped crack by Yang et al. (2021). Yang et al. (2022) studied an infinite three-dimensional isotropic elastic solid with a penny-shaped crack whose boundary is enhanced by the incorporation of surface elasticity in terms of its torsional deformation. Madani and Kebli (2019) solved the problem of axisymmetric torsion of an elastic layer with a penny-shaped crack by a cylindrical rigid disc at the symmetry plane. Madani and Kebli (2019) studied a cracked semi-infinite medium under the torsion of a rigid disc using dual integral equations. Using dual integral equations, Hankel and Weber-Orr transform, Pinchas Malits (2020) investigated the rotation of an elastic body by an embedded semi-infinite rigid cylinder with a penny-shaped crack. The torsion of an elastic layer attached to a rigid circular base with a circular rigid punch is solved by Kebli et al. (2020). The solution of an axisymmetric problem of a penny-shaped crack near and parallel to a graded interface was given by Chen et al. (2022). An investigation into the fracture mechanics of elastic cracked materials exposed to transient dynamic loading has been done by Menshykov et al. (2020). Stress intensity factors around multiple radial cracks within circular shafts with an FG coating layer under transient torsional loading have been analyzed by Mahmoodi et al. (2022). In view of the above literature survey, we present our thesis chapters as follows:

Only numerical techniques may be used to evaluate stresses and strains because

of the complicated geometries and loads placed on composite materials. In our investigations, we have studied some mixed type “boundary value problems”. To solve these problems, we have used some standard methods and techniques, which are presented briefly in Chapter 2.

In Chapter 3, the first problem, shear wave propagation through an orthotropic strip with an edge crack has been analyzed. Dual integral equations have been developed for the solution of the governing mixed boundary value problem with the aid of the Hankel transform technique. Then, the dual integral equations have been transformed into a second kind of Fredholm integral equation employing Abel’s transformation. The numerical calculations of stress intensity factor and crack opening displacement are performed utilizing the Fox & Goodwin method and displayed graphically. Elastic constants of two orthotropic materials have been used to illustrate the influence of material orthotropy and normalized strip width on SIF and COD.

Secondly, we investigated the motion of a semi-infinite moving crack inside a semi-infinite half-space of an orthotropic medium subjected to an anti-plane shear wave. The crack is located at a finite depth from the surface of the semi-infinite orthotropic medium. Our aim is to examine how such anisotropy and geometric parameters can be adjusted to reduce the magnitude of the stress intensity factor to control the crack propagation near the crack tip region. As mathematical tools, Fourier transformation and inverse Fourier transformation techniques are employed to convert the governing mixed boundary value problem to the well-known Wiener-Hopf equation with suitable boundary conditions. Some physical quantities, such as stress intensity factor (SIF) at the crack tip and crack opening displacement (COD) around the crack tip, have been derived. A graphical exhibition has been carried out to show the impact of relevant parameters such as crack velocity, layer depth from the surface to crack and orthotropic material properties on SIF and COD. The numerical results show that SIF decay with crack depth from the layer. It is also observed that SIF decreases with an increase in crack velocity and finally tends to zero as crack velocity approaches near SH-wave velocity. Also, the value of COD decays as we move along the damage near the crack tip along the negative x-axis and finally tends to zero at the crack tip. This behaviour of COD is consistent with the physical nature of the semi-infinite crack of the problem. The results are

validated for isotropic material with some reported work and are well in agreement. The study of these physical quantities (SIF, COD) ensures the arrest of the onset of crack expansion by monitoring geometric parameters and wave velocity to avoid fracture.

In Chapter 4, we studied the influence of a suddenly applied impact load due to torsion upon a crack in the form of a penny sandwiched in between 2 elastic layers inserted in an elastic media. Hankel and Laplace's transformations are utilized to resolve the axisymmetric model with mixed boundary conditions into two dual integral equations. The equations are further simplified into a 2nd kind integral equation Fredholm type which is then numerically solved. Stress intensity factor (SIF) around the crack rim has been derived and is then displayed taking several geometric parameters and set of composite mediums.

Lastly, in Chapter 5, we have considered the torsional wave propagation of a penny-shaped crack in an orthotropic layer and two circular discs bonded between the layer and half-spaces. A general solution for the system is presented as a set of dual integral equations using the Hankel transform technique. Using Abel's transform method, the equations have been transformed into Fredholm integral equations of the second kind, which have been solved numerically to compute the stress intensity factors (SIFs) near the rims of crack and discs. Numerical results are obtained using material constants of two orthotropic mediums to demonstrate the impact of material non-homogeneity, normalized disc radius, and layer depth on SIFs and portrayed by virtue of graphs. The analysis of the physical quantity SIF in the present model leads to speculation about the stability of composites against the propagation of cracks in layered engineering solids by surveilling geometric parameters of orthotropic materials and layer depth.

*Chapter-2*  
*Methodology*



# Chapter 2

## Methodology

Mixed boundary value problems are linked to wave propagation and diffraction problems. Near the crack edges, the stress singularity is crucial in view of its practical usage. Also, results of dynamic-crack propagation research are relevant in numerous applications. Generally, the aim of structural engineering is to resist a propagating crack once it begins. If cracks or inclusions occur in finite or infinite elastic strips, the problem becomes more onerous. The orthotropic anisotropy has a significant impact on the influence of multilayer composites with fractures and inclusions in fracture analysis. Evaluation of stresses and strains can only be done numerically due to the complicated geometries and loads placed on composite materials. In our research work, we have studied some mixed boundary value problems.

Integral equations are often employed to address this kind of boundary value problem. By using Hankel, Laplace, or Fourier transforms, the axisymmetric mixed boundary value problem can initially be reduced into a pair involving dual integral equations. The dual integral equation can be inverted into a second kind integral equation of Fredholm type employing Abel's integral formula or Hankel's transform. It is often necessary to apply the Wiener-Hopf technique in such cases.

Methods for numerical calculation and solving boundary value problems in elasticity are listed below.

1. Dual Integral Equation Method

2. Abel's Integral Equation Solution
3. Integral Equation Solution following the Hankel Transform approach
4. Linear non-singular Integral Equations numerical solution by Fox and Goodwin Method
5. Numerical Inversion of Laplace Transform
6. Gaussian Integration
7. Wiener-Hopf Method

## 2.1 Dual Integral Equation Method

When a mixed boundary value problem is given, this method can be used successfully. At first, this problem is reduced to a dual integral equation system using Fourier transform or otherwise. Then this method is used to reduce dual integral equations set in a single Fredholm type integral equation of some unknown variable. After resolving the Fredholm integral equation, the desired function is obtained by performing simple integration.

Let us suppose that formulation of the model based on mixed boundary conditions is done with suitable integral transformation to derive a equation set of dual integrals as:

$$\int_0^{\infty} x^{-1} [1 + K(x)] S(x) J_{\nu}(rx) dx = f(r), \quad 0 \leq r \leq a, \quad (2.1.1)$$

$$\int_0^{\infty} S(x) J_{\nu}(rx) dx = g(r), \quad r > a, \quad (2.1.2)$$

where  $K(x)$ ,  $f(r)$  and  $g(r)$  represents known functions. As reported by Noble (1963), considering  $\nu > -\frac{1}{2}$

$$S(x) = \sqrt{\frac{2x}{\pi}} \left\{ \int_0^a t^{1/2} \theta(t) J_{\nu-\frac{1}{2}}(xt) dt + \int_a^{\infty} t^{\nu+\frac{1}{2}} G(t) J_{\nu-\frac{1}{2}}(xt) dt \right\},$$

where  $\theta(t)$  satisfies the Fredholm integral equation

$$\theta(t) + \frac{1}{\pi} \int_0^a M(\tau, t) \theta(\tau) d\tau = t^{-\nu} F(t) - H(t), \quad 0 \leq t \leq a, \quad (2.1.3)$$

in which

$$M(\tau, t) = \pi \sqrt{\tau t} \int_0^\infty x K(x) J_{\nu-\frac{1}{2}}(\tau x) J_{\nu-\frac{1}{2}}(tx) dx,$$

$$F(t) = \frac{d}{dt} \int_0^t f(r) r^{\nu+1} (t^2 - r^2)^{-1/2} dr,$$

$$H(t) = t^{1/2} \int_0^\infty x K(x) J_{\nu-\frac{1}{2}}(xt) dx \int_a^\infty \xi^{\nu+\frac{1}{2}} G(\xi) J_{\nu-\frac{1}{2}}(x\xi) d\xi,$$

$$G(\xi) = \int_\xi^\infty g(r) r^{-\nu+1} (r^2 - \xi^2)^{-1/2} dr.$$

The above given integral equations is also further solved for  $\theta(t)$  and consequently  $S(x)$  can be determined.

## 2.2 Abel's Integral Equation Solution

In 1823, Abel studied how a particle moves when it is pulled downward by gravity along an unknown smooth curve at a vertical plane. The particle moves from high vertical height point  $\zeta$  to a low point  $a$  for time  $u(\zeta)$ . To determine the curve's equation, the Abel's problem is developed. Abel used the singular integral equation to calculate the sliding particle's motion equation along a smooth curve.

Abel used the singular integral equation to calculate the sliding particle's motion equation along a smooth curve.

$$u(\zeta) = \int_a^\zeta \frac{q(t) dt}{\sqrt{\zeta - t}}, \quad (2.2.1)$$

In the above equation  $u(\zeta)$  represents pre-determined data function and  $q(\zeta)$  is the solution to be calculated. Equation (2.2.1) is in form of the Abel's Integral Equation which is also termed as the 1st kind Volterra integral equation. In this equation the kernel  $K(\zeta, t)$  is expressed as

$$K(\zeta, t) = \frac{1}{\sqrt{\zeta - t}} \longrightarrow \infty \text{ as } t \longrightarrow \zeta, \quad (2.2.2)$$

and the solution is of the form

$$q(\zeta) = \frac{1}{\pi} \frac{d}{d\zeta} \int_a^\zeta \frac{u(t) dt}{\sqrt{\zeta - t}} = \frac{u(a)}{\pi\sqrt{\zeta - a}} + \frac{1}{\pi} \int_a^\zeta \frac{u'(t) dt}{\sqrt{\zeta - t}}. \quad (2.2.3)$$

## 2.3 Integral Equation Solution following the Hankel Transform approach

Bessel functions serve as the kernels of “Hankel Transforms”, which are one type of integral transformations. They are sometimes known as Bessel transforms. Hankel transformations may be quite helpful when dealing with models that exhibit circular symmetry. This transform could be used to convert Laplace’s partial differential equation in cylindrical coordinates to an ordinary differential equation. Let  $g(r)$  is a function defined when  $r \geq 0$ . The  $\nu$ th order “Hankel transform” of  $g(r)$  can be prescribed as

$$G_\nu(s) \equiv \int_0^\infty r g(r) J_\nu(sr) dr. \quad (2.3.1)$$

In the above equation,  $J_\nu(sr)$  denotes first kind Bessel function with order  $\nu$  and  $r J_\nu(sr)$  represents kernel related to the transformation. If  $\nu > -\frac{1}{2}$ , an inversion formula is formed immediately by Hankels repeated integral:

$$g(r) \equiv \int_0^\infty s G_\nu(s) J_\nu(sr) ds. \quad (2.3.2)$$

The Hankel transform’s two most significant special types are found when  $\nu$  takes the values 0 and 1. Conditions that are sufficient but not essential for the validity of (2.3.1) and (2.3.2) are

1. Here  $g(r) = O(r^{-k})$ ,  $r \rightarrow \infty$ , where  $k > \frac{3}{2}$ .
2. Piecewise continuous function  $g'(r)$  exists throughout all bounded subinterval of  $[0, \infty)$ .
3.  $g(r)$  could be described as  $\frac{[g(r+) + g(r-)]}{2}$ .

It is possible to relax the above conditions.

## 2.4 Linear non-singular Integral Equations numerical solution by Fox and Goodwin Method

We will use the continental convention of calling Fredholm type equations those with constant limits in the integral and Volterra type equations those with variable limits. Fredholm type first and second kind equations are given by:

$$\int_a^b k(x, y)f(y) dy = g(x), \tag{2.4.1}$$

$$\int_a^b k(x, y)f(y) dy = g(x) + f(x). \tag{2.4.2}$$

For frequent occurrence another equation can be given as:

$$\lambda \int_a^b k(x, y)f(y) dy = g(x). \tag{2.4.3}$$

In Equations (2.4.1) and (2.4.2), the wanted function is given by  $f$ , all other functions are known either numerically, graphically or analytically. Both the eigenvalue  $\lambda$  and eigenfunction  $f$  appearing in Equation (2.4.3) are to be determined.

To describe the integral in each instance as a finite sum of terms of the type  $a_r k(x_s, y_r)f(y_r)$ , we must first look at certain numerical integration formulas.

### Numerical Integration:

Difference-based equations are often preferable over Lagrangian-based ones. The former may be truncated when contributions are negligible, but the degree of a suitable Lagrangian polynomial is unknown without considering the differences. The best finite-difference integration formulas are expressed as follows:

$$\frac{1}{h} \int_a^{a+nh} f(x)dx = \frac{1}{2}f_0 + f_1 + \dots + f_{n-1} + \frac{1}{2}f_n + \Delta, \tag{2.4.4}$$

where  $f_0 = f(a)$ ,  $f_r = f(a + rh)$  and  $\Delta$ , denotes difference correction related to the function  $f$ .

For the simplest scenario, when  $n = 1$ , and the integral is calculated between neighbouring pivotal points, we get the expression using central differences.

$$\frac{1}{h} \int_a^{a+h} f(x)dx = \frac{1}{2}(f_0 + f_1) - \frac{1}{12}\mu\delta^2 f_{\frac{1}{2}} + \frac{11}{720}\mu\delta^4 f_{\frac{1}{2}}, \quad (2.4.5)$$

and in the general case,

$$\frac{1}{h} \int_a^{a+nh} f(x)dx = \frac{1}{2}f_0 + f_1 + \dots + f_{n-1} + \frac{1}{2}f_n + \Delta, \quad (2.4.6)$$

$$\Delta = \left(-\frac{1}{12}\Delta^1 + \frac{1}{24}\Delta^2 - \frac{19}{720}\Delta^3 \dots\right)(f_n - f_0). \quad (2.4.7)$$

These formulas all make use of differences discovered at pivotal points beyond the integration range. Equation (2.4.7) may be converted into a formula that only uses pivot points within the range by rewriting the difference correction as:

$$\Delta = -\left(\frac{1}{12}\nabla^1 + \frac{1}{24}\nabla^2 + \frac{19}{720}\nabla^3 \dots\right)f_n + \left(\frac{1}{12}\Delta^1 - \frac{1}{24}\Delta^2 + \frac{19}{720}\Delta^3 \dots\right)f_0. \quad (2.4.8)$$

This is Gregory's integration formula's difference correction.

Our major ally in solving Fredholm type integral equations is the Gregory formula. We are only interested in its solution at pivotal points under a designated integration range; the kernel can not even be described beyond the range, making it difficult to employ formulas like (2.4.6). Less terms are involved in the correction, and the accuracy is somewhat improved due to the lower coefficient.

**Solution of second kind Fredholm's equation:**

We begin by addressing 2nd kind Fredholm's equation which is represented in equation (2.4.2).

Equation (2.4.2) may be written as follows using Equation (2.4.4) as the integral's representation:

$$h[\frac{1}{2}k(x, 0)f_0 + k(x, 1)f_1 + \dots + k(x, n - 1)f_{n-1} + \frac{1}{2}k(x, n)f_n + \Delta(x)] = g(x) + f(x),$$

where  $k(x, y)$  value at point  $(x, sh)$  is indicated by  $k(x, s)$ . We may then substitute the integral equation with a set of  $(n+1)$  linear simultaneous equation taking into account all of the pivotal points as

$$h[\frac{1}{2}k(r, 0)f_0 + k(r, 1)f_1 + \dots + k(r, n - 1)f_{n-1} + \frac{1}{2}k(r, n)f_n + \Delta_r] = g_r + f_r,$$

Where  $r$  now takes the values  $0, 1, \dots, n$ . and  $k(r, s)$  signifies  $k(x, y)$  value on point  $(rh, sh)$ . We may formulate the equations in the following form by combining the  $f_r$  on the left with those on the right.

$$\begin{aligned} \{1 - \frac{1}{2}hk(0, 0)\}f_0 - hk(0, 1)f_1 \dots - hk(0, n - 1)f_{n-1} - \frac{1}{2}hk(0, n)f_n &= -g_0 + h\Delta_0, \\ -\frac{1}{2}hk(1, 0)f_0 + \{1 - hk(1, 1)\}f_1 \dots - hk(1, n - 1)f_{n-1} - \frac{1}{2}hk(1, n)f_n &= -g_1 + h\Delta_1, \\ \dots \dots \dots \dots \dots \dots \dots \dots \dots \dots \dots \dots \dots \dots \dots \dots \dots & \dots \dots \dots \dots \dots \dots \dots \dots \dots \dots \dots \dots \dots \dots \dots \dots \dots \\ -\frac{1}{2}hk(n - 1, 0)f_0 - hk(n - 1, 1)f_1 \dots + \{1 - hk(n - 1, n - 1)\}f_{n-1} - \frac{1}{2}hk(n - 1, n)f_n &= -g_{n-1} + h\Delta_{n-1}, \\ -\frac{1}{2}hk(n, 0)f_0 - hk(n, 1)f_1 \dots - hk(n, n - 1)f_{n-1} + \{1 - \frac{1}{2}hk(n, n)\}f_n &= -g_n + h\Delta_n. \end{aligned} \tag{2.4.9}$$

We will quickly discuss a few options for solving these problems.

The  $\Delta_r$  are linear functions of the  $f_r$  when the Gregory formula is used. These linear functions would be known if we also knew the order of the most recent significant difference in (2.4.8). The  $\Delta_r$  in (2.4.9) could therefore be moved to the left, leading to a set of expressions for the  $f_r$  that only had distinct coefficients and



the  $g_r$  on the right. This is practically equal to representing the integral using a Lagrangian formula.

As an alternative, we may select a very tiny interval  $h$  with the goal of making the  $\Delta_r$  insignificant. This might require solving a large number of linear equations, which would require a lot of work and present the risk of mistakes due to improper conditioning. Finally, we may calculate the equation while accounting for up to fourth and sixth differences, respectively, and compare the outcomes.

It appears more appealing to take an iterative approach. By ignoring the  $\Delta_r$  in Equations (2.4.9), the simplest quadrature formula is used in this technique to get a first approximation to the desired answer. We next use the roughly determined estimated  $f_r$  to compute and difference the values  $k(x, 0)f_0$ ,  $k(x, 1)f_1$ , etc. for each  $x$ . Then, all the  $\Delta_r$  may be computed and added in right-hand sides of Equation (2.4.9) for correction. Next, necessary corrections to  $f$  are acquired trivially and the method is then repeated until there is no more change.

This method may be represented symbolically as follows. We solve the equations sequentially if  $A$  signifies coefficient matrix (square) related to  $f_r$ , the vector  $g$  having coefficients  $g_r$  and the vector  $\Delta$  admits  $\Delta_r$  as components.

$$\begin{aligned}
 Af^{(0)} &= -g, \\
 Af^{(1)} &= h\Delta(f^{(0)}), \\
 Af^{(2)} &= h\Delta(f^{(1)}), \\
 &\dots\dots\dots,
 \end{aligned}$$

the final solution being given by

$$f = f^{(0)} + f^{(1)} + f^{(2)} + \dots$$

For models containing differential equations of the boundary-value type, this method is the exact same as that of Fox (1949).

Of course, picking the interval  $h$  was rather arbitrary. The number of linear equations should be kept to a minimum; but the interval shouldn't be so wide that the finite-difference expressions become useless. The procedure protects against the danger of getting inaccurate findings from this cause since the differences are investigated. Additionally, the truncation point should not be the same for every  $x$ , ensuring that neither too few differences nor too many differences are kept in the quadrature equations.

## 2.5 Numerical Inversion of Laplace Transform

Below given is the Laplace transform  $H(s)$  of  $h(t)$ :

$$H(s) = \int_0^{\infty} e^{-st} h(t) dt, \quad s \geq 0 \quad (s = \text{transform parameter}).$$

Here, Zakian's Algorithm is used for the Laplace inversion.

### Zakian's Algorithm:

This represents a class of algorithms, where calculation of the function  $h(t)$  has been performed as the total sum of  $H(s)$  as

$$h(t) = \sum_{j=1}^M K_j H(s_j),$$

where a specific technique determines the values of  $K_j, s_j$  and  $M$ . The condition that the time function may be connected with a finite series involving exponential functions is a critical aspect of the derivation.

$$\sum_{j=1}^M K_j e^{\alpha_j t} .$$

This specification is significant because it shows how well Zakian's Algorithm performs for systems that are slightly underdamped and slightly overdamped. However, it is inaccurate for systems that oscillate for a long time. The following equation denotes Zakian's Algorithm and enables us to get the numerical value of  $h(t)$  for known value of  $H(s)$  and time  $t$ .

$$h(t) = \frac{2}{t} \sum_{j=1}^5 \text{REAL} \left( K_j H \left( \frac{\alpha_j}{t} \right) \right).$$

Table 2.1 provides the set of 5 complex constants for  $\alpha_j$ .

Table 2.1: Five constant set for  $\alpha_j$  and  $K_j$  for the Zakian's approach.

i	$\alpha_j$	$K_j$
1	12.83767675 + i 1.666063445	-36902.08210 + i 196990.4257
2	12.22613209 + i 5.012718792	61277.02524 - i 95408.62551
3	10.93430308 + i 8.409673116	-28916.56288 + i 18169.18531
4	8.776434715 + i 11.92185389	4655.361138 - i 1.901528642
5	5.225453361 + i 15.72952905	-118.7414011 - i 141.3036911

The Zakian algorithm computes rapidly and is easy to use. But it can be noticed that it is impossible to determine the primary value,  $h(t)$  at  $t = 0$ . Additionally,  $h(t)$  becomes incorrect in oscillatory systems after around the second cycle.

## 2.6 Gaussian Integration

The Gauss quadrature formula was introduced by the famous German mathematician Karl Friedrich Gauss (1777-1855). He proved that the points of subdivision should not be equidistant, but must be symmetrically placed with respect to the midpoint of the interval of integration. Gauss integration is based on the fact that the accuracy of numerical integration can be improved by selecting the function values sensibly rather than on the basis of equal spacing.

Thus, we have

$$\int_a^b f(x) dx \simeq \sum_{i=0}^n c_i f(x_i), \quad x_i = a + ih, \quad h = \frac{b-a}{n}. \quad (2.6.1)$$

where the coefficients  $c_i$ 's are the parameters which are the weighting factors applied to the function values. Gauss observed that if we do not restrict the function values to be evaluated at predetermined equally spaced  $x$ -values, an  $(n+1)$  term formula will contain  $(2n+2)$  parameters. The Gaussian Quadrature is written in the form

$$\int_{-1}^1 F(u) du = \sum_{i=1}^n w_i F(u_i), \quad (2.6.2)$$

where  $n$  values of  $u_i$  and  $n$  values of weights  $w_i$  are  $2n$  unknowns. The  $2n$  unknowns are derived such that the above formula give exact values for  $F(u)$  being a polynomial of degree less than or equal to  $2n-1$ .

Let us consider

$$F(u) = \sum_{k=0}^{2n-1} a_k u^k. \quad (2.6.3)$$

Now, substituting (2.6.2) in (2.6.3), we obtain

$$\int_{-1}^1 \left( \sum_{k=0}^{2n-1} a_k u^k \right) du = \sum_{i=1}^n a_k u^k,$$

$$\text{or } 2a_0 + \frac{2}{3}a_2 + \frac{2}{5}a_4 + \dots + \frac{2a_{2n-2}}{2n-1} = \sum_{i=1}^n w_i \left[ \sum_{k=0}^{2n-1} a_k u^k \right].$$

The above equations must be true for all polynomials of degree less than or equal to  $2n-1$ , i.e. for all  $a_k$  and, hence, equating the coefficients of  $a_k$  on either side, we get the following  $2n$  equations

$$\begin{aligned} w_1 + w_2 + \dots + w_n &= 2, \\ u_1 w_1 + u_2 w_2 + \dots + u_n w_n &= 0, \\ u_1^2 w_1 + u_2^2 w_2 + \dots + u_n^2 w_n &= \frac{2}{3}, \\ &\vdots \\ u_1^{2n-1} w_1 + u_2^{2n-1} w_2 + \dots + u_n^{2n-1} w_n &= 0. \end{aligned} \tag{2.6.4}$$

The above is a set of  $2n$  equations in the  $2n$  unknowns  $w_1, w_2, \dots, w_n$  and  $u_1, u_2, \dots, u_n$ . It is obvious that the equations are quite complicated, and it is cumbersome to solve them by ordinary methods of algebra.

However, it can be shown by using the theory of orthogonal polynomials that the  $u'_i$ s are the zeros of the Legendre Polynomial  $P_n(u)$  of degree  $n$ . Substituting the values of  $u'_i$ s in any set of  $n$  equations from (2.6.4), the weights  $w_i$  can be determined. The values of these  $2n$  parameters are listed in the table for various values of  $n$ . The abscissa and the weights are irrational numbers, and their values have been provided in Table 2.2.

Table 2.2: Gauss Quadrature Table

$n$	$w_i$	$x_i$	$n$	$w_i$	$x_i$
1	2.0	0.0	8	0.1012285363	$\pm 0.9602898565$
2	1.0	$\pm 0.5773502692$		0.2223810345	$\pm 0.7966664774$
3	0.5555555556	$\pm 0.7745966692$		0.3137066459	$\pm 0.5255324099$
	0.8888888889	0.0		0.3626837834	$\pm 0.1834346425$
4	0.3478548451	$\pm 0.8611363116$	9	0.0812743883	$\pm 0.9681602395$
	0.6521451549	$\pm 0.3399810436$		0.1806481607	$\pm 0.8360311073$
5	0.2369268851	$\pm 0.9061798459$		0.2606106964	$\pm 0.6133714327$
	0.4786286705	$\pm 0.5384693101$		0.3123470770	$\pm 0.3242534234$
	0.5688888889	0.0	0.3302393550	0.0	
6	0.1713244924	$\pm 0.9324695142$	10	0.0666713443	$\pm 0.9739065285$
	0.3607615730	$\pm 0.6612093865$		0.1494513492	$\pm 0.8650633667$
	0.4679139346	$\pm 0.2386191861$		0.2190863625	$\pm 0.6794095683$
7	0.1294849662	$\pm 0.9491079123$		0.2692667193	$\pm 0.4333953941$
	0.2797053915	$\pm 0.7415311856$	0.2955242247	$\pm 0.1488743390$	
	0.3818300505	$\pm 0.4058451514$			
	0.4179591837	0.0			

It is to be noted that the Gaussian formula is applied for the limits of integration  $-1$  to  $1$ . To use the Gaussian quadrature for evaluating  $\int_a^b f(x) dx$ , we can use a transformation of variable to change the limits of integration to  $(-1, 1)$  in the form  $x = \frac{b-a}{2} u + \frac{b+a}{2}$ . So that

$$\int_a^b f(x) dx = \frac{b-a}{2} \int_{-1}^1 f\left(\frac{b-a}{2} u + \frac{b+a}{2}\right) du.$$

#### Errors in Gaussssian Formula

1. One-point formula  $E_1 =$  high error.
2. Two-point formula  $E_2 = -\frac{F^4(\xi)}{135}$ ,  $-1 < \xi < 1$ .
3. Three-point formula  $E_3 = -\frac{F^4(\xi)}{15750}$ ,  $-1 < \xi < 1$ .
4. Four -point formula  $E_4 = -\frac{F^8(\xi)}{3471875}$ ,  $-1 < \xi < 1$ .
5. Five-point formula  $E_5 = -\frac{F^{10}(\xi)}{123773650}$ ,  $-1 < \xi < 1$  where  $F^i(\xi)$  means  $\frac{d^i}{dx^i}(F(\xi))$ .

## 2.7 Wiener-Hopf Method

Noble (1958) developed the Wiener-Hopf approach for solution of integral equations in the following general form

$$f(x) + \int_0^{\infty} k(x-\eta)f(\eta)d\eta = g(x), \quad 0 \leq x < \infty. \quad (2.7.1)$$

Here the kernel  $k(x)$  can be described in  $-\infty < x < \infty$ . The function  $g(x)$  is described in  $0 \leq x < \infty$ , and undefined in  $-\infty < x < 0$ . The function  $f(x)$  is identically zero in  $-\infty < x < 0$  and to be measured within range  $0 \leq x < \infty$ .

Particularly instrumental to solve (2.7.1) is a convolution theorem stating:

$$\int_{-\infty}^{\infty} e^{-\zeta x} dx \int_{-\infty}^{\infty} k(x-\eta)f(\eta)d\eta = k^*f^*, \quad (2.7.2)$$

where  $f^*(\zeta)$  and  $k^*(\zeta)$  are the 2 sided Laplace transforms of  $f(x)$  and  $k(x)$ . Equation (2.7.1) will not be complicated to resolve when the integral equation were described for the entire range of  $x$  such as  $-\infty < x < \infty$ . So, Equation (2.7.1) can be rewritten as

$$f_+(x) + \int_{-\infty}^{\infty} k(x-\eta)f_+(\eta)d\eta = g_+(x) + h_-(x), \quad (2.7.3)$$

where

$$f_+(x) = \begin{cases} f(x), & x \geq 0 \\ 0, & x < 0 \end{cases} \quad (2.7.4)$$

$$h_-(x) = \begin{cases} 0, & x \geq 0 \\ h(x), & x < 0 \end{cases} \quad (2.7.5)$$

It is noted that for  $x \geq 0$ , Equation (2.7.3) just reduced to Equation (2.7.1). For  $x < 0$ , we have

$$\int_{-\infty}^{\infty} k(x - \eta) f_+(\eta) = h_-(x). \quad (2.7.6)$$

Suppose,  $\gamma$  a real number may be estimated so that  $k(x)e^{-\gamma x}$  is integrable absolutely for  $-\infty < x < \infty$ . Further, it can be considered that  $f_+(x)e^{-\gamma x}$  and  $g_+(x)e^{-\gamma x}$  are integrable absolutely for  $0 < x < \infty$  and also that  $h_-(x)e^{-\gamma x}$  is integrable absolutely for  $-\infty < x < 0$ . So, the transforms are defined as:

$$k^*(\zeta) = \int_{-\infty}^{\infty} e^{-\zeta x} k(x) dx, \quad (2.7.7)$$

$$f_+^*(\zeta) = \int_0^{\infty} e^{-\zeta x} f_+(x) dx, \quad (2.7.8)$$

$$g_+^*(\zeta) = \int_0^{\infty} e^{-\zeta x} g_+(x) dx, \quad (2.7.9)$$

$$h_-^*(\zeta) = \int_{-\infty}^0 e^{-\zeta x} h_-(x) dx. \quad (2.7.10)$$

$k^*(\zeta)$  is regular for  $\mathbf{R}(\zeta) = \gamma$ .  $f_+^*(\zeta)$  and  $g_+^*(\zeta)$  become regular when  $\mathbf{R}(\zeta) > \gamma$  and  $h_-^*$  become regular when  $\mathbf{R}(\zeta) < \gamma$ . In addition to this, using the convolution theorem from Equation (2.7.3) we get:-

$$f_+^* + k^* f_+^* = g_+^* + h_-^*, \quad (2.7.11)$$

on the line  $\mathbf{R}(\zeta) = \gamma$ .

It can be further assumed that,  $1 + k^*(\zeta)$  don't have roots on  $\mathbf{R}(\zeta) = \gamma$ . With some weak conditions,  $1 + k^*(\zeta)$  could be factored, that is  $1 + k^*(\zeta)$  is specified as:

$$1 + k^* = m_+^* m_-^*. \quad (2.7.12)$$

Here  $m_+^*$  as well as  $(m_+^*)^{-1}$  are bounded on  $\mathbf{R}(\zeta) = \gamma$ , and regular for  $\mathbf{R}(\zeta) > \gamma$ , whereas  $m_-^*$  and  $(m_-^*)^{-1}$  are also bounded on  $\mathbf{R}(\zeta) = \gamma$ , but regular on  $\mathbf{R}(\zeta) < \gamma$ . Equation (2.7.1) can be written as

$$m_+^* f_+^* = \frac{g_+^*}{m_-^*} + \frac{h_-^*}{m_-^*}. \quad (2.7.13)$$



Subsequently the term  $\frac{g_+^*}{m_-^*}$  may usually be split up in the following way :

$$\frac{g_+^*}{m_-^*} = n_+^* + n_-^*, \quad (2.7.14)$$

where  $n_+^*$  is regular in  $\mathbf{R}(\zeta) > \gamma$  and  $n_-^*$  is regular in  $\mathbf{R}(\zeta) < \gamma$ . Substitution of Equation (2.7.14) into Equation (2.7.13) yields

$$m_+^* f_+^* - n_+^* = \frac{h_-^*}{m_-^*} + n_-^* \quad \text{on} \quad \mathbf{R}(\zeta) = \gamma. \quad (2.7.15)$$

Now, we describe the functions

$$e_+^*(\zeta) = m_+^* f_+^* - n_+^*, \quad (2.7.16)$$

and

$$e_-^*(\zeta) = \frac{h_-^*}{m_-^*} - n_-^*. \quad (2.7.17)$$

Then,  $e_+^*(\zeta)$  is regular for  $\mathbf{R}(\zeta) > \gamma$  and  $e_-^*(\zeta)$  is regular for  $\mathbf{R}(\zeta) < \gamma$ , whereas for  $\mathbf{R}(\zeta) = \gamma$  the functions  $e_+^*(\zeta)$  and  $e_-^*(\zeta)$  are continuous and identical with one another. On the basis of functional analysis theorem,  $e_+^*(\zeta)$  might further be taken as the analytic continuation of  $e_-^*(\zeta)$  and vice versa. Therefore, the functions  $e_+^*(\zeta)$  as well as  $e_-^*(\zeta)$  present one and the same entire function  $e^*(\zeta)$  (a function that is regular throughout the whole  $\zeta$ -plane). In following step, Liouville's theorem is used, which describes: If  $e^*(\zeta)$  is entire and  $|e^*(\zeta)|$  become bounded considering every values of  $\zeta$  within the complex plane, then  $e^*(\zeta)$  should be a constant. To find the constant's exact value, calculation of the value of either  $e_+^*(\zeta)$  or  $e_-^*(\zeta)$  at one specific value of  $\zeta$  is required. Generally, it may be illustrated that  $e^*(\zeta) = 0(1)$  for  $|\zeta| \rightarrow \infty$ . So, conclusions can be drawn with help of Liouville's theorem that  $e^*(\zeta) \equiv 0$  and as a consequence, the following equation can be obtained using Equation (2.7.16)

$$f_+^* = \frac{n_+^*}{m_+^*}. \quad (2.7.18)$$

The two-sided Laplace transform's inversion integral may then be used to derive the

function  $f(x)$ . The numerous stages that led to the solution of Equation (2.7.1) will be outlined below:

1. The definition range of integral equation is extended to:  $-\infty < x < \infty$ .
2. A two-sided Laplace transform is then applied.
3. Line of juncture is determined.
4. Factorization is then conducted.

$$1 + k^* = m_+^* m_-^*,$$

and rewrite

$$m_+^* f_+^* = \frac{g_+^*}{m_-^*} + \frac{h_-^*}{m_-^*}.$$

5. Split up the term

$$\frac{g_+^*}{m_-^*} = n_+^* + n_-^*,$$

and below relation is achieved:

$$m_+^* f_+^* - n_+^* = \frac{h_-^*}{m_-^*} + n_-^* = \text{entire function.}$$

6. The Liouville's theorem is applied for concluding the entire function C.
7. Observing the nature of  $f(x)$  for small values of  $x$ , calculate  $C$ . Physical factors are often able to predict this behaviour.
8. Inverse transform is evaluated.

The hardest component of the process is often factorization. It may be important to highlight that the 2 half-planes of regularity do not always overlap in the current explanation of the Wiener-Hopf approach. Simply having the two half-planes border along the line  $\mathbf{R}(\zeta) = \gamma$  is sufficient. Also to be observed is the fact that the whole

---

function should not be bounded and might instead be  $O(\zeta^{1/2})$  as  $|\zeta| \rightarrow \infty$ . The function's constant nature may then be deduced using an extension of Liouville's theorem.

One of the most striking features of the mathematical description of natural phenomena by means of a partial differential equation is the comparative ease with which solutions can be obtained for certain geometrical shapes, for example, circles and infinite strips, by the method of separation of variables. But for geometrical shapes outside the scope of the method of separation of variables, it is quite difficult to find solution. This is where the Wiener-Hopf technique comes quite handy and provides a significant extension to the range of problems which can be solved using Fourier, Laplace and Mellin integrals.

*Chapter-3*  
*Interaction of Shear Wave with Cracks*

# Chapter 3

## Interaction of Shear Wave with Cracks

### 3.1 Edge crack subject to anti-plane shear wave in an orthotropic strip

- Introduction

In general, it is familiar that orthotropic materials have intrinsic material properties that differ from each other along three symmetric plane which are mutually orthogonal. These planes intersect to form three mutually perpendicular axes known as principal axes of material symmetry. Because of its high anisotropy nature, orthotropic materials are widely used in a variety of fields such as material science, structural engineering, aerospace engineering, geophysics, etc. To get advanced mechanical performance, orthotropic materials are designed with multidirectional laminates. The high-stiffness, high-strength and lightweight phenomena of orthotropic materials make it extremely desirable in the application of aircraft, automotive, marine, energy, infrastructure, biomedical, and recreational (sports) industries [Daniel et al. (2006), Sun et al. (2022)]. When influenced by anti-plane shear wave propagation, this orthotropic materials, which are made by two or more different laminates, can fail prematurely due to propagation of cracks created at the time of manufacture. Our main aim is to resist the stress initiated by controlling a physical quantity named as stress intensity factor (SIF). Also, length of displacement between two edges of the crack is called crack opening displacement (COD) is a physical quantity leading to fracture toughness of a solid material and vanishes at the crack tip. So,

the study of analysis of these physical quantities related to orthotropic materials in presence of edge crack reveals an emerging area of research in designing engineering structures and machines.

Various crack problems in orthotropic strips [ Nandi and Mandal (2017), Das et al. (2008), X.-F. Li (2005), Monfared and Ayatollahi (2013), Basak and Mandal (2017), Naskar and Mandal (2022)] have been analyzed extensively because of rigorous usage of composite materials in engineering fields. The problem of shear wave propagation in orthotropic media has received much attention in a large number of articles. Using the Fourier series method, X.-F. Li (2003) derived the solution concerning an orthotropic strip of finite width having two mode-III collinear cracks. Lü et al. (2011) addressed the dynamic fracture problems related to asymmetrical mode-III crack inside a solid made of orthotropic media. A finite orthotropic plate has been considered with an edge crack under anti-plane shear by Wang et al. (1992). Y. Wang et al. (1992) calculated stress intensity factors of an edge cracked body by shear force with the aid of integral transform method. Panja and Mandal (2021) calculated stress intensity factors for a griffith crack situated within a strip of infinite length influenced by magnetoelastic shear wave. Guo et al. (2005) examined the fracture behavior caused by an edge crack inside a functionally graded orthotropic strip. Several moving crack problems influenced by shear wave have been investigated in an orthotropic strip by Ayatollahi et al. (2012) and in an infinite strip of functionally graded material (FGM) by Bi et al. (2003). Considering several defects and cracks in functionally graded orthotropic strips, stress intensity factors has been determined by Ayatollahi and Bahgeri (2013) subject to anti-plane time- harmonic concentrated loads and Asadi et al. (2012) due to anti-plane shear deformation.

The problem of a cracked functionally graded orthotropic strip has been addressed by Mausavi and Paavola (2013). Again, Mausavi and Fariborz (2012) analyzed anti-plane stress fields caused by viscous damping in a cracked graded orthotropic layer. The solution was derived by Bayat et al. (2015) for an orthotropic strip reinforced by a piezoelectric coating having several defects. Adopting the distribution dislocation technique, Ayatollahi and Fariborz (2009) deduced stress intensity factors of a strip with cracks and cavities due to time-harmonic anti-plane vibrations. Ing and Ma (2003) investigated stress wave scattering of horizontally polarized shear waves

in anisotropic material with finite cracks. Mostly in the above pieces of literatures, the model was solved by converting into a integral equation of singular type using Laplace and Fourier technique.

In addition, the effective crack problems (including edge crack) with shear wave propagation entailing properties of orthotropic solid composites has been extensively studied. Among these are, scattering phenomena of shear waves within a functionally graded strip having a vertical edge crack by Li et al. (2006); behavior concerning an interfacial edge crack within a semi-infinite strip sandwiched through a functionally graded interlayer due to impact of shear wave by H. J. Choi (2018); influence of the magneto-electro-elastic impact of a strip with multiple and edge cracks based on transient loading by Bagheri and Manfredi (2018); behaviour of edge interfacial cracks situated within dissimilar strips sandwiched by a functionally graded interlayer due to antiplane deformation by H. J. Choi (2020); mode III fatigue crack propagation in an orthotropic piezoelectric ceramic strip by Narita and Shindo (1999); interface stress analysis of nano defects situated in an orthotropic material induced by shear loading by Xiao et al. (2016). Analysis of p-wave through an orthotropic strip was addressed by Basu and Mandal (2016) for two rigid strips, by Nandi et al. (2015) with an edge crack, by Basak and Mandal (2015) for a asymmetric crack. Recently, in our previous literature [Karan et al. (2021)], we studied semi-infinite moving crack in an orthotropic strip under the effect of shear wave propagation.

The technology of orthotropic composites has experienced remarkable development in various fields like structural design, material characterization, and optimization. Evidently, an analysis of stress in orthotropic strips weakened by edge crack owing to shear wave propagation, has not attracted much attention. In the present article, stress analysis is carried out for an edge crack with anti-plane shear wave in an orthotropic strip. Dual integral equations have been developed to solve the governing mixed boundary value problem with aid of Hankel transform technique. Then, the dual integral equations were converted into a second kind integral equation of Fredholm type employing Abel's transformation. The numerical calculations of SIF and COD are performed utilizing the Fox & Goodwin method and displayed graphically. Elastic constants of two orthotropic materials have been used to illustrate the influence of orthotropic non-homogeneity and normalized strip width

upon SIF and COD. This study will be useful to compare the fracture toughness of orthotropic composite materials with edge cracks by arresting crack propagation in several engineering structures.

### • Formulation of the Elasticity Problem

In the present study, an infinitely long orthotropic strip with finite width  $D$  consisting an edge crack with length  $b$  subject to shear wave propagation has been considered. As shown in Fig.3.1, an edge crack of finite length is located at  $0 \leq X \leq b$ ,  $-\infty < Z < \infty$ ,  $Y = 0$  referring to Cartesian axes  $(X, Y, Z)$ . By letting  $\frac{X}{b} = x$ ,  $\frac{Y}{b} = y$ ,  $\frac{D}{b} = d$ , all the lengths have been normalized with reference to  $b$  and then the crack's location becomes  $0 \leq x \leq 1$ ,  $-\infty < z < \infty$ ,  $y = 0$ . The plane of analysis is taken to be the  $x - y$  plane. Let the edge crack is influenced due to time-harmonic shear-wave incident normally along direction of the positive  $y$ -axis.

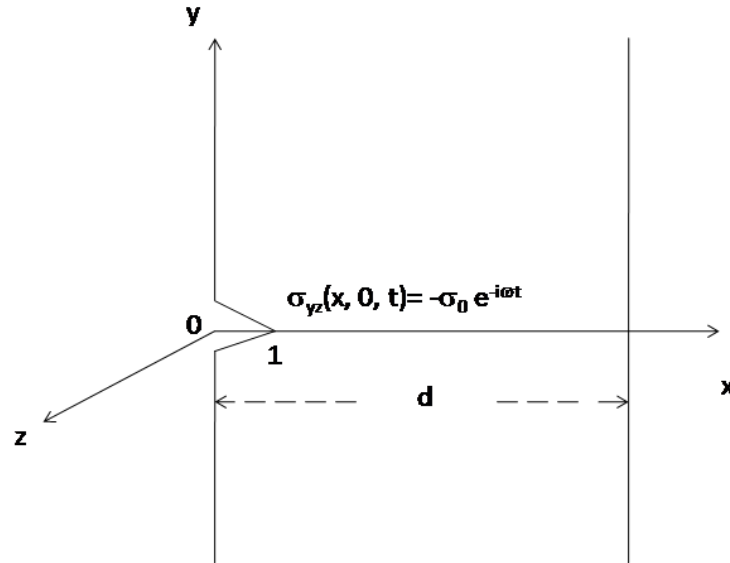


Fig.3.1 Cracked orthotropic strip



Due to the shear wave motion, the displacement components can be considered as  $u_x = 0$ ,  $u_y = 0$ , and  $u_z = u_z(x, y, t)$ . For an orthotropic solid, the anti-plane equation of motion takes a form similar to that below [Mandal and Mandal (2021)]:

$$C_{55} \frac{\partial^2 u_z}{\partial x^2} + C_{44} \frac{\partial^2 u_z}{\partial y^2} = \frac{b^2}{c_s^2} \frac{\partial^2 u_z}{\partial t^2}, \quad (3.1.1)$$

where  $C_{44}, C_{55}$  are orthotropic shear moduli along  $x$  and  $y$  directions respectively, and  $c_s = \sqrt{\frac{C_{55}}{\rho}}$  is SH-wave velocity depending on the orthotropic medium.

By substituting  $u_z(x, y, t) = U_z(x, y)e^{-i\omega t}$ , the Equation (3.1.1) is converted to

$$C_{55} \frac{\partial^2 U_z}{\partial x^2} + C_{44} \frac{\partial^2 U_z}{\partial y^2} + \frac{b^2 \omega^2}{c_s^2} U_z = 0. \quad (3.1.2)$$

The nonzero component of the stress tensor can be expressed as follows:

$$\begin{aligned} \sigma_{xz}(x, y) &= C_{55} \frac{\partial U_z(x, y)}{\partial x}, \\ \sigma_{yz}(x, y) &= C_{44} \frac{\partial U_z(x, y)}{\partial y}. \end{aligned}$$

Application of the standard Hankel integral transform, Equation (3.1.2) admits solution as

$$\begin{aligned} U_z(x, y) &= \int_{-\infty}^{\infty} D_1(\zeta) e^{-\phi y} e^{i\zeta x} d\zeta + \\ &\int_0^{\infty} \left[ D_2(\lambda) e^{\psi x} + D_3(\lambda) e^{-\psi x} \right] \sin(\lambda y) d\lambda, \end{aligned} \quad (3.1.3)$$

with

$$\begin{aligned} \phi &= \sqrt{Q(\zeta^2 - k_s^2)}, & \zeta > k_s \\ &= -i\sqrt{Q(k_s^2 - \zeta^2)}, & \zeta < k_s \end{aligned}$$

and

$$\begin{aligned} \psi &= \sqrt{\frac{1}{Q}(\lambda^2 - k_s^2)}, & \lambda > k_s \\ &= -i\sqrt{\frac{1}{Q}(k_s^2 - \lambda^2)}, & \lambda < k_s \end{aligned}$$

and  $Q = \frac{C_{55}}{C_{44}}$ ,  $k_s^2 = \frac{b^2\omega^2}{c_s^2 C_{55}}$ . In Equation (3.1.3),  $D_1(\zeta)$ ,  $D_2(\lambda)$  and  $D_3(\lambda)$  appears as unknown functions to be evaluated utilizing boundary conditions.

When  $y = 0$ , the boundary conditions can be prescribed as

$$\sigma_{yz}(x, 0) = -\sigma_0, \quad 0 \leq x \leq 1, \quad (3.1.4)$$

$$U_z(x, 0) = 0, \quad 1 \leq x \leq d. \quad (3.1.5)$$

The two edges of the infinite strip appears as liberated out of traction. Therefore, at the edges  $x = 0$  and  $x = d$ , we have the following boundary conditons

$$\sigma_{xz}(0, y) = 0, \quad |y| < \infty, \quad (3.1.6)$$

$$\sigma_{xz}(d, y) = 0, \quad |y| < \infty. \quad (3.1.7)$$

The expressions for stresses  $\tau_{\theta z}$  now becomes

$$\begin{aligned} \sigma_{yz}(x, y) = & -C_{44} \int_{-\infty}^{\infty} \phi D_1(\zeta) e^{-\phi y} e^{i\zeta x} d\zeta + \\ & C_{44} \int_0^{\infty} \lambda \left[ D_2(\lambda) e^{\psi x} + D_3(\lambda) e^{-\psi x} \right] \cos(\lambda y) d\lambda, \end{aligned} \quad (3.1.8)$$

$$\begin{aligned} \sigma_{xz}(x, y) = & iC_{44} \int_{-\infty}^{\infty} \zeta D_1(\zeta) e^{-\phi y} e^{i\zeta x} d\zeta + \\ & C_{44} \int_0^{\infty} \psi \left[ D_2(\lambda) e^{\psi x} - D_3(\lambda) e^{-\psi x} \right] \sin(\lambda y) d\lambda. \end{aligned} \quad (3.1.9)$$

## • Derivation of Integral Equation

The following dual integral equations has been obtained utilizing boundary conditions (3.1.4) and (3.1.5) as

$$\int_{-\infty}^{\infty} \phi D_1(\zeta) e^{i\zeta x} d\zeta = \frac{\sigma_0}{C_{44}} + \int_0^{\infty} \lambda \left[ D_2(\lambda) e^{\psi x} + D_3(\lambda) e^{-\psi x} \right] d\lambda, \quad 0 \leq x \leq 1, \quad (3.1.10)$$

and

$$\int_{-\infty}^{\infty} D_1(\zeta) e^{i\zeta x} d\zeta = 0, \quad 1 \leq x \leq d. \quad (3.1.11)$$

Boundary conditions (3.1.6) and (3.1.7) with the help of inverse Fourier sine and cosine transform leads to the unknown functions  $D_2(\lambda)$  and  $D_3(\lambda)$  in terms of  $D_1(\zeta)$  as following

$$D_2(\lambda) = \frac{2i\lambda}{\pi\psi(e^{2d\psi} - 1)} \left( \int_{-\infty}^{\infty} \frac{\zeta D_1(\zeta)}{\phi^2 + \lambda^2} d\zeta - e^{d\psi} \int_{-\infty}^{\infty} \frac{\zeta D_1(\zeta) e^{id\zeta}}{\phi^2 + \lambda^2} d\zeta \right), \quad (3.1.12)$$

$$D_3(\lambda) = \frac{2i\lambda}{\pi\psi(1 - e^{-2d\psi})} \left( \int_{-\infty}^{\infty} \frac{\zeta D_1(\zeta)}{\phi^2 + \lambda^2} d\zeta - e^{-d\psi} \int_{-\infty}^{\infty} \frac{\zeta D_1(\zeta) e^{id\zeta}}{\phi^2 + \lambda^2} d\zeta \right). \quad (3.1.13)$$

Utilizing Equations (3.1.12) and (3.1.13) into Equation (3.1.10), dual integral equations concerning the unknown function  $D_1(\zeta)$  can be derived as follows

$$\int_0^{\infty} \zeta (1 + G(\zeta)) D_1(\zeta) \cos(\zeta x) d\zeta = R(x), \quad 0 \leq x \leq 1, \quad (3.1.14)$$

$$\int_0^{\infty} D_1(\zeta) \cos(\zeta x) d\zeta = 0, \quad 1 \leq x \leq d, \quad (3.1.15)$$

where

$$G(\zeta) = \left( \frac{\phi}{\sqrt{Q}\zeta} - 1 \right), \quad (3.1.16)$$

with

$$R(x) = \frac{\sigma_0}{C_{44}\sqrt{Q}} + \frac{1}{\sqrt{Q}} \int_0^{\infty} \lambda [D_2(\lambda) e^{\psi x} + D_3(\lambda) e^{-\psi x}] d\lambda, \quad 0 \leq x \leq 1. \quad (3.1.17)$$

To convert above system of Equation (3.1.14) and Equation (3.1.15) to a second kind Fredholm integral equation,  $D_1(\zeta)$  is taken as

$$D_1(\zeta) = \frac{\sigma_0}{2C_{44}\sqrt{Q}} \int_0^1 \eta p(\eta) J_0(\zeta\eta) d\eta, \quad (3.1.18)$$

that satisfy Equation (3.1.15) and  $p(\eta)$  is an unknown function to be evaluated.

The Equation (3.1.14) with aid of expression (3.1.18) yields a second kind Fredholm integral equation as

$$p(\eta) + \int_0^1 \mu p(\mu) M_1(\mu, \eta) d\mu = \frac{2C_{44}}{\pi\sigma_0} \int_0^t \frac{R(x)}{\sqrt{\eta^2 - x^2}} dx, \quad (3.1.19)$$

where

$$M_1(\mu, \eta) = \int_0^\infty \zeta G(\zeta) J_0(\zeta\mu) J_0(\zeta\eta) d\zeta. \quad (3.1.20)$$

Putting the expression of  $D_1(\zeta)$  from Equation (3.1.18) into (3.1.17), we get

$$\int_0^t \frac{R(x)}{\sqrt{\eta^2 - x^2}} dx = \frac{\pi\sigma_0}{2C_{44}\sqrt{Q}} \left[ 1 + \int_0^1 \mu p(\mu) \left( M_2(\mu, \eta) + M_3(\mu, \eta) \right) d\mu \right] d\mu, \quad (3.1.21)$$

with

$$M_2(\mu, \eta) = \int_0^\infty \frac{\zeta^2 I_0(\psi\mu)}{\psi(e^{2d\psi} - 1)} \left( I_0(\psi\eta) + L_0(\psi\eta) \right) d\lambda, \quad (3.1.22)$$

and

$$M_3(\mu, \eta) = \int_0^\infty \frac{\zeta^2 I_0(\psi\mu) e^{-2d\psi}}{\psi(1 - e^{-2d\psi})} \left( I_0(\psi\eta) - L_0(\psi\eta) \right) d\lambda, \quad (3.1.23)$$

where  $I_0()$  represents modified Bessel function with an imaginary argument with zero order and  $L_0()$  represents modified Struve function with zero order. Employing Abel's transformation in Equation (3.1.19) and Equation (3.1.21), we obtained the following second kind integral equation of Fredholm type

$$p(\eta) + \int_0^1 \mu p(\mu) M(\mu, \eta) d\mu = 1, \quad (3.1.24)$$

where the kernel  $M(\mu, \eta) = M_1(\mu, \eta) - M_2(\mu, \eta) - M_3(\mu, \eta)$ .

Applying the process of contour integration technique, the integral  $M_1(\mu, \eta)$  in (3.1.20) can be transformed into integral with finite limit as

$$M_1(\mu, \eta) = -ik_s^2 \int_0^1 \sqrt{1 - \gamma^2} J_0(k_s\gamma\mu) H_0^{(1)}(k_s\gamma\eta) d\gamma, \quad (3.1.25)$$

$$\begin{aligned} M_2(\mu, \eta) + M_3(\mu, \eta) = & - \int_0^{k_s} \frac{\lambda^2 J_0(\psi'\mu) J_0(\psi'\eta) e^{i\psi'd}}{\psi' \sin(\psi'd)} d\lambda \\ & + \int_{k_s}^\infty \frac{\lambda^2 I_0(\psi\mu) I_0(\psi\eta) e^{-\psi d}}{\psi \sinh(\psi d)} d\lambda, \end{aligned} \quad (3.1.26)$$

where  $\psi' = \sqrt{\frac{1}{Q}(k_s^2 - \lambda^2)}$ .

Letting  $\lambda^2 = k_s^2(1 - \delta^2)$  and  $\lambda^2 = k_s^2(1 + \delta^2)$  in the integrals  $\int_0^{k_s}$  and  $\int_{k_s}^\infty$  respectively, we obtain

$$\begin{aligned} M_2(\mu, \eta) + M_3(\mu, \eta) = & -\sqrt{Q}k_s^2 \int_0^1 \frac{\sqrt{1 - \delta^2} J_0\left(\frac{k_s \delta \mu}{\sqrt{Q}}\right) J_0\left(\frac{k_s \delta \eta}{\sqrt{Q}}\right) e^{i\frac{k_s \delta d}{\sqrt{Q}}}}{\sin\left(\frac{k_s \delta d}{\sqrt{Q}}\right)} d\delta \\ & + \sqrt{Q}k_s^2 \int_0^\infty \frac{\sqrt{1 + \delta^2} I_0\left(\frac{k_s \delta \mu}{\sqrt{Q}}\right) I_0\left(\frac{k_s \delta \eta}{\sqrt{Q}}\right) e^{-\frac{k_s \delta d}{\sqrt{Q}}}}{\sinh\left(\frac{k_s \delta d}{\sqrt{Q}}\right)} d\delta. \end{aligned} \quad (3.1.27)$$

### • Quantities of Physical Interest

With aid of Equations (3.1.8), (3.1.12), and (3.1.13), the expression of shear stress  $\sigma_{yz}(x, 0)$  near rim of the crack may be expressed as

$$\sigma_{yz}(x, 0) = \frac{\sigma_0 x}{\sqrt{x^2 - 1}} p(1) + O(1), \quad x > 1. \quad (3.1.28)$$

Stress intensity factor (SIF) is a quantity of physical interest representing state of stress originated in a cracked structure. Denoting dimensionless SIFs as  $K_{III}$ , we define it as

$$K_{III} = \lim_{x \rightarrow 1^+} \left| \frac{\sqrt{x - 1} \sigma_{yz}(x, 0)}{\sigma_0} \right|. \quad (3.1.29)$$

Finally, using Equation (3.1.26), SIF can be written as

$$K_{III} = \frac{|p(1)|}{\sqrt{2}}. \quad (3.1.30)$$

The jump of the displacement  $L(x)$ , called crack opening displacement(COD) in the plane of the edge crack can be derived from

$$L(x) = U_z(x, 0^+) - U_z(x, 0^-). \quad (3.1.31)$$

Substitution of Equation (3.1.3) into the relation (3.1.26) leads to

$$L(x) = 2 \int_0^\infty D_1(\zeta) e^{i\zeta x} d\zeta, \quad x > 1, \quad (3.1.32)$$

which with the help of expression (3.1.18) can be written as

$$L(x) = \frac{2\sigma_0}{C_{44}} \left| \int_x^1 \frac{\eta p(\eta)}{\sqrt{\eta^2 - x^2}} d\eta \right|. \quad (3.1.33)$$

The value of crack opening displacement can be assumed for the static case as

$$L_0 = \frac{2\sigma_0}{C_{44}}.$$

Finally, we obtained normalized COD with reference to the static crack opening displacement  $L_0$  as

$$L = \frac{L(x)}{L_0} = \left| \sqrt{(1-x^2)}p(1) - \int_x^1 \sqrt{\eta^2 - x^2} p'(\eta) d\eta \right|, \quad x < 1. \quad (3.1.34)$$

### • Numerical and Graphical Demonstration

To explain the theoretical results graphically, numerical values concerning stress intensity factor (SIF) near the crack rim and normalized crack opening displacement (COD) are calculated from Equations (3.1.30) and (3.1.34) respectively.

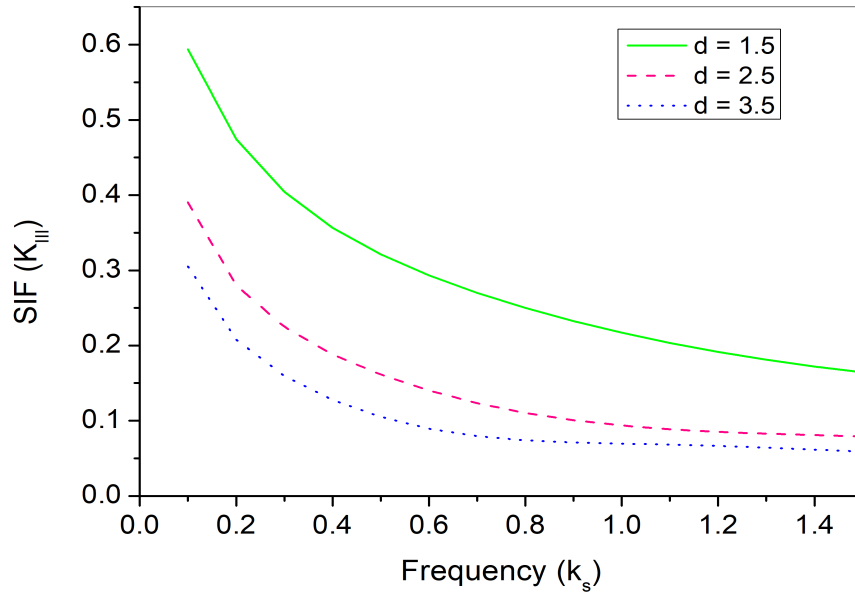


**Fig.3.2** Variation of SIF with frequency  $k_s$  for Type-I medium

Numerical computations are performed with the help of the Fox & Goodwin (1953) method and Gauss quadrature rule by use of the MATLAB software. We considered elastic constants for two sets of medium as listed in Table 3.1 [Lü et al. (2001), Mandal and Mandal (2021)].

**Table 3.1. Elastic constants of orthotropic medium**

Elastic medium	$C_{44}(GPA \ unit)$	$C_{55}(GPA \ unit)$
Type-I	5.40	5.50
Type-II	5	10.0

Here, numerical values of normalized SIF ( $K_{III}$ ) against dimensionless frequency  $k_s$  have been portrayed through graphs as shown in Figs.3.2 – 3.3. To inspect the influence of normalized strip width  $d = \frac{D}{b}$  and the anisotropy nature of orthotropic medium on SIF, three distinct strip width, namely ( $d = 1.5, 2.5, 3.5$ ) have been considered.

From Figs.3.2 – 3.3, it might be noticed that the peak value of SIF at the crack tip for Type-I medium (Fig.3.2) is higher than that for Type-II medium (Fig.3.3) with the same frequency  $k_s$ . For all values of the dimensionless frequency  $k_s$ , it seems that with the decrease of strip width ( $d$ ), the peak value of SIF will increase gradually. In addition, based on Figs.3.2 – 3.3 we may conclude that the curve of SIF attains a peak value first and then diminishes gradually as an increase in the magnitude of frequency. So, the peak value of SIF may be raised or reduced by differing the strip width and orthotropic medium.

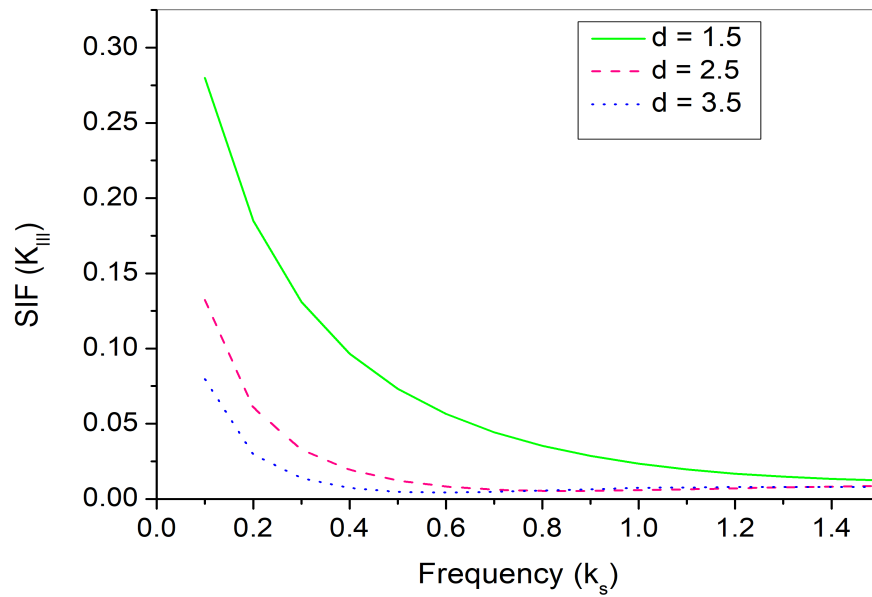


Fig.3.3 Variation of SIF with frequency  $k_s$  for Type-II medium

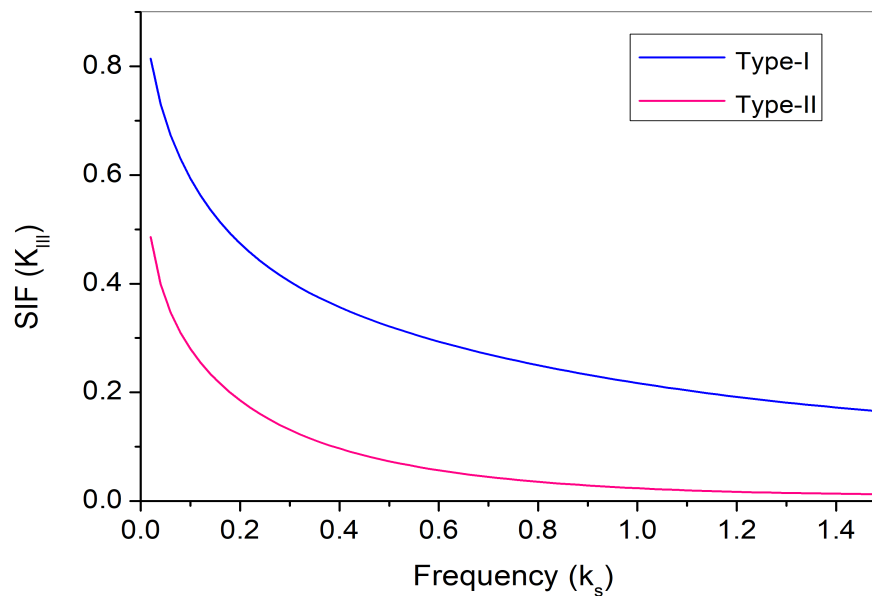


Fig.3.4 Variation of SIF with frequency  $k_s$  with strip width  $d = 1.5$

In Fig.3.4, SIF values have been plotted for two different orthotropic mediums (Type-I, Type-II) against frequency  $k_s$  with fixed strip width  $d = 1.5$  to observe



the effect of orthotropic nature on SIF. It is observed that SIF is higher for Type-I medium than for Type-II medium with the same strip width. So, conclusion can be drawn as the Type-I medium seems elastically stronger compared with the Type-II medium.

Generally, it is observed that crack begins to propagate within engineering solids when the SIF values exceed a certain limit (depending on medium orthotropy) termed critical SIF. In structural engineering, the main aim is to resist the onset of crack within a composite medium to avoid damage to solid bodies by controlling SIF within a specific range that is critical SIF. Considering this fact, we may conclude that SIF values might be controlled by monitoring the width of the strip ( $d$ ) and geometric parameters of the orthotropic medium, which is rightly envisioned in fracture analysis.

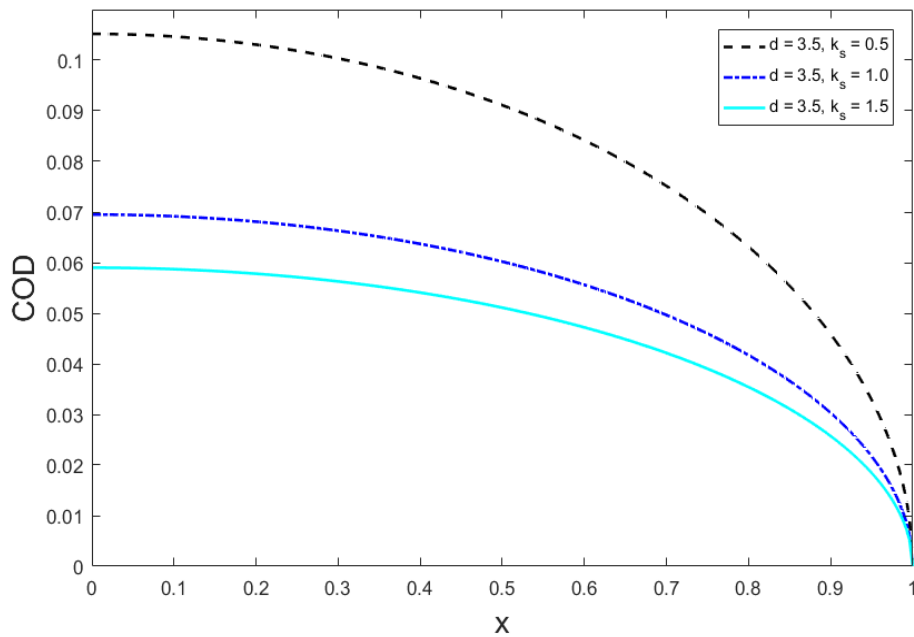


**Fig.3.5** COD versus distance  $x$  for Type-I medium (fixed normalized strip width  $d = 3.5$ ).

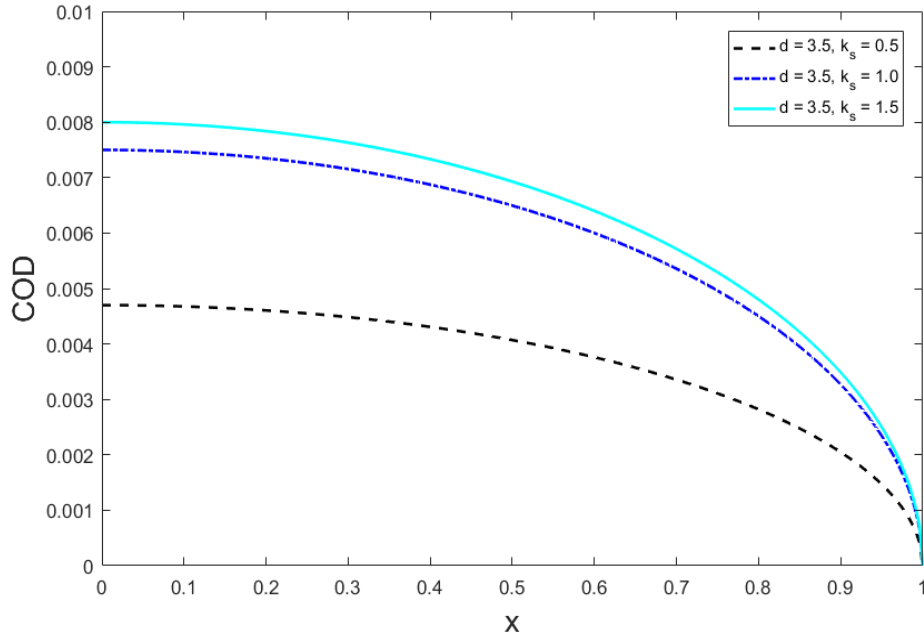


**Fig.3.6 COD versus distance  $x$  for Type-II medium (fixed normalized strip width  $d = 3.5$ ).**

From all configurations of COD (Figs.3.5-3.10), it is noticed that COD values diminish when we move forward along the crack rim across the direction of the  $x$ -axis and ultimately approach near zero at the tip of the crack ( $x = 1$ ). Figs.(3.5–3.6) describes the effect of frequency  $k_s$  (taking  $k_s = 0.5, 1.0, 1.5$ ) with constant normalized strip width  $d = 3.5$  in the case of Type-I and Type-II medium, respectively. The fact can be revealed as the rise of frequency  $k_s$  leads to a decrease in COD gradually for Type-I medium (Fig.3.5) and an increase in COD gradually for Type-II medium (Fig.3.6).

Furthermore, the effect of COD on different normalized strip width  $d = 1.5, 2.5, 3.5$  keeping frequency  $k_s = 1.5$  constant has been plotted through Figs.3.7 – 3.8 taking both (Type-I and Type-II) medium, respectively. The conclusion can be drawn as COD is higher for a lower value of strip width when the frequency is retained constant for both materials.

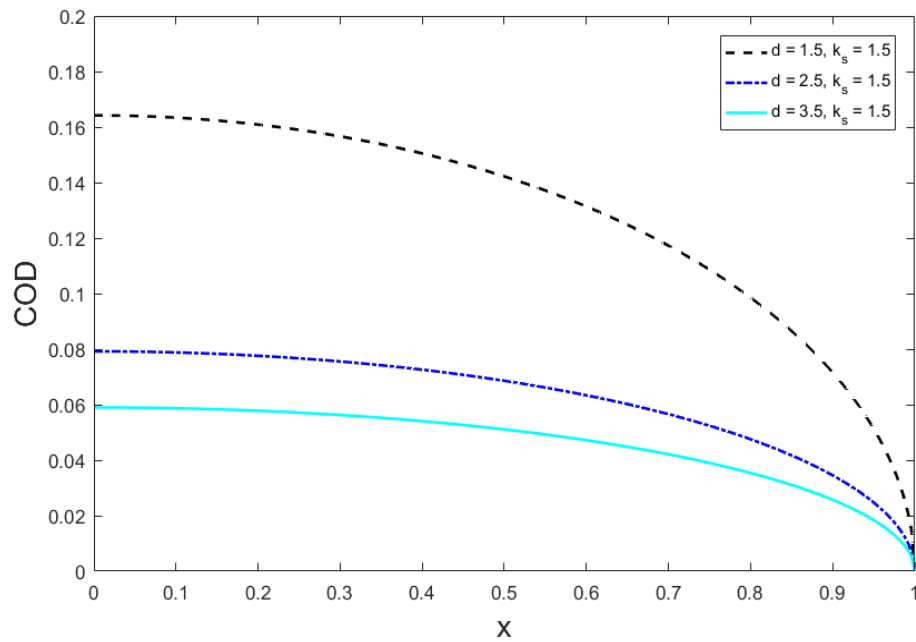


Fig.3.7 COD versus distance  $x$  for Type-I medium (fixed frequency  $k_s = 1.5$ ).

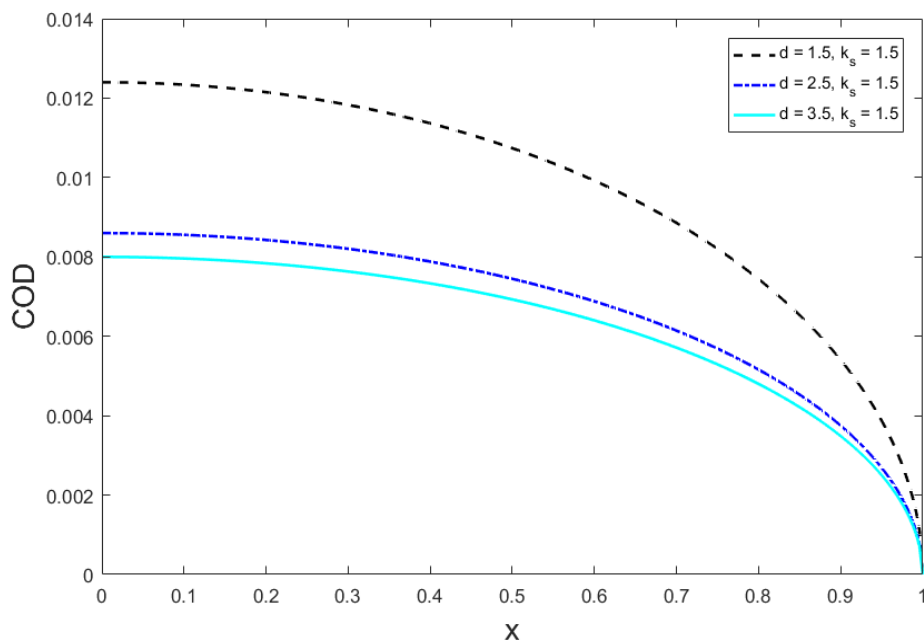
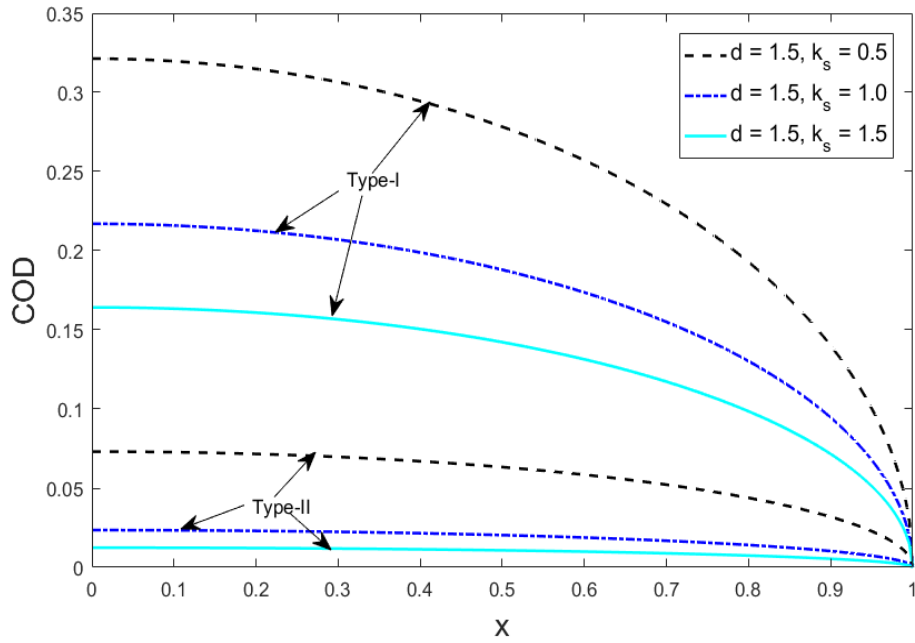
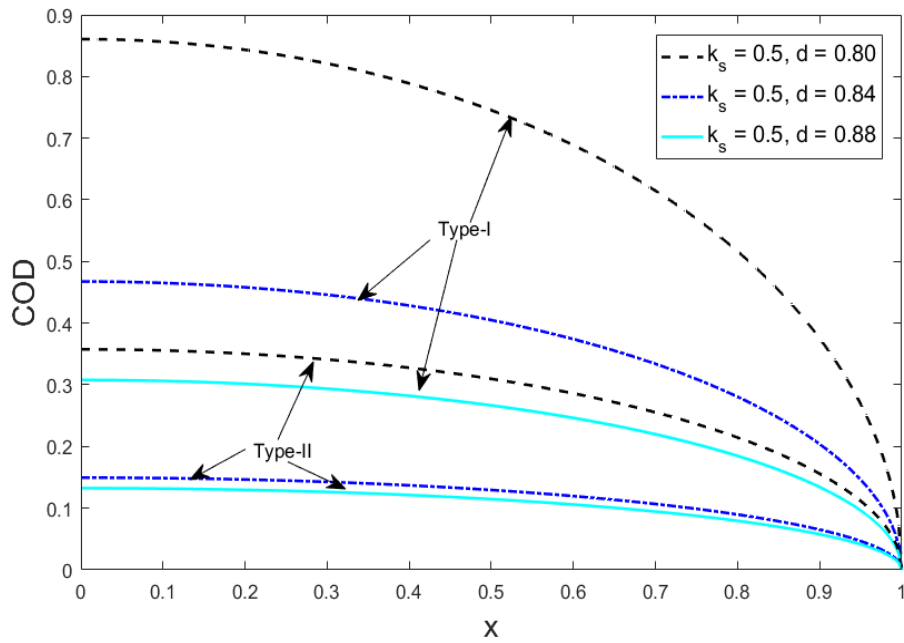


Fig.3.8 COD versus distance  $x$  for Type-II medium (fixed frequency  $k_s = 1.5$ ).



**Fig.3.9** COD versus distance  $x$  for different values frequency of  $k_s$  with strip width  $d = 1.5$ .



**Fig.3.10** COD versus distance  $x$  for different values of strip width  $d$  with frequency  $k_s = 0.5$ .

In addition, Figs.3.9 and 3.10 have been plotted to compare the influence of material constants of orthotropic mediums on COD taking various combinations of strip width  $d$  and dimensionless frequency  $k_s$ . Here, COD is decreasing with distance  $x$  like previous Figs. of COD. Fig.3.9 describes nature of COD taking two different orthotropic medium (Type-I and Type-II) for three values of dimensionless frequency  $k_s = 0.5, 1.0, 1.5$  with fixed strip width  $d = 1.5$ . We can conclude that COD values are higher for Type-I medium than for Type-II medium when strip width  $d$  remains the same.

Next, Fig.3.10 describes nature of COD taking both orthotropic medium (Type-I and Type-II) for three distinct strip width  $d = 0.80, 0.84, 0.88$  with fixed dimensionless frequency  $k_s = 0.5$ . It can conclude from Fig.3.10 that COD values are higher for Type-I medium than for Type-II medium when frequency  $k_s$  is kept constant. So, the values of COD are changing considerably for different orthotropic mediums. Therefore, elastic constants of orthotropic mediums have admit a remarkable influence upon the values of COD.

## • Conclusion

Stress analysis of a crack on the edge of an orthotropic strip with finite width subject to anti-plane shear wave propagation has been executed in this formulation. Abel's transform technique is utilized to solve the mixed boundary value problem by converting it into dual integral equations and then second kind integral equation of Fredholm type. To illustrate the influence of material orthotropy, several graphs have been presented for SIF and COD with varying different geometric parameters.

It was observed that the strip width and geometric parameter have a revealing effect on SIF and COD. So, SIF and COD may be kept in control surveiling these geometric parameters so that crack propagation can be arrested to avoid damage to solids. This theoretical analysis is formulated to address characterization, structural design analysis, and optimization of composite materials with pre-existing cracks.

## 3.2 Interaction of shear waves with semi-infinite moving crack inside of a orthotropic media

- **Introduction**

Orthotropic material being a composite material have unique mechanical properties since they have three orthogonal planes of symmetry. Some of this material like Prepreg, Carbon fiber, Epoxy has found in high-performance structural applications such as designing of aircraft, aerospace, corrosion- resistance equipment, marine, load-bearing components for vehicles, metal and polymer-forming process [A.K. Kaw (2006), Vasiliev and Morozov (2018)]. Their rigorous anisotropic properties in addition to the presence of moving cracks have a strong application in Seismology. Area inside the Earth and the geological structure adjacent to surface are considered as a composite material formed by rocks, crystalline minerals, etc. which is highly anisotropic. When an earthquake arises, waves travel across different anisotropic parts of the earth. Crack started to propagate in different modes (II, III, or in a mixture of mode of II and III) due to sliding motion as a consequence of Earthquake [B. K. Broberg (1999)]. Semi-infinite moving crack is acknowledged as a well-known failure model within orthotropic composites. So, it intrigued significant interest to develop methods for describing the behavior of orthotropic bodies with semi-infinite moving cracks under the influence of shear wave. Hence, this model may be adopted in several field like construction, seismic, geology, and earthquake disaster prevention as well [Mandal and Mandal (2022), Gupta and Bhengra (2017)]. Investigation of composites with semi-infinite moving cracks under shear wave incidence are very little due to its abundance of parameters which may effect phenomena of propagation of crack. So, in order to ensure safe and robust structures, it has become crucial to analyze the failure of composites caused by propagation of crack.

The study of moving semi-infinite crack model based on Weiner-Hopf technique has been described first by E. H. Yofee (1951). The solution of semi-infinite crack problem located inside an infinitely isotropic strip with finite width considering

displaced and clamped boundary perpendicular to the crack was given by W. H. Knauss (1966) where Weiner-Hopf technique was employed to find stress intensity factor. Later, that work has been modified by J. R. Rice (1967). A method was proposed by F. Nilsson (1972, 1973) using the Weiner-Hopf technique to solve a semi-infinite crack propagating inside an isotropic strip. After that, this same method was used by Atkinson and Popelar (1979), H. G. Georgiadis (1986), Kousionelos and Williams (1982) in their respective solutions.

Although traveling cracks in elastic material under longitudinal wave was introduced first by McClintock and Sukhatme (1960), later in many engineering smart structures such as the couple stress elastic materials, orthotropic thin plate, elastic plate carrying an electric current, semi-infinite cracks appeared [Thomson and Abrahams (2007), Abraham and Lawrie (2012), Morini et al. (2014)]. An interfaced crack (mode-III) located between two distinct layers of equal thickness has been studied by X. F. Li (2001). Wang et al. (2001) discussed the process to find dynamic SIF of a crack (semi-infinite) in orthotropic solid under the impact of concentrated shear load. Using Laplace and Fourier transformation method, he problem was reduced to the solution and finally, the Weiner-Hopf technique has been employed to find SIF. De and Patra (1990), Das and Ghosh (1992), Ma et al. (2005) studied the dynamic griffith crack behavior in isotropic and orthotropic elastic materials.

Wu et al. (2002) introduced the analytical expression for complex SIF and release rate of energy concerning a semi-infinite interfacial crack sandwiched by two distinct elastic strips using conformal mapping technique. Sarkar et al. (1991) analyzed scattering of the anti-plane shear wave upon a crack (semi-infinite) moving uniformly across the interface between two distinct semi-infinite medium. Solving the boundary value problem with the help of Fourier transform and Weiner-Hopf technique, they found that SIF is influenced by the motion of the crack expansion, the incidence angle formed by the incoming wave, and properties of elastic material. An effective approach for finding fields of stress and displacement along interface between two dissimilar orthotropic mediums containing a crack moving under a dynamic loads (mode I, mode II) has been investigated by K. H. Lee (2000). Analysis of four coplanar moving Griffith cracks subject to anti-plane stress inside an infinite strip has been treated by Sarkar et al. (1996). A moving semi-infinite crack (mode III) located between two sandwiched layers that are orthotropic has been

solved analytically by Singh et al. (2008). Hongmin et al. (2008) considered the investigation of semi-infinite crack within an infinite orthotropic functionally graded medium. They solved the problem involving two impact loads (opening mode, in-plane shear mode). Basak et al. (2017). addressed the problem of semi-infinite crack moving, considering a orthotropic strip with boundaries displaced normally. Here, applying Fourier transformation method the boundary value problem was reduced to the well-known Weiner-Hopf equation to be solved in asymptotic behaviour to obtain the physical quantities like stress intensity factor and crack opening displacement. Fracture analysis regarding a semi-infinite crack located between two distinct orthotropic composite materials was treated by Junlin and Shaoqin (2010) using the composite complex function method. Different moving cracks in a piezoelectric strip and layers have been analyzed by Bagheri et al. (2016) and Nourazar and Ayatollahi (2016). Propagation of anti-plane moving griffith crack was solved by Hu and Li (2005) and Jin et al. (2003).

In most of the above studies, the problems were assumed on anisotropic and isotropic media by different ( finite or semi-infinite ) moving crack. Very recently, P. Mandal (2022) studied the problem of semi-infinite crack (mode-III) moving inside the semi-infinite isotropic medium considering an isotropic case. To date, however, fracture analysis for the case of semi-infinite moving crack inside semi-infinite orthotropic media has not received much attention. Therefore, in the current investigation, the emphasis is on finding the theoretical and analytical nature of a moving semi-infinite crack at a finite depth from the surface of a orthotropic medium influenced by shear load applied on the surface. Fourier transformation method is applied to convert the mixed boundary value type problem for obtaining solution to the well-known Weiner-Hopf equation. Further, the expressions for SIF and COD by solving the Weiner-Hopf equation have been derived asymptotically. The results show that the corresponding SIF and COD are influenced by crack propagation velocity, layer width, and material constants. The discussion about these quantities of physical interest (SIF, COD) ensures the arrest of crack propagation by monitoring geometric parameters of the orthotropic material. Our prime objective is to reduce damages in buildings fracture, geophysical interpretation of seismic waves by controlling the onset of crack growth within a structure.



• Formulation of the Problem

We consider a horizontal semi-infinite moving crack with crack tip coincides with the origin of the moving coordinates. Let  $(X, Y, Z)$  be the fixed cartesian co-ordinates which are the axes of symmetry of the orthotropic material. Then the crack position is  $-\infty < X < 0, Y = 0$ . We assume that the crack is propagating with a constant velocity  $V$  along the positive  $X$ -axis parallel to the surface of the semi-infinite orthotropic medium at a depth ‘ $d$ ’ from the surface. So, at any time  $t$ , the position of the crack is  $-\infty < X < Vt, Y = 0$  (Fig.3.11).

Since the crack motion is maintained under anti-plane shear mode, the displacement vector takes the form  $(0, 0, U_Z)$ . Here,  $U_Z$  is the only nonvanishing out-of-plane component of displacement in the  $Z$ -direction presented as

$$U_Z = U_Z(X, Y, t)$$

from which relation between nonzero shear stress and displacement component for orthotropic materials (mode-III) are as follows

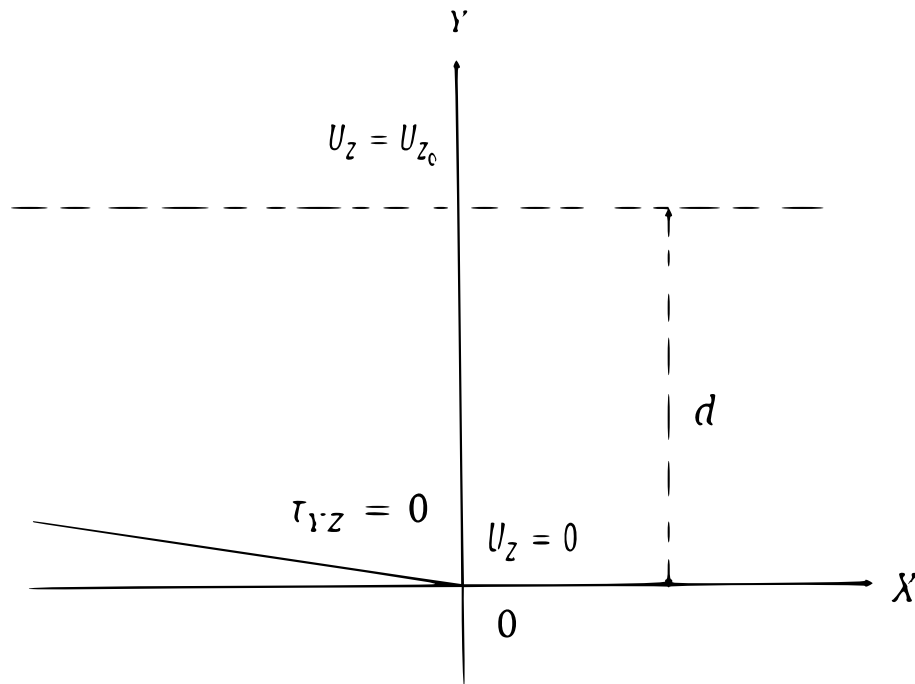


Fig.3.11 Semi-infinite crack moving inside of a semi-infinite orthotropic media

$$\begin{aligned}\tau_{XZ} &= C_{55} \frac{\partial U_Z}{\partial X}, \\ \tau_{YZ} &= C_{44} \frac{\partial U_Z}{\partial Y},\end{aligned}\tag{3.2.1}$$

where  $C_{44}$  and  $C_{55}$  represent the principal shear moduli directed along  $X$  and  $Y$  –axes of the orthotropic material respectively. The anti-plane equation of motion requires the gratification of the following wave equation for orthotropic medium [G. C. Sih (1981)],

$$C_{55} \frac{\partial^2 U_Z}{\partial X^2} + C_{44} \frac{\partial^2 U_Z}{\partial Y^2} = \rho \frac{\partial^2 U_Z}{\partial t^2}\tag{3.2.2}$$

where,  $\rho$  is the material density. It is convenient to define the constant

$$\beta = \sqrt{\frac{C_{44}}{C_{55}}}$$

while the SH-wave velocity of orthotropic material designated by  $C_S$ , is

$$C_S = \sqrt{\frac{C_{55}}{\rho}}$$

so that Equation (3.2.2) can be cast into the form

$$\frac{\partial^2 U_Z}{\partial X^2} + \beta^2 \frac{\partial^2 U_Z}{\partial Y^2} = \frac{1}{C_S^2} \frac{\partial^2 U_Z}{\partial t^2}\tag{3.2.3}$$

To make the crack stationary, a moving framework  $x = X - Vt$ ,  $y = Y$  (Galilean transformation) has been introduced which reduces the number of independent variables to the same as for static deformations. Therefore the displacement Equation (3.2.3) in the moving coordinate system  $(x, y, z)$  become

$$G^2 \frac{\partial^2 u_z}{\partial x^2} + \frac{\partial^2 u_z}{\partial y^2} = 0\tag{3.2.4}$$

where  $G^2 = \frac{1}{\beta^2} (1 - \frac{V^2}{C_S^2})$ ,  $V$  is the crack velocity, and  $u_z(x, y) = U_Z(X, Y, t)$  is the displacement along the moving coordinate  $z$ .

We may also transform the moving coordinates simply by replacing  $X$  and  $Y$  in Equation (3.2.1) by  $x$  and  $y$ , respectively and  $U_Z$  by  $u_z$ . The mixed boundary conditions on and outside the crack for  $y = 0$  are given by

$$\tau_{yz}(x, 0) = 0, \quad x < 0 \quad (3.2.5)$$

$$u_z(x, 0) = 0, \quad x > 0 \quad (3.2.6)$$

Stress and displacement across the surface  $y = d$  are

$$\tau_{yz}(x, d) = 0, \quad -\infty < x < \infty \quad (3.2.7)$$

$$u_z(x, d) = u_{z_0}, \quad -\infty < x < \infty \quad (3.2.8)$$

where  $u_{z_0}$  is constant displacement applied at the surface boundary  $y = d$ . For applying the Weiner-Hopf technique, we consider a different set of boundary conditions by superimposing a constant load  $p_0$  in the original system which does not affect the value of SIF obtained by solving the modified problem. The new boundary conditions are (Fig.3.12)

$$\tau_{yz}(x, 0) = p_0, \quad x < 0 \quad (3.2.9)$$

$$u_z(x, 0) = 0, \quad x > 0 \quad (3.2.10)$$

$$\tau_{yz}(x, d) = 0, \quad -\infty < x < \infty \quad (3.2.11)$$

$$u_z(x, d) = 0, \quad -\infty < x < \infty \quad (3.2.12)$$

The above two problems are identical for a particular value of  $p_0$ . For generalized

plane stress problems, the appropriate value of  $p_0$  is given by  $(-\frac{C_{44}u_{z0}}{d})$ . The complete procedure to find the value of  $p_0$  has been elaborated in the work of Georgiadis and Papadopoulos (1988).

To proceed for the solution, we introduce the standard definition of complex Fourier transform pair as

$$\bar{g}(\xi, y) = \frac{1}{\sqrt{2\pi}} \int_{-\infty}^{\infty} g(x, y) e^{i\xi x} dx \quad (3.2.13)$$

and

$$g(x, y) = \frac{1}{\sqrt{2\pi}} \int_{-\infty}^{\infty} \bar{g}(\xi, y) e^{-i\xi x} d\xi \quad (3.2.14)$$

where  $\xi = \eta + i\gamma$ , is to be understood as a complex variable in the Fourier transform plane,  $\eta$  and  $\gamma$  being the real and imaginary parts of the complex variable  $\xi$ .

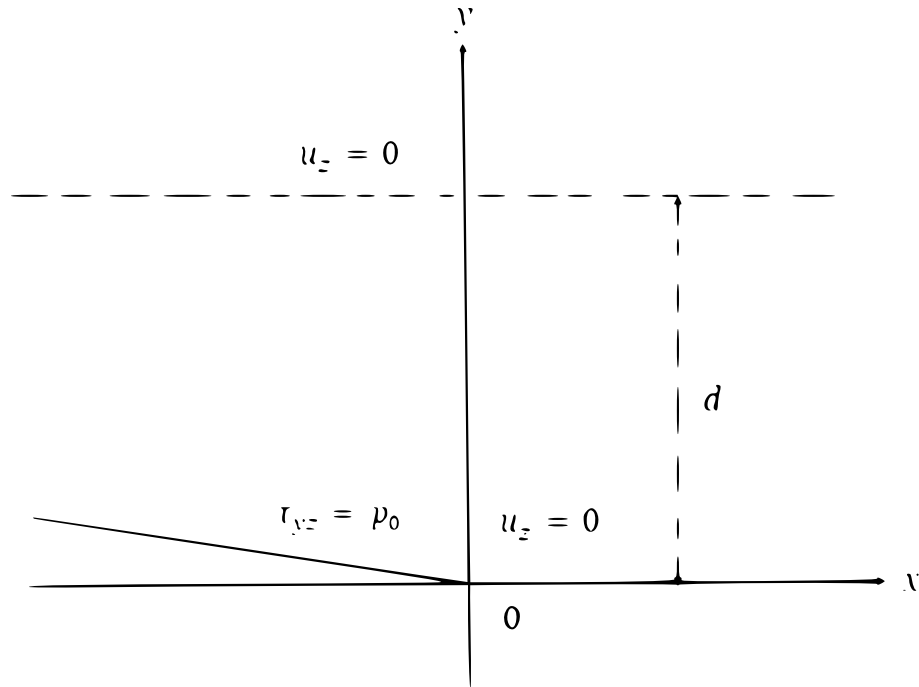


**Fig.3.12** Transformed geometry of the semi-infinite crack

According to Nilsson (1973), the boundary condition (3.2.9) in lieu of constant load  $p_0$  can be written with a slight modification as follows

$$\tau_{yz}(x, 0) = p_0 e^{\delta x}, \quad x < 0 \quad (3.2.15)$$

where  $\delta > 0$ , which is a very small quantity and tending to zero.

Applying the Fourier transform, the boundary conditions (3.2.10) and (3.2.11) will become

$$\bar{\tau}_{yz}(\xi, d) = 0 \quad (3.2.16)$$

$$\bar{u}_z(\xi, d) = 0 \quad (3.2.17)$$

After applying the Fourier transform on the variable  $\xi$  the solution of the Equation (3.2.4) is obtained as

$$\begin{aligned} \bar{u}_z(\xi, y) &= A_1(\xi) e^{-G\xi y} + A_2(\xi) e^{G\xi y}, & 0 \leq y \leq d \\ &= A_3(\xi) e^{G\xi y}, & -\infty < y \leq 0 \end{aligned} \quad (3.2.18)$$

provided that the crack velocity ( $V$ ) is less than the shear wave velocity ( $C_S$ ) of the material. Here  $\bar{u}_z(\xi, y)$  be the Fourier transform of displacement component  $u_z(x, y)$  and  $A_1(\xi)$ ,  $A_2(\xi)$ ,  $A_3(\xi)$  are unknown functions of the transformed variable  $\xi$  which are not independent.

Shear stress now becomes

$$\begin{aligned} \bar{\tau}_{yz}(\xi, y) &= C_{44}G\xi[A_2(\xi)e^{G\xi y} - A_1(\xi)e^{-G\xi y}], & 0 \leq y \leq d \\ &= C_{44}A_3(\xi)G\xi e^{G\xi y}, & -\infty < y \leq 0 \end{aligned} \quad (3.2.19)$$

## • Solution Procedure

Let us introduce two unknown functions for determining the complete solution by Weiner -Hopf method

$$\tau_{yz}(x, 0) = r(x), \quad x > 0, \quad (3.2.20)$$

$$u_z(x, 0) = s(x), \quad x < 0, \quad (3.2.21)$$

By taking both sides Fourier transformation of Equations (3.2.20) and (3.2.21), we obtain

$$\bar{r}_+(\xi) = \frac{1}{\sqrt{2\pi}} \int_0^\infty r(x)e^{i\xi x} dx, \quad (3.2.22)$$

$$\bar{s}_-(\xi) = \frac{1}{\sqrt{2\pi}} \int_{-\infty}^0 s(x)e^{i\xi x} dx, \quad (3.2.23)$$

where the (+) and (−) subscript denote that the functions are analytic above or below a certain line in the complex  $\xi$  – plane.

The functions  $\bar{r}(x)$  and  $\bar{s}(x)$  are bounded at infinity as the stress and displacements are tending to zero at infinity which is obvious from the physical nature of the problem. So we assume the following bounds

$$|\bar{r}(x)| < Rx^{-l_r}, \quad \text{as } x \rightarrow \infty \quad (3.2.24)$$

$$|\bar{s}(x)| < S|x|^{-l_s}, \quad \text{as } x \rightarrow -\infty \quad (3.2.25)$$

where  $l_r > 0$ ,  $l_s > 0$ ,  $R > 0$  and  $S > 0$ . Here  $R$  and  $S$  are finite. Now it can be shown that the functions  $\bar{r}_+(\xi)$  and  $\bar{s}_-(\xi)$  are analytic for  $\gamma \geq 0$  and  $\gamma \leq 0$  respectively.

Making use of the boundary conditions (3.2.9) and (3.2.10) with the help of the Equations (3.2.22) and (3.2.23), we get a pair of Equations as follows

$$\bar{\tau}_{yz}(\xi, 0) = \bar{r}_+(\xi) + \frac{p_0}{\sqrt{2\pi}(\delta + i\xi)} \quad (3.2.26)$$

$$\bar{u}_z(\xi, 0) = \bar{s}_-(\xi) \quad (3.2.27)$$

Now Equation (3.2.26) can be rewritten as

$$\bar{r}_+(\xi) = \bar{\tau}_{yz}(\xi, 0) - \frac{p_0}{\sqrt{2\pi}(\delta + i\xi)} \quad (3.2.28)$$

With the help of boundary condition (3.2.17), we get

$$A_2(\xi) = -A_1(\xi)e^{-2G\xi d} \quad (3.2.29)$$

At  $y = 0$ , the solutions are

$$\bar{u}_z(\xi, 0) = A_1(\xi) + A_2(\xi), \quad 0 \leq y \leq d \quad (3.2.30)$$

and

$$\bar{u}_z(\xi, 0) = A_3(\xi), \quad -\infty \leq y \leq 0 \quad (3.2.31)$$

Equation (3.2.30) in view of (3.2.27) and (3.2.29), assumes the form

$$A_1(\xi) = \frac{\bar{s}_-(\xi)}{1 - e^{-2G\xi d}} \quad (3.2.32)$$

From Equations (3.2.27) and (3.2.31), we obtain

$$A_3(\xi) = \bar{s}_-(\xi) \quad (3.2.33)$$

Substitution of the values of stress from (3.2.19) into the Equation (3.2.28) and then using (3.2.26) and (3.2.32) renders the well-known Weiner-Hopf Equation of the unknown functions as  $\bar{r}_+(\xi)$  and  $\bar{s}_-(\xi)$

$$\bar{r}_+(\xi) = T(\xi)\bar{s}_-(\xi) - \frac{p_0}{\sqrt{2\pi}(\delta + i\xi)} \quad (3.2.34)$$

where the kernel  $T(\xi)$  is given by

$$T(\xi) = \frac{-C_{44}G\xi(1 + e^{-2G\xi d})}{1 - e^{-2G\xi d}} \quad (3.2.35)$$

• **Solution of the Weiner- Hopf Equation**

In order to solve the Equation (3.2.34), it is necessary to split the kernel  $T(\xi)$  in the following form [B. Noble (1958)]

$$T(\xi) = T_+(\xi)T_-(\xi) \tag{3.2.36}$$

where the functions  $T_+(\xi)$  and  $T_-(\xi)$  both are analytic and non-zero for  $\gamma > \gamma_1$  ( $\gamma_1 < 0$ ) and  $\gamma < \gamma_2$  ( $\gamma_2 > 0$ ).

Consequently, Equation (3.2.34) by virtue of (3.2.36) becomes

$$\frac{\bar{r}_+(\xi)}{T_+(\xi)} = T_-(\xi)\bar{s}_-(\xi) - \frac{p_0}{\sqrt{2\pi}(\delta + i\xi)T_+(\xi)} \tag{3.2.37}$$

The last term of Equation (3.2.37) has been decomposed as a sum of two analytic functions given by

$$\frac{p_0}{\sqrt{2\pi}(\delta + i\xi)T_+(\xi)} = D_+(\xi) + D_-(\xi) \tag{3.2.38}$$

where the functions  $D_+(\xi)$  and  $D_-(\xi)$  can be obtained as

$$D_+(\xi) = \frac{p_0}{\sqrt{2\pi}(\delta + i\xi)} \left[ \frac{1}{T_+(\xi)} - \frac{1}{T_+(i\delta)} \right] \tag{3.2.39}$$

$$D_-(\xi) = \frac{p_0}{\sqrt{2\pi}(\delta + i\xi)T_+(i\delta)} \tag{3.2.40}$$

We have checked the analyticity of the functions  $D_+(\xi)$  and  $D_-(\xi)$  and these two functions are non-zero in  $\gamma > \gamma_1$  and  $\gamma < \delta$  respectively. Rearranging the Equation (3.2.37), with the help of (3.2.38), we get

$$\frac{\bar{r}_+(\xi)}{T_+(\xi)} + D_+(\xi) = T_-(\xi)\bar{s}_-(\xi) - D_-(\xi) \tag{3.2.41}$$

From Equation (3.2.41), it is observed that the region of analyticity of the functions  $\bar{r}_+(\xi)$ ,  $\bar{s}_-(\xi)$ ,  $T_+(\xi)$ ,  $T_-(\xi)$ ,  $D_+(\xi)$  and  $D_-(\xi)$  are  $\gamma \geq 0$ ,  $\gamma \leq 0$ ,  $\gamma > \gamma_1$  ( $\gamma_1 < 0$ ),  $\gamma < \gamma_2$  ( $\gamma_2 > 0$ ),  $\gamma > \gamma_1$  ( $\gamma_1 < 0$ ) and  $\gamma < \delta$  respectively. The left side



and the right side of the Equation (3.2.41), both are analytic at the region of the upper half-plane  $\gamma \geq 0$  and the lower half-plane  $\gamma \leq 0$  where  $\delta(> 0)$  is a very small quantity. The common part of analyticity is the line  $\gamma = 0$ . The Equation (3.2.41) is analytic and single-valued in the whole complex  $\xi - plane$  by analytic continuation. By considering the large values of  $\xi$ , the functions  $T_+(\xi)$  and  $T_-(\xi)$  tend to be  $\xi^{\frac{1}{2}}$  and the functions  $\bar{r}_+(\xi)$  and  $\bar{s}_-(\xi)$  will be bounded. Now we consider both sides of the Equation (3.2.41) equal to  $F(\xi)$ . This function is analytic and the function  $F(\xi)$  is tending to  $\xi^{-\frac{1}{2}}$  for large value of  $\xi$  in the upper half-plane  $\gamma \geq 0$ . Moreover using the same arguments on the right-hand side of the Equation (3.2.41) is analytic and tending to  $\xi^{\frac{1}{2}}$  for large value of  $\xi$  in the lower half-plane  $\gamma \leq 0$ . It can be culminated that the function  $F(\xi)$  is identically zero by the extended Liouville's theorem.

$$F(\xi) = 0 \quad (3.2.42)$$

Now utilizing (3.2.39 – 3.2.41), the functions of interest can be found from (3.2.42) as

$$\bar{r}_+(\xi) = \frac{p_0}{\sqrt{2\pi}(\delta + i\xi)} \left[ \frac{T_+(\xi)}{T_+(\delta)} - 1 \right] \quad (3.2.43)$$

$$\text{and} \quad \bar{s}_-(\xi) = \frac{p_0}{\sqrt{2\pi}(\delta + i\xi)T_+(i\delta)T_-(\xi)} \quad (3.2.44)$$

So we may take  $\delta \rightarrow 0$  for constant loading and consequently the above expressions become

$$\bar{r}_+(\xi) = \frac{p_0}{\sqrt{2\pi}i\xi} \left[ \frac{T_+(\xi)}{T_+(0)} - 1 \right] \quad (3.2.45)$$

$$\text{and} \quad \bar{s}_-(\xi) = \frac{p_0}{\sqrt{2\pi}i\xi T_+(0)T_-(\xi)} \quad (3.2.46)$$

Nilsson (1972) introduced a process where SIF can be obtained by only knowing the values of  $T(\xi)$  for very large and small values of  $\xi$ .

After algebraic manipulation, we get the following asymptotic values of the kernel  $T(\xi)$ :

$$\lim_{\xi \rightarrow \infty} \frac{T(\xi)}{\xi} = -C_{44}G \quad (3.2.47)$$

and

$$\lim_{\xi \rightarrow 0} T(\xi) = -\frac{C_{44}}{d} \quad (3.2.48)$$

The Equations (3.2.45) and (3.2.46) can be written for large values of  $\xi$  as

$$\lim_{\xi \rightarrow \infty} \bar{r}_+(\xi) = \lim_{\xi \rightarrow \infty} \frac{p_0}{\sqrt{2\pi i T_+(0)} \xi^{\frac{1}{2}}} \frac{T_+(\xi)}{\xi^{\frac{1}{2}}} \quad (3.2.49)$$

$$\lim_{\xi \rightarrow \infty} \bar{s}_-(\xi) = \lim_{\xi \rightarrow \infty} \frac{p_0}{\sqrt{2\pi i T_+(0)} \xi^{\frac{3}{2}}} \frac{\xi^{\frac{1}{2}}}{T_-(\xi)} \quad (3.2.50)$$

Taking inverse fourier transform on (3.2.49) and (3.2.50) with the help of Equations (3.2.47) and (3.2.48), we finally obtain the following expressions for the unknown functions

$$\lim_{x \rightarrow 0^+} r(x) = -p_0 \sqrt{\frac{Gd}{\pi}} x^{-\frac{1}{2}} \quad (3.2.51)$$

$$\lim_{x \rightarrow 0^-} s(x) = -p_0 \sqrt{\frac{d}{\pi C_{44}^2 G}} (-x)^{\frac{1}{2}} \quad (3.2.52)$$

From the definition of the function  $r(x)$ , Equation (3.2.51) represents distribution of the shear stress component  $\tau_{yz}$  along the  $x$ -axis just outside the crack and the structure of the shear stress component in Equation (3.2.51) reveals a square root singularity at the crack tip which is very much expected in the field of Fracture Mechanics. Furthermore, the Equation (3.2.52) represents the displacement  $u_z$  in

the vicinity of the crack tip. This quantity known as Crack Opening Displacement (COD) is also important in view of the physical nature of the crack.

### • Quantities of Physical Interest

The quantity that reveals state of stress (SIF) at the crack tip, denoted by  $K_{III}$  is defined by

$$K_{III} = \lim_{x \rightarrow 0^+} \sqrt{2\pi x} \tau_{yz}(x, 0) \quad (3.2.53)$$

In this case, the SIF can be found as

$$SIF = K_{III} = -p_0 \sqrt{2Gd} \quad (3.2.54)$$

Therefore, the SIF of the original problem (normalized with respect to  $u_{z_0}$ ) is given by

$$SIF = K_{III} = C_{44} \sqrt{\frac{2G}{d}} \quad (3.2.55)$$

Next the Crack Opening Displacement (COD) is defined by

$$COD = u_z(x, 0^+) - u_z(x, 0^-) \quad (3.2.56)$$

In this problem , the COD can be written as

$$COD = -2p_0 \sqrt{\frac{d}{\pi C_{44}^2 G}} (-x)^{\frac{1}{2}} \quad (3.2.57)$$

Therefore, COD of the original problem (normalized with respect to  $u_{z_0}$ ) is

$$COD = 2\sqrt{\frac{1}{\pi G d}} (-x)^{\frac{1}{2}} \quad (3.2.58)$$

### • Numerical Results and Discussion

Analytical expressions need to be translated into numerical solutions for better understanding of the nature of the physical quantities in the light of relevant

parameters. The normalized SIF ( $K_{III}$ ) and normalized COD with respect to  $u_{z_0}$  depend on crack velocity ( $V$ ), crack depth ( $d$ ) and material constants ( $C_{44}, C_{55}, \rho$ ). Therefore, the numerical solutions of (3.2.55) and (3.2.58) are facily obtained to show the effects of the material orthotropy on the SIF and COD by virtue of graphs.

The general theoretical upper limit [B. K. Broberg (1999)] of crack propagation velocity is the SH-wave velocity ( $C_S$ ) for mode III cracks i.e.  $0 < V < C_S$ . In particular, SIF at the crack tip asymptotically vanishes when  $V \rightarrow C_S$ .

Material constants (n unit  $GPA$ ) and densities (*in unit  $gm/cm^3$* ) of two orthotropic materials are provided [J. G. Yu (2011)] in Table 3.2.

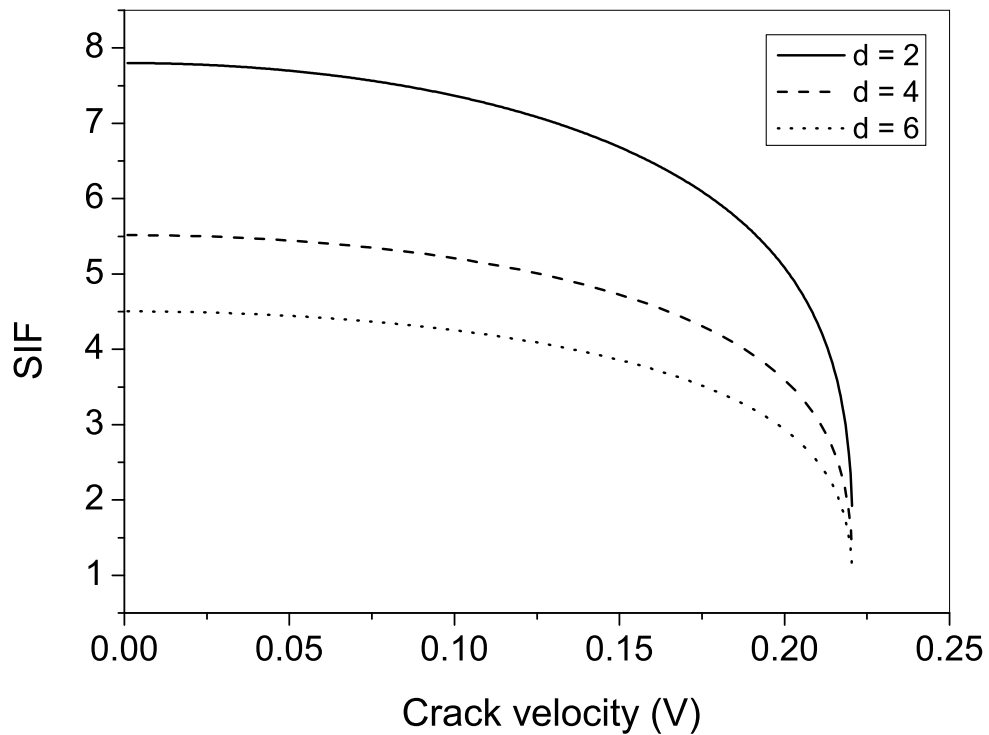


**Fig.3.13** Variation of anti-plane shear SIF with crack velocity  $V$  for Type - I material.

**Table 3.2: Engineering elastic constants of two materials**

	Name of the material	$C_{44}$	$C_{55}$	$\rho$
Type - I	Prepreg	7.8	7.8	1.595
Type - II	Carbon fiber	6.15	6.15	1.5

The velocity of SH-wave for Type-I and Type-II material are  $C_S^I = 2.2114 \text{ cm}/\mu\text{s}$  and  $C_S^{II} = 2.0248 \text{ cm}/\mu\text{s}$ . Fig.3.13 and Fig.3.14 show the variation of the normalized SIF ( $K_{III}/u_{z0}$ ) against crack velocity ( $V$  in  $\text{cm}/\mu\text{s}$ ) for various values of the crack depth  $d = 2, 4, 6 \text{ cm}$ . It is seen that with the increase in the value of  $V$ , the stress intensity factor decreases and finally tends to zero as  $V$  approaches to SH-wave velocity  $C_S$ .

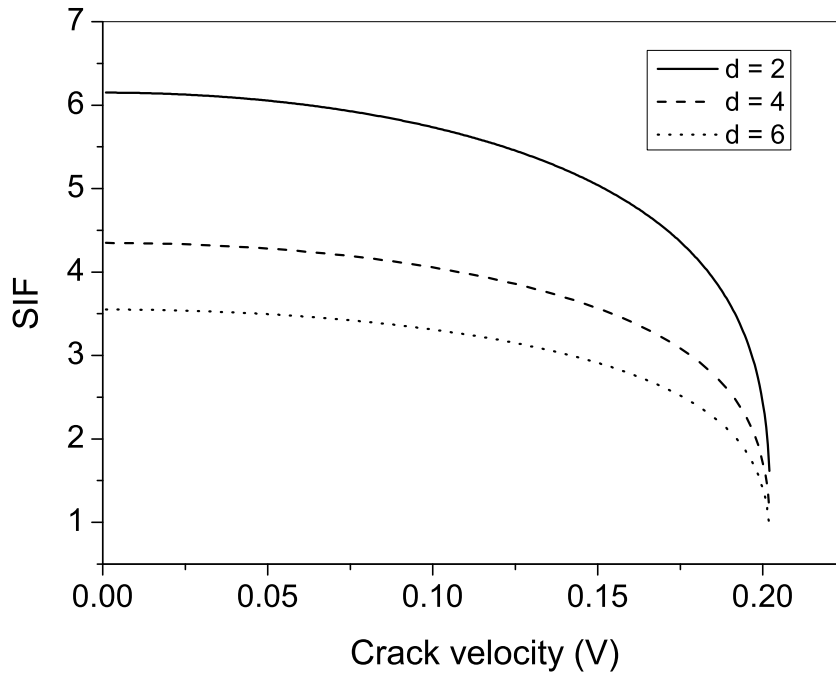


**Fig.3.14 Variation of anti-plane shear SIF with crack velocity V for Type - II material.**

The graph is not valid for super SH-wave velocities ( $V > C_S$ ) as  $C_S$  is the theoretical upper limit of crack propagation velocity  $V$ . In addition, the effect

of crack depth  $d$  on the SIF is also shown in Figs.3.13-3.14. The increase in the crack depth  $d$  induces the decrement in stress intensity factor for all values of crack velocity ( $V$ ). This represents the physical significance of the expression of SIF from Equation (3.2.55) which can be justified with the fact that the impact of the constant displacement at the crack tip region becomes lower as the crack depth becomes higher.

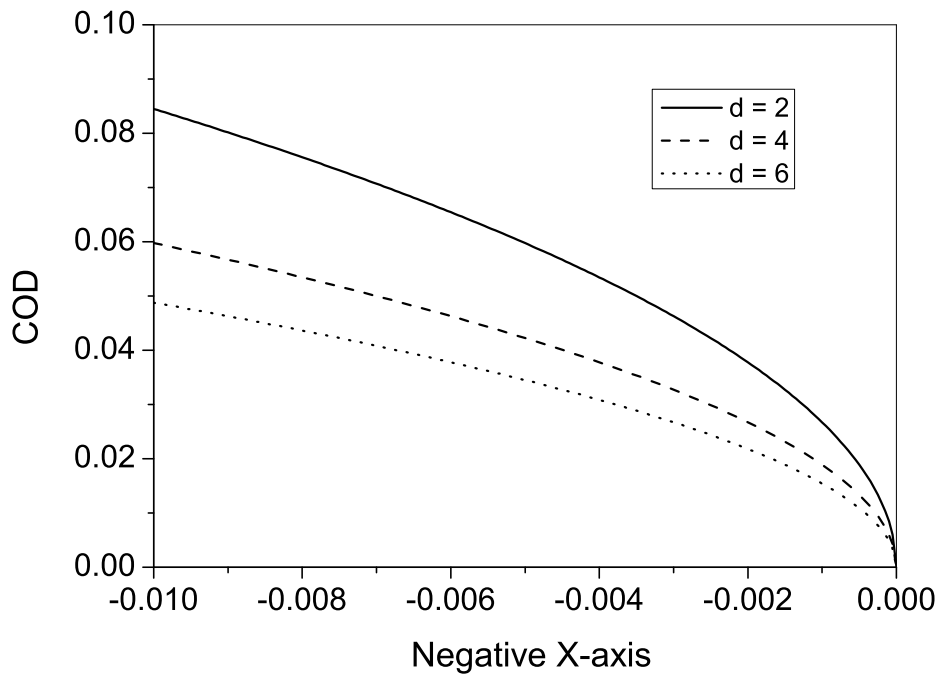


**Fig.3.15** Variation of COD with distance  $x$  for Type - I material (fixed crack velocity  $V = 0.1$  in  $\text{cm}/\mu\text{s}$ .)

Also, it is observed from Fig.3.13 and Fig.3.14 that the values of SIF of Type-I material are greater than the values of Type-II material. So the peak value of  $K_{III}$  can either be raised or lowered by varying the material constants. As the SIF and the toughness of the material are directly proportional to each other, fracture toughness of Type-I material is more than Type-II material.

Our primary motivation in fracture mechanics is to resist the process of propagation of fracture. When SIF at the crack tip region exceeds a particular limit known

as critical SIF, it leads to failure of the composite which involves the cracking of the orthotropic material at relatively high velocities known as crack propagation. So, we want to control the value of SIF, so that SIF can't exceed the critical SIF. For this reason, by varying different geometric parameters (like crack velocity, the width of layer), we may control the magnitude of SIF which helps to prevent crack growth leading to a safe structure. For this purpose, we observe the cases when SIF is decreasing (Figs.3.13 – 3.14). If we observe the case when SIF is increasing, then SIF may exceed critical SIF that leads to crack growth which is not expected in a practical situation. Therefore, these results can be used to control the geometric parameters of these materials concerning for the magnitude of SIF which will help to prevent the expansion of the semi-infinite crack.

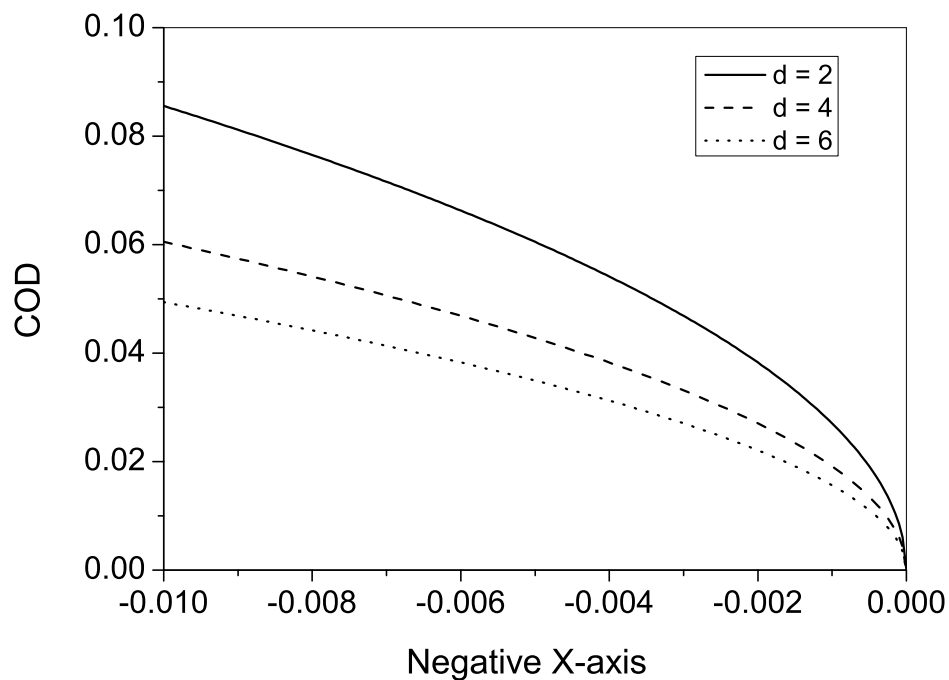


**Fig.3.16** Variation of COD with distance  $x$  for Type - II material  
(fixed crack velocity  $V = 0.1$  in  $\text{cm}/\mu\text{s}$ .)

From all figures of COD ( Figs.3.15 – 3.18), it is observed that the value of COD decreases as we approach near the crack tip along the negative x-axis and finally wiped out at the crack tip i.e. origin. This result is very much agreed with the physical nature of the crack.

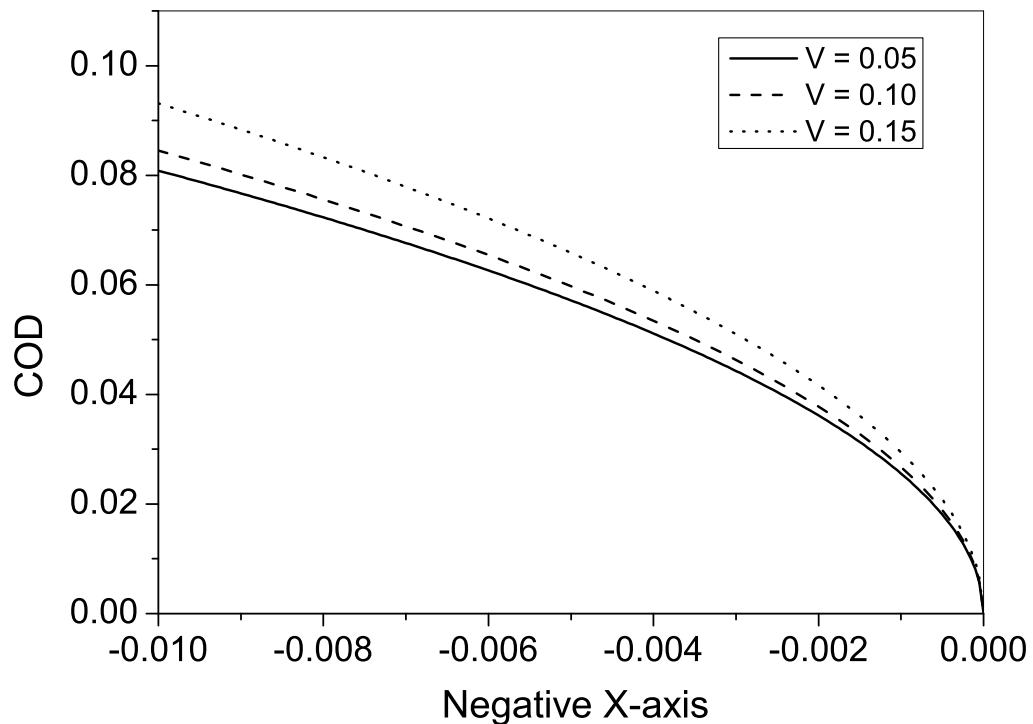


**Fig.3.17** Variation of COD with distance x for Type - I material (fixed crack depth  $d = 2$  cm).

Figs.3.15 and 3.16 illustrate the effect of crack depth  $d$  ( $d = 2, 4, 6$  cm) on the COD for fixed value of  $V = 0.1$  cm/ $\mu$ s and it is observed that COD decreases with the increasing value of  $d$  which signifies the Equation (3.2.58) physically.



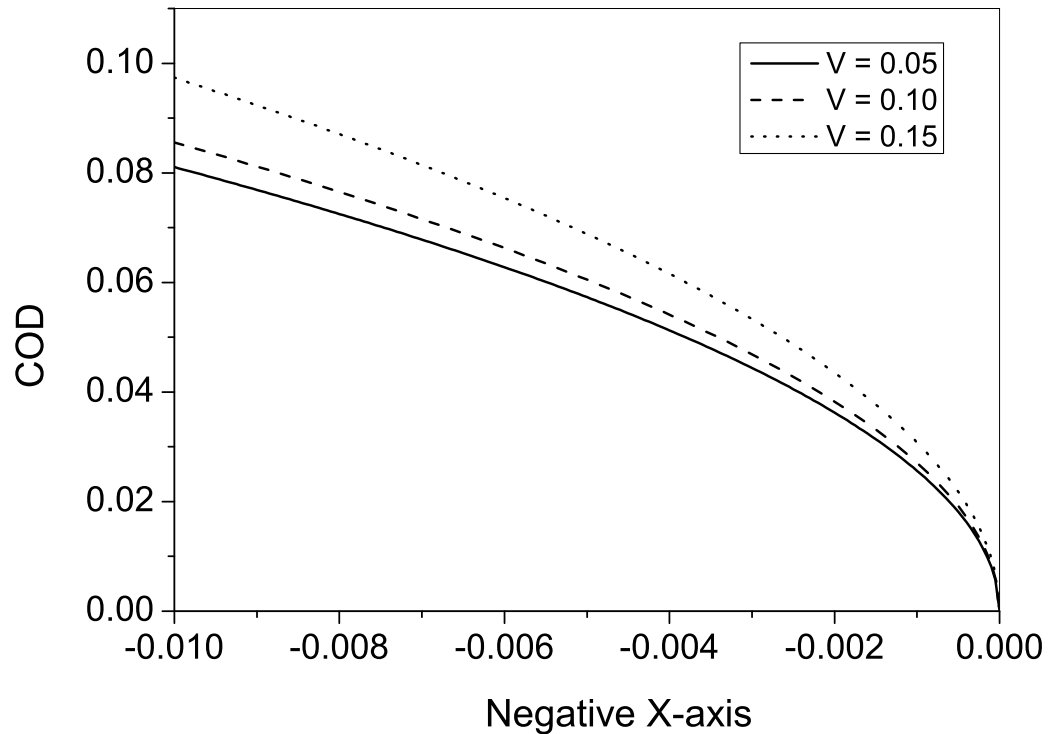


**Fig.3.18** Variation of COD with distance  $x$  for Type - II material (fixed crack depth  $d = 2$  cm).

Again, Figs.3.17–3.18 show the effect of crack velocity  $V$  ( $V = 0.05, 0.10, 0.15$  cm/ $\mu$ s) on the COD for fixed value of crack depth  $d = 2$  cm. It is seen that COD increases with the increasing value of  $V$  subjected to same crack depth. Further investigation disclosed that the variation of crack opening displacement is found to be prominent for different orthotropic materials.

Further, semi-infinite mode-III crack inside the semi-infinite orthotropic medium has been considered following the model developed by P. Mandal (2022) in isotropic medium.

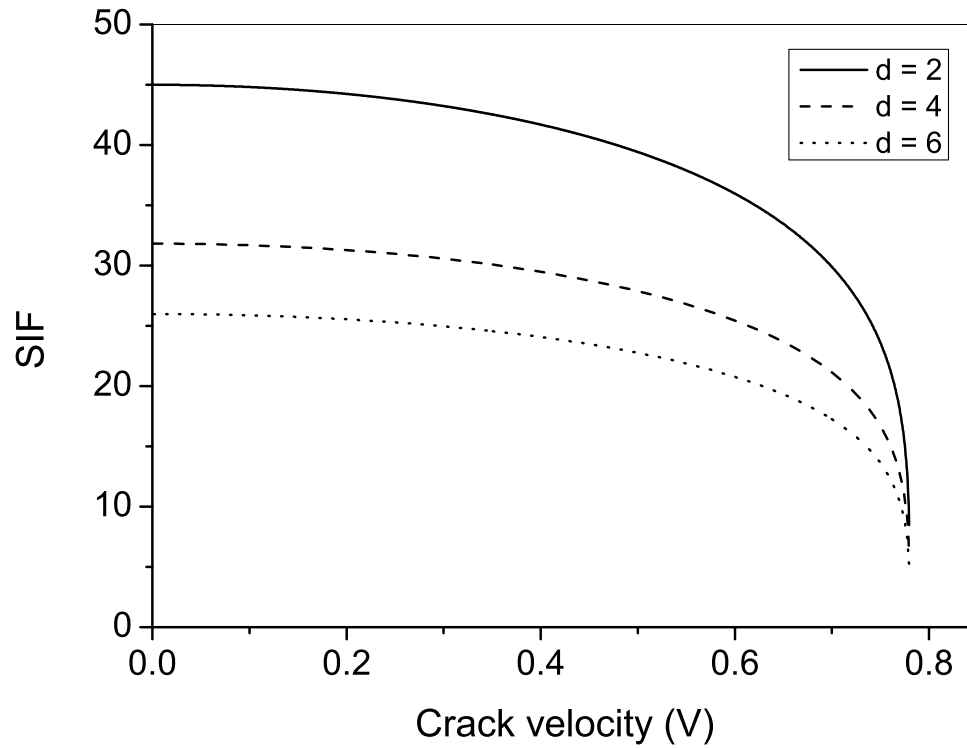


**Fig.3.19** Variation of anti-plane shear SIF with crack velocity V for Isotropic medium.

For validation of this work, we converted this orthotropic medium problem to isotropic medium problem by putting  $C_{44} = C_{55} = \mu$ , where  $\mu$  is shear modulus of the isotropic material and we deduce the following expressions

$$\beta = 1, \text{ shear wave velocity} = C_S = \sqrt{\frac{\mu}{\rho}}$$

$$G^2 = \left(1 - \frac{V^2}{C_S^2}\right)$$

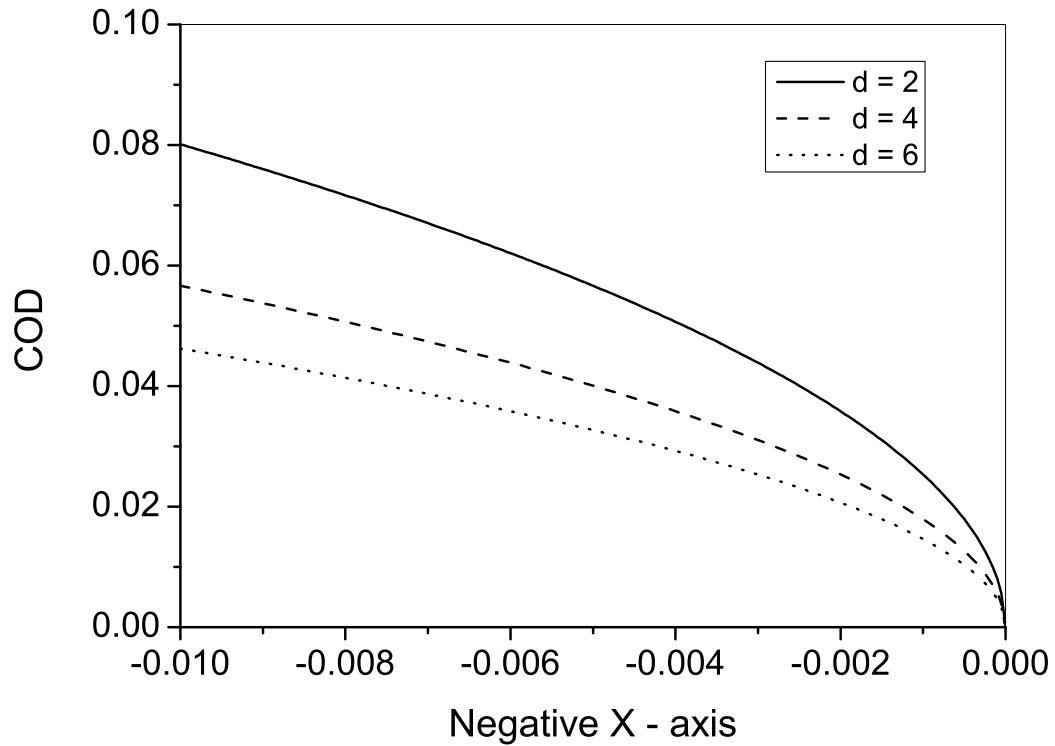


**Fig.3.20** Variation of COD with distance x for Isotropic medium  
(fixed crack velocity  $V = 0.1 \text{ cm}/\mu\text{s.}$ )

The above expressions and governing Equation (3.2.4) are identical to those obtained by the work of P. Mandal (2022) for isotropic elastic medium. Also, it is found that the corresponding SIF and COD for the Type - I material (copper) are identical to that of P. Mandal's (2022) findings. Henceforth, the obtained graphs represented in Figs.3.19 – 3.21 are of similar with Figs.3, 5a, 5b of the paper of P. Mandal (2022).

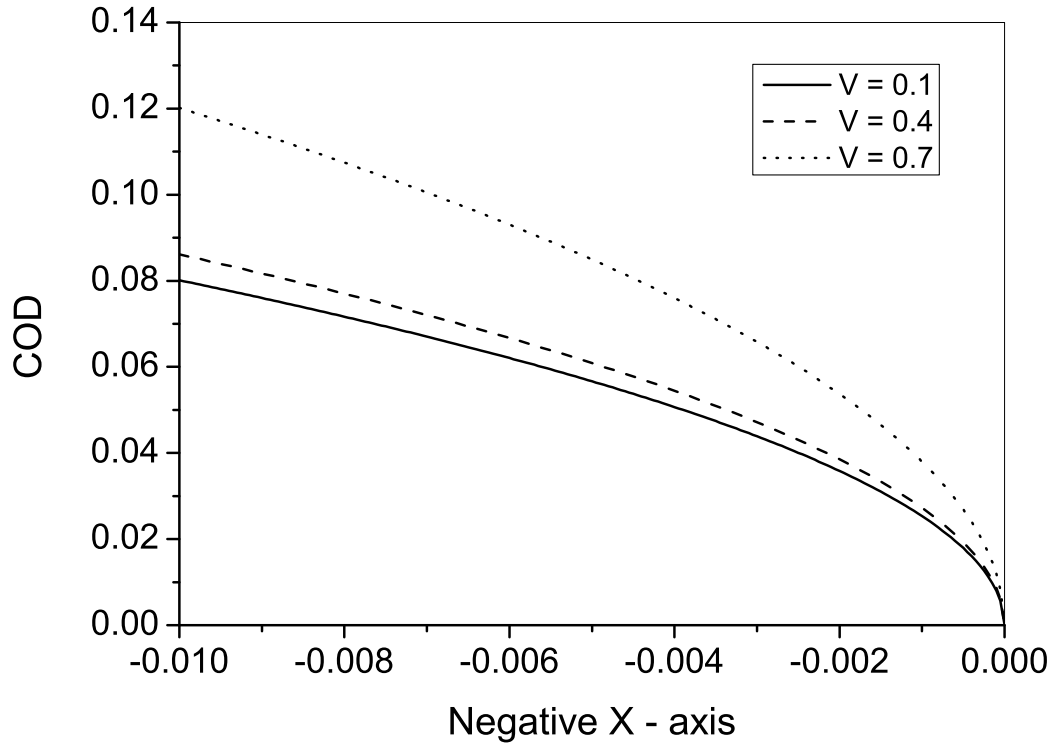


Fig.3.21 Variation of COD with distance x for Isotropic medium (fixed crack depth  $d = 2$  cm).

### • Conclusion

The problem of a moving semi-infinite crack in semi-infinite orthotropic medium has been investigated subject to SH-wave incidence. The mixed boundary value problem has been reduced to the standard Wiener-Hopf equation by applying Fourier transformation. Due to the complex nature of the kernel, the Wiener-Hopf equation has been solved only for the asymptotic case which is sufficient to obtain SIF and COD. By plotting the numerical values of SIF and COD, the dependency of the material constants ( $C_{44}$ ,  $C_{55}$ ,  $\rho$ ) crack propagation velocity ( $V$ ) as well as crack depth ( $d$ ) on SIF and COD have been shown by virtue of graphs. The predicted

behavior of SIF and COD graphs were similar and in good agreement with available literature data.

Based on the numerical calculations outlined above, the following conclusions have been established.

1) The values of SIF and COD can be controlled and arrested within a certain range by varying the above-mentioned parameters to avoid the process of propagation of fracture if the manuscripted model is considered practically for an experiment.

2) The material properties are also playing a vital role here. Two types of orthotropic materials have been used here to obtain the above SIF and COD graphs. It has been concluded that Type-I material is elastically harder than Type-II material. Damage of solid material, earth's surface building is subjected to the propagation of cracks due to seismic hazards, earthquake which is a big challenge in the fields of construction engineering and geophysics as well. The proposed model offers a useful means by which mechanical design of large composite structures can be done to prevent earthquake disasters.

## *Chapter-4*

*Impact of a torsional load on a penny-shaped crack sandwiched between two elastic layers embedded in an elastic medium*

# Chapter 4

## Impact of a torsional load on a penny-shaped crack sandwiched between two elastic layers embedded in an elastic medium

- **Introduction**

As composite materials render advantages such as low weight, strength ratio, corrosion resistance, and high fatigue strength, they have become an essential commodity in modern times. There are many composite materials that are used in the manufacture of aircraft structures, golf clubs, medical equipment, electronic packaging, space vehicles, and homes construction. Increasing commercial applications of composite materials have also been observed. Nonhomogeneous, multiphased, and anisotropic are the characteristics of advanced composite materials. It complicates stress analysis for fracture, especially if the loading is dependent on time and the crack grows at sharp edges.

It is important to investigate the effect of cracks and inclusions on the performance of engineered composite systems. The dynamic problem of torsional impact is one of the important part in view of construction technology and fabrication process. The crack is mainly generated by impact of torsional load. The problem of sudden

---

Published in Acta Mechanica, Vol. 229(4), pp. 1759-1772, 2018, DOI:10.1007/s00707-017-2073-3.

impact of torsional load in half-space are investigated by M. L. Ghosh (1964), G. Eason (1966), R. Shail (1970). Shibuya (1975) analyzed the impact of torsion on a thick elastic plate.

Sih and Chen (1980) developed an effective method for finding dynamic stresses in layered composites with cracks. Keer and Jabali (1974) solved the problem of oscillation due to torsion attached to a layer bonded to an half-space. The concept of penny-shaped crack has been first considered in 1970's by Arin and Erdogan (1971, 1972), Kassir and Bregman (1972), and E. P. Chen (1979). In these studies, some numerical examples are discussed to find stress intensity factors and the strain energy release rate at the edge of the crack with different material properties Within a power law infinite solid medium, the stress analysis for cracks like penny-shaped and plane strain have been studied by He and Hutchinson (1981). Ueda et al. (1983, 1984) also analyzed the impact of torsion upon a penny-shaped interface crack . In both the cases, with the help of Laplace and Hankel transformation, the model is reduced to the solution of a pair of dual integral equations. An integral transformation method has been applied to solve the equations and the result has been expressed in terms of the second kind integral equations of Fredholm type.

Applying numerical method of inverse Laplace transform, the time dependent solution has been obtained and depending upon time and elastic constants of medium the values of stress intensity factor (SIF) have been calculated. The mechanics of interface crack (penny-shaped) between different nonhomogeneous layers and two different transversely isotropic half-spaces a influenced by axisymmetric torsion have been studied by Saxena and Dhaliwala (1990, 1993). Das et al. (1998) determined the stress intensity factors for a crack at the interface of an orthotropic half-plane connected with different orthotropic layer having punch. In this study, simultaneous integral equations was derived with help of chebyshev polynomials. In a FGM interlaying between different half-spaces, Li and Weng (2002) solved the dynamic fracture problem using a penny-shaped crack as a model. Menshykov et al. (2008) derived effect of tension-compression wave which are incident normally to an penny-shaped crack and due to time-harmonic waves, Mykhaskiv and Khay (2009) discussed state of stress of rigid disc interacting with penny-shaped cracks. Lee and Tran (2010) considered interaction of a penny-shaped crack, inclusions, and voids. An analysis



of the fracture of a half-space compressed by a penny-shaped crack at a short distance from the surface has been presented by M.V. Dovzhik (2012). In his study, D.-S. Lee (2013) examined stress analysis for a penny-shaped crack that appears in a plate effected by uniform shear. Recently Basu and Mandal (2016) addressed the nature of how a penny-shaped crack situated in a layer bonded between two similar half-spaces is affected by a torsional impact load.

In most of the above discussed literature, the problem due to impact of torsion upon penny-shaped crack within a layer bonded to a half-space, a non-homogeneous layer at the interface of two different half-planes, within an unbounded thermo-elastic medium or in a layer bonded by two similar half-space has been considered. But the torsional problem of penny-shaped crack bonded by two isotropic layers sandwiched by another isotropic media has not been treated yet. So in this investigation, impact caused by torsion upon a penny-shaped crack bonded by two dissimilar isotropic layers sandwiched by another isotropic media has been analyzed. With the help of Hankel and Laplace transformations, the second kind integral equation of Fredholm type has been derived to be solved with aid of the Fox and Goodwin (1953) technique. After taking numerical inversion of Laplace Transform, numerical values of stress intensity factor (SIF) has been derived at the crack tip for several geometric parameter and set of mediums to compare the bonded strength of the materials.

### • **Formulation of the Problem and Method of Solution**

A study is made of torsional load on a penny-shaped crack with radius  $a$  which lies between two dissimilar elastic layer each of thickness  $b$  with material properties  $\mu_1, \nu_1, \rho_1$  (type - I) and  $\mu_2, \nu_2, \rho_2$  (type - II) in cylindrical co-ordinates  $(r, \theta, z)$ . This two layers are embedded in an infinite elastic medium with properties  $\mu_3, \nu_3, \rho_3$  (type - III) as shown in Fig.4.1. Due to the symmetry of the problem, let the load is of magnitude  $\sigma_0$  which is applied suddenly at time  $t = 0$  so that the surface on the upper and lower sides will have an opposite movement.

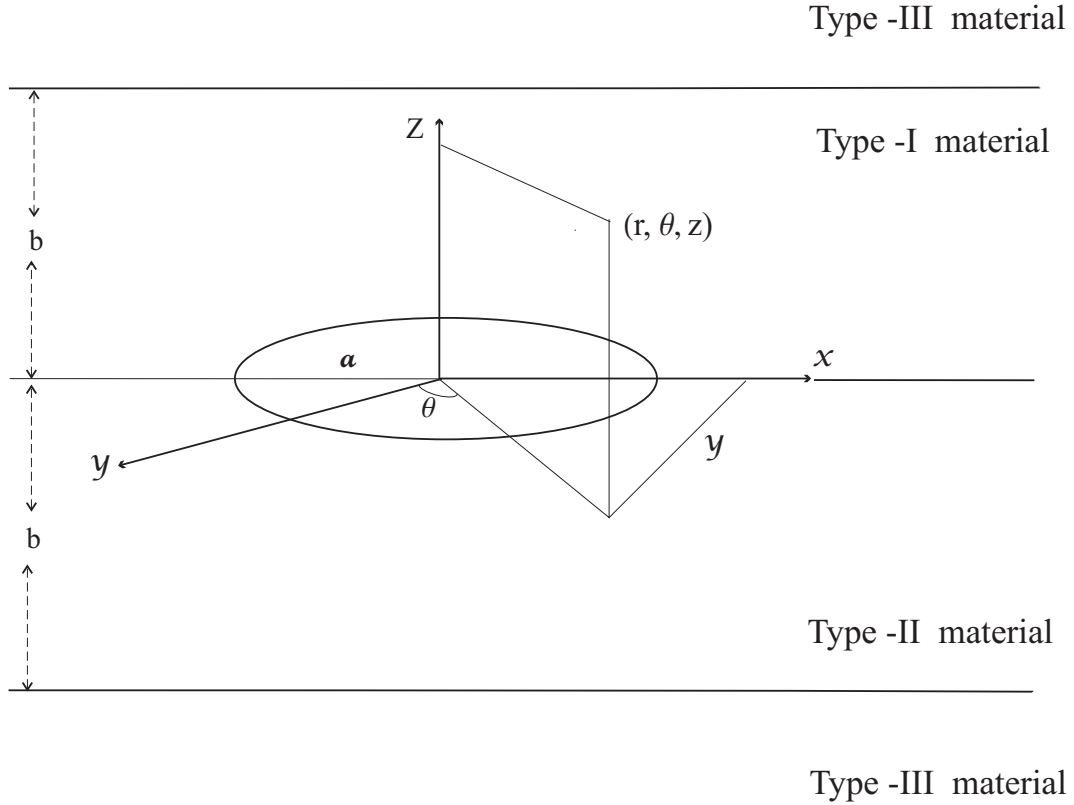


**Fig.4.1 Geometry of the composite model.**

In this study,  $u_\theta$  is the non-zero displacement component and the non-zero stress component  $\sigma_{\theta z}$  is defined by the relation

$$\sigma_{\theta z} = \mu \frac{\partial u_\theta}{\partial z}, \quad (4.1)$$

where  $\mu$  is the shear modulus of the elastic material.

The displacement component  $u_\theta$  satisfies the partial differential equation [G. C. Sih (1977)]

$$\frac{\partial^2 u_\theta}{\partial r^2} + \frac{1}{r} \frac{\partial u_\theta}{\partial r} - \frac{u_\theta}{r^2} + \frac{\partial^2 u_\theta}{\partial z^2} = \frac{1}{c_j^2} \frac{\partial^2 u_\theta}{\partial t^2} \quad (j = 1, 2, 3), \quad (4.2)$$

where  $c_j = \left(\frac{\mu_j}{\rho_j}\right)^{\frac{1}{2}}$  is velocity of shear wave and the density of the material is  $\rho$ . In Equation (4.2), subscripts “1”, “2” and “3” have been used to refer type-I, type-II and type-III material respectively.

To eliminate the time variable from Equation (4.2), Laplace transform pair have

been used which are defined as

$$\bar{h}(p) = \int_0^{\infty} h(t)e^{-pt} dt, \quad (4.3)$$

$$h(t) = \frac{1}{2\pi i} \int_{Br} \bar{h}(p)e^{pt} dp, \quad (4.4)$$

where  $Br$  is the Bromwich integral.

Applying Laplace transformation, the Equation (4.2) transformed to

$$\frac{\partial^2 \bar{u}_\theta}{\partial r^2} + \frac{1}{r} \frac{\partial \bar{u}_\theta}{\partial r} - \frac{\bar{u}_\theta}{r^2} + \frac{\partial^2 \bar{u}_\theta}{\partial z^2} = \frac{p^2}{c_j^2} \bar{u}_\theta \quad (j = 1, 2, 3). \quad (4.5)$$

At the plane  $z = 0$  the boundary condition for  $r \leq a$  and  $r > a$  are

$$\sigma_{\theta z}^{(1)}(r, 0, t) = \sigma_{\theta z}^{(2)}(r, 0, t) = \sigma_0 \left( \frac{r}{a} \right) H(t), \quad 0 \leq r \leq a, \quad (4.6)$$

$$u_\theta^{(1)}(r, 0, t) = u_\theta^{(2)}(r, 0, t), \quad r > a, \quad (4.7)$$

where  $H(t)$  is the Heaviside unit step function.

Also the interfaced layer  $z = \pm b$  are bonded perfectly to the elastic medium. The continuity conditions at the interface are given by

$$\sigma_{\theta z}^{(1)}(r, b, t) = \sigma_{\theta z}^{(3)}(r, b, t), \quad (4.8)$$

$$u_\theta^{(1)}(r, b, t) = u_\theta^{(3)}(r, b, t), \quad (4.9)$$

$$\sigma_{\theta z}^{(2)}(r, -b, t) = \sigma_{\theta z}^{(3)}(r, -b, t), \quad (4.10)$$

$$u_\theta^{(2)}(r, -b, t) = u_\theta^{(3)}(r, -b, t). \quad (4.11)$$

With help of the Laplace transform, the boundary and continuity equations (4.6) – (4.11) can be written as :

$$\bar{\sigma}_{\theta z}^{(1)}(r, 0, p) = \bar{\sigma}_{\theta z}^{(2)}(r, 0, p) = \frac{\sigma_0 \left(\frac{r}{a}\right)}{p}, \quad 0 \leq r \leq a, \quad (4.12)$$

$$\bar{u}_{\theta}^{(1)}(r, 0, p) = \bar{u}_{\theta}^{(2)}(r, 0, p), \quad r > a, \quad (4.13)$$

$$\bar{\sigma}_{\theta z}^{(1)}(r, b, p) = \bar{\sigma}_{\theta z}^{(3)}(r, b, p), \quad (4.14)$$

$$\bar{u}_{\theta}^{(1)}(r, b, p) = \bar{u}_{\theta}^{(3)}(r, b, p), \quad (4.15)$$

$$\bar{\sigma}_{\theta z}^{(2)}(r, -b, p) = \bar{\sigma}_{\theta z}^{(3)}(r, -b, p), \quad (4.16)$$

$$\bar{u}_{\theta}^{(2)}(r, -b, p) = \bar{u}_{\theta}^{(3)}(r, -b, p). \quad (4.17)$$

To solve the Equation (4.5), Hankel transform has been used and the displacement component in Laplace transform domain for the region *I* ( $0 < z < b$ ), region *II* ( $-b < z < 0$ ), region *III* ( $|z| \geq b$ ) are in the following form :

$$\bar{u}_{\theta}^{(1)}(r, z, p) = \int_0^{\infty} [A_1(s, p) e^{-\gamma_1 z} + A_2(s, p) e^{\gamma_1 z}] J_1(sr) ds, \quad (4.18)$$

$$\bar{u}_{\theta}^{(2)}(r, z, p) = \int_0^{\infty} [A_3(s, p) e^{-\gamma_2 z} + A_4(s, p) e^{\gamma_2 z}] J_1(sr) ds, \quad (4.19)$$

$$\bar{u}_{\theta}^{(3)}(r, z, p) = \int_0^{\infty} A_5(s, p) e^{-\gamma_3(z-b)} J_1(sr) ds, \quad z \geq b, \quad (4.20)$$

$$\bar{u}_{\theta}^{(3)}(r, z, p) = \int_0^{\infty} A_6(s, p) e^{\gamma_3(z+b)} J_1(sr) ds, \quad z \leq -b. \quad (4.21)$$

where

$$\begin{aligned} \gamma_1 &= (s^2 + k_1^2)^{\frac{1}{2}}, \quad \gamma_2 = (s^2 + k_2^2)^{\frac{1}{2}}, \quad \gamma_3 = (s^2 + k_3^2)^{\frac{1}{2}}, \\ k_1 &= p/c_1, \quad k_2 = p/c_2, \quad k_3 = p/c_3, \\ c_1 &= \sqrt{\frac{\mu_1}{\rho_1}}, \quad c_2 = \sqrt{\frac{\mu_2}{\rho_2}}, \quad c_3 = \sqrt{\frac{\mu_3}{\rho_3}}. \end{aligned} \quad (4.22)$$

and  $J_1$  is the 1st kind Bessel function with order one.

In Equations (4.18) – (4.21),  $A_i$  ( $i = 1, 2, \dots, 6$ ) are the constants to be found out later. With the help of Equations (4.18) – (4.21), stress components  $\bar{\tau}_{\theta z}$  are obtained

as

$$\bar{\sigma}_{\theta z}^{(1)} = -\mu_1 \int_0^\infty \gamma_1 [A_1(s, p) e^{-\gamma_1 z} - A_2(s, p) e^{\gamma_1 z}] J_1(sr) ds, \quad (4.23)$$

$$\bar{\sigma}_{\theta z}^{(2)} = -\mu_2 \int_0^\infty \gamma_2 [A_3(s, p) e^{-\gamma_2 z} - A_4(s, p) e^{\gamma_2 z}] J_1(sr) ds. \quad (4.24)$$

and

$$\bar{\sigma}_{\theta z}^{(3)} = -\mu_3 \int_0^\infty \gamma_3 [A_5(s, p) e^{-\gamma_3(z-b)}] J_1(sr) ds, \quad z \geq b, \quad (4.25)$$

$$= \mu_3 \int_0^\infty \gamma_3 [A_6(s, p) e^{\gamma_3(z+b)}] J_1(sr) ds, \quad z \leq -b. \quad (4.26)$$

Using the above expressions, the boundary conditions (4.12) and (4.13) yield

$$\begin{aligned} & \mu_1 \int_0^\infty \gamma_1 [A_1(s, p) - A_2(s, p)] J_1(sr) ds \\ &= \mu_2 \int_0^\infty \gamma_2 [A_3(s, p) - A_4(s, p)] J_1(sr) ds, \end{aligned} \quad (4.27)$$

$$\begin{aligned} & \int_0^\infty [A_1(s, p) + A_2(s, p)] J_1(sr) ds = \\ & \int_0^\infty [A_3(s, p) + A_4(s, p)] J_1(sr) ds. \end{aligned} \quad (4.28)$$

and from the continuity conditions (4.14) – (4.17), we obtain

$$\begin{aligned} & \mu_1 \int_0^\infty \gamma_1 [A_1(s, p) e^{-\gamma_1 b} - A_2(s, p) e^{\gamma_1 b}] J_1(sr) ds \\ &= \mu_3 \int_0^\infty \gamma_3 A_5(s, p) J_1(sr) ds, \end{aligned} \quad (4.29)$$

$$- \int_0^\infty [A_1(s, p) e^{-\gamma_1 b} + A_2(s, p) e^{\gamma_1 b}] J_1(sr) ds = \int_0^\infty A_5(s, p) J_1(sr) ds, \quad (4.30)$$

$$\begin{aligned} & -\mu_2 \int_0^\infty \gamma_2 [A_3(s, p) e^{\gamma_2 b} - A_4(s, p) e^{-\gamma_2 b}] J_1(sr) ds \\ &= \mu_3 \int_0^\infty \gamma_3 A_6(s, p) J_1(sr) ds, \end{aligned} \quad (4.31)$$

$$\int_0^\infty [A_3(s, p) e^{\gamma_2 b} + A_4(s, p) e^{-\gamma_2 b}] J_1(sr) ds = \int_0^\infty A_6(s, p) J_1(sr) ds. \quad (4.32)$$

Inverting equations (4.27)–(4.32) using inverse Hankel transformation, the following relations are derived :

$$\gamma_1 [A_1(s, p) - A_2(s, p)] = G_1 \gamma_2 [A_3(s, p) - A_4(s, p)], \quad (4.33)$$

$$A_1(s, p) + A_2(s, p) = A_3(s, p) + A_4(s, p), \quad (4.34)$$

$$\gamma_1 [A_1(s, p) e^{-\gamma_1 b} - A_2(s, p) e^{\gamma_1 b}] = G_2 \gamma_3 A_5(s, p), \quad (4.35)$$

$$A_1(s, p) e^{-\gamma_1 b} + A_2(s, p) e^{\gamma_1 b} = A_5(s, p), \quad (4.36)$$

$$-\gamma_2 [A_3(s, p) e^{\gamma_2 b} - A_4(s, p) e^{-\gamma_2 b}] = G_3 \gamma_3 A_6(s, p), \quad (4.37)$$

$$A_3(s, p) e^{\gamma_2 b} + A_4(s, p) e^{-\gamma_2 b} = A_6(s, p). \quad (4.38)$$

where  $G_1 = \mu_2/\mu_1$ ,  $G_2 = \mu_3/\mu_1$ ,  $G_3 = \mu_3/\mu_2$ .

After solving the Equations (4.33)–(4.38) for  $A_2(s, p)$ ,  $A_3(s, p)$ ,  $A_4(s, p)$ ,  $A_5(s, p)$ ,  $A_6(s, p)$  in terms of  $A_1(s, p)$ , the expression for constants can be written as

$$A_2(s, p) = \left( \frac{\gamma_1 - G_2 \gamma_3}{\gamma_1 + G_2 \gamma_3} \right) e^{-2\gamma_1 b} A_1(s, p), \quad (4.39)$$

$$A_3(s, p) = G A_1(s, p), \quad (4.40)$$

$$A_4(s, p) = \left( \frac{\gamma_2 + G_3 \gamma_3}{\gamma_2 - G_3 \gamma_3} \right) e^{2\gamma_2 b} G A_1(s, p), \quad (4.41)$$

$$A_5(s, p) = \frac{2\gamma_1}{(\gamma_1 + G_2 \gamma_3)} e^{-\gamma_1 b} A_1(s, p), \quad (4.42)$$

$$A_6(s, p) = \frac{2\gamma_2 e^{\gamma_2 b}}{(\gamma_2 - G_3 \gamma_3)} G A_1(s, p), \quad (4.43)$$

where

$$G = \left[ 1 - \left( \frac{\gamma_1 - G_2 \gamma_3}{\gamma_1 + G_2 \gamma_3} \right) e^{-2\gamma_1 b} \right] / \frac{G_1 \gamma_2}{\gamma_1} \left[ 1 - \left( \frac{\gamma_2 + G_3 \gamma_3}{\gamma_2 - G_3 \gamma_3} \right) e^{2\gamma_2 b} \right].$$

Applying (4.18), (4.19) and (4.23) in the boundary conditions (4.13) and (4.12),

the following dual integral equations has been deduced involving the unknown function  $B(s, p)$ .

$$\int_0^\infty B(s, p) J_1(sr) ds = 0, \quad r > a, \quad (4.44)$$

$$\int_0^\infty s P_1(s, p) B(s, p) J_1(sr) ds = -\frac{\sigma_0(\frac{r}{a})}{p\mu_1}, \quad 0 \leq r \leq a, \quad (4.45)$$

where

$$B(s, p) = \left[ \left\{ 1 + \left( \frac{\gamma_1 - G_2\gamma_3}{\gamma_1 + G_2\gamma_3} \right) e^{-2\gamma_1 b} \right\} - G \left\{ 1 + \left( \frac{\gamma_2 + G_3\gamma_3}{\gamma_2 - G_3\gamma_3} \right) e^{2\gamma_2 b} \right\} \right] A_1(s, p), \quad (4.46)$$

and

$$P(s, p) = \frac{\gamma_1 \left[ 1 - \left( \frac{\gamma_1 - G_2\gamma_3}{\gamma_1 + G_2\gamma_3} \right) e^{-2\gamma_1 b} \right]}{s \left[ \left\{ 1 + \left( \frac{\gamma_1 - G_2\gamma_3}{\gamma_1 + G_2\gamma_3} \right) e^{-2\gamma_1 b} \right\} - G \left\{ 1 + \left( \frac{\gamma_2 + G_3\gamma_3}{\gamma_2 - G_3\gamma_3} \right) e^{2\gamma_2 b} \right\} \right]}. \quad (4.47)$$

To convert the dual integral Equations (4.44) and (4.45) to a second kind of Fredholm integral equation, the form of  $B(s, p)$  to satisfy Equation (4.44) automatically can be considered as

$$B(s, p) = \frac{4\sigma_0 a^{\frac{5}{2}}}{3\mu_1 p (2\pi)^{\frac{1}{2}}} \sqrt{s} \int_0^1 \sqrt{\eta} \Phi(\eta, p) J_{\frac{3}{2}}(s a \eta) d\eta, \quad (4.48)$$

where  $\Phi(\eta, p)$  is unknown function to be determined.

Using the formula

$$J_{\frac{3}{2}}(s_1 \eta) = -\frac{\sqrt{\eta}}{s_1} \frac{d}{d\eta} \left\{ \eta^{-\frac{1}{2}} J_{\frac{1}{2}}(s_1 \eta) \right\}, \quad s_1 = sa,$$

$B(s, p)$  may be written like

$$B\left(\frac{s_1}{a}, p\right) = \frac{4\sigma_0 a^2}{3\mu_1 p (2\pi s_1)^{\frac{1}{2}}} \left[ \int_0^1 \Phi_1(\eta, p) J_{\frac{1}{2}}(s_1 \eta) d\eta - \Phi(1, p) J_{\frac{1}{2}}(s_1) \right], \quad (4.49)$$

where

$$\Phi_1(\eta, p) = \eta^{-\frac{1}{2}} \frac{d}{d\eta} [\eta \Phi(\eta, p)]. \quad (4.50)$$

When  $s_1$  is large, the expression of  $P\left(\frac{s_1}{a}, p\right)$  approaches to  $1/G_4$  so that

$$1 - G_4 P\left(\frac{s_1}{a}, p\right) \longrightarrow 0 \quad \text{as } s_1 \longrightarrow \infty,$$

where  $G_4 = 1 + \frac{\mu_1}{\mu_2} = 1 + \frac{1}{G_1}$ .

Now the expression of Equations (4.45) in dimensionless quantities are

$$\int_0^\infty s_1 B\left(\frac{s_1}{a}, p\right) J_1(\mathcal{R} s_1) ds_1 = -\frac{\sigma_0 a^2 G_4 \mathcal{R}}{p \mu_1} + \int_0^\infty s_1 \left[1 - G_4 P\left(\frac{s_1}{a}, p\right)\right] B\left(\frac{s_1}{a}, p\right) J_1(\mathcal{R} s_1) ds_1, \quad (R < 1)$$

where  $\mathcal{R} = \frac{r}{a}$ .

With the help of Equations (4.49) and using the result

$$\int_0^\infty t^{\frac{1}{2}} J_1(at) J_{\frac{1}{2}}(bt) dt = \begin{cases} 0 & , 0 < a < b, \\ \sqrt{\frac{2}{\pi}} \frac{\sqrt{b}}{a \sqrt{a^2 - b^2}} & , 0 < b < a. \end{cases}$$

the above equation becomes

$$\begin{aligned} \int_0^{\mathcal{R}} \frac{\sqrt{\eta}}{\sqrt{\mathcal{R}^2 - \eta^2}} \Phi_1(\eta, p) d\eta \\ = -\frac{3\pi G_4 \mathcal{R}^2}{4} + \frac{\sqrt{\pi} \mathcal{R}}{\sqrt{2}} \int_0^1 \sqrt{\eta} \Phi(\eta, p) d\eta \int_0^\infty s_1^{\frac{3}{2}} M\left(\frac{s_1}{a}, p\right) J_1(\mathcal{R} s_1) J_{\frac{3}{2}}(\eta s_1) ds_1 \\ = Q(\mathcal{R}) \end{aligned} \quad (4.51)$$

where  $M\left(\frac{s_1}{a}, p\right) = 1 - G_4 P\left(\frac{s_1}{a}, p\right)$ ,

and  $Q(\mathcal{R}) = -\frac{3\pi G_4 \mathcal{R}^2}{4} + \sqrt{\frac{\pi}{2}} \mathcal{R} \int_0^1 \sqrt{\eta} \Phi(\eta, p) d\eta \int_0^\infty s_1^{\frac{3}{2}} M\left(\frac{s_1}{a}, p\right) J_1(\mathcal{R} s_1) J_{\frac{3}{2}}(\eta s_1) ds_1$ .

By setting Abel's integral as

$$\sqrt{\eta} \Phi_1(\eta, p) = \frac{2}{\pi} \frac{d}{d\eta} \int_0^\eta \frac{\mathcal{R} Q(\mathcal{R})}{\sqrt{\eta^2 - \mathcal{R}^2}} d\mathcal{R},$$



and with the help of expression (4.50), Equation (4.51) becomes

$$\eta\Phi(\eta, p) = \frac{2}{\pi} \int_0^\eta \frac{\mathcal{R}}{\sqrt{\eta^2 - \mathcal{R}^2}} \left[ \frac{-3\pi G_4 \mathcal{R}^2}{4} + \sqrt{\frac{\pi}{2}} \mathcal{R} \int_0^1 \sqrt{u} \Phi(u, p) du \right. \\ \left. \times \int_0^\infty s_1^{\frac{3}{2}} M\left(\frac{s_1}{a}, p\right) J_1(\mathcal{R} s_1) J_{\frac{3}{2}}(u s_1) ds_1 \right] d\mathcal{R}, \quad (4.52)$$

which can be converted by using Hankel transform in to a second kind integral equation of Fredholm type as

$$\Phi(\eta, p) + \int_0^1 \Phi(u, p) L_3(\eta, u, p) du = -G_4 \eta^2, \quad (4.53)$$

$$\text{where } L_3(\eta, u, p) = -\sqrt{\eta u} \int_0^\infty s_1 \left[ 1 - G_4 P\left(\frac{s_1}{a}, p\right) \right] J_{\frac{3}{2}}(u s_1) J_{\frac{3}{2}}(\eta s_1) ds_1. \quad (4.54)$$

### • Stress Intensity Factor

For determining stress intensity factor (SIF)  $K_1(t)$  from  $K_1^*(p)$ , we expressed the components of stress in the matrix layer with reference to local co-ordinates  $(r_1, \theta_1)$  (when  $r_1$  is very small) as following

$$\left. \begin{aligned} r &= a + r_1 \cos \theta_1, \\ z &= r_1 \sin \theta_1. \end{aligned} \right\} \quad (4.55)$$

where  $x = r \cos \theta$  and  $y = r \sin \theta$ .

Equation (4.23) can be written as

$$\bar{\sigma}_{\theta z}^{(1)}(r, 0, p) = -\mu_1 \int_0^\infty s P(s, p) B(s, p) J_1(sr) ds, \quad (r > a). \quad (4.56)$$

Now, letting  $P(s, p) \rightarrow 1/G_4$  as  $s \rightarrow \infty$ , the Equation (4.56) becomes

$$\bar{\sigma}_{\theta z}^{(1)}(r, 0, p) = \frac{4\sigma_0}{3\pi p G_4} \left[ \frac{\phi(1, p)}{\mathcal{R}\sqrt{\mathcal{R}^2 - 1}} - \int_0^1 \frac{\sqrt{\eta}}{\mathcal{R}\sqrt{\mathcal{R}^2 - \eta^2}} \phi_1(\eta, p) d\eta \right] \\ = \frac{4\sigma_0}{3\pi p G_4} \frac{\phi(1, p)}{(\mathcal{R}\sqrt{\mathcal{R}^2 - 1})} + O(1), \quad (\mathcal{R} > 1). \quad (4.57)$$

Derivation of singularity requires calculation of the term  $|\bar{\sigma}_{\theta z}^{(1)}(r, 0, p)|$ . Therefore,

$$\begin{aligned} |\bar{\sigma}_{\theta z}^{(1)}(r, 0, p)| &= \frac{4\sigma_0}{3\pi p G_4} \frac{\phi(1, p)}{(\mathcal{R}\sqrt{\mathcal{R}^2 - 1})} \quad (\mathcal{R} > 1) \\ &= \frac{4\sigma_0}{3\pi p G_4} \frac{\phi(1, p)}{(\frac{r}{a}\sqrt{\frac{r}{a} - 1} \sqrt{\frac{r}{a} + 1})} \quad (r > a) \\ &= \frac{4\sigma_0}{3\pi p G_4} \frac{\sqrt{a}\phi(1, p)}{(\frac{r}{a}\sqrt{r_1} \sqrt{\frac{r}{a} + 1})} \quad (r > a). \end{aligned} \quad (4.58)$$

where  $r_1 = r - a$ .

The formula to define stress-intensity factor in Laplace transform domain is as following

$$K_1^*(p) = \lim_{r \rightarrow a} [|\bar{\sigma}_{\theta z}^{(1)}(r, 0, p)| \sqrt{r - a}]. \quad (4.59)$$

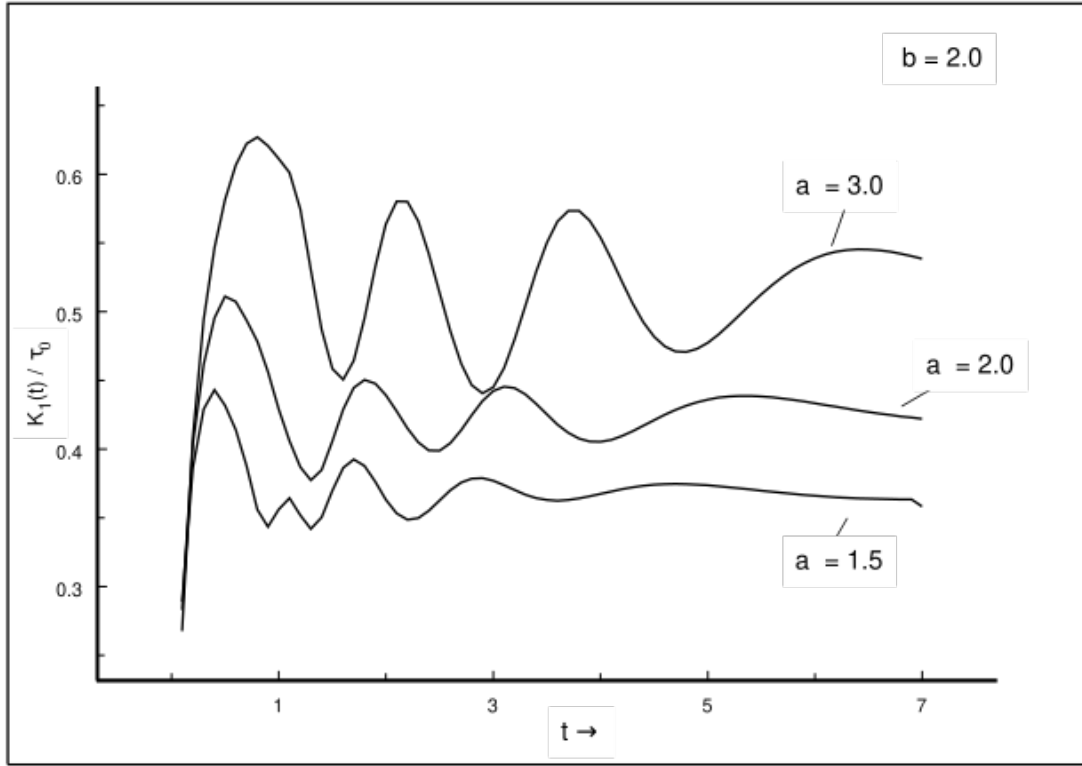
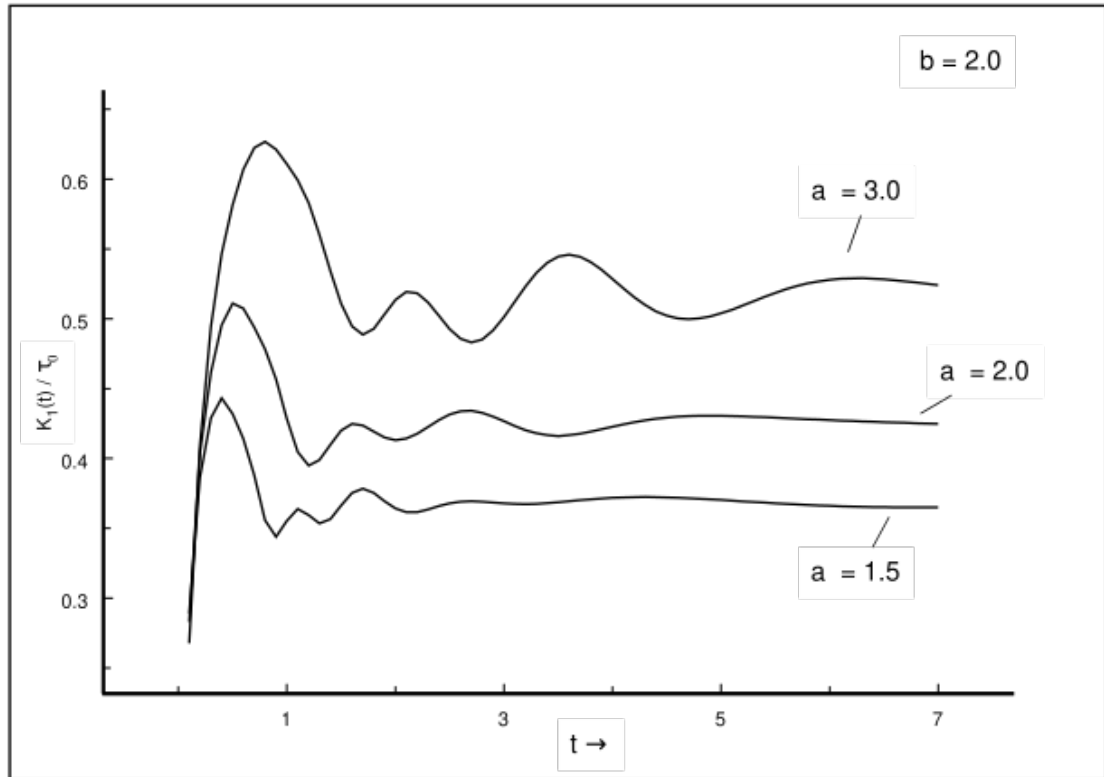


Fig.4.2 Normalized stress intensity factor against time t for set-I materials (b = 2.0)



**Fig.4.3** Normalized stress intensity factor against time  $t$  for set-II materials ( $b = 2.0$ )

With the help of Equation (4.58), the Equation (4.59) becomes

$$K_1^*(p) = \frac{2\sqrt{2a}\sigma_0}{3\pi G_4} \frac{\phi(1,p)}{p}. \quad (4.60)$$

Applying Laplace inversion method, the expression of  $K_1(t)$  has been obtained as

$$K_1(t) = \frac{2\sqrt{2a}}{3\pi G_4} \frac{\sigma_0}{2\pi i} \int_{Br} \frac{\phi(1,p)}{p} e^{pt} dp, \quad (4.61)$$

where  $Br$  is denoted by Bromwich contour.

• Numerical Results and Discussions

The Equation (4.53) has been solved to obtain  $\phi(1, p)$  by the Fox and Goodwin numerical method (1953). After solving the integral Equation (4.53), Zakian Algorithm (1969, 1970) has been used for the Laplace inversion of (4.61) to find the stress intensity factor  $K_1(t)$  at the crack rim considering two dissimilar set of composite material. Then, the value of  $K_1(t)/\sigma_0$  has been displayed along time  $t$  for several values of  $a$  and  $b$ . We considered the numerical values of material constants for two sets of composite material as listed in Tables 4.1 and 4.2 [D. Roylance (1995)].

**Table 4.1. Elastic constants**

Set I	Name of the material	$\rho$ (Density, $Mg/m^3$ )	$\mu$ (Shear Modulus)
Type-I	Aluminum alloy (7075-T6)	2.7	28
Type-II	Brass (70Cu30Zn, annealed)	8.4	39
Type-III	Nickel alloys	8.5	70

**Table 4.2. Elastic constants**

Set II	Name of the material	$\rho$ (Density, $Mg/m^3$ )	$\mu$ (Shear Modulus)
Type-I	Brass (70Cu30Zn, annealed)	8.4	39
Type-II	Aluminum alloy (7075-T6)	2.7	28
Type-III	Nickel alloys	8.5	70

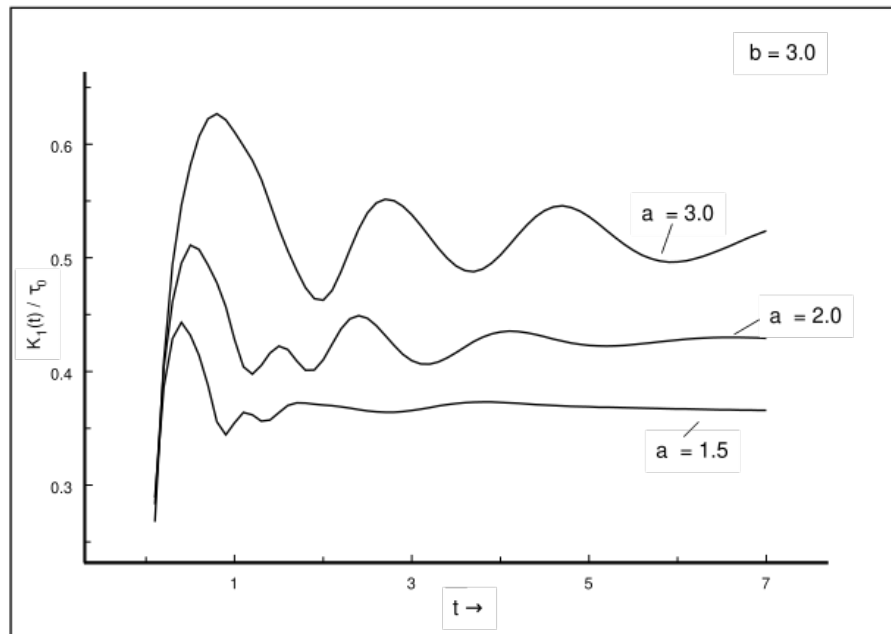


Fig.4.4 Normalized stress intensity factor against time  $t$  for set-I materials ( $b = 3.0$ )

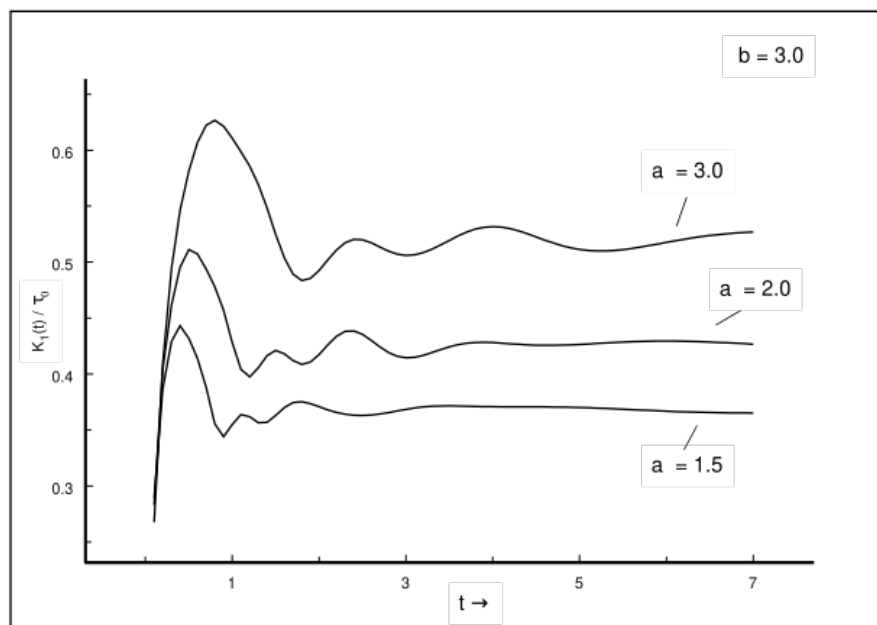


Fig.4.5 Normalized stress intensity factor against time  $t$  for set-II materials ( $b = 3.0$ )

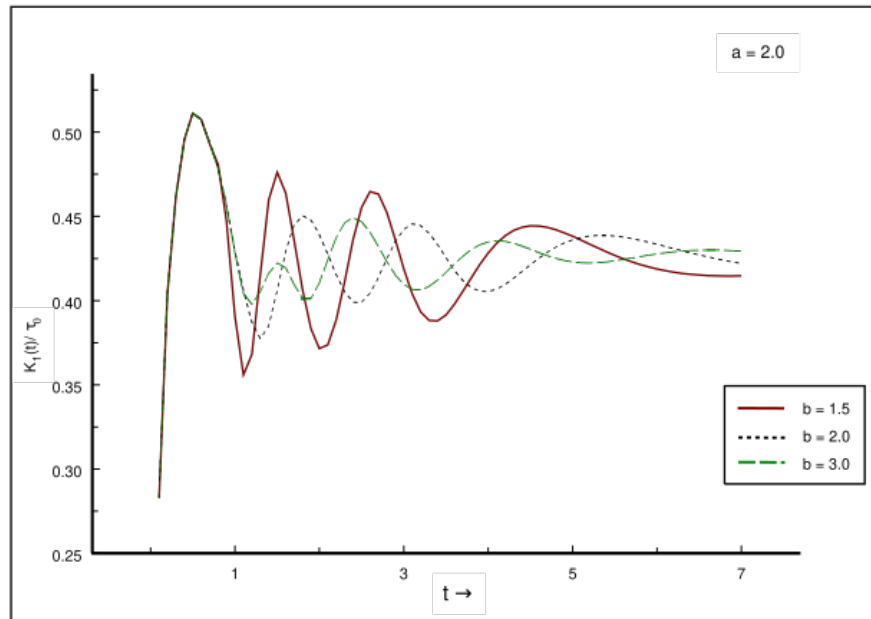


Fig.4.6 Normalized stress intensity factor against time  $t$  for set-I materials ( $a = 2.0$ )

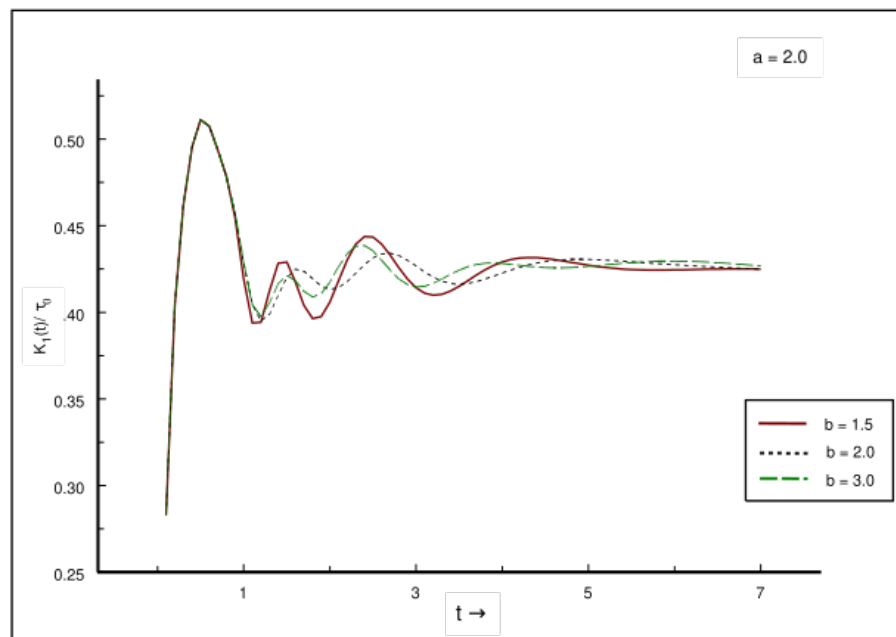


Fig.4.7 Normalized stress intensity factor against time  $t$  for set-II materials ( $a = 2.0$ )

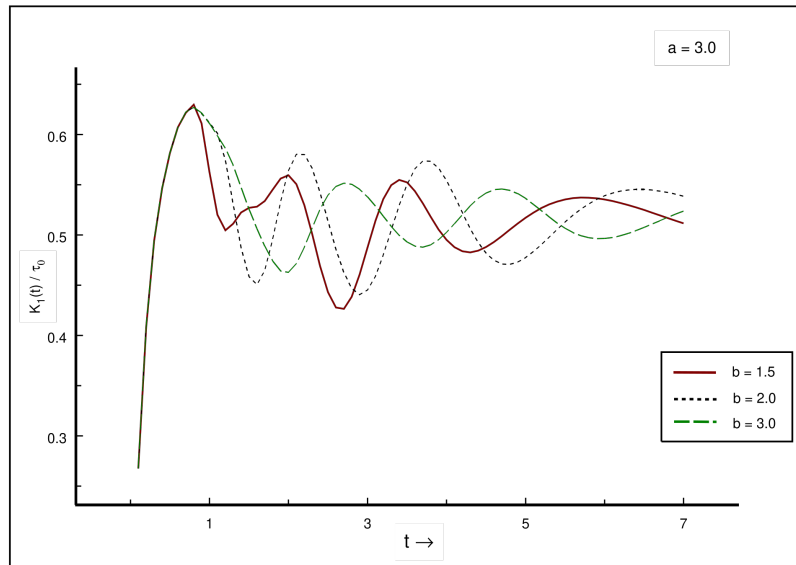


Fig.4.8 Normalized stress intensity factor against time  $t$  for set-I materials ( $a = 3.0$ )

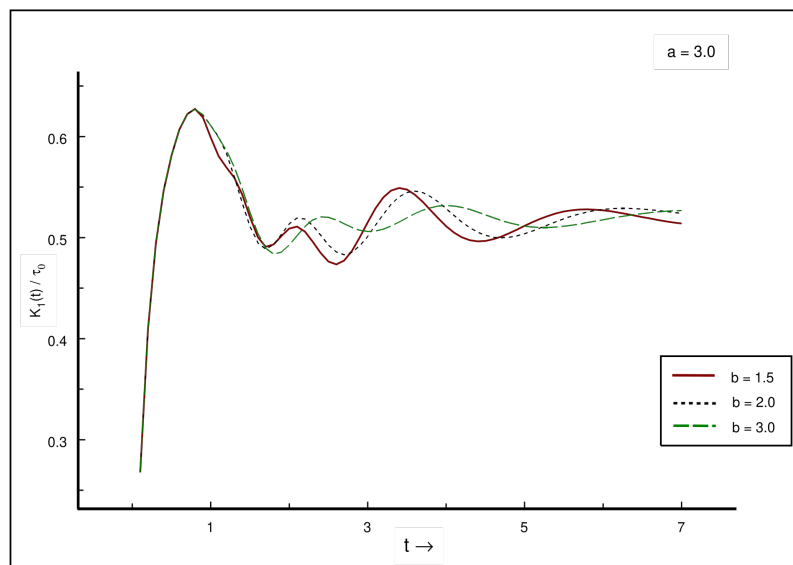


Fig.4.9 Normalized stress intensity factor against time  $t$  for set-II materials ( $a = 3.0$ )

In Figs.(4.2) and (4.4),  $K_1(t)/\sigma_0$  has been plotted against  $t$  for set - I materials and in Figs.(4.3) and (4.5) for set - II materials taking several crack radius  $a$  (1.5, 2.0, 3.0) and thickness of layer  $b$  (2.0, 3.0). Again,  $K_1(t)/\sigma_0$  has been plotted against  $t$  in Figs.(4.6) and (4.8) for set-I materials and in Figs.(4.7) and (4.9). for set-II materials for different layer thickness  $b$  (1.5, 2.0, 3.0) for the crack radius  $a = 2.0$  and  $a = 3.0$ . As  $t$  increases, SIF value first increases and reaches its maximum value nearly at  $t=0.5$ , then decreases to its minimum value close to  $t=1.0$ , then reveals wave-like behavior and finally decreases with time  $t$ . In case of set-I materials, it is found SIF to be more wavy than set-II materials. It is also seen that for fixed  $b$ , SIF is higher for higher value of crack radius  $a$  (Figs.4.2 – 4.5).

If the system of equilibrium is disturbed by applying sudden torsion, then it reaches to maximum angular displacement with respect to equilibrium position. At that moment, due to this displacement an internally developed reacting force act on the material for which it move opposite direction to that of the initial position and then again it moves to the other extreme due to inertia. Here, it is clearly identified that at first, there is a raise in SIF values reaching to its peak value, which later on, diminishes with time  $t$  revealing damped oscillation. This nature of SIF helps to prevent the crack in solid to propagate. In the case concerning set-II materials, elastic limit of those materials is higher than set-I materials. It can be concluded that set-II materials is elastically harder than the other.

## • Conclusions

A penny-shaped crack sandwiched between two different isotropic layers embedded in an isotropic medium, whose propagation is arrested by calculating SIF at the crack tip, is the main objective for this investigation. Dynamic fractures develop when stress waves and crack interact which are seriously impeded by experimental measurement techniques because of its inherent time dependency and it is enormously difficult to measure the quantities of interest without interfering with the process being observed here. This model of experiment can be further used in the study of strength of these type of composite materials.



## *Chapter-5*

*Torsional wave propagation on a penny-shaped crack in an orthotropic layer sandwiched between two rigid discs bonded by an orthotropic elastic half-space*

# Chapter 5

## Torsional wave propagation on a penny-shaped crack in an orthotropic layer sandwiched between two rigid discs bonded by an orthotropic elastic half-space

- **Introduction**

An orthotropic material is one with material properties that differ from each other along three rotationally symmetric axes which are mutually orthogonal. High anisotropy of these materials with nine elastic constants are very useful in fabrication process. Continued works [AA. Lukyanov (2010), Swain (2017), Nath and Afsar (2009)] have been carried out upon modeling wave propagation through layered orthotropic materials for application in fields of non-destructive evaluation such as geophysics, aircraft engineering, aerospace engineering, acoustics, civil engineering etc. In fracture analysis, the response of layered composites having cracks and inclusion is highly influenced by the orthotropic anisotropy. Our main objective is to resist the stress initiated by controlling a physical quantity named as stress intensity factor. In this context, taking a look at orthotropic layered structures with

---

Published in Waves in Random and Complex Media, 2022, DOI:10.1080/17455030.2022.2132315.

the presence of cracks and inclusion reveals an emerging area of research in designing engineering structures and machines.

A wide variety of analytical and closed-form solutions for different wave propagation including torsion in various anisotropic layered systems have been discussed by many researchers such as Kumari and Sharma (2014), Chattopadhyay (2013), Guillen-Rujano (2021), Kumari et al. (2015), Alam et al. (2018), Alvarez and Bisagni (2020)]. The study of impact of torsional load on several axisymmetric crack within orthotropic strip coated FGM orthotropic was proposed by Bagherpoor and Pourseifi (2022) using the distributed dislocation technique. Effected by a twisting load, displacement of crack within a half-space surface was reported by Skalsky et al. (2013) applying the Fourier transformation technique. Investigation regarding stresses associated with torsional study of cracks in circular bars with a piezoelectric coating and surface cracks in semi-elliptical form within a cylindrical bar due to pure tension through closed form is presented in papers by Hassani and Faal (2016) and Ramezani et al. (2022) respectively. Trivedi et al. (2022) determined SIF for an edge crack influenced by time harmonic wave in orthotropic strip and orthotropic vertical semi-infinite strip utilizing Fourier transformation and Schmidh method.

Among the problems related to multilayered anisotropic media, Wang et al. (2000) studied stress behaviour regarding interface crack in the shape of a penny caused by the action of dynamic torsional load on different layers made of orthotropic media. The impact due to torsion near a penny-shaped crack has been considered within a strip made of transversely isotropic material by Feng and Zou (2003). Here, the nature of stress around the crack rim has been derived employing Bessel function concerning asymptotic behavior. The impact of a sudden load caused by torsion upon a penny-shaped crack within a isotropic layer bonded by two another elastic half-space was considered by Basu and Mandal (2016). Erdogan and Arin (1972) analyzed axially symmetric elastostatic problem for a penny-shaped interface crack between an elastic layer and half-space. Stress intensity factors have been determined for a interfaced crack in the shape of a penny within two different half-space (transversely isotropic) bonded with each other by Saxena and Dhaliwal (1990). In all the pieces of literature mentioned above, for the purpose of obtaining the solution, mainly employing Hankel transforms, the mixed boundary type problems were converted to dual integral equations first and then transformed to the reduction to

second kind integral equations of Fredholm type. Behaviour of stress around a crack in the form a penny was evaluated by Lee and Tran (2010), by Ueda et al. (1984) in a layered composite under the torsional impact, by Li and Weng (2002) within an FGM interlayer between two different half-spaces subject to torsional impact load, by Saxena et al. (1993) for two dissimilar bonded elastic layers subjected to axially symmetric torsion.

Several studies were carried out to examine the effects of stresses arised within composites due to subsurface disk-shaped torsion (mode-III type) cracks by V. Bohdanov (2015), around two coaxial cylindrical cracks by S. Itou (2013). Here, tensile stress is applied to cracks in normal direction. Based on interaction integral method, the SIFs for circular arc-shaped cracks in orthotropic nonhomogeneous media is derived by Yu and Wang (2019).

Recently, Madani and Kebli (2019), first implemented the torsional wave propagation in a composite media with two rigid discs and a cracked isotropic layer. Based on the study above, in the context of applications of composite materials [Afsar et al. (2008)] such as orthotropic laminates, the above types of problems may provide a basis for designing layered composite structures. In many actual-world situations like impresser and turbine disks, various pipes where the geometry type and pressure are axially symmetric, composite materials have faced several types of waves and disturbances.

Also, in the field of engineering foundation, various shapes of inclusion as circular, strip, rectangular, and other types have been used to make the desired foundation. To get a high level of mechanical performance like high-stiffness, lightweight phenomena, flexibility, durability, etc, orthotropic materials are designed multi-directinal laminates by combining two or more materials. So, orthotropic solids may be considered as composite material. In composite materials, crack-like flaws may be initiated during the manufacturing process. In light of this, the stress behavior of orthotropic composites influenced by torsional wave attains a significant field of research in geomechanics as well as applied mechanics. This communication aims to illustrate the nature of stress on geometric parameters of the assumed model for torsional wave propagation.

In what follows, the present article derives fracture analysis of composite orthotropic medium with penny-shaped crack and two circular discs subjected to the axisymmetric torsional response. The geometry of the orthotropic composite is modeled based on a layer with finite depth bonded by two dissimilar orthotropic half-spaces. Hankel transform technique was utilized to obtain a set of pair of integral equations. With help of Abel's transform technique, the set of integral equations were expressed in terms of Fredholm integral equations of the second kind. The integral equations are solved numerically by applying the Simpson quadrature formula to compute the stress intensity factors (SIFs) near the rims of the crack and discs. Stress intensity factors (SIFs) have been computed considering material constants of two different orthotropic materials as the layer ( $L_1$ ) and the half-spaces ( $L_2$ ) and charted graphically. The graphs reveal that the material non-homogeneity, disc size, crack size, and layer depth have a significant influence on SIFs. The study can serve as a guideline in controlling failure mechanisms, failure propagation, fracture toughness, and the overall stress-strain behavior of composite materials. It is possible to use the conclusions obtained as a guide to engineering practice by comparing the hardness against failure revealed by orthotropic solids.

### • Formulation of the Elasticity Problem

Schematic illustration (Fig.5.1) of a crack (radius  $h_1$ ) shaped like a penny is taken into account in an orthotropic layer ( $L_1$ ) of thickness  $2d$  where the media have a symmetry along the  $z$ -axis. The orthotropic layer ( $L_1$ ) and half-space ( $L_2$ ) are connected by two rigid discs. Two rigid discs having radius  $h_2$  are symmetrically placed between the layer ( $L_1$ ) and half-space ( $L_2$ ) in the planes  $z = \pm d$  and are twisted by the axisymmetric torsion. The coordinate system in cylindrical polar form  $(r, \theta, z)$  yield displacement components showing a form similar to that below:

$$u_r = 0, \quad u_\theta = u_\theta(r, z), \quad u_z = 0.$$

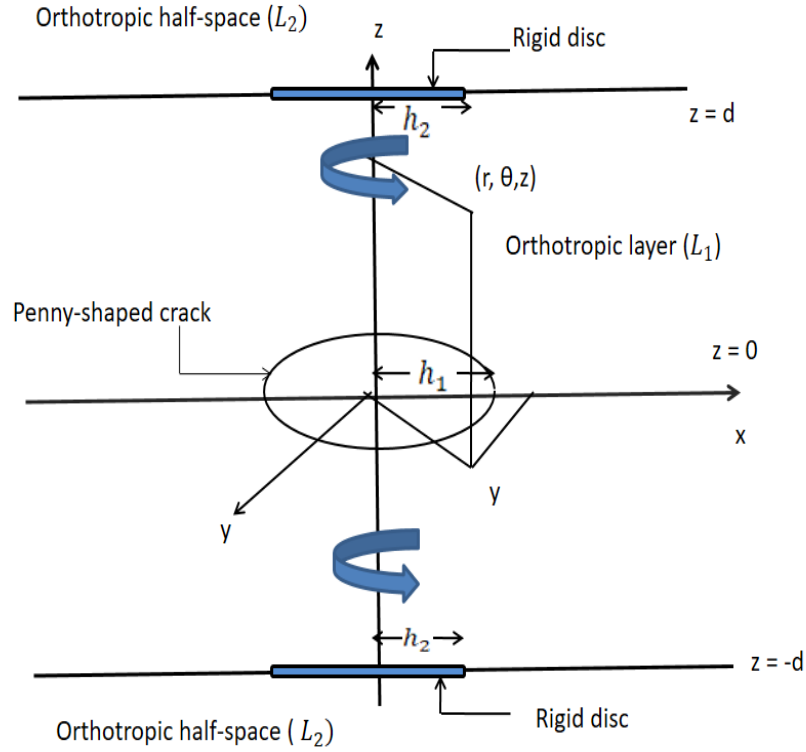


**Fig.5.1 Geometry and notation of the problem**

The governing wave equation concerning orthotropic material [Hassani et al. (2018)] takes the form

$$\frac{\partial^2 u_\theta^{(j)}}{\partial r^2} + \frac{1}{r} \frac{\partial u_\theta^{(j)}}{\partial r} - \frac{u_\theta^{(j)}}{r^2} + C^{(j)} \frac{\partial^2 u_\theta^{(j)}}{\partial z^2} = 0 \quad (j = 1, 2). \quad (5.1)$$

where  $C^{(j)} = \frac{C_{44}^{(j)}}{C_{66}^{(j)}}$ , and  $C_{44}^{(j)}, C_{66}^{(j)}$  are orthotropic shear moduli in the radial and circumferential direction. Throughout the manuscript, superscripts "1", "2" have been used to refer sandwiched orthotropic layer ( $L_1$ ), orthotropic half-space ( $L_2$ ),

respectively. The nonzero component of stress tensor can be expressed as follows:

$$\begin{aligned}\sigma_{\theta r}^{(j)} &= C_{66}^{(j)} \left( \frac{\partial u_{\theta}^{(j)}}{\partial r} - \frac{u_{\theta}^{(j)}}{r} \right), \\ \sigma_{\theta z}^{(j)} &= C_{44}^{(j)} \left( \frac{\partial u_{\theta}^{(j)}}{\partial z} \right).\end{aligned}$$

The regularity conditions at infinity are

$$\begin{aligned}\lim_{r,z \rightarrow \infty} u_{\theta}^{(j)}(r, z) &= 0, \\ \lim_{r,z \rightarrow \infty} \sigma_{\theta z}^{(j)}(r, z) &= 0.\end{aligned}\tag{5.2}$$

The boundary conditions regarding the formulated problem can be stated as:

$$\sigma_{\theta z}^{(1)}(r, 0^+) = 0, \quad 0 \leq r \leq h_1,\tag{5.3}$$

$$u_{\theta}^{(1)}(r, 0^+) = 0, \quad r > h_1,\tag{5.4}$$

$$u_{\theta}^{(1)}(r, d^-) = u_{\theta}^{(2)}(r, d^+) = \omega r, \quad 0 \leq r \leq h_2.\tag{5.5}$$

Also, the interfaces  $z = \pm d$  between the rigid discs and orthotropic half-spaces are bonded perfectly. So, at the interface  $z = \pm d$  we find the continuity conditions as

$$\sigma_{\theta z}^{(1)}(r, d^-) = \sigma_{\theta z}^{(2)}(r, d^+) = 0, \quad r > h_2,\tag{5.6}$$

$$u_{\theta}^{(1)}(r, d^-) = u_{\theta}^{(2)}(r, d^+) = 0, \quad r > h_2.\tag{5.7}$$

Application of the standard Hankel integral transform to the regularity condition given by Equation (5.2), the solution of Equation (5.1) for the orthotropic layer  $L_1$  ( $|z| \leq d$ ), and orthotropic half-space  $L_2$  ( $|z| \geq d$ ) can be taken as

$$u_{\theta}^{(1)}(r, z) = \int_0^{\infty} \left[ E(\zeta) e^{-\frac{\zeta z}{\sqrt{c^{(1)}}}} + F(\zeta) e^{\frac{\zeta z}{\sqrt{c^{(1)}}}} \right] J_1(\zeta r) d\zeta,\tag{5.8}$$

and

$$u_{\theta}^{(2)}(r, z) = \int_0^{\infty} \left[ G(\zeta) e^{-\frac{\zeta z}{\sqrt{c^{(2)}}}} \right] J_1(\zeta r) d\zeta,\tag{5.9}$$

where  $J_1(\cdot)$  is the first kind of Bessel function of order one and  $C^{(1)} = \frac{C_{44}^{(1)}}{C_{66}^{(1)}}$ ,  $C^{(2)} = \frac{C_{44}^{(2)}}{C_{66}^{(2)}}$ . In Equations (5.8) – (5.9),  $E(\zeta)$ ,  $F(\zeta)$ ,  $G(\zeta)$  represents unknown functions to be derived from boundary conditions. The expressions for stresses  $\tau_{\theta z}$  now becomes

$$\sigma_{\theta z}^{(1)}(r, z) = P^{(1)} \int_0^\infty \zeta \left[ -E(\zeta) e^{-\frac{\zeta z}{\sqrt{C^{(1)}}}} + F(\zeta) e^{\frac{\zeta z}{\sqrt{C^{(1)}}}} \right] J_1(\zeta r) d\zeta, \quad (5.10)$$

$$\sigma_{\theta z}^{(2)}(r, z) = -P^{(2)} \int_0^\infty \zeta \left[ G(\zeta) e^{-\frac{\zeta z}{\sqrt{C^{(2)}}}} \right] J_1(\zeta r) d\zeta, \quad (5.11)$$

where

$$P^{(1)} = \sqrt{C_{44}^{(1)} \cdot C_{66}^{(1)}}, \quad P^{(2)} = \sqrt{C_{44}^{(2)} \cdot C_{66}^{(2)}}.$$

### • Derivation of Integral Equation

Using the above expressions, the continuity condition (5.7) yields

$$G(\zeta) = E(\zeta) e^{\zeta d Q_3} + F(\zeta) e^{\zeta d Q_4}, \quad (5.12)$$

where

$$Q_3 = \frac{1}{\sqrt{C^{(2)}}} - \frac{1}{\sqrt{C^{(1)}}}, \quad Q_4 = \frac{1}{\sqrt{C^{(2)}}} + \frac{1}{\sqrt{C^{(1)}}},$$

and we derived the following set of dual integral equations utilizing boundary conditions Equation (5.3) – (5.6)

$$\int_0^\infty \zeta \left[ F(\zeta) - E(\zeta) \right] J_1(\zeta r) d\zeta = 0, \quad 0 \leq r \leq h_1, \quad (5.13)$$

$$\int_0^\infty \left[ E(\zeta) + F(\zeta) \right] J_1(\zeta r) d\zeta = 0, \quad r > h_1, \quad (5.14)$$

$$\int_0^\infty \left[ E(\zeta) e^{-\frac{\zeta d}{\sqrt{C^{(1)}}}} + F(\zeta) e^{\frac{\zeta d}{\sqrt{C^{(1)}}}} \right] J_1(\zeta r) d\zeta = \omega r, \quad 0 \leq r \leq h_2, \quad (5.15)$$



$$\int_0^{\infty} \zeta \left[ F(\zeta) e^{\frac{\zeta d}{\sqrt{c^{(1)}}}} \right] J_1(\zeta r) d\zeta = 0, \quad r > h_2. \quad (5.16)$$

The above set of dual integral equations were converted to a set of integral equations of Fredholm type incorporating two auxiliary functions  $m_1(x)$ ,  $m_2(x)$  as follows:

$$E(\zeta) + F(\zeta) = \sqrt{\zeta} \int_0^{h_1} \left[ \sqrt{x} m_1(x) \right] J_{\frac{3}{2}}(\zeta x) dx, \quad (5.17)$$

$$F(\zeta) e^{\frac{\zeta d}{\sqrt{c^{(1)}}}} = \sqrt{\zeta} \int_0^{h_2} \left[ \sqrt{x} m_2(x) \right] J_{\frac{1}{2}}(\zeta x) dx. \quad (5.18)$$

After solving the unknown functions, we get

$$\begin{aligned} E(\zeta) &= \sqrt{\zeta} \int_0^{h_1} \left[ \sqrt{x} m_1(x) \right] J_{\frac{3}{2}}(\zeta x) dx \\ &\quad - \sqrt{\zeta} e^{-\frac{\zeta d}{\sqrt{c^{(1)}}}} \int_0^{h_2} \left[ \sqrt{x} m_2(x) \right] J_{\frac{1}{2}}(\zeta x) dx, \end{aligned} \quad (5.19)$$

$$F(\zeta) = \sqrt{\zeta} e^{-\frac{\zeta d}{\sqrt{c^{(1)}}}} \int_0^{h_2} \left[ \sqrt{x} m_2(x) \right] J_{\frac{1}{2}}(\zeta x) dx. \quad (5.20)$$

Now, Equations (5.13) and (5.15) become in the following form

$$\begin{aligned} &\int_0^{h_1} \sqrt{x} m_1(x) dx \int_0^{\infty} \zeta^{\frac{3}{2}} g_1(\zeta) J_{\frac{3}{2}}(\zeta x) J_1(\zeta r) d\zeta + \\ &\int_0^{h_2} \sqrt{x} m_2(x) dx \int_0^{\infty} \zeta^{\frac{3}{2}} g_2(\zeta) J_{\frac{1}{2}}(\zeta x) J_1(\zeta r) d\zeta = 0, \quad r < h_1, \end{aligned} \quad (5.21)$$

and

$$\begin{aligned} &\int_0^{h_1} \sqrt{x} m_1(x) dx \int_0^{\infty} \zeta^{\frac{1}{2}} g_3(\zeta) J_{\frac{3}{2}}(\zeta x) J_1(\zeta r) d\zeta + \\ &\int_0^{h_2} \sqrt{x} m_2(x) dx \int_0^{\infty} \zeta^{\frac{1}{2}} g_4(\zeta) J_{\frac{1}{2}}(\zeta x) J_1(\zeta r) d\zeta = \omega r, \quad r < h_2, \end{aligned} \quad (5.22)$$

where

$$g_1(\zeta) = 1, \quad g_2(\zeta) = -2e^{-\frac{\zeta d}{\sqrt{C(1)}}},$$

$$g_3(\zeta) = e^{-\frac{\zeta d}{\sqrt{C(1)}}}, \quad g_4(\zeta) = 1 - e^{-\frac{2\zeta d}{\sqrt{C(1)}}}.$$

Using the following results

$$\int_0^\infty \zeta^{\frac{1}{2}} J_2(\zeta r) J_{\frac{3}{2}}(\zeta x) dx = \begin{cases} 0 & ; x > r, \\ \sqrt{\frac{2}{\pi}} \frac{x^{\frac{3}{2}}}{r^2 \sqrt{r^2 - x^2}} & ; x < r. \end{cases}$$

and

$$\zeta J_1(\zeta r) = \frac{1}{r^2} \frac{d}{dr} [r^2 J_2(\zeta r)],$$

the Equation (5.21) converted to Abel equation as

$$\begin{aligned} \sqrt{\frac{2}{\pi}} \int_0^r \frac{x^2 m_1(x)}{\sqrt{r^2 - x^2}} dx + r^2 \int_0^{h_1} \sqrt{x} m_1(x) dx \int_0^\infty \zeta^{\frac{1}{2}} (g_1(\zeta) - 1) J_{\frac{3}{2}}(\zeta x) J_2(\zeta r) d\zeta \\ + r^2 \int_0^{h_2} \sqrt{x} m_2(x) dx \int_0^\infty \zeta^{\frac{1}{2}} g_2(\zeta) J_{\frac{1}{2}}(\zeta x) J_2(\zeta r) d\zeta = 0, \quad r < h_1, \end{aligned} \quad (5.23)$$

which can be inverted by using Abel transform as follows

$$\begin{aligned} x^2 m_1(x) = \sqrt{\frac{2}{\pi}} \frac{d}{dx} \int_0^x \frac{r^3}{\sqrt{x^2 - r^2}} \left[ - \int_0^{h_1} \sqrt{\lambda} m_1(\lambda) d\lambda \int_0^\infty \zeta^{\frac{1}{2}} (g_1(\zeta) - 1) J_{\frac{3}{2}}(\zeta \lambda) J_2(\zeta r) d\zeta \right. \\ \left. - \int_0^{h_2} \sqrt{\lambda} m_2(\lambda) d\lambda \int_0^\infty \zeta^{\frac{1}{2}} g_2(\zeta) J_{\frac{1}{2}}(\zeta \lambda) J_2(\zeta r) d\zeta \right] dx, \quad r < h_1. \end{aligned} \quad (5.24)$$

With the help of the formula

$$\sqrt{\frac{2}{\pi}} \frac{d}{dt} \int_0^x \frac{r^3}{\sqrt{x^2 - r^2}} J_2(\zeta r) dr = \sqrt{\zeta} x^{\frac{5}{2}} J_{\frac{3}{2}}(\zeta x),$$

the Equation (5.24) is rewritten as a second kind of Fredholm integral equation in the following form

$$\begin{aligned} m_1(x) + x^{\frac{1}{2}} \int_0^{h_1} \lambda^{\frac{1}{2}} m_1(\lambda) P(x, \lambda) d\lambda + x^{\frac{1}{2}} \int_0^{h_2} \lambda^{\frac{1}{2}} m_2(\lambda) Q(x, \lambda) d\lambda \\ = 0, \quad r < h_1, \end{aligned} \quad (5.25)$$

where

$$\begin{aligned} P(x, \lambda) &= \int_0^\infty \zeta (g_1(\zeta) - 1) J_{\frac{3}{2}}(\zeta x) J_{\frac{3}{2}}(\zeta \lambda) d\zeta, \\ Q(x, \lambda) &= \int_0^\infty \zeta g_2(\zeta) J_{\frac{3}{2}}(\zeta x) J_{\frac{3}{2}}(\zeta \lambda) d\zeta. \end{aligned}$$

Following a similar type of analysis, we get another Fredholm integral equation of the second kind from Equation (5.22) as

$$\begin{aligned} m_2(x) + x^{\frac{1}{2}} \int_0^{h_1} \lambda^{\frac{1}{2}} m_1(\lambda) R(x, \lambda) d\lambda + x^{\frac{1}{2}} \int_0^{h_2} \lambda^{\frac{1}{2}} m_2(\lambda) S(x, \lambda) d\lambda \\ = \frac{4\omega}{\sqrt{2\pi}} x, \quad 0 < x < h_2, \end{aligned} \quad (5.26)$$

where

$$\begin{aligned} R(x, \lambda) &= \int_0^\infty \zeta g_3(\zeta) J_{\frac{1}{2}}(\zeta x) J_{\frac{3}{2}}(\zeta \lambda) d\zeta, \\ S(x, \lambda) &= \int_0^\infty \zeta (g_4(\zeta) - 1) J_{\frac{1}{2}}(\zeta x) J_{\frac{1}{2}}(\zeta \lambda) d\zeta. \end{aligned}$$

We then introduced dimensionless variables ( $\xi$  and  $\mu$ ) as:

$$\begin{aligned} \lambda = h_1 \xi, \quad 0 < \lambda < h_1; \quad x = h_1 \mu, \quad 0 < x < h_1; \\ \lambda = h_2 \xi, \quad 0 < \lambda < h_2; \quad x = h_2 \mu, \quad 0 < x < h_2. \end{aligned}$$

Then, Equations (5.25) and (5.26) have been multiplied by  $\frac{\sqrt{2\pi} m_1(h_1 \mu)}{4h_1 \omega}$  and

$\frac{\sqrt{2\pi}m_2(h_2\mu)}{4h_2\omega}$  respectively and rewritten in terms of the dimensionless variables to obtain the non-dimensional form:

$$\begin{aligned} M_1(x) + a^2\mu^{\frac{1}{2}} \int_0^1 \xi^{\frac{1}{2}} M_1(\xi) P(\mu, \xi) d\xi + \frac{\mu^{\frac{1}{2}}}{a^{\frac{1}{2}}} \int_0^1 \xi^{\frac{1}{2}} M_2(\xi) Q(\mu, \xi) d\xi \\ = 0, \quad \mu < 1, \end{aligned} \quad (5.27)$$

$$\begin{aligned} M_2(x) + a^{\frac{5}{2}}\mu^{\frac{1}{2}} \int_0^1 \xi^{\frac{1}{2}} M_1(\xi) R(\mu, \xi) d\xi + \mu^{\frac{1}{2}} \int_0^1 \xi^{\frac{1}{2}} M_2(\xi) S(\mu, \xi) d\xi \\ = \mu, \quad \mu < 1, \end{aligned} \quad (5.28)$$

where

$$\begin{aligned} P(\mu, \xi) &= 0, \quad Q(\mu, \xi) = \int_0^\infty \eta g_2(\eta) J_{\frac{3}{2}}(\eta a \mu) J_{\frac{1}{2}}(\eta \xi) d\eta, \\ R(\mu, \xi) &= \int_0^\infty \zeta g_3(\eta) J_{\frac{1}{2}}(\eta \mu) J_{\frac{3}{2}}(\eta a \xi) d\eta, \quad S(\mu, \xi) = \int_0^\infty \eta (g_4(\eta) - 1) J_{\frac{1}{2}}(\eta \mu) J_{\frac{1}{2}}(\eta \xi) d\eta. \end{aligned}$$

In the above system, we have used the following transformations:

$$M_1(\mu) = \frac{\sqrt{2\pi}}{4h_1\omega} m_1(h_1\mu), \quad M_2(\mu) = \frac{\sqrt{2\pi}}{4h_2\omega} m_2(h_2\mu), \quad a = \frac{h_1}{h_2}, \quad \zeta = \frac{\eta}{h_2}, \quad D = \frac{d}{h_2}.$$

### • The Solution Method of Integral Equations

The Fredholm integral Equations (5.27) and (5.28) have been solved by applying Gaussian quadrature formula. Here the interval  $[0, 1]$  has been divided into  $T$  equal sub-interval each of length  $\frac{1}{T}$ . Next, Equations (5.27) and (5.28) can be written as:

$$\begin{aligned} M_{1\alpha} + \frac{1}{T a^{\frac{1}{2}}} \mu_\alpha^{\frac{1}{2}} \sum_{\beta=1}^T (\mu_\beta^{\frac{1}{2}} M_{2\beta} Q_{\alpha\beta}) = 0, \quad \alpha, \beta = 1, 2, \dots, T \\ M_{2\alpha} + \frac{a^{\frac{5}{2}}}{T} \mu_\alpha^{\frac{1}{2}} \sum_{\beta=1}^T (\mu_\beta^{\frac{1}{2}} M_{1\beta} R_{\alpha\beta}) + \frac{1}{T} \mu_\alpha^{\frac{1}{2}} \sum_{\beta=1}^T (\mu_\beta^{\frac{1}{2}} M_{2\beta} S_{\alpha\beta}) = \mu_\alpha, \quad \alpha, \beta = 1, 2, \dots, T \end{aligned}$$

with the following notations

$$\begin{aligned}\mu &= \mu_\alpha = \frac{2\alpha - 1}{2T}, \quad \xi = \mu_\beta = \frac{2\beta - 1}{2T}, \\ M_1(\mu_\alpha) &= M_{1\alpha}, \quad M_2(\mu_\alpha) = M_{2\alpha}, \quad Q(\mu_\alpha, \mu_\beta) = Q_{\alpha\beta}, \\ R(\mu_\alpha, \mu_\beta) &= R_{\alpha\beta}, \quad S(\mu_\alpha, \mu_\beta) = S_{\alpha\beta}, \\ Q_{\alpha\beta} &= \int_0^\infty \eta g_2(\eta) J_{\frac{3}{2}}(\eta a \mu_\alpha) J_{\frac{1}{2}}(\eta \mu_\beta) d\eta, \\ R_{\alpha\beta} &= \int_0^\infty \eta g_3(\eta) J_{\frac{1}{2}}(\eta \mu_\alpha) J_{\frac{3}{2}}(\eta a \mu_\beta) d\eta, \\ S_{\alpha\beta} &= \int_0^\infty \eta (g_4(\eta) - 1)(\eta) J_{\frac{1}{2}}(\eta \mu_\alpha) J_{\frac{1}{2}}(\eta \mu_\beta) d\eta.\end{aligned}$$

Also, the unknown functions  $E(\zeta)$ ,  $F(\zeta)$ ,  $G(\zeta)$  can be approximated from Equations (5.12), (5.19), (5.20) as following for numerical computation:

$$\begin{aligned}G(\eta) &= E(\eta)e^{\eta D Q_3} + F(\eta)e^{\eta D Q_4}, \\ E(\eta) &= \frac{4h_2^2\omega}{\sqrt{2\pi T}}\eta^{\frac{1}{2}}\sum_{\alpha=1}^T \mu_\alpha^{\frac{1}{2}} \left[ a^{\frac{5}{2}} M_{1\alpha} J_{\frac{3}{2}}(\eta a \mu_\alpha) - e^{-\frac{\eta D}{\sqrt{c^{(1)}}}} M_{2\alpha} J_{\frac{1}{2}}(\eta \mu_\alpha) \right], \\ F(\eta) &= \frac{4h_2^2\omega}{\sqrt{2\pi T}}\eta^{\frac{1}{2}}e^{-\frac{\eta D}{\sqrt{c^{(1)}}}} \sum_{\alpha=1}^T \left[ \mu_\alpha^{\frac{1}{2}} M_{2\alpha} J_{\frac{1}{2}}(\eta \mu_\alpha) \right].\end{aligned}$$

## • Quantities of Physical Interest

The stress intensity factors (SIFs) near the vicinity of the crack and near the rim of the disc can be illustrated as follows:

$$K_{h_1} = \lim_{r \rightarrow h_1^+} \sqrt{2\pi(r - h_1)} \sigma_{\theta z}^{(1)}(r, z)|_{z=0}, \quad (5.29)$$

$$K_{h_2} = \lim_{r \rightarrow h_2^-} \sqrt{2\pi(h_2 - r)} \sigma_{\theta z}^{(1)}(r, z)|_{z=d}. \quad (5.30)$$

From Equation (5.10), the expression of stress across the plane  $z = 0$  for  $r \geq h_1$  and  $z = d$  becomes

$$\begin{aligned}\sigma_{\theta z}^{(1)}(r, 0) &= P^{(1)} \int_0^\infty \zeta^{\frac{3}{2}} \left[ - \int_0^{h_1} x^{\frac{1}{2}} m_1(x) J_{\frac{3}{2}}(\zeta x) dx + \right. \\ &\quad \left. 2e^{\frac{-\zeta d}{\sqrt{c^{(1)}}}} \int_0^{h_2} x^{\frac{1}{2}} m_2(x) J_{\frac{1}{2}}(\zeta x) dx \right] J_1(\zeta x) d\zeta, \quad (5.31)\end{aligned}$$

$$\begin{aligned} \sigma_{\theta z}^{(1)}(r, d) = & P^{(1)} \int_0^\infty \zeta^{\frac{3}{2}} \left[ -e^{\frac{-\zeta d}{\sqrt{c^{(1)}}}} \int_0^{h_1} x^{\frac{1}{2}} m_1(x) J_{\frac{3}{2}}(\zeta x) dx + \right. \\ & \left. (1 + e^{\frac{-2\zeta d}{\sqrt{c^{(1)}}}}) \int_0^{h_2} x^{\frac{1}{2}} m_2(x) J_{\frac{1}{2}}(\zeta x) dx \right] J_1(\zeta r) d\zeta. \end{aligned} \quad (5.32)$$

Using the following relation,

$$J_1(\zeta r) = -\frac{1}{\zeta} \frac{d}{dr} J_0(\zeta r),$$

we obtain

$$\begin{aligned} \sigma_{\theta z}^{(1)}(r, 0) = & P^{(1)} \int_0^{h_1} x^{\frac{1}{2}} m_1(x) dx \int_0^\infty \zeta^{\frac{1}{2}} J_{\frac{3}{2}}(\zeta x) J_0(\zeta r) d\zeta + \\ & 2P^{(1)} \int_0^{h_2} x^{\frac{1}{2}} m_2(x) dx \int_0^\infty \zeta^{\frac{3}{2}} e^{\frac{-\zeta d}{\sqrt{c^{(1)}}}} J_{\frac{1}{2}}(\zeta x) J_1(\zeta r) d\zeta, \end{aligned} \quad (5.33)$$

$$\begin{aligned} \sigma_{\theta z}^{(1)}(r, d) = & -P^{(1)} \int_0^{h_2} x^{\frac{1}{2}} m_2(x) dx \int_0^\infty \zeta^{\frac{1}{2}} J_{\frac{1}{2}}(\zeta x) J_0(\zeta r) d\zeta - P^{(1)} \int_0^{h_1} x^{\frac{1}{2}} m_1(x) dx \\ & \int_0^\infty \zeta^{\frac{3}{2}} e^{\frac{-\zeta d}{\sqrt{c^{(1)}}}} J_1(\zeta r) d\zeta + P^{(1)} \int_0^{h_2} x^{\frac{1}{2}} m_2(x) dx \int_0^\infty \zeta^{\frac{3}{2}} e^{\frac{-2\zeta d}{\sqrt{c^{(1)}}}} J_{\frac{1}{2}}(\zeta x) J_1(\zeta r) d\zeta. \end{aligned} \quad (5.34)$$

Based on the the formula  $J_\nu(\zeta) \simeq \sqrt{\frac{2}{\pi\zeta}} \cos(\zeta - \frac{\pi\nu}{2} - \frac{\pi}{4})$  for asymptotic behaviour of the first kind of Bessel function for large values of  $\zeta$ , we get the relations as

$$\begin{aligned} J_{\frac{3}{2}}(\zeta x) & \simeq \sqrt{\frac{2}{\pi\zeta x}} \cos(\zeta x - \pi) = -\sqrt{\frac{2}{\pi\zeta x}} \cos(\zeta x), \\ J_{\frac{1}{2}}(\zeta x) & \simeq \sqrt{\frac{2}{\pi\zeta x}} \cos(\zeta x - \frac{\pi}{2}) = -\sqrt{\frac{2}{\pi\zeta x}} \sin(\zeta x). \end{aligned}$$

Next, we use the following integral formula

$$\begin{aligned} \int_0^\infty \cos(\zeta x) J_0(\zeta r) d\zeta & = \begin{cases} 0 & , \quad r < x, \\ \frac{1}{\sqrt{r^2 - x^2}} & , \quad r > x. \end{cases} \\ \text{and } \int_0^\infty \sin(\zeta x) J_0(\zeta r) d\zeta & = \begin{cases} 0 & , \quad r > x, \\ \frac{1}{\sqrt{x^2 - r^2}} & , \quad r < x. \end{cases} \end{aligned}$$

to get

$$\sigma_{\theta z}^{(1)}(r, 0) = -\sqrt{\frac{2}{\pi}} P^{(1)} \frac{d}{dr} \int_0^{h_1} \frac{m_1(x)}{\sqrt{r^2 - x^2}} dx + \chi_1(r), \quad (5.35)$$

$$\sigma_{\theta z}^{(1)}(r, d) = -\sqrt{\frac{2}{\pi}} P^{(1)} \frac{d}{dr} \int_0^{h_2} \frac{m_2(x)}{\sqrt{x^2 - r^2}} dx + \chi_2(r), \quad (5.36)$$

where

$$\begin{aligned} \chi_1(r) &= 2P^{(1)} \int_0^{h_2} x^{\frac{1}{2}} m_2(x) dx \int_0^\infty \zeta^{\frac{3}{2}} e^{\frac{-\zeta d}{\sqrt{c^{(1)}}}} J_{\frac{1}{2}}(\zeta x) J_1(\zeta r) d\zeta, \\ \chi_2(r) &= -P^{(1)} \int_0^{h_1} x^{\frac{1}{2}} m_1(x) dx \int_0^\infty \zeta^{\frac{3}{2}} e^{\frac{-\zeta d}{\sqrt{c^{(1)}}}} J_1(\zeta r) d\zeta + \\ &P^{(1)} \int_0^{h_2} x^{\frac{1}{2}} m_2(x) dx \int_0^\infty \zeta^{\frac{3}{2}} e^{\frac{-2\zeta d}{\sqrt{c^{(1)}}}} J_{\frac{1}{2}}(\zeta x) J_1(\zeta r) d\zeta. \end{aligned}$$

Then, we obtain by integrating

$$\sigma_{\theta z}^{(1)}(r, 0) = -\sqrt{\frac{2}{\pi}} P^{(1)} \left[ \frac{h_1 m_1(h_1)}{r \sqrt{r^2 - h_1^2}} - \int_0^{h_1} \frac{x m_1'(x)}{r \sqrt{r^2 - x^2}} dx \right] + \chi_1(r), \quad (5.37)$$

$$\sigma_{\theta z}^{(1)}(r, d) = -\sqrt{\frac{2}{\pi}} P^{(1)} \left[ \frac{h_2 m_2(h_2)}{r \sqrt{h_2^2 - r^2}} - \int_r^{h_2} \frac{x m_2'(x)}{r \sqrt{x^2 - r^2}} dx \right] + \chi_2(r). \quad (5.38)$$

So, SIFs at  $r = h_1$  and  $r = h_2$  can be written as

$$K_{h_1} = \lim_{r \rightarrow h_1^+} \sqrt{2\pi(r - h_1)} P^{(1)} \sqrt{\frac{2}{\pi}} \left( \frac{h_1 m_1(h_1)}{r \sqrt{r^2 - h_1^2}} \right), \quad (5.39)$$

$$K_{h_2} = \lim_{r \rightarrow h_2^+} \sqrt{2\pi(h_2 - r)} P^{(1)} \sqrt{\frac{2}{\pi}} \left( \frac{h_2 m_2(h_2)}{r \sqrt{h_1^2 - r^2}} \right). \quad (5.40)$$

Next, applying the transformations

$$m_1(h_1) = \frac{4h_1\omega}{\sqrt{2\pi}} M_{1T} \quad \text{and} \quad m_2(h_2) = \frac{4h_2\omega}{\sqrt{2\pi}} M_{2T},$$

we can write

$$K_{h_1} = \frac{4\omega P^{(1)}\sqrt{h_1}}{\sqrt{\pi}} M_{1T}, \quad (5.41)$$

$$K_{h_2} = \frac{4\omega P^{(1)}\sqrt{h_2}}{\sqrt{\pi}} M_{2T}. \quad (5.42)$$

## • Numerical and Graphical Demonstration

To explain the theoretical results graphically, numerical values of the SIFs are calculated near the edge concerning the penny-shaped crack and near the rim of circular disc from Equations (5.41) and (5.42) respectively. We use here Gaussian quadrature rule and the numerical computations are performed by using MATLAB software. We considered elastic constants and densities concerning orthotropic layer and half-space as listed in Table 5.1 [Panja and Mandal (2022)].

**Table 5.1: Elastic constants of layer ( $L_1$ ) and half-space ( $L_2$ )**

Elastic medium	$C_{44}(GPA \text{ unit})$	$C_{66}(GPA \text{ unit})$	$\rho(kg/m^3)$
Orthotropic layer ( $L_1$ )	5.35	6.47	3400
Orthotropic half-space ( $L_2$ )	4.35	5.0	9890



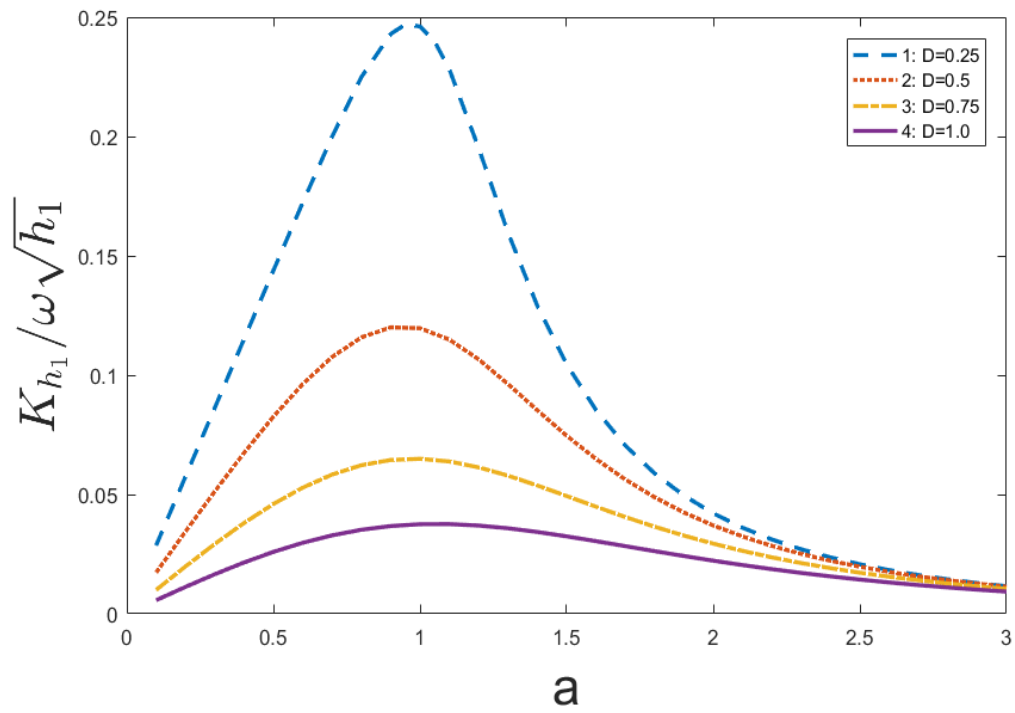


Fig.5.2 SIF as a function of the ratio of  $h_1/h_2 = a$  for crack

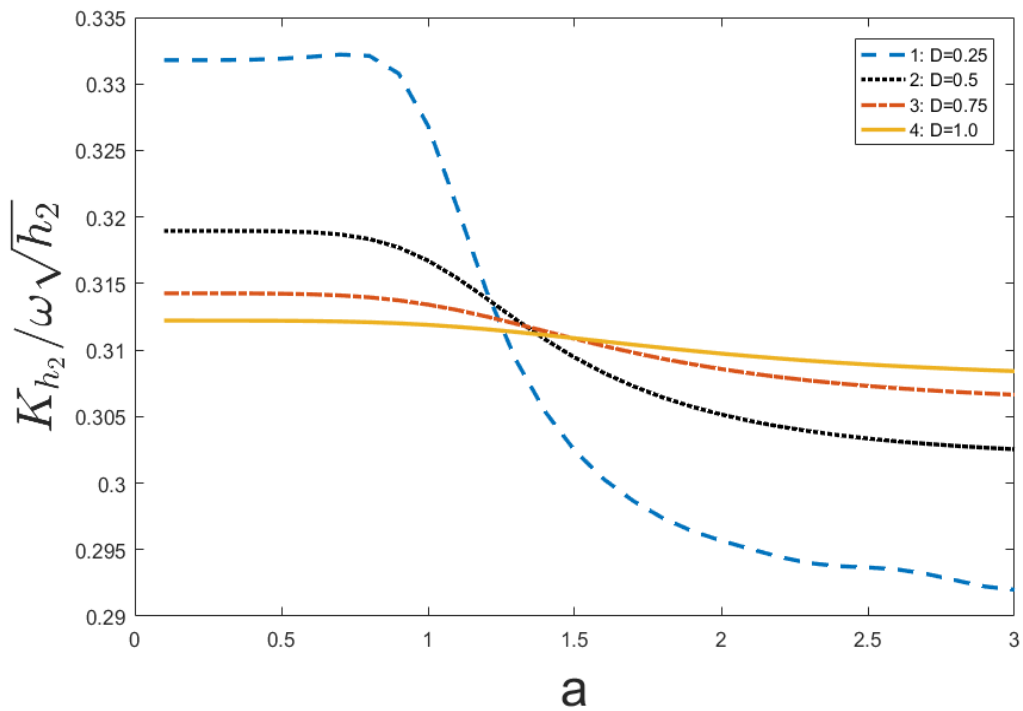


Fig.5.3 SIF as a function of the ratio of  $h_1/h_2 = a$  for circular disc

In this section, numerical values of normalized SIFs along with the ratio of crack radius  $h_1$ , to radius  $h_2$  of disc (i.e.  $a = h_1/h_2$ ) are displayed through graphical demonstrations as shown in Figs.5.2 – 5.3. In order to explore the effect of normalized layer depth ( $D = d/h_2$ ) on SIFs, four values of layer depth, namely  $D = 0.25, 0.50, 0.75, 1.0$  has been considered.

From Fig.5.2, it can be observed that the depth of the orthotropic layer has significant effects on the normalized SIFs for the penny-shaped crack. Considering any values of the ratio ' $a$ ', it seems that with the decrease of layer depth ( $D$ ), the peak SIFs will increase gradually. Also, it is seen that the curve of SIFs gradually increases first, attains to peak value at  $a = 1.0$ , and then decreases with an increase of the ratio ' $a$ '.

In Fig.5.3, The SIFs at the rim of circular discs versus the ratio  $a$  of the crack radius with disc radius has been depicted. Here, the ratio  $a$  have a revealing influence on the values of SIFs, in which a rise in this ratio leads to a lower value of SIF. Furthermore, like Fig.5.2, this figure suggests that the peak value of SIF increases when layer depth  $D$  decreases.

Based on Figs.5.2 – 5.3, we may conclude that the values of SIFs variate in large scale for large values of ' $a$ ' than those of the smaller values. Lastly, the highest value regarding SIFs may be increased or diminished with change of the layer depth (i.e. the width between the circular disc and penny-shaped crack). Within engineering solids, it has been seen that onset of fracture occurs when the numerical values of SIFs cross a certain limit (depending on material anisotropy) named as critical SIFs. Our main objective in fracture analysis of composite medium is to prevent the crack propagation to avoid damage of solid structure by controlling the values of SIFs within a certain range called critical SIFs. In this regard, these results indicate that by modifying crack and disc size ( $a$ ) and layer depth ( $D$ ), the magnitude of SIFs can be controlled which is expected in fracture mechanics for safe structure. Therefore, the analysis can help us in studying the fracture toughness of composite orthotropic bodies with cracks and inclusion under stress.

Now, the outcomes of the problem have been compared with reference to current available literature [Madani and Kebli (2019)] for isotropic material. Axisymmetric torsion applied upon an internally cracked isotropic medium with 2 embedded rigid

discs have been investigated by Madani and Kebli (2019). The presented model was formulated for a cracked orthotropic layer with two rigid discs bonded by the layer and half-spaces under axially symmetric torsion. To verify our results with an isotropic case, we substitute  $C_{44} = C_{66} = \mu$  ( $\mu$  is shear modulus of the isotropic medium) to convert the problem of orthotropic medium to isotropic medium. The following expressions of stress and governing partial differential equation have been obtained

$$\begin{aligned}\sigma_{\theta r}^{(j)} &= \mu^{(j)} \left( \frac{\partial u_{\theta}^{(j)}}{\partial r} - \frac{u_{\theta}^{(j)}}{r} \right), \\ \sigma_{\theta z}^{(j)} &= \mu^{(j)} \left( \frac{\partial u_{\theta}^{(j)}}{\partial z} \right).\end{aligned}\tag{5.43}$$

$$\frac{\partial^2 u_{\theta}^{(j)}}{\partial r^2} + \frac{1}{r} \frac{\partial u_{\theta}^{(j)}}{\partial r} - \frac{u_{\theta}^{(j)}}{r^2} + C^{(j)} \frac{\partial^2 u_{\theta}^{(j)}}{\partial z^2} = 0 \quad (j = 1, 2).\tag{5.44}$$

In our problem, some terms have been converted to following forms which are similar to isotropic case.

$$C^{(j)} = \frac{C_{44}^{(j)}}{C_{66}^{(j)}} = \frac{\mu^{(j)}}{\mu^{(j)}} = 1, \quad P^{(1)} = \mu^{(1)}, \quad P^{(2)} = \mu^{(2)}.$$

Finally, the forms of SIF near the crack rim and disc rim become

$$K_{h_1} = \frac{4\omega\mu^{(1)}\sqrt{h_1}}{\sqrt{\pi}} M_{1T},\tag{5.45}$$

$$K_{h_2} = \frac{4\omega\mu^{(1)}\sqrt{h_2}}{\sqrt{\pi}} M_{2T}.\tag{5.46}$$

The expressions stated above and Equations (5.43), (5.44), (5.45), (5.46) are exactly the same as that expressions and equations (1), (2), (56), (57) respectively of the work of Madani and Kebli (2019) for isotropic case. Similar expressions can be found in all the other expressions. Therefore, according to Madani and Kebli (2019), our results are consistent.

- **Conclusion**

In this research, the problem was formulated for a cracked orthotropic layer with two rigid discs bonded by the layer and dissimilar orthotropic half-spaces under axially symmetric torsion. Hankel transform was employed to obtain a set of dual integral equation. Further, the set of dual integral equations has been converted into a pair of second kind integral equations of Fredholm type by virtue of Abel's transforms and appropriate integral formula. Finally, to unfold the impact of layer depth and normalized disc size on SIFs, numerical implementations have been carried out using a quadrature rule and expressed through graphical presentation.

It has been observed that the SIFs diminish with the increase of layer depth i.e. the distance of crack and disc. Also, the curve of SIFs shows a wave like nature and decreases as the ratio disc radius to crack radius increases and gradually tends to a static value. So, we can say that SIFs values at the vicinity of crack and disc may be prevented in a specific range by changing several geometric parameters (layer depth, disc size and crack size). The technology of layered composites has experienced a significant development in the field of structural design, process engineering, macromechanics, material characterization, and optimization. The influence of torsional waves can not be avoided to prevent damage to solids by an earthquake and many more real situations. So the present study confirms the importance of stress analysis of orthotropic composites under a torsional wave. The proposed model can provide an analytical approach of characterizing structural behavior, stress analysis, nondestructive evaluation of material integrity, and comparing the resistance of composite anisotropic bodies with cracks and inclusion against crack growth.

## *Bibliography*

## Bibliography

1. ABBAS, I. A. (2016): Finite element analysis of internal penny-shaped crack problem in an unbounded thermoelastic medium, *J. Therm. Stresses*, Vol. 39(10), pp.1171-1181.
2. ABRAHAMAS, I.D. AND LAWRIE, J.B. (2012): Scattering of flexural waves by a semi-infinite crack in an elastic plate carrying an electric current, *Math. Mech. Solids.*, Vol. 17(1), pp. 43–58.
3. ACHENBACH, J. (2012): Wave propagation in elastic solids, *Elsevier*.
4. ACHENBACH, J.D. (1976): Wave propagation, elastodynamic stress intensity factors and fracture, *Theoretical and Applied Mechanics*, ed. W.T. Koiter, *Proc. 14th IUTAM congress, North -Holland publishing co., Amsterdam*.
5. AFSAR, A., DEB NATH, S., AHMED, S.R. AND SONG, J. (2008): Displacement potential based finite difference solution to elastic field in a cantilever beam of orthotropic composite, *Mech. Adv. Mater. Struct.*, Vol. 15(5), pp. 386-399.
6. AHMAD, F., ABBASSI, F., PARK, M.K. AND J.-W. HONG, J.-W. (2019): Numerical investigation to evaluate effect of fiber orientation on penetration-resistance of an aircraft composite material, *Mech. Adv. Mater. Struct.*, Vol. 26(19), pp. 1613–1621.
7. AIZIKOVICH, S.M., GALYBIN, A.N., and KRENEV, L.I. (2015): Semi-analytical solution for mode I penny-shaped crack in a soft inhomogeneous layer, *Int. J. Solids Struct.*, Vol. 53, pp. 129-137.
8. ALAM, P., KUNDU, S., GUPTA, S. AND SAHA, A. (2018): Study of torsional wave in a poroelastic medium sandwiched between a layer and a half-space of

- heterogeneous dry sandy media, *Waves Random Complex Media*, Vol. 28(1), pp. 182-201.
9. ÁLVAREZ, J.G. AND BISAGNI, C. (2020): Closed-form solutions for thermomechanical buckling of orthotropic composite plates, *Compos. Struct.*, Vol. 233, p. 111622.
  10. ANDERSON, T.L. (2017): Fracture Mechanics: Fundamentals and Applications, *Fourth Edition (4th ed.)*, CRC Press, <https://doi.org/10.1201/9781315370293>.
  11. ANGEL, Y.C. and ACHENBACH, J.D. (1985): Reflection and transmission of elastic waves by a periodical array of cracks, *J. Appl. Mech.*, Vol. 52, pp. 33-41.
  12. ATKINSON, C. AND POPELAR, C.H. (1979): Antiplane dynamic crack propagation in a viscoelastic strip, *J. Mech. Phys. Solids.*, Vol. 27(5), pp. 431-439.
  13. ASADI, E., FARIBORZ, S.J. AND FOTUHI, A.R. (2012): Anti-plane analysis of orthotropic strips with defects and imperfect fgm coating, *Eur. J. Mech. A Solids.*, Vol. 34, pp. 12-20.
  14. AYATOLLAHI, M. AND FARIBORZ, S. (2009): Antiplane elastodynamic analysis of a strip weakened by multiple defects, *Appl. Math. Modell.*, Vol. 33(7), pp. 3258-3268.
  15. AYATOLLAHI, M., FAAL, R. AND TARKIAN, O. (2012): Anti-plane analysis of an orthotropic strip weakened by several moving cracks, *Appl. Math. Modell.*, Vol. 36(2), pp. 596-604.
  16. AYATOLLAHI, M. AND BAGHERI, R. (2013): Dynamic behavior of several cracks in functionally graded strip subjected to anti-plane time-harmonic concentrated loads, *Acta Mech. Solida Sin.*, Vol. 26(6), pp. 691-705.
  17. BAGHERI, R., AYATOLLAHI, M. AND MOUSAVI, S.M. (2016): Analytical solution of multiple moving cracks in functionally graded piezoelectric strip, *J. Appl. Math. Mech.*, Vol. 36(6), pp. 777-792.

18. BAGHERI, R. AND MONFARED, M. (2018): Magneto-electro-elastic analysis of a strip containing multiple embedded and edge cracks under transient loading, *Acta Mech.*, Vol. 229(12), pp. 4895–4913.
19. BAGHERPOOR, F. AND POURSEIFI, M. (2022): Dynamic mode III stress intensity factors of multiple axisymmetric interfacial cracks in an FGM coated orthotropic layer, *Int. J. Comput. Methods. Eng.*, pp. 1-17.
20. BASAK, P. AND MANDAL, S. (2015): P-wave interaction by an asymmetric crack in an orthotropic strip, *Int. J. Appl. Comput. Math.*, Vol. 1(1), pp. 157–170.
21. BASAK, P. AND MANDAL, S. (2017): Semi-infinite moving crack in an orthotropic strip, *Int. J. Solids. Struct.*, Vol. 128, pp. 221–230.
22. BASAK, P. AND MANDAL, S. (2019): Semi-infinite moving crack between two bonded dissimilar isotropic strips, *Meccanica*, Vol. 54(6), pp. 855–871.
23. BASU, S. AND MANDAL, S.C. (2016): Impact of torsional load on a penny-shaped crack in an elastic layer sandwiched between two elastic half-spaces, *Int. J. Appl. Comput. Math.*, Vol. 2, pp. 533–543.
24. BASU, S. AND MANDAL, S. (2016): P-wave interaction with a pair of rigid strips embedded in an orthotropic strip, *J. Theor. Appl. Mech.*, Vol. 54(2), pp. 579–592.
25. BAYAT, J., AYATOLLAHI, M. AND BAGHERI, R. (2015): Fracture analysis of an orthotropic strip with imperfect piezoelectric coating containing multiple defects, *Theor. Appl. Fract. Mech.*, Vol. 77, pp. 41–49.
26. BERINCI, A. and ERDOL, R. (2004): A layered composite containing a crack in its lower layer loaded by rigid stamp, *Euro. J. Mech.A Solids*, Vol. 23(6), pp. 909-924.
27. BI, X., CHENG, J. AND CHEN, X. (2003): Moving crack for functionally graded material in an infinite length strip under antiplane shear, *Theor. Appl. Fract. Mech.*, Vol. 39(1), pp. 89–97.



28. BOHDANOV, V. (2015): Influence of initial stresses on the fracture of composite material weakened by a subsurface mode III crack, *J. Math. Sci.*, Vol. 205(5), pp. 621-634.
29. BREKHOVSKIKH, L.M. (1960): Waves in layered media, *Academic Press, New York*.
30. BROBERG, B.K. (1999): Cracks and fracture, *Academic Press, San Diego (CA)*.
31. BROWN, J.W. AND CHURCHILL, R.V. (2009): Complex Variables and Applications, 8th edn, pp. 298–299, *McGraw-Hill, New York*.
32. CHATTOPADHYAY, A., GUPTA, S., KUMARI, P. AND SHARMA, V. (2013): Torsional wave propagation in non-homogeneous layer between non-homogeneous half-spaces, *Int. J. Numer. Anal. Methods. Geomech.*, Vol. 37(10), pp. 1280-1291.
33. CHEN, E.P. (1979): Elastodynamic response of a penny-shaped crack in a cylinder of a finite radius, *Int. J. Eng. Sci.*, Vol. 17(4), pp. 379–385.
34. CHEN, S., CHEN, L. AND PAN, E. (2007): Vertical vibration of a flexible plate with rigid core on saturated ground, *J. Eng. Mech.*, Vol. 133(3), pp. 326–337.
35. CHEN, X., YUE, Z. AND WANG, S. (2022): Complete solution for the axisymmetric problem of a pennyshaped crack near and parallel to an arbitrarily graded interface in FGMs, *Int. J. Solids Struct.*, Vol. 254, p. 111849.
36. CHOI, H.J. (2018): Transient response of an edge interfacial crack in bonded dissimilar strips with a functionally graded interlayer under an antiplane shear impact, *Theor. Appl. Fract. Mech.*, Vol. 93, pp. 177–182.
37. CHOI, H.J. (2020): Transient interaction of edge interfacial cracks in bonded dissimilar strips with a functionally graded interlayer: Antiplane deformation, *Theor. Appl. Fract. Mech.*, Vol. 107, p. 102513.
38. COCHARD, A.P. and RICE, J.R. (1997): A spectral method for numerical elastodynamic fracture analysis without spatial replication of the rupture event, *J. Appl. Mech.*, Vol. 45, p. 1393.

39. CRACIUN, E. AND BARBU, L. (2015): Compact closed form solution of the incremental plane states in a pre-stressed elastic composite with an elliptical hole, *ZAMM-J. Appl. Math. Mech.*, Vol. 95(2), pp. 193-199.
40. DANIEL, I.M., ISHAI, O., DANIEL, I.M. AND DANIEL, I. (2006): Engineering mechanics of composite materials. *Oxford university press, New York*, Vol. 1994.
41. DAS, S., CHAKRABORTY, S., SRIKANTH, N. AND GUPTA, M. (2008): Symmetric edge cracks in an orthotropic strip under normal loading, *Int. J. Fract.*, Vol. 153(1), pp. 77-84.
42. DAS, A.N. AND GHOSH, M.L. (1992): Two coplanar Griffith cracks moving along the interface of two dissimilar elastic medium, *Eng. Fract. Mech.*, Vol. 41, pp. 59-69.
43. DE, J. and PATRA, B. (1990): Moving Griffith crack in an orthotropic strip, *Int. J. Eng. Sci.*, Vol. 28(8), pp. 809-819.
44. DE SARKAR, P.K. (1983): On diffraction of SH-waves by cut in non homogeneous solids, *Proc. Indian Acad. Sci. (Math. Sci.)*, Vol. 92(1), pp. 41-47.
45. DAS, S., PATRA, B. AND DEBNATH, L. (1998): Stress intensity factors for an interfacial crack between an orthotropic half-plane bonded to a dissimilar orthotropic layer with a punch, *Comput. Math. Appl.*, Vol. 35(12), pp. 27-40.
46. DING, S.H. and LI, X. (2014): The collinear crack problem for an orthotropic functionally graded coating-substrate structure, *Arch. Appl. Mech.*, Vol. 84(3), pp. 291-307.
47. DOVZHIK, M. V.(2012): Fracture of a half-space compressed along a penny-shaped crack located at a short distance from the surface, *Int. Appl. Mech.*, Vol. 48(3), pp. 294-304.
48. EASON, G. (1966): The displacements produced in an elastic half-space by a suddenly applied surface force, *J. Inst. Math. Appl.*, Vol. 2, pp. 299-326.

49. EMENOGU, N. G., NNADI, J. N. AND OGBONNA, N. (2022): Closed form solution for a semi-infinite crack moving in an infinite orthotropic material with a circular crack breaker under antiplane strain, *J. Egypt. Math. Soc.*, Vol. 30(1), pp. 1–11.
50. ERDOGAN, F. AND ARIN, K. (1972): Penny-shaped interface crack between an elastic layer and a half space, *Int. J. Eng. Sci.*, Vol. 10(2), pp. 115–125.
51. ESKANDARI-GHADI, M., FALLAHI, M. AND ARDESHIR-BEHRESTAGHI, A.(2010): Forced vertical vibration of rigid circular disc on a transversely isotropic half-space, *J. Eng. Mech.*, Vol. 136(7), pp. 913–922.
52. FAKOOR, M. AND MANAFI FARID, H. (2019): Mixed-mode I/II fracture criterion for crack initiation assessment of composite materials, *Acta Mech.*, Vol. 230(1), pp. 281–301.
53. FENG, W. AND ZOU, Z. (2003): Dynamic stress field for torsional impact of a penny-shaped crack in a transversely isotropic functional graded strip, *Int. J. Eng. Sci.*, Vol. 41(15), pp. 1729-1739.
54. FOTUHI, A.R. and FARIBORZ, S.J. (2007): Stress analysis of orthotropic planes weakened by cracks, *Appl. Math. Model.*, Vol. 31(6), pp. 1133-1148.
55. FOX, L. AND GOODWIN, E.T. (1953): The numerical solution of non-singular linear integral equations, *Phil. Trans. Series A, Mathematical and Physical Sciences*, Vol. A245(902), pp. 501–534.
56. FREUND, L.B. (1976): The analysis of elastodynamic crack tip stress fields, *Mechanics Today, ed. S. Nemat Nasser, Vol. II, Pergamon Press, New York.*
57. FREUND, L.B. (1972a): Crack propagation in an elastic solid subjected to general loading-I. Constant rate of extension, *J. Mech. Phys. Solids*, Vol. 20(3), pp. 129-140.
58. FREUND, L.B. (1972b): Crack propagation in an elastic solid subjected to general loading-II, Nonuniform rate of extension, *J. Mech. Phys. Solids*, Vol. 20(3), pp. 141-152.

59. FREUND, L.B. (1973): Crack propagation in an elastic solid subjected to general loading-III. Stress wave loading, *J. Mech. Phys. Solids*, Vol. 21(2), pp. 47-61.
60. FREUND, L.B. (1974): Crack propagation in an elastic solid subjected to general loading-IV, Obliquely incident stress pulse, *J. Mech. Phys. Solids*, Vol. 22(3), pp. 137-146.
61. FREUND, B. (1998): Dynamic fracture mechanics, *Cambridge university press*.
62. GARD, A.C. (1981): Stress distribution near periodic cracks at the interface of two bonded dissimilar orthotropic half-planes, *Int. J. Eng. Sci.*, Vol. 19(8), pp. 1101-1114.
63. GEORGIADIS, H.G. (1986): Complex variable and integral transform methods for elastodynamic solutions of cracked orthotropic strips, *Eng. Fract. Mech.*, Vol. 24(5), pp. 727-735.
64. GEORGIADIS, H.G. AND PAPADOPOULOS, G.A. (1988): Cracked orthotropic strip with clamped boundaries, *J. Appl. Math. Phys.*, Vol. 39, pp. 573-578.
65. GEUBELLE, P.H. and RICE, J.R. (1995): A spectral method for three-dimensional elastodynamic fracture processes, *J. Mech. Phys. Solids*, Vol. 43(1), pp. 1791-1824.
66. GHOSH, M.L. (1964): Disturbance in an elastic half space due to an impulsive twisting moment applied to an attached rigid circular disc, *Appl. Sci. Res.*, Vol. 14(1), pp. 31-42.
67. GILBERT, R. P. and LEE, D. S.(2015): Penny-Shaped Crack in a Poroelastic Plate, *J. Comput. Acoustics*, Vol. 23(02), p. 1550012.
68. GOU, L.C., WU and ZENG, T. (2005): The dynamic response of an edge crack in a functionally graded orthotropic strip, *Mech. Res. Commun.*, Vol. 32(4), pp. 385-400.
69. GRAFF, KARL F. (1973): Wave motion in elastic solids, *Ohio State University Press*.

70. GRIFFITH, A.A. (1920): The phenomena of rupture and flow in solids, *Phil. Trans. Roy. Soc. (London)*, Vol. A221(582-593), pp. 163-198.
71. GUILLÉN-RUJANO, R., AVILÉS, F., VIDAL-LESSO, A. AND HERNANDEZ-PEREZ, A. (2021): Closed-form solution and analysis of the plate twist test in sandwich and laminated composites, *Mech. Mater.*, Vol. 155, p. 103753.
72. GUPTA, S. AND BHENGRA, N. (2017): Implementation of finite difference approximation on the SH-wave propagation in a multilayered magnetoelastic orthotropic composite medium, *Acta. Mech.*, Vol. 228(10), pp. 3421-3444.
73. GUO, L.-C., WU, L.-Z. AND ZENG, T. (2005): The dynamic response of an edge crack in a functionally graded orthotropic strip, *Mech. Res. Commun.*, Vol. 32(4), pp. 385–400.
74. HADI HAFEZI, M., NIK ABDULLAH, N., CORREIA, J.F. AND DE JESUS, A.M. (2012): An assessment of a strain-life approach for fatigue crack growth, *Int. J. Struct. Integr.*, Vol. 3(4), pp. 344–376.
75. HANGAMIN, X., XUEFENG, Y., XIQIAO, F. AND YANG, YEH. H. (2008): Dynamic stress intensity factors of a semi-infinite crack in an orthotropic functionally graded material, *Mech. Mater.*, Vol. 40(1–2), pp. 37–47.
76. HASSANI, A., HASSANI, A. AND MONFARED, M.M. (2018): Torsional analysis of an orthotropic long cylinder weakened by multiple axisymmetric cracks, *J. Comput. Appl. Res. Mech. Eng.*, Vol. 8(1), pp. 49-60.
77. HASSANI, A. AND FAAL, R. (2016): Torsion analysis of cracked circular bars actuated by a piezoelectric coating, *Smart Mater. Struct.*, Vol. 25(12), p. 125030.
78. HE, M.Y. AND HUTCHINSON, J.W. (1981): The penny shaped crack and the plane strain crack in an infinite body of power law material, *J. Appl. Mech.*, Vol. 48, pp. 830–840.
79. HE, D., GUO, Z. AND MA, H. (2021): Penny-shaped crack simulation with a single high order smooth boundary element, *Eng. Anal. Bound. Elem.*, Vol. 124, pp. 211-220.

80. HOPKINSON, B. (1913): Discussion to paper by C.E. Inglis (see Inglis 1913), *Trans. Inst. Navel Architects*, Vol. 55, p. 232.
81. HU, K. AND LI, G. (2005): Constant moving crack in a magnetoelastic material under anti-plane shear loading, *Int. J. Solid. Struct.*, Vol. 42, pp. 2823–2835.
82. HU, K. and CHEN, Z. (2015): Mode-I crack in a magnetoelastic layer sandwiched by two elastic half-planes, *Eng. Fract. Mech.*, Vol. 134, pp. 79-94.
83. HUANG, G.Y., WANG, Y.S., and YU, S.W. (2005): Stress concentration at a penny-shaped crack in a non homogeneous medium under torsion, *Acta Mech.*, Vol. 180(1), pp. 107-115.
84. HUANG, K.-X., SHUI, G.-S., WANG, Y.-Z. AND WANG, Y.-S. (2021): Elastic wave scattering by a pair of parallel semi-infinite cracks in mechanical metamaterials with multi resonators, *Int. J. Fract.*, Vol. 232(2), pp. 199–212.
85. HUANG, Y. AND WANG, X. (2022): On the fracture toughness testing for single-edge notched bend specimen of orthotropic materials, *Compos. Struct.*, Vol. 281, pp. 114970.
86. HUDSON, J. A. (1980): The excitation and propagation of elastic waves, *Cambridge University Press, Cambridge*.
87. ING, Y.-S AND MA, C.-C. (2003): Dynamic fracture analysis of finite cracks by horizontally polarized shear waves in anisotropic solids, *J. Mech. Phys. Solids.*, Vol. 51(11-12), pp. 1987–2021.
88. IRWIN, G.R. (1957): Analysis of stresses and strain near the end of the crack traversing a plate, *J. Appl. Mech.*, Vol. 24, p. 361.
89. ITOU, S. (2001): Transient dynamic stress intensity factors around a crack in a nonhomogeneous interfacial layer between two dissimilar elastic half-planes, *Int. J. Solids Struct.*, Vol. 38, pp. 3631–3645.
90. ITOU, S. (2012): Stress intensity factors for two parallel interface cracks between a nonhomogeneous bonding layer and two dissimilar orthotropic half-planes under tension, *Int. J. Fract.*, Vol. 175(2), pp. 187-192.

91. ITOU, S. (2013): Stress intensity factors around two coaxial cylindrical cracks in composite materials, *Mech. Adv. Mater. Struct.*, Vol. 20(9), pp. 721-729.
92. JIN, B., SOH, A.K. AND ZHONG, Z. (2003): Propagation of an anti-plane moving crack in a functionally graded piezoelectric strip, *Arch. Appl. Mech.*, Vol. 73, pp. 252-260.
93. JUNLIN, LI. AND SHAOQIN, Z. (2010): Fracture analysis of semi-infinite interface crack between two dissimilar orthotropic composite materials, *Key. Eng. Mater.*, Vol. 417-418, pp. 429-432.
94. KADIOĞLU, F.S. (2005): Edge crack in a transversely isotropic hollow cylinder, *Eng. Fract. Mech.*, Vol. 72(14), pp. 2159-2173.
95. KANNINEN, M.F. (1978): A critical appraisal of solution techniques in dynamic fracture mechanics, Numerical Methods in Fracture Mechanics, ed. A.R. Luxmoore and D.R.J. Owen. *University College of Swansea, U.K.*
96. KARAN, S., MANDAL, P., BASU, S. AND MANDAL, S.C. (2021): Interaction of shear waves with semiinfinite moving crack inside of a orthotropic media, *Waves Random and Complex Media*, pp. 1-17.
97. KASSIR, M.K. AND BREGMAN, A.M. (1972): The stress-intensity factor for a penny-shaped crack between two dissimilar materials, *J. Appl. Mech.*, Vol. 39(1), pp. 308-310.
98. KAW, A.K. (2006): Mechanics of composite materials. 2nd ed., *CRC Press, London, Taylor and Francis Group*, ISBN NO.- 978-0-8493-1343-1.
99. KEBLI, B., BERKANE, S. AND GUERRACHE, F.(2020): An axisymmetric torsion problem of an elastic layer on a rigid circular base, *J. Solid Mech.*, Vol. 12(1), pp. 204-218.
100. KEBLI, B. AND MADANI, F. (2020): The reissner-sagoci problem for an interfacial crack in an elastic bilayer medium under torsion of an embedded rigid circular disc, *Theor. Appl. Fract. Mech.*, Vol. 110, p. 102825.
101. KEER, L.M., JABALI, H.H. AND CHANTARAMUNGKORN, K. (1974): Torsional oscillation of a layer bonded to an elastic half-space, *Int. J. Solids Struct.*, Vol. 10(1), pp. 1-13.

102. KNAUSS, W.H. (1966): Stresses in an infinite strip containing a semi-finite crack, *J. Appl. Mech.*, Vol. 33(2), pp. 356–362.
103. KNOPS, R. and PAYNE, L.E. (1971): Uniqueness theorems in linear elasticity, Springer-verlag, New York.
104. KOLSKY, H. (1963): Stress waves in solids, *Dover publications, Inc. New York*.
105. KOSTROV, B.V. (1966): Unsteady propagation of longitudinal shear cracks, *Appl. Math. Mech.*, Vol. 30, p. 1241. English translation from PMM, Vol. 30, p. 1042.
106. KOUSIOUNELOS, P.N. AND WILLIAMS, JR. J.H. (1982): Dyanamic fracture of unidirectional graphite fiber composite strips, *Int. J. Fract.*, Vol. 20(1), pp. 47–63.
107. KUMARI, P. AND SHARMA, V. (2014): Propagation of torsional waves in a viscoelastic layer over an inhomogeneous half space, *Acta Mech.*, Vol. 225(6), pp. 1673-1684.
108. KUMARI, P., SHARMA, V. AND MODI, C. (2015): Propagation of torsional waves in an inhomogeneous layer sandwiched between inhomogeneous semi-infinite strata, *J. Eng. Math.*, Vol. 90(1), pp. 1-11.
109. KUNA, M. (2013): Finite Elements in Fracture Mechanics Theory-Numerics-Applications, *Springer*.
110. KUNDU, T. (2008): Fundamentals of Fracture Mechanics, *CRC Press, Boca Raton*.
111. LEE, K.H. (2000): Stress and displacement fields for propagating the crack along the interface of dissimilar orthotropic materials under dynamic mode I and mode II load, *J. Appl. Mech.*, Vol. 67(1), pp. 223–228.
112. LEE, D.-S. (2013) : Penny-shaped crack in a plate of finite thickness subjected to a uniform shearing stress, *Z. Angew. Math. Phys.*, Vol. 64, pp. 361–369.



113. LEE, H.K., TRAN, X.H.(2010): On stress analysis for a penny-shaped crack interacting with inclusions and voids, *Int. J. Solids Struct.*, Vol. 47(5), pp. 549-558.
114. LEE, DOO-SUNG (2013): Penny-shaped crack in a plate of finite thickness subjected to a uniform shearing stress, *Z. Angew. Math. Phys.*, Vol. 64(2), pp. 361- 369.
115. LEKHINISKII, S.G. (1963): Theory of elasticity of an Anisotropic Elastic Body, *Holden-Day, San Francisco*.
116. LEKHINISKII, S.G. (1963): Theory of Elasticity of an Anisotropic Elastic Body, *Holden-Day, San Francisco*.
117. LI, Q., RICOEUR, A., KUNA, M. (2011): Coulomb traction on a penny-shaped crack in a three dimensional piezoelectric body, *Arch. Appl. Mech.*, Vol. 81(6), pp. 685 - 700 .
118. LI, X.F. (2001): Closed-form solution for a mode-III interface crack between two bonded dissimilar elastic layers, *Int. J. Fract.*, Vol. 109(2), pp. 3–8.
119. LI, C. AND WENG, G.J. (2002): Dynamic fracture analysis for a penny-shaped crack in an FGM interlayer between dissimilar half spaces, *Math. Mech. Solids*, Vol. 7(2), pp. 149–163.
120. LI, X.-F. (2003): Closed-form solution for two collinear mode-iii cracks in an orthotropic elastic strip of finite width, *Mech. Res. Commun.*, Vol. 30(4), pp. 365–370.
121. LI, X.-F. (2005): Two perfectly-bonded dissimilar orthotropic strips with an interfacial crack normal to the boundaries, *Appl. Math. Comput.*, Vol. 163(2), pp. 961–975.
122. LI, L., ZHOU, Z.-G.AND WANG, B. (2006): Scattering of anti-plane shear waves in a functionally graded material strip with an off-center vertical crack, *Appl. Math. Mecha.*, Vol. 27(6), pp. 731–739.
123. LI, C., ZOU, Z. AND DUAN, Z. (1999): Torsional impact of transversely isotropic solid with functionally graded shear moduli and a penny-shaped crack, *Theor. Appl. Fract. Mech.*, Vol. 32(3), pp. 157-163.

124. LI, P.-D., LI, X.-Y., KANG, G.-Z. AND MÜLLER, R. (2017): Three-dimensional fundamental solution of a penny-shaped crack in an infinite thermo-magneto-electro-elastic medium with transverse isotropy, *Int. J. Mech. Sci.*, Vol. 130, pp. 203–220.
125. LÜ, N., CHENG, J. AND CHENG, Y. (2001): Mode III interface crack propagation in two joined media with weak dissimilarity and strong orthotropy, *Theor. Appl. Fract. Mech.*, Vol. 36(3), pp. 219–231.
126. LÜ, N.-C., CHENG, Y.-H., WANG, Y.-T. AND CHENG, J. (2011): Fracture dynamics problems of orthotropic solids under anti-plane shear loading, *Nonlinear Dyn.*, Vol. 63(4), pp. 793–806.
127. LUKYANOV, A.A. (2010): Modeling shock waves in composite materials, *Mech. Adv. Mater. Struct.*, Vol. 17(5), pp. 304-312.
128. MA, L., WU, L. AND GUO, L. (2005): On the moving griffith crack in a nonhomogeneous orthotropic strip, *Int. J. Fract.*, Vol. 136(1), pp. 187–205.
129. MADANI, F. AND KEBLI, B. (2019): Axisymmetric torsion of an elastic layer sandwiched between two elastic half-spaces with two interfaced cracks, *Stud. Geotech. Mech.*, Vol. 41(2), pp. 57-66.
130. MAHMOODI, E., MALEKZADEH, P. AND MOHEBPOUR, S.R. (2022): Dynamic torsional analysis of a functionally graded coated circular shafts weakened by multiple radial cracks, *Theor. Appl. Fract. Mech.*, Vol. 121, pp. 103493.
131. MALITS, P.(2020): Torsion of a cracked elastic body by an embedded semi-infinite rigid cylinder, *Z. fur Angew. Math. Phys.*, Vol. 71(1), pp. 1–19.
132. MANDAL, P. (2020): Moving semi-infinite mode - III crack inside the semi-infinite elastic media, *J. Theor. Appl. Mech.*, Vol. 58(3), pp. 649-659.
133. MANDAL, P. AND MANDAL, S.C. (2021): Sh-waves interaction with crack at orthotropic interface, *Waves Random and Complex Media*, Vol. 31(6), pp. 2074–2088.

134. MANDAL, S.C. and GHOSH, M.L. (1993): Diffraction of torsional elastic waves by rigid annular disk at a bimaterial interface, *Eng. Trans.*, Vol. 41(1), pp. 97-116.
135. MANDAL, S.C. and GHOSH, M.L. (1994): Interaction of elastic waves with a periodic array of coplanar Griffith cracks in an orthotropic elastic medium, *Int. J. Eng. Sci.*, Vol. 32(1), pp. 167-178.
136. MANNA, S.K., GOSH, S. AND MANDAL, S.C. (2003): Torsional oscillation of rigid disk in an infinite cylinder, *J. Tech. Phys.*, Vol. 44(4), pp. 341-347.
137. MATBULY, M.S. (2008): Analysis of mode-III crack perpendicular to the interface between two dissimilar strips, *Acta Mech. Sin.*, Vol. 24(4), pp. 433-438.
138. MATYSIAK, S.J. and PAUK, V.J. (2003): Edge crack in an elastic layer resting on Winkler foundation, *Eng. Fract. Mech.*, Vol. 70(17), pp. 2353-2361.
139. MCCLINTOCK, F.A. AND SUKHATME, S.P. (1960): Travelling cracks in elastic material under longitudinal shear, *J. Mech. Phys. Solids.*, Vol. 8(3), pp. 187-193.
140. MENSHYKOV, O. V., Menshykov, V.A., Guz, I.A. (2008): The contact problem for an open penny-shaped crack under normally incident tension-compression wave, *Eng. Fract. Mech.*, Vol. 75(5), pp. 1114-1126.
141. MENSHYKOV, O., MENSHYKOVA, M. AND GUZ, I.(2020): Contact problems for cracks under impact loading, *Procedia Struct. Integr.*, Vol. 28, pp. 1621-1628.
142. MENSHYKOV, O.V., MENSHYKOV, V.A. AND GUZ, I.A. (2008): The contact problem for an open penny-shaped crack under normally incident tension-compression wave, *Eng. Fract. Mech.*, Vol. 75(5), pp. 1114-1126.
143. MONFARED, M.M. AND AYATOLLAHI, M. (2013): Dynamic stress intensity factors of multiple cracks in an orthotropic strip with FGM coating, *Eng. Fract. Mech.*, Vol. 109, pp. 45-57.

144. MORINI, L., PICCOLROAZ, A. AND MISHURIS, G. (2014): Remarks on the energy release rate for an antiplane moving crack in couple stress elasticity, *Int. J. Solids. Struct.*, Vol. 51(18), pp. 3087–3100.
145. MORRISEY, J.W. and RICE, J.R. (1998): Crack from waves, *J. Mech. Phys. Solids*, Vol. 46(3), pp. 467-487.
146. MORTEZA, E.G., AMMAR, M., and AZIZOLLAH, A.B. (2011): Rocking vibration of a rigid circular disc in a transversely isotropic full-space, *Int. J. Numer. Anal. Methods Geomech.*, Vol. 35(14), pp. 1587-1603.
147. MOUSAVI, S. AND FARIBORZ, S. (2012): Anti-plane elastodynamic analysis of cracked graded orthotropic layers with viscous damping, *Appl. Math. Modell.*, Vol. 36(4), pp. 1626–1638.
148. MOUSAVI, S.M. AND PAAVOLA, J. (2013): Analysis of cracked functionally graded piezoelectric strip, *Int. J. Solids. Struct.*, Vol. 50(14-15), pp. 2449–2456.
149. MUNSHI, N. AND MANDAL, S.C.(2006): Diffraction of p-waves by edge crack in an infinitely long elastic strip, *JSME Int. J. A-Solid M.*, Vol. 49(1), pp. 116–122.
150. MURAKAMI, Y.(1987): Stress intensity factors, *Pergamon Books Inc., Elmsford, NY*.
151. MYKHAS'KIV, V.V., KHAY, O.M. (2009): Interaction between rigid-disc inclusion and penny-shaped crack under elastic time-harmonic wave incidence, *Int. J. Solids Struct.*, Vol. 46(3), pp. 602-616.
152. MYKHASKIV , V. AND STANKEVYCH, V. (2019): Elastodynamic problem for a layered composite with penny-shaped crack under harmonic torsion, *ZAMM-J. Appl. Math. Mech.*, Vol. 99(5), p. e201800193.
153. MYKHASKIV, V., ZHBADYNSKYI, I.Y. AND ZHANG, C.(2019): On propagation of time-harmonic elastic waves through a double-periodic array of penny-shaped cracks, *Eur. J. Mech. A Solids*, Vol. 73, pp. 306–317.

154. NAGAI, M., IKEDA, T., and MIYAZAKI, N. (2007): Stress intensity factor analysis of a three-dimensional interface crack between dissimilar anisotropic materials, *Eng. Fract. Mech.*, Vol. 74(16), pp. 2481-2497.
155. NANDI, A., BASAK, P. AND MANDAL, S. (2015): Diffraction of p-waves by edge crack in an infinite orthotropic strip, *Int. J. Appl. Comput. Math.*, Vol. 1(4), pp. 543-557.
156. NANDI, A. AND MANDAL, S. (2017): Elastodynamic response of symmetric edge cracks in an orthotropic strip, *Int. J. Appl. Comput. Math.*, Vol. 3(3), pp. 2611-2625.
157. NARITA, F. AND SHINDO, Y. (1999): Fatigue crack propagation in a piezoelectric ceramic strip subjected to mode III loading, *Acta Mech.*, Vol. 137(1), pp. 55-63.
158. NASKAR, S. AND MANDAL, S.C. (2022): Moving semi-infinite crack between dissimilar orthotropic strips, *Waves Random and Complex Media*, pp. 1-16.
159. NATH, S.D.. AND AFSAR, A. (2009): Analysis of the effect of fiber orientation on the elastic field in a stiffened orthotropic panel under uniform tension using displacement potential approach, *Mech. Adv. Mater. Struct.*, Vol. 16(4), pp. 300-307.
160. NAYFEH, A.H. (1995): Wave propagation in layered anisotropic media: With application to composites, *Elsevier*.
161. NILSSON, F. (1972): Dynamic stress-intensity factors for finite strip problems, *Int. J. Fract.*, Vol. 9(4), pp. 403-411.
162. NILSSON, F. (1973): Erratum to dynamic stress intensity factors for finite strip problems, *Int. J. Fract.*, Vol. 9(4), p. 477.
163. NOBLE, B. (1958): Methods based on the Wiener-Hopf Technique, *Pergamon Press, New York*.
164. NOURAZAR, M. AND AYATOLLAHI, M. (2016): Multiple moving interfacial cracks between two dissimilar piezoelectric layers under electromechanical loading, *Smart. Mater. Struct.*, Vol. 25(7), p. 075011.

165. OBREZANOVA, O. AND WILLIS, J.(2008): Stability of an intersonic shear crack to a perturbation of its edge, *J. Mech. Phys. Solids*, Vol. 56(1), pp. 51–69.
166. OROWON, E. (1952): Fundamental of Brittle behaviour in metals. In fatigue and Fracture of Metals, edited by W.M. Murray, *John Wiley, New York*, p. 139.
167. PANJA, S.K. AND MANDAL, S. (2021): Interaction of magnetoelastic shear waves with a griffith crack in an infinite strip, *J. Eng. Math.*, Vol. 126(1), pp. 1–11.
168. PANJA, S.K. AND MANDAL, S.C. (2022): Propagation of love wave in multilayered viscoelastic orthotropic medium with initial stress, *Waves Random Complex Media*, Vol. 32(2), pp. 1000-1017.
169. PARIHAR, K.S. and LALITHA, S. (1987): Cracks located on a single line in an orthotropic elastic medium in which body forces are acting, *Int. J. Eng. Sci.*, Vol. 25(6), pp. 735-754.
170. PARTON, V.Z. and MOROZOV, E. M. (1978): Elastic plastic fracture mechanics, *Mir Publishers. Moscow*.
171. PAYTON, R.C. (2012): Elastic wave propagation in transversely isotropic media, *Springer, Berlin*.
172. RABIEIFAR, A., POURSEIFI, M. AND DERILI, H. (2018): Transient analysis for torsional impact of multi-ple axisymmetric cracks in the functionally graded orthotropic medium, *IMA J.Appl. Math.*, Vol. 83(1), pp. 131-147.
173. RAMEZANI, M., RAMESH, S., PURBOLAKSONO, J. AND DAS, R. (2021): Closed-form solutions of stress intensity factors for semi-elliptical surface cracks in a cylindrical bar under pure tension, *Acta Mech. Solida Sin.*, pp. 1-13.
174. RICE, J.R. (1967): Discussion: stresses in an infinite strip containing a semi-infinite crack, *J. Appl. Mech.*, Vol. 34(1), pp. 248–249.
175. RICE, J.R. (1968): A path independent integral and approximate analysis of strain concentration by notches and cracks, *J. Appl. Mech.*, Vol. 35, pp. 379-386.

176. RICE, R.G. AND DO, D.D. (1995) : Applied Mathematics and Modeling for Chemical Engineers, *Wiley, New York*.
177. ROYLANCE, D. (1995): Mechanics of Materials, *Wiley, New York*.
178. ROGOWSKI, B. (2014): The analysis of A mode I conducting crack under general applied loads in piezo-electromagnetic-elastic-layer, *Int. J. Eng. Sci.*, Vol. 75, pp. 11-30.
179. SARKAR, J., GHOSH, M.L., and MANDAL, S.C. (1991): Scattering of antiplane shear wave by a propagating crack at the interface of two dissimilar elastic media, *Proc. Indian Acad. Sci. (Math. Sci.)*, Vol. 101(3), pp. 183-194.
180. SARKAR, J.K., GHOSH, M.L. AND MANDAL, S.C. (1996): Four coplanar griffith cracks moving in an infinitely long elastic strip under antiplane shear stress, *Proc. Indian. Acad. Sci. Math. Sci.*, Vol. 106(1), pp. 91–103.
181. SAXENA, H.S. AND DHALIWALA, R.S. (1990): A penny-shaped crack at the interface of two bonded dissimilar transversely isotropic elastic half-spaces, *Eng. Fract. Mech.*, Vol. 37(4), pp. 891–899.
182. SAXENA, H.S., DHALIWALA, R.S., HE, W. AND ROKNE, J.G. (1993): Penny-shaped interface crack between dissimilar nonhomogeneous elastic layers under axially symmetric torsion, *Acta Mech.*, Vol. 99(1), pp. 201–211.
183. SELVADURAI, A.P.S. (2002): Mechanics of a rigid circular disc bonded to a cracked elastic half-space, *Int. J. Solid Struct.*, Vol. 39(24), pp. 6035-6053.
184. SELVADURAI, A. AND SAMEA, P. (2021): Mechanics of a pressurized penny-shaped crack in a poroelastic halfspace, *Int. J. Eng. Sci.*, Vol. 163, p. 103472.
185. SHAIL, R. (1970): The impulsive Reissner–Sagocci problem, *J. Math. Mech.*, Vol. 19, pp. 709–716.
186. SHAH, R.C. AND KOBAYASHI, A.S. (1971): Stress intensity factor for an elliptical crack under arbitrary normal loading, *Eng. Fract. Mech.*, Vol. 3(1), pp. 71–96.

187. SHIAH, Y., HWU, C. AND YAO, J.J. (2019): Boundary element analysis of the stress intensity factors of plane interface cracks between dissimilarly adjoined anisotropic materials, *Eng. Anal. Bound.*, Vol. 106, pp. 68–74.
188. SHIBUYA, T. (1975): On the torsional impact of a thick elastic plate, *Int. J. Solids Struct.*, Vol. 11(7-8), pp. 803–811.
189. SIH, G. AND CHEN, E. (1972): Torsion of a laminar composite debonded over a penny-shaped area, *J. Franklin Inst.*, Vol. 293(4), pp. 251-261.
190. SIH, G.C. (1977): Mechanics of Fracture, *Noordhoff International Publishing, Leyden*, Vol. 4.
191. SIH, G.C. AND CHEN, E.P. (1981): Mechanics of fracture, *London: Martinus Nijhoff Publishers*, Vol. 6.
192. SINGH, B.M., ROKNE, J. AND DHALIWAL, R.S. (2008): Closed-form solutions for a mode-III moving interface crack at the interface of two bonded dissimilar orthotropic elastic layers, *Math. Probl. Eng.*, Vol. 2008, pp. 1–10.
193. SINGH, A., DAS, S., ALTENBACH, H. AND CRACIUN, E.-M. (2020): Semi-infinite moving crack in an orthotropic strip sandwiched between two identical half planes, *ZAMM-J. Appl. Math. Mech.*, Vol. 100(2), p. e201900202.
194. SKALSKY, V., STANKEVYCH, O. AND SERHIYENKO, O. (2013): Wave displacement field at a half-space surface caused by an internal crack under twisting load, *Wave Motion*, Vol. 50(2), pp. 326-333.
195. SUN, D.-L., ZHANG, X.-Y. AND LI, X.-F. (2022): Interaction of multiple parallel cracks in a prestressed orthotropic elastic plane, *Eur. J. Mech. A Solids.*, p. 104704.
196. SWAIN, A., BAAD, S. AND ROY, T. (2017): Modeling and analyses of thermo-elastic properties of radially grown carbon nanotubes-based woven fabric hybrid composite materials, *Mech. Adv. Mater. Struct.*, Vol. 24(14), pp. 1206–1220.
197. TAVANGARI, A. and N, SALEHZADEH. (2014) : Obtain the stress intensity factor in a medium containing a penny shaped crack by the Ritz method, *Int.J.of Mech. Mechatron. Eng.*, Vol. 8(9), pp. 1596-1599.



198. THOMSON, I. AND ABRAHAMAS, I.D. (2007): Diffraction of flexural waves by cracks in orthotropic thin elastic plates, Part II. Far field analysis, *Proc. R. Soc. A.*, Vol. 463(2082), pp. 1615–1638.
199. TRIVEDI, N., DAS, S. AND CRACIUN, E.-M. (2022): The mathematical study of an edge crack in two different specified models under time-harmonic wave disturbance, *Mech. Compos. Mater.*, Vol. 58(1), pp. 1-14.
200. UEDA, S., SHINDO, Y. AND ATSUMI, A. (1984): Torsional impact response of a penny-shaped interface crack in a layered composite, *Eng. Fract. Mech.*, Vol. 19(6), pp. 1095–1104.
201. VASILIEV, V.V. AND MOROZOV, E.V. (2018): Advanced mechanics Of composite materials and structures, 4th ed., *Elsevier Science, Netherlands*, ISBN NO.- 0081022093.
202. WANG, Y. (1992): Analysis of an edge-cracked body subjected to a longitudinal shear force, *Eng. Fract. Mech.*, Vol. 42(1), pp. 45–50.
203. WANG, Y., CHEUNG, Y. AND WOO, C. (1992): Anti-plane shear problem for an edge crack in a finite orthotropic plate, *Eng. Fract. Mech.*, Vol. 42(6), pp. 971–976.
204. WANG, B.L., HAN, J.C., and DU, S.Y. (1999): Functionally graded penny-shaped cracks under dynamic loading, *Theo. Appl. Fract. Mech.*, Vol. 32(3), pp. 165-175.
205. WANG, B.L., HAN, J.C., and DU, S.Y. (2000): Fracture mechanics for multilayers with penny-shaped cracks under dynamic torsional loading, *Int. J. Eng. Sci.*, Vol. 38(8), pp. 893-901.
206. WANG, B., HAN, J. AND DU, S. (2000): Fracture mechanics for multilayers with penny-shaped cracks subjected to dynamic torsional loading, *Int. J. Eng. Sci.*, Vol. 38(8), pp. 893-901.
207. WANG, C.Y., RUBIO-GONZALE, C. AND MASSON, J.J. (2001): The dynamics stress intensity factor for a semi-infinite crack in orthotropic materials with concentrated shear impact loads, *Int. J. Solids. Struct.*, Vol. 38(8), pp. 1265–1280.

208. WEIBULL, W. (1939a): A statistical theory of the strength of materials, *Proc. Royal Academy Eng. Sc.*, Vol. 15.
209. WEIBULL, W. (1939b): The phenomena of rupture and solids, *Proceedings of the Royal Swedish Institute for Engineering Research*, Vol. 153.
210. WILLIS, J. AND MOVCHAN, N. (2007): Crack front waves in an anisotropic medium, *Wave Motion*, Vol. 44(6), pp. 458–471.
211. WU, T.-H., LI, X.-Y. AND TANG, H.-P. (2021): Three-dimensional fields in an infinite transversely isotropic magneto-electro-elastic space with multiple coplanar penny-shaped cracks, *Int. J. Eng. Sci.*, Vol. 159, p. 103434.
212. WU, X.F., LILLA, E. AND ZOU, W.S. (2002): A semi-infinite interfacial crack between two bonded dissimilar elastic strips, *Arch. Appl. Mech.*, Vol. 72(8), pp. 630–636.
213. XIAO, J., SHI, C., XU, Y. AND ZHANG, F. (2016): Interface stress of orthotropic materials with a nanodefekt under antiplane shear loading, *J. Mech. Mater. Struct.*, Vol. 11(5), pp. 491–504.
214. YANG, J., JIN, X., JIN, N. (2014): A penny-shaped crack in transversely isotropic magneto-electro-thermo-elastic medium subjected to uniform symmetric heat flux, *Int. J. Solids Struct.*, Vol. 51(9), pp. 1792–1808.
215. YANG, Y., HU, Z.-L., GHARAH, A., SCHIAVONE, P. AND LI, X.-F. (2021): Torsion of an elastic medium containing a nanosized penny-shaped crack with surface effects, *Int. J. Fract.*, Vol. 231(2), pp. 189–199.
216. YANG, Y., SCHIAVONE, P. AND LI, X.-F. (2022): Torsional deformation of an infinite elastic solid weakened by a penny-shaped crack in the presence of surface elasticity and dugdale plastic zone, *Int. J. Solids Struct.*, Vol. 254, p. 111858.
217. YOFFE, E.H. (1951): The moving Griffith crack, *Philos Magaz.*, Vol. 42(330), pp. 739–750.
218. YOSIBASH, Z., OMER, N., and DAUGE, M. (2008): Edge stress intensity functions in 3-D anisotropic composites, *Compos. Sci. Technol.*, Vol. 68(5), pp. 1216–1224.

- 
219. YU, J.G., RATOLOJANAHARY, F.E. AND LEFEBVRE, J.E. (2011): Guided waves in functionally graded viscoelastic plates, *Compos. Struct.*, Vol. 93(11), p. 2674.
  220. YU, H. AND WANG, B. (2019): Stress intensity factor evaluations for a curved crack in orthotropic particulate composites using an interaction integral method, *Mech. Adv. Mater. Struct.*, Vol. 26(7), pp. 631-638.
  221. ZAKIAN, V. (1969): Numerical inversions of Laplace transforms, *Electron. Lett.*, Vol. 5(6), pp. 120–121.
  222. ZAKIAN, V. (1970): Optimization of numerical inversion of Laplace transforms, *Electron. Lett.*, Vol. 21(6), pp. 677–679.
  223. ZHANG, C. and GROSS, D. (1998): On wave propagation in elastic solids with cracks. *Int. Ser. Advances Fract.*, Vol. 2.

*List of Publications and Communicated  
Papers*

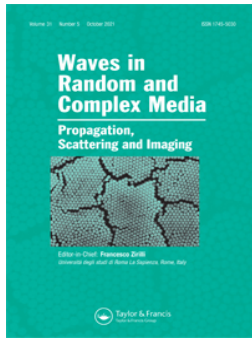
## List of Published Papers

1. Torsional wave propagation on a penny-shaped crack in an orthotropic layer sandwiched between two rigid discs bonded by an orthotropic elastic half-space. WAVES IN RANDOM AND COMPLEX MEDIA, 2022, DOI:10.1080/17455030.2022.2132315.
2. Interaction of shear wave with semi-infinite moving crack inside of a orthotropic media. WAVES IN RANDOM AND COMPLEX MEDIA, pp. 1-17, 2021, DOI:10.1080/17455030.2021.1987583.
3. Impact of torsional load on a penny-shaped crack sandwiched between two elastic layers embedded in an elastic medium. ACTA MECHANICA, Vol. 229(4), pp. 1759-1772, 2018, DOI:10.1007/s00707-017-2073-3.

## List of Communicated Papers

1. Edge crack subject to anti-plane shear wave in an orthotropic strip (INTERNATIONAL JOURNAL OF APPLIED AND COMPUTATIONAL MATHEMATICS).

\*\*\*\*\*



## Interaction of shear waves with semi-infinite moving crack inside of a orthotropic media

Somashri Karan, Palas Mandal, Sanjoy Basu & Subhas Chandra Mandal

To cite this article: Somashri Karan, Palas Mandal, Sanjoy Basu & Subhas Chandra Mandal (2021): Interaction of shear waves with semi-infinite moving crack inside of a orthotropic media, Waves in Random and Complex Media, DOI: [10.1080/17455030.2021.1987583](https://doi.org/10.1080/17455030.2021.1987583)

To link to this article: <https://doi.org/10.1080/17455030.2021.1987583>



Published online: 08 Nov 2021.



Submit your article to this journal [↗](#)



View related articles [↗](#)



View Crossmark data [↗](#)



# Interaction of shear waves with semi-infinite moving crack inside of a orthotropic media

Somashri Karan<sup>a</sup>, Palas Mandal<sup>b</sup>, Sanjoy Basu<sup>c</sup> and Subhas Chandra Mandal<sup>a</sup>

<sup>a</sup>Department of Mathematics, Jadavpur University, Kolkata, India; <sup>b</sup>Department of Aerospace Engineering, IIT Bombay, Mumbai, India; <sup>c</sup>Department of Mathematics, Arignar Anna Government Arts and Science College, Karaikal, India

## ABSTRACT

The present work investigates the motion of a semi-infinite moving crack inside a semi-infinite half-space of orthotropic medium subjected to anti-plane shear wave. The crack is located at a finite depth from the surface of semi-infinite orthotropic medium. Our aim is to examine how such anisotropy and geometric parameters can be adjusted to reduce the magnitude of stress intensity factor (SIF) to control the crack propagation near the crack tip region. As mathematical tools, Fourier transformation and inverse Fourier transformation techniques are employed to convert the governing mixed boundary value problem to the well-known Weiner-Hopf equation with suitable boundary conditions. Some physical quantities such as SIF at the crack tip and crack opening displacement (COD) around the crack tip have been derived. Graphical exhibition has been carried out to show the impact of relevant parameters such as crack velocity, layer depth from the surface to crack and orthotropic material properties on SIF and COD. The numerical results show that SIF decay with crack depth from the layer. It is also observed that SIF decreases with an increase in crack velocity and finally tends to zero as crack velocity approaches near SH-wave velocity. Also, the value of COD decays as we move along the damage near the crack tip along negative x-axis and finally tends to zero at the crack tip. This behavior of COD is consistent with the physical nature of the semi-infinite crack of the problem. The results are validated for isotropic material with some reported work and are well in agreement. The study of these physical quantities (SIF, COD) ensures the arrest of onset of crack expansion by monitoring geometric parameters and wave velocity to avoid fracture.

## ARTICLE HISTORY

Received 16 January 2021  
Accepted 22 September 2021

## KEYWORDS

Semi-infinite moving crack; orthotropic media; SH-wave; Weiner-Hopf technique; stress intensity factor; crack opening displacement

## 1. Introduction

Orthotropic material being a composite material have unique mechanical properties since they have three orthogonal planes of symmetry. Some of this material like Prepreg, Carbon fiber, Epoxy has found in high-performance structural applications such as designing of aircraft, aerospace, corrosion-resistance equipment, marine, load-bearing components for vehicles, metal and polymer-forming process [1,2]. Their rigorous anisotropic properties

**CONTACT** Sanjoy Basu  basu1982@gmail.com

in addition to the presence of moving cracks have a strong application in Seismology. Earth's interior and the geological structure near-surface are considered as a composite material formed by rocks, crystalline minerals, etc. which is highly anisotropic. When an earthquake arises, waves travel across different anisotropic parts of the earth. Earthquake sliding motion constitutes a prominent example of dynamic crack propagation in modes II, III, or in a mixed mode of II and III [3]. Semi-infinite moving crack is one of the most common failure methods in orthotropic laminates. So, it intrigued significant interest to develop methods for describing the behavior of orthotropic bodies with semi-infinite moving cracks under the influence of shear wave. Hence, this model can be utilized in the field of construction engineering, seismic engineering, geology, geophysics, and earthquake disaster prevention as well [4,5]. Only a few problems of composites with semi-infinite moving cracks under shear wave incidence have been studied due to its multitude of parameters which can effect crack propagation. So, analytical modeling of composite failure by crack propagation has become vital to ensure safe and robust structures.

The study of moving semi-infinite crack model based on Weiner-Hopf technique has been described first by Yofee [6] and the problem of a semi-infinite crack running with a constant velocity in an infinite solid had been addressed here. The solution of semi-infinite crack problem situated in an infinitely isotropic strip of finite width considering displaced clamped boundaries normal to the crack was given by Knauss [7] where Weiner-Hopf technique was employed to find stress intensity factor. Later, that work has been modified by Rice [8]. A method was proposed by Nilsson [9,10] using the Weiner-Hopf technique to solve a moving semi-infinite crack in an isotropic strip. After that, the same technique was used by Atkinson et al. [11], Georgiadis [12], Kousionelos et al. [13] in their respective solutions.

Although traveling cracks in elastic material under longitudinal wave was introduced first by McClintock et al. [14] in 1960, later in many engineering smart structures such as the couple stress elastic materials, orthotropic thin plate, elastic plate carrying an electric current, semi-infinite cracks appeared [15–17]. A mode-III crack at the interface between two dissimilar layers of equal thickness has been studied by Li [18]. Wang et al. [19] discussed the process to find dynamic SIF for a semi-infinite crack in orthotropic materials with concentrated shear impact loads. Laplace and Fourier transforms are used to reduce the problem to the solution which has been solved by the Weiner-Hopf technique to find SIF. De and Patra [20], Das and Ghosh [21], Ma et al. [22] studied the dynamic griffith crack behavior in isotropic and orthotropic elastic materials.

Wu et al. [23] introduced the analytical expression for complex SIF and energy release rate for a semi-infinite interfacial crack between two bonded dissimilar elastic strips using conformal mapping technique. Sarkar et al. [24] analyzed scattering of the antiplane shear wave by a semi-infinite crack running uniformly along with the interface of two dissimilar semi-infinite elastic media. Solving the boundary value problem with the help of Fourier transform and Weiner-Hopf technique, they found that SIF is influenced by the speed of the crack growth, the incidence angle of the incoming wave, and material properties of elastic media. An effective approach for finding stress and displacement fields along the interface of two dissimilar orthotropic mediums containing a crack moving under a dynamic mode I and mode II load has been investigated by Lee [25]. Four coplanar Griffith cracks moving in an infinite elastic strip under anti-plane shear stress has been treated by Sarkar et al. [26]. A (mode III) moving semi-infinite crack at the interface of two bonded orthotropic layers has been solved analytically by Singh et al. [27]. Hongmin et al. [28]



considered the problem of semi-infinite crack in an infinite orthotropic functionally graded material. They solved the problem for two impact loading modes, i.e. opening and in-plane shear. Basak et al. addressed the problem of semi-infinite moving crack, considering a orthotropic strip due to normally displaced boundaries. Applying Fourier transform technique the boundary value problem has been reduced to the standard Weiner-Hopf equation which has been solved in asymptotic cases to obtain the physical quantities like stress intensity factor and crack opening displacement [29]. Fracture analysis of a semi-infinite crack between two dissimilar orthotropic composite materials has been treated by Junlin et al. [30] using the composite complex function method. Different moving cracks in a piezoelectric strip and layers have been analyzed by Bagheri et al. [31] and Nourazar and Ayatollahi [32]. Propagation of anti-plane moving griffith crack was solved by Hu and Li [33] and Jin et al. [34].

In most of the above studies, the problems were assumed on anisotropic and isotropic media by different (griffith or semi-infinite) moving crack. Very recently, Mandal [35] studied the problem of moving semi-infinite mode-III crack inside the semi-infinite elastic media considering an isotropic case. To date, however, fracture analysis for the case of semi-infinite moving crack inside semi-infinite orthotropic media has not received much attention. Therefore, the focus of the present work is concentrated to find the theoretical and analytical behavior of a moving semi-infinite crack at a finite depth from the surface of a orthotropic elastic medium subjected to shear load applied on the surface. Fourier transform is used to convert the mixed boundary value problem to the solution of the well-known Weiner-Hopf equation. Further, the analytical expressions of SIF and COD by solving the Weiner-Hopf equation have been derived asymptotically. The results show that the corresponding SIF and COD are influenced by crack propagation velocity, layer width, and material constants. The study of these physical quantities (SIF, COD) ensures the arrest of propagation of crack by monitoring geometric parameters of the orthotropic material. Our prime objective is to reduce damages in buildings fracture, geophysical interpretation of seismic waves by controlling the onset of crack growth within a structure.

## 2. Formulation of the problem

We consider a horizontal semi-infinite moving crack with crack tip coincides with the origin of the moving coordinates. Let  $(X, Y, Z)$  be the fixed cartesian co-ordinates which are the axes of symmetry of the orthotropic material. Then the crack position is  $-\infty < X < 0$ ,  $Y = 0$ . We assume that the crack is propagating with a constant velocity  $V$  along the positive  $X$ -axis parallel to the surface of the semi-infinite orthotropic medium at a depth ' $d$ ' from the surface. So, at any time  $t$ , the position of the crack is  $-\infty < X < Vt$ ,  $Y = 0$  (Figure 1).

Since the crack motion is maintained under anti-plane shear mode, the displacement vector takes the form  $(0, 0, U_Z)$ . Here,  $U_Z$  is the only nonvanishing out-of-plane component of displacement in the  $Z$ -direction presented as

$$U_Z = U_Z(X, Y, t)$$

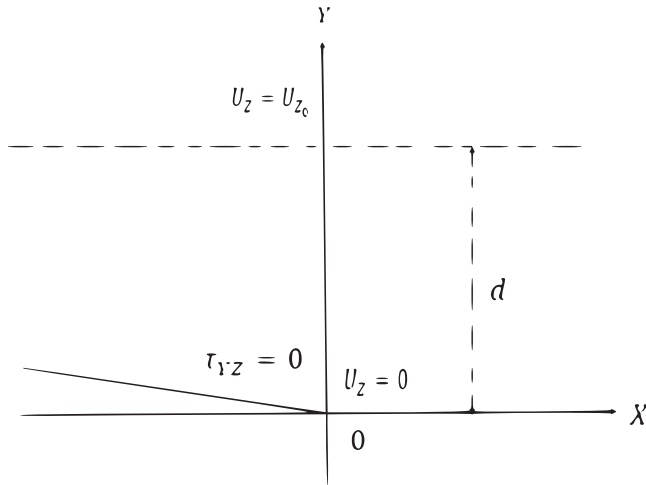


**Figure 1.** Semi-infinite crack moving inside of a semi-infinite orthotropic media.

from which relation between nonzero shear stress and displacement component for orthotropic materials (mode-III) are as follows

$$\begin{aligned}\tau_{XZ} &= C_{55} \frac{\partial U_Z}{\partial X}, \\ \tau_{YZ} &= C_{44} \frac{\partial U_Z}{\partial Y},\end{aligned}\quad (1)$$

where  $C_{44}$  and  $C_{55}$  represent the principal shear moduli directed along  $X$  and  $Y$  axes of the orthotropic material, respectively. The anti-plane equation of motion requires the gratification of the following wave equation for orthotropic medium [36],

$$C_{55} \frac{\partial^2 U_Z}{\partial X^2} + C_{44} \frac{\partial^2 U_Z}{\partial Y^2} = \rho \frac{\partial^2 U_Z}{\partial t^2} \quad (2)$$

where  $\rho$  is the material density. It is convenient to define the constant

$$\beta = \sqrt{\frac{C_{44}}{C_{55}}}$$

while the SH-wave velocity of orthotropic material designated by  $C_S$ , is

$$C_S = \sqrt{\frac{C_{55}}{\rho}}$$

so that Equation (2) can be cast into the form

$$\frac{\partial^2 U_Z}{\partial X^2} + \beta^2 \frac{\partial^2 U_Z}{\partial Y^2} = \frac{1}{C_S^2} \frac{\partial^2 U_Z}{\partial t^2} \quad (3)$$

To make the crack stationary, a moving framework  $x = X - Vt$ ,  $y = Y$  (Galilean transformation) has been introduced which reduces the number of independent variables to the

same as for static deformations. Therefore, the displacement Equation (2) in the moving coordinate system  $(x, y, z)$  become

$$G^2 \frac{\partial^2 u_z}{\partial x^2} + \frac{\partial^2 u_z}{\partial y^2} = 0 \quad (4)$$

where  $G^2 = \frac{1}{\beta^2} (1 - \frac{V^2}{C_\xi^2})$ ,  $V$  is the crack velocity, and  $u_z(x, y) = U_Z(X, Y, t)$  is the displacement along the moving coordinate  $z$ .

We may also transform the moving coordinates simply by replacing  $X$  and  $Y$  in Equations (1) by  $x$  and  $y$ , respectively, and  $U_Z$  by  $u_z$ . The mixed boundary conditions on and outside the crack for  $y = 0$  are given by

$$\tau_{yz}(x, 0) = 0, \quad x < 0 \quad (5)$$

$$u_z(x, 0) = 0, \quad x > 0 \quad (6)$$

Stress and displacement across the surface  $y = d$  are

$$\tau_{yz}(x, d) = 0, \quad -\infty < x < \infty \quad (7)$$

$$u_z(x, d) = u_{z_0}, \quad -\infty < x < \infty \quad (8)$$

where  $u_{z_0}$  is constant displacement applied at the surface boundary  $y = d$ . For applying the Weiner-Hopf technique, we consider a different set of boundary conditions by superimposing a constant load  $p_0$  in the original system which does not affect the value of SIF obtained by solving the modified problem. The new boundary conditions are (Figure 2)

$$\tau_{yz}(x, 0) = p_0, \quad x < 0 \quad (9)$$

$$u_z(x, 0) = 0, \quad x > 0 \quad (10)$$

$$\tau_{yz}(x, d) = 0, \quad -\infty < x < \infty \quad (11)$$

$$u_z(x, d) = 0, \quad -\infty < x < \infty \quad (12)$$

The above two problems are identical for a particular value of  $p_0$ . For generalized plane stress problems, the appropriate value of  $p_0$  is given by  $(-\frac{C_{44}u_{z_0}}{d})$ . The complete procedure to find the value of  $p_0$  has been elaborated in the work of Georgiadis et al. [37].

To proceed for the solution, we introduce the standard definition of complex Fourier transform pair as

$$\bar{g}(\xi, y) = \frac{1}{\sqrt{2\pi}} \int_{-\infty}^{\infty} g(x, y) e^{i\xi x} dx \quad (13)$$

and

$$g(x, y) = \frac{1}{\sqrt{2\pi}} \int_{-\infty}^{\infty} \bar{g}(\xi, y) e^{-i\xi x} d\xi \quad (14)$$

where  $\xi = \eta + i\gamma$ , is to be understood as a complex variable in the Fourier transform plane,  $\eta$  and  $\gamma$  being the real and imaginary parts of the complex variable  $\xi$ .

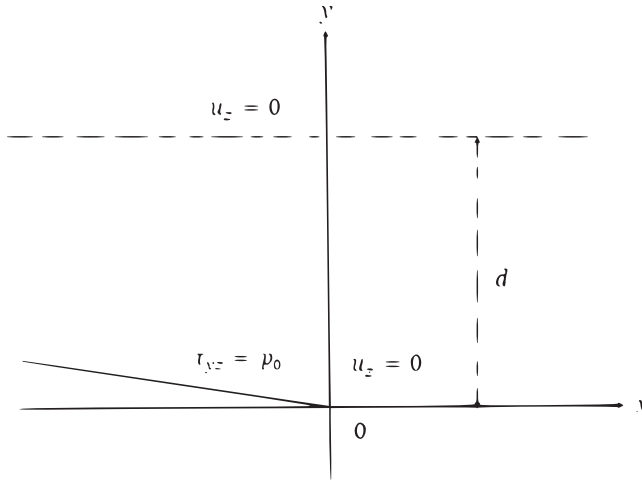


**Figure 2.** Transformed geometry of the semi-infinite crack.

According to Nilsson [10], the boundary condition (9) in lieu of constant load  $p_0$  can be written with a slight modification as follows

$$\tau_{yz}(x, 0) = p_0 e^{\delta x}, \quad x < 0 \quad (15)$$

where  $\delta > 0$ , which is a very small quantity and tending to zero.

Applying the Fourier transform, the boundary conditions 10 and 11 will become

$$\bar{\tau}_{yz}(\xi, d) = 0 \quad (16)$$

$$\bar{u}_z(\xi, d) = 0 \quad (17)$$

After applying the Fourier transform on the variable  $\xi$ , the solution of the equation of (4) is obtained as

$$\begin{aligned} \bar{u}_z(\xi, y) &= A_1(\xi) e^{-G\xi y} + A_2(\xi) e^{G\xi y}, \quad 0 \leq y \leq d \\ &= A_3(\xi) e^{G\xi y}, \quad -\infty < y \leq 0 \end{aligned} \quad (18)$$

provided that the crack velocity ( $V$ ) is less than the shear wave velocity ( $C_S$ ) of the material. Here  $\bar{u}_z(\xi, y)$  be the Fourier transform of displacement component  $u_z(x, y)$  and  $A_1(\xi)$ ,  $A_2(\xi)$ ,  $A_3(\xi)$  are unknown functions of the transformed variable  $\xi$  which are not independent.

Shear stress now becomes

$$\begin{aligned} \bar{\tau}_{yz}(\xi, y) &= C_{44} G \xi [A_2(\xi) e^{G\xi y} - A_1(\xi) e^{-G\xi y}], \quad 0 \leq y \leq d \\ &= C_{44} A_3(\xi) G \xi e^{G\xi y}, \quad -\infty < y \leq 0 \end{aligned} \quad (19)$$

### 3. Solution procedure

Let us introduce two unknown functions for determining the complete solution by Weiner-Hopf method

$$\tau_{yz}(x, 0) = r(x), \quad x > 0, \quad (20)$$

$$u_z(x, 0) = s(x), \quad x < 0, \quad (21)$$

By taking both sides fourier transformation of Equations (20) and (21), we obtain

$$\bar{r}_+(\xi) = \frac{1}{\sqrt{2\pi}} \int_0^{\infty} r(x)e^{i\xi x} dx, \quad (22)$$

$$\bar{s}_-(\xi) = \frac{1}{\sqrt{2\pi}} \int_{-\infty}^0 s(x)e^{i\xi x} dx, \quad (23)$$

where the (+) and (-) subscript denote that the functions are analytic above or bellow a certain line in the complex  $\xi - plane$ .

The functions  $\bar{r}(x)$  and  $\bar{s}(x)$  are bounded at infinity as the stress and displacements are tending to zero at infinity which is obvious from the physical nature of the problem. So we assume the following bounds

$$|\bar{r}(x)| < Rx^{-l_r}, \quad as \ x \rightarrow \infty \quad (24)$$

$$|\bar{s}(x)| < S|x|^{-l_s}, \quad as \ x \rightarrow -\infty \quad (25)$$

where  $l_r > 0$ ,  $l_s > 0$ ,  $R > 0$  and  $S > 0$ . Here  $R$  and  $S$  are finite. Now it can be shown that the functions  $\bar{r}_+(\xi)$  and  $\bar{s}_-(\xi)$  are analytic for  $\gamma \geq 0$  and  $\gamma \leq 0$ , respectively.

Making use of the boundary conditions (9)and (10) with the help of the Equations (22) and (23), we get a pair of equations as follows

$$\bar{\tau}_{yz}(\xi, 0) = \bar{r}_+(\xi) + \frac{p_0}{\sqrt{2\pi}(\delta + i\xi)} \quad (26)$$

$$\bar{u}_z(\xi, 0) = \bar{s}_-(\xi) \quad (27)$$

Now Equation (26) can be rewritten as

$$\bar{r}_+(\xi) = \bar{\tau}_{yz}(\xi, 0) - \frac{p_0}{\sqrt{2\pi}(\delta + i\xi)} \quad (28)$$

With the help of boundary condition (17), we get

$$A_2(\xi) = -A_1(\xi)e^{-2G\xi d} \quad (29)$$

At  $y = 0$ , the solutions are

$$\bar{u}_z(\xi, 0) = A_1(\xi) + A_2(\xi), \quad 0 \leq y \leq d \quad (30)$$

and

$$\bar{u}_z(\xi, 0) = A_3(\xi), \quad -\infty \leq y \leq 0 \quad (31)$$

Equation (30) in view of (27) and (29) assumes the form

$$A_1(\xi) = \frac{\bar{s}_-(\xi)}{1 - e^{-2G\xi d}} \quad (32)$$

From Equations (27) and (31), we obtain

$$A_3(\xi) = \bar{s}_-(\xi) \quad (33)$$

Substitution of the values of stress from (19) into the Equation (28) and then using (26) and (32) renders the well-known Wiener-Hopf equation of the unknown functions as  $\bar{r}_+(\xi)$  and  $\bar{s}_-(\xi)$

$$\bar{r}_+(\xi) = T(\xi)\bar{s}_-(\xi) - \frac{p_0}{\sqrt{2\pi}(\delta + i\xi)} \quad (34)$$

where the kernel  $T(\xi)$  is given by

$$T(\xi) = \frac{-C_{44}G\xi(1 + e^{-2G\xi d})}{1 - e^{-2G\xi d}} \quad (35)$$

#### 4. Solution of the Wiener-Hopf equation

In order to solve the Equation (34), it is necessary to split the kernel  $T(\xi)$  in the following form (Noble [38])

$$T(\xi) = T_+(\xi)T_-(\xi) \quad (36)$$

where the functions  $T_+(\xi)$  and  $T_-(\xi)$  both are analytic and non-zero for  $\gamma > \gamma_1$  ( $\gamma_1 < 0$ ) and  $\gamma < \gamma_2$  ( $\gamma_2 > 0$ ).

Consequently, Equation (34) by virtue of (36) becomes

$$\frac{\bar{r}_+(\xi)}{T_+(\xi)} = T_-(\xi)\bar{s}_-(\xi) - \frac{p_0}{\sqrt{2\pi}(\delta + i\xi)T_+(\xi)} \quad (37)$$

The last term of Equation (37) has been decomposed as a sum of two analytic functions given by

$$\frac{p_0}{\sqrt{2\pi}(\delta + i\xi)T_+(\xi)} = D_+(\xi) + D_-(\xi) \quad (38)$$

where the functions  $D_+(\xi)$  and  $D_-(\xi)$  can be obtained as

$$D_+(\xi) = \frac{p_0}{\sqrt{2\pi}(\delta + i\xi)} \left[ \frac{1}{T_+(\xi)} - \frac{1}{T_+(i\delta)} \right] \quad (39)$$

$$D_-(\xi) = \frac{p_0}{\sqrt{2\pi}(\delta + i\xi)T_+(i\delta)} \quad (40)$$

We have checked the analyticity of the functions  $D_+(\xi)$  and  $D_-(\xi)$  and these two functions are non-zero in  $\gamma > \gamma_1$  and  $\gamma < \delta$ , respectively. Rearranging the Equation (37), with the help of (38), we get

$$\frac{\bar{r}_+(\xi)}{T_+(\xi)} + D_+(\xi) = T_-(\xi)\bar{s}_-(\xi) - D_-(\xi) \quad (42)$$

From Equation (42), it is observed that the region of analyticity of the functions  $\bar{r}_+(\xi)$ ,  $\bar{s}_-(\xi)$ ,  $T_+(\xi)$ ,  $T_-(\xi)$ ,  $D_+(\xi)$  and  $D_-(\xi)$  are  $\gamma \geq 0$ ,  $\gamma \leq 0$ ,  $\gamma > \gamma_1$  ( $\gamma_1 < 0$ ),  $\gamma < \gamma_2$  ( $\gamma_2 > 0$ ),

$\gamma > \gamma_1$  ( $\gamma_1 < 0$ ) and  $\gamma < \delta$ , respectively. The left side and the right side of Equation (41), both are analytic at the region of the upper half-plane  $\gamma \geq 0$  and the lower half-plane  $\gamma \leq 0$  where  $\delta (> 0)$  is a very small quantity. The common part of analyticity is the line  $\gamma = 0$ . Equation (41) is analytic and single-valued in the whole complex  $\xi - plane$  by analytic continuation. By considering the large values of  $\xi$ , the functions  $T_+(\xi)$  and  $T_-(\xi)$  tend to be  $\xi^{\frac{1}{2}}$  and the functions  $\bar{r}_+(\xi)$  and  $\bar{s}_-(\xi)$  will be bounded. Now we consider both sides of the Equation (41) equal to  $F(\xi)$ . This function is analytic and the function  $F(\xi)$  is tending to  $\xi^{-\frac{1}{2}}$  for large value of  $\xi$  in the upper half-plane  $\gamma \geq 0$ . Moreover using the same arguments on the right-hand side of Equation (41) is analytic and tending to  $\xi^{\frac{1}{2}}$  for large value of  $\xi$  in the lower half-plane  $\gamma \leq 0$ . It can be culminated that the function  $F(\xi)$  is identically zero by the extended Liouville's theorem.

$$F(\xi) = 0 \quad (42)$$

Now utilizing (39)–(41), the functions of interest can be found from (42) as

$$\bar{r}_+(\xi) = \frac{p_0}{\sqrt{2\pi}(\delta + i\xi)} \left[ \frac{T_+(\xi)}{T_+(\delta)} - 1 \right] \quad (43)$$

and

$$\bar{s}_-(\xi) = \frac{p_0}{\sqrt{2\pi}(\delta + i\xi)T_+(i\delta)T_-(\xi)} \quad (44)$$

So we may take  $\delta \rightarrow 0$  for constant loading and consequently the above expressions become

$$\bar{r}_+(\xi) = \frac{p_0}{\sqrt{2\pi}i\xi} \left[ \frac{T_+(\xi)}{T_+(0)} - 1 \right] \quad (45)$$

and

$$\bar{s}_-(\xi) = \frac{p_0}{\sqrt{2\pi}i\xi T_+(0)T_-(\xi)} \quad (46)$$

Nilsson [9] introduced a process where SIF can be obtained by only knowing the values of  $T(\xi)$  for very large and small values of  $\xi$ .

After algebraic manipulation, we get the following asymptotic values of the kernel  $T(\xi)$ :

$$\lim_{\xi \rightarrow \infty} \frac{T(\xi)}{\xi} = -C_{44}G \quad (47)$$

and

$$\lim_{\xi \rightarrow 0} T(\xi) = -\frac{C_{44}}{d} \quad (48)$$

The Equations (45) and (46) can be written for large values of  $\xi$  as

$$\lim_{\xi \rightarrow \infty} \bar{r}_+(\xi) = \lim_{\xi \rightarrow \infty} \frac{p_0}{\sqrt{2\pi}iT_+(0)\xi^{\frac{1}{2}}} \frac{T_+(\xi)}{\xi^{\frac{1}{2}}} \quad (49)$$

$$\lim_{\xi \rightarrow \infty} \bar{s}_-(\xi) = \lim_{\xi \rightarrow \infty} \frac{p_0}{\sqrt{2\pi}iT_+(0)\xi^{\frac{3}{2}}} \frac{\xi^{\frac{1}{2}}}{T_-(\xi)} \quad (50)$$

Taking inverse fourier transform on (49) and (50) with the help of Equations (47) and (48), we finally obtain the following expressions for the unknown functions

$$\lim_{x \rightarrow 0^+} r(x) = -p_0 \sqrt{\frac{Gd}{\pi}} x^{-\frac{1}{2}} \quad (51)$$

$$\lim_{x \rightarrow 0^-} s(x) = -p_0 \sqrt{\frac{d}{\pi C_{44}^2 G}} (-x)^{\frac{1}{2}} \quad (52)$$

From the definition of the function  $r(x)$ , Equation (51) represents distribution of the shear stress component  $\tau_{yz}$  along the  $x$ -axis just outside the crack and the structure of the shear stress component in Equation (51) reveals a square root singularity at the crack tip which is very much expected in the field of Fracture Mechanics. Furthermore, the Equation (52) represents the displacement  $u_z$  in the vicinity of the crack tip. This quantity known as Crack Opening Displacement (COD) is also important in view of the physical nature of the crack.

## 5. Quantities of physical interest

The quantity that reveals state of stress (SIF) at the crack tip, denoted by  $K_{III}$  is defined by

$$K_{III} = \lim_{x \rightarrow 0^+} \sqrt{2\pi x} \tau_{yz}(x, 0) \quad (53)$$

In this case, the SIF can be found as

$$SIF = K_{III} = -p_0 \sqrt{2Gd} \quad (54)$$

Therefore, the SIF of the original problem (normalized with respect to  $u_{z_0}$ ) is given by

$$SIF = K_{III} = C_{44} \sqrt{\frac{2G}{d}} \quad (55)$$

Next the COD is defined by

$$COD = u_z(x, 0^+) - u_z(x, 0^-) \quad (56)$$

In this problem, the COD can be written as

$$COD = -2p_0 \sqrt{\frac{d}{\pi C_{44}^2 G}} (-x)^{\frac{1}{2}} \quad (57)$$

Therefore, COD of the original problem (normalized with respect to  $u_{z_0}$ ) is

$$COD = 2 \sqrt{\frac{1}{\pi Gd}} (-x)^{\frac{1}{2}} \quad (58)$$

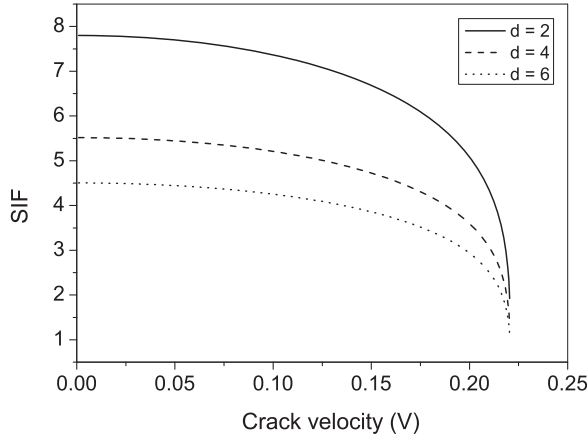
## 6. Numerical results and discussion

Analytical expressions need to be translated into numerical solutions for better understanding of the nature of the physical quantities in the light of relevant parameters. The



**Table 1.** Engineering elastic constants of two orthotropic materials.

	Name of the material	$C_{44}$	$C_{55}$	$\rho$
Type-I	Prepreg	7.8	7.8	1.595
Type-II	Carbon fiber	6.15	6.15	1.5


**Figure 3.** Variation of anti-plane shear SIF with crack velocity  $V$  for Type-I material.

normalized SIF ( $K_{III}$ ) and normalized COD with respect to  $u_{z_0}$  depend on crack velocity ( $V$ ), crack depth ( $d$ ) and material constants ( $C_{44}$ ,  $C_{55}$ ,  $\rho$ ). Therefore, the numerical solutions of (55) and (58) are readily obtained to show the effects of the material orthotropy on the SIF and COD by virtue of graphs.

The general theoretical upper limit (Broberg [3]) of crack propagation velocity is the SH-wave velocity ( $C_5$ ) for mode III cracks i.e.  $0 < V < C_5$ . In particular, SIF at the crack tip asymptotically vanishes when  $V \rightarrow C_5$ .

Material constants (in unit *GPA*) and densities (in unit *gm/cm<sup>3</sup>*) of two orthotropic materials are provided (Yu et al. [39]) in Table 1.

The velocity of SH-wave for Type-I and Type-II material are  $C_5^I = 2.2114 \text{ cm}/\mu\text{s}$  and  $C_5^{II} = 2.0248 \text{ cm}/\mu\text{s}$ . Figures 3 and 4 show the variation of the normalized SIF ( $K_{III}/u_{z_0}$ ) against crack velocity ( $V$  in *cm/μs*) for various values of the crack depth  $d = 2, 4, 6$  cm. It is seen that with the increase in the value of  $V$ , the stress intensity factor decreases and finally tends to zero as  $V$  approaches to SH-wave velocity  $C_5$ .

The graph is not valid for super SH-wave velocities ( $V > C_5$ ) as  $C_5$  is the theoretical upper limit of crack propagation velocity  $V$ . In addition, the effect of crack depth  $d$  on the SIF is also shown in Figures 3 and 4. The increase in the crack depth  $d$  induces the decrement in stress intensity factor for all values of crack velocity ( $V$ ). This represents the physical significance of the expression of SIF from Equation (55) which can be justified with the fact that the impact of the constant displacement at the crack tip region becomes lower as the crack depth becomes higher.

Also, it is observed from Figures 3 and 4 that the values of SIF of Type-I material are greater than the values of Type-II material. So the peak value of  $K_{III}$  can either be raised or lowered by varying the material constants. As the SIF and the toughness of the material

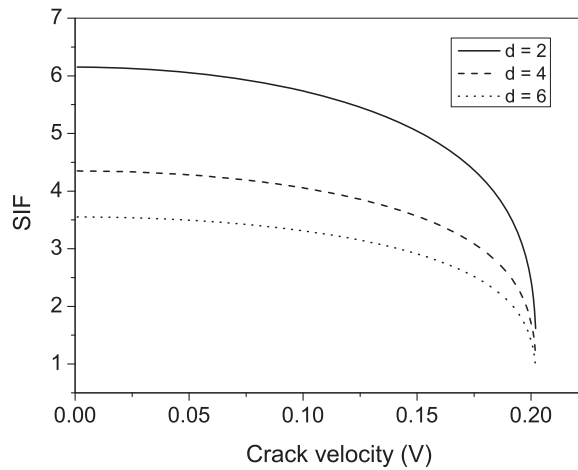


**Figure 4.** Variation of anti-plane shear SIF with crack velocity  $V$  for Type-II material.

are directly proportional to each other, fracture toughness of Type-I material is more than Type-II material.

Our primary motivation in fracture mechanics is to resist the process of propagation of fracture. When SIF at the crack tip region exceeds a particular limit known as critical SIF, it leads to failure of the composite which involves the cracking of the orthotropic material at relatively high velocities known as crack propagation. So, we want to control the value of SIF, so that SIF can't exceed the critical SIF. For this reason, by varying different geometric parameters (like crack velocity, the width of layer), we may control the magnitude of SIF which helps to prevent crack growth leading to a safe structure. For this purpose, we observe the cases when SIF is decreasing (Figures 3 and 4). If we observe the case when SIF is increasing, then SIF may exceed critical SIF that leads to crack growth which is not expected in a practical situation. Therefore, these results can be used to control the geometric parameters of these materials concerning for the magnitude of SIF which will help to prevent the expansion of the semi-infinite crack.

From all figures of COD (Figures 5–8), it is observed that the value of COD decreases as we approach near the crack tip along the negative  $x$ -axis and finally wiped out at the crack tip i.e. origin. This result is very much agreed with the physical nature of the crack.

Figures 5 and 6 illustrate the effect of crack depth  $d$  ( $d = 2, 4, 6$  cm) on the COD for fixed value of  $V = 0.1$  cm/ $\mu$ s and it is observed that COD decreases with the increasing value of  $d$  which signifies the Equation (58) physically.

Again, Figures 7 and 8 show the effect of crack velocity  $V$  ( $V = 0.05, 0.10, 0.15$  cm/ $\mu$ s) on the COD for fixed value of crack depth  $d = 2$  cm. It is seen that COD increases with the increasing value of  $V$  subjected to same crack depth. Further investigation disclosed that the variation of crack opening displacement is found to be prominent for different orthotropic materials.

Further, semi-infinite mode-III crack inside the semi-infinite orthotropic medium has been considered following the model developed by Mandal [35].

For validation of this work, we converted this orthotropic medium problem to isotropic medium problem by putting  $C_{44} = C_{55} = \mu$ , where  $\mu$  is shear modulus of the isotropic

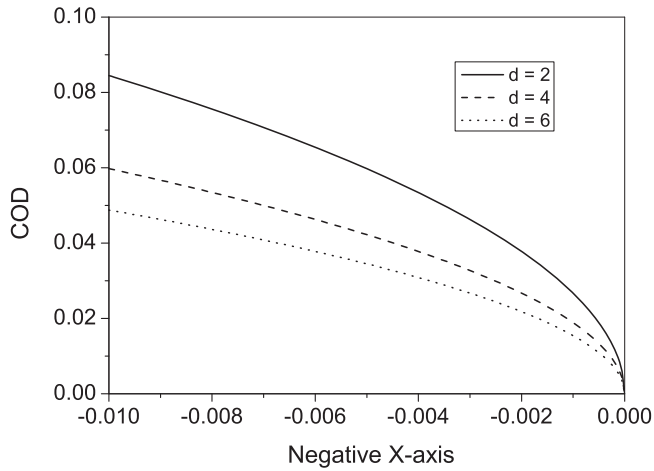


**Figure 5.** Variation of COD with distance  $x$  for Type-I material (fixed crack velocity  $V = 0.1$  in  $\text{cm}/\mu\text{s}$ ).

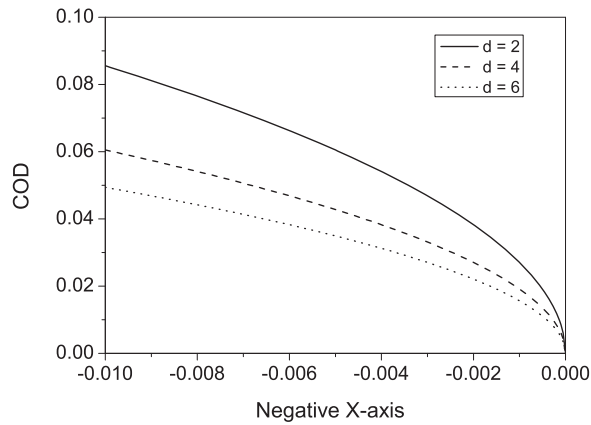


**Figure 6.** Variation of COD with distance  $x$  for Type-II material (fixed crack velocity  $V = 0.1$  in  $\text{cm}/\mu\text{s}$ ).

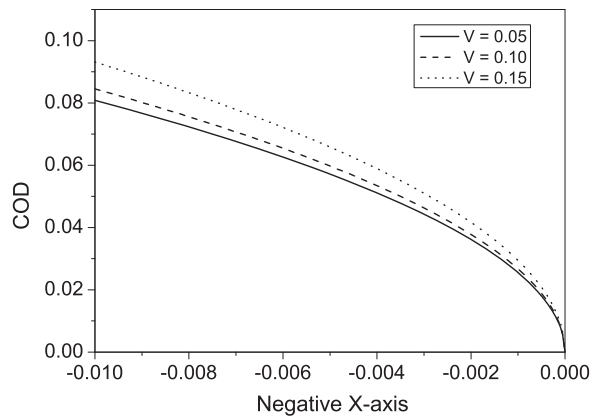


**Figure 7.** Variation of COD with distance  $x$  for Type-I material (fixed crack depth  $d = 2$  cm).

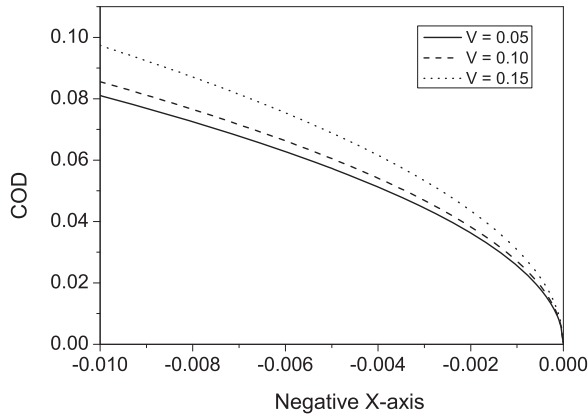


**Figure 8.** Variation of COD with distance  $x$  for Type-II material (fixed crack depth  $d = 2$  cm).

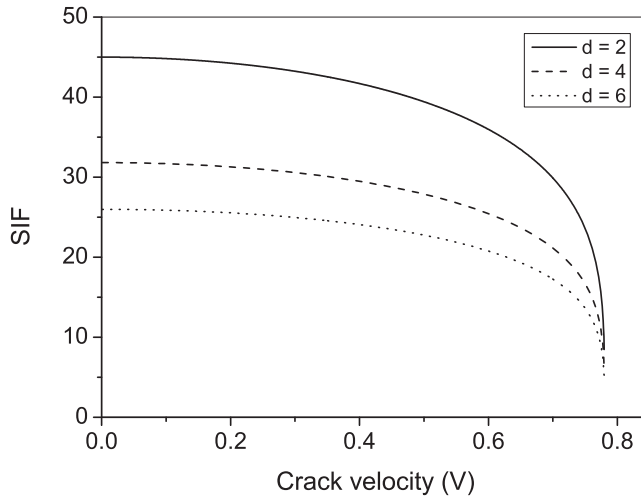


**Figure 9.** Variation of anti-plane shear SIF with crack velocity  $V$  for Isotropic medium.

material and we deduce the following expressions

$$\beta = 1, \text{ shear wave velocity} = C_S = \sqrt{\frac{\mu}{\rho}}$$

$$G^2 = \left(1 - \frac{V^2}{C_S^2}\right)$$

The above expressions and governing Equation (4) are identical to those obtained by the work of Mandal [35] for isotropic elastic medium. Also, it is found that the corresponding SIF and COD for the Type-I material (copper) are identical to that of Mandal’s [35] findings. Henceforth, the obtained graphs represented in Figures 9–11 are of similar with Figures 3, 5a,b of the paper of Mandal [35].

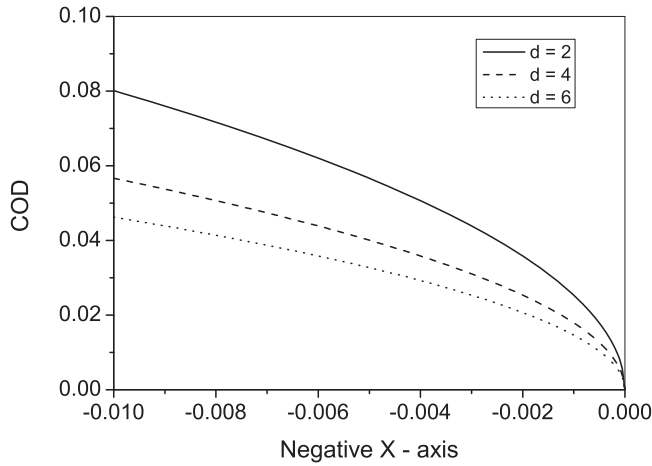


**Figure 10.** Variation of COD with distance  $x$  for Isotropic medium (fixed crack velocity  $V = 0.1 \text{ cm}/\mu\text{s}$ ).

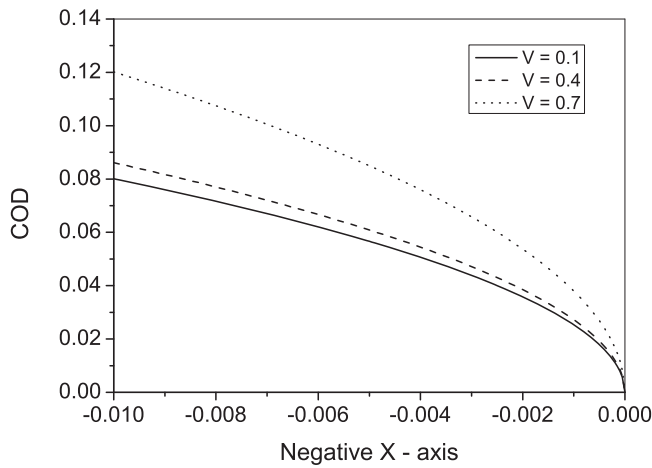


**Figure 11.** Variation of COD with distance  $x$  for Isotropic medium (fixed crack depth  $d = 2 \text{ cm}$ ).

## 7. Conclusion

The problem of a moving semi-infinite crack in semi-infinite orthotropic medium has been investigated subject to SH-wave incidence. The mixed boundary value problem has been reduced to the standard Wiener-Hopf equation by applying Fourier transformation. Due to the complex nature of the kernel, the Wiener-Hopf equation has been solved only for the asymptotic case which is sufficient to obtain SIF and COD. By plotting the numerical values of SIF and COD, the dependency of the material constants ( $C_{44}, C_{55}, \rho$ ) crack propagation velocity ( $V$ ) as well as crack depth ( $d$ ) on SIF and COD have been shown by virtue of graphs. The predicted behavior of SIF and COD graphs were similar and in good agreement with available literature data.

Based on the numerical calculations outlined above, and with reference to Figure 3 through Figure 8, the following conclusions have been established.

(1) The values of SIF and COD can be controlled and arrested within a certain range by varying the above-mentioned parameters to avoid the process of propagation of fracture if the manuscripted model is considered practically for an experiment.

(2) The material properties are also playing a vital role here. Two types of orthotropic materials have been used here to obtain the above SIF and COD graphs. It has been concluded that Type-I material is elastically harder than Type-II material. Damage of solid material, earth's surface building is subjected to the propagation of cracks due to seismic hazards, earthquake which is a big challenge in the fields of construction engineering and geophysics as well. The proposed model offers a useful means by which mechanical design of large composite structures can be done to prevent earthquake disasters.

## Acknowledgments

The authors are grateful to the referees for their valuable suggestions for the improvement of the manuscript.

## Disclosure statement

No potential conflict of interest was reported by the author(s).

## Funding

The research work is supported by Rashtriya Uchcharat Shiksha Abhiyan (RUSA)-2.0, Jadavpur University, Kolkata-700032, West Bengal, India [grant number R-11/475/19].

## References

- [1] Kaw AK. Mechanics of composite materials. 2nd ed., London: CRC Press, Taylor and Francis Group; 2006. ISBN NO.- 978-0-8493-1343-1.
- [2] Vasiliev VV, Morozov EV. Advanced mechanics Of composite materials and structures. 4th ed., Netherlands: Elsevier Science; 2018. ISBN NO.- 0081022093.
- [3] Broberg BK. Cracks and fracture. San Diego (CA): Academic Press; 1999.
- [4] Mandal P, Mandal S C. SH-wave interaction with crack at orthotropic interface. Waves Random Complex Media. 2020;1–15. DOI: 10.1080/17455030.2020.1720043.
- [5] Gupta S, Bhengra N. Implementation of finite difference approximation on the SH-wave propagation in a multilayered magnetoelastic orthotropic composite medium. Acta Mech. 2017;228(10):3421-3444.
- [6] Yoffe EH. The moving Griffith crack. Philos Magaz. 1951;42:739–750.
- [7] Knauss WH. Stresses in an infinite strip containing a semi-finite crack. J Appl Mech. 1966;33(2):356–362.
- [8] Rice JR. Discussion: stresses in an infinite strip containing a semi-infinite crack. J Appl Mech. 1967;34(1):248–249.
- [9] Nilsson F. Dynamic stress-intensity factors for finite strip problems. Int J Fract. 1972;9(4):403–411.
- [10] Nilsson F. Erratum to dynamic stress intensity factors for finite strip problems. Int J Fract. 1973;9(4):477.
- [11] Atkinson C, Popelar CH. Antiplane dynamic crack propagation in a viscoelastic strip. J Mech Phys Solids. 1979;27(5):431–439.
- [12] Georgiadis HG. Complex variable and integral transform methods for elastodynamic solutions pf cracked orthotropic strips. Eng Fract Mech. 1986;24(5):727–735.
- [13] Kousiounelos PN, Williams Jr JH. Dyanamic fracture of unidirectional graphite fiber composite strips. Int J Fract. 1982;20:47–63.

- [14] McClintock FA, Sukhatme SP. Travelling cracks in elastic material under longitudinal shear. *J Mech Phys Solids*. 1960;8(3):187–193.
- [15] Thomson I, Abrahams ID. Diffraction of flexural waves by cracks in orthotropic thin elastic plates, Part II. Far field analysis. *Proc R Soc A*. 2007;463:1615–1638.
- [16] Abrahams ID, Lawrie JB. Scattering of flexural waves by a semi-infinite crack in an elastic plate carrying an electric current. *Math Mech Solids*. 2012;17(1):43–58.
- [17] Morini L, Piccolroaz A, Mishuris G. Remarks on the energy release rate for an antiplane moving crack in couple stress elasticity. *Int J Solids Struct*. 2014;51(18):3087–3100.
- [18] Li XF. Closed-form solution for a mode-III interface crack between two bonded dissimilar elastic layers. *Int J Fract*. 2001;109:L3–L8.
- [19] Wang CY, Rubio-Gonzalez C, Masson JJ. The dynamics stress intensity factor for a semi-infinite crack in orthotropic materials with concentrated shear impact loads. *Int J Solids Struct*. 2001;38:1265–1280.
- [20] Dey J, Patra B. Moving griffith crack in orthotropic strip. *Int J Eng Sci*. 1990;28(8):809–819.
- [21] Das AN, Ghosh ML. Two coplanar Griffith cracks moving along the interface of two dissimilar elastic medium. *Eng Fract Mech*. 1992;41:59–69.
- [22] Ma L, Wu L, Guo L. On the moving griffith crack in a nonhomogeneous orthotropic strip. *Int J Fract*. 2005;136(1):187–205.
- [23] WU XF, Lilla E, Zou WS. A semi-infinite interfacial crack between two bonded dissimilar elastic strips. *Arch Appl Mech*. 2002;72:630–636.
- [24] Sarkar J, Ghosh ML, Mandal SC. Scattering of antiplane shear wave by a propagating crack at the interface of two dissimilar elastic media. *Proc Indian Academy Math Sci*. 1991;101:183–194.
- [25] Lee KH. Stress and displacement fields for propagating the crack along the interface of dissimilar orthotropic materials under dynamic mode I and mode II load. *J Appl Mech*. 2000;67:223–228.
- [26] Sarkar JK, Ghosh ML, Mandal SC. Four coplanar griffith cracks moving in an infinitely long elastic strip under antiplane shear stress. *Proc Indian Acad Sci Math Sci*. 1996;106(1):91–103.
- [27] Singh BM, Rokne J, Dhaliwal RS. Closed-form solutions for a mode-III moving interface crack at the interface of two bonded dissimilar orthotropic elastic layers. *Math Probl Eng*. 2008;2008:1–10.
- [28] Hangamin X, Xuefeng Y, Xiqiao F, Yang Yeh H. Dynamic stress intensity factors of a semi-infinite crack in an orthotropic functionally graded material. *Mech Mater*. 2008;40(1–2):37–47.
- [29] Basak P, Mandal SC. Semi-infinite moving crack in an orthotropic strip. *Int J Solids Struct*. 2017;128:221–330.
- [30] Junlin Li, Shaoqin Z. Fracture analysis of semi-infinite interface crack between two dissimilar orthotropic composite materials. *Key Eng Mater*. 2010;417–418:429–432.
- [31] Bagheri R, Ayatollahi M, Mousavi SM. Analytical solution of multiple moving cracks in functionally graded piezoelectric strip. *J Appl Math Mech*. 2016;36(6):777–792.
- [32] Nourazar M, Ayatollahi M. Multiple moving interfacial cracks between two dissimilar piezoelectric layers under electromechanical loading. *Smart Mater Struct*. 2016;25(7):075011.
- [33] Hu K, Li G. Constant moving crack in a magneto-electroelastic material under anti-plane shear loading. *Int J Solids Struct*. 2005;42:2823–2835.
- [34] Jin B, Soh AK, Zhong Z. Propagation of an anti-plane moving crack in a functionally graded piezoelectric strip. *Arch Appl Mech*. 2003;73:252–260.
- [35] Mandal P. Moving semi-infinite mode - III crack inside the semi-infinite elastic media. *J Theor Appl Mech*. 2020;58(3):649–659–659.
- [36] Sih GC, Chen EP. *Mechanics of fracture*. Vol. 6, London: Martinus Nijhoff Publishers; 1981.
- [37] Georgiadis HG, Papadopoulos GA. Cracked orthotropic strip with clamped boundaries. *J Appl Math Phys*. 1988;39:573–578.
- [38] Noble B. *Method based on the Eimer-Hopf technique*. New York: Pergamon Press; 1958.
- [39] Yu JG, Ratolojanahary FE, Lefebvre JE. Guided waves in functionally graded viscoelastic plates. *Compos Struct*. 2011;93(11):2674.

S. Karan · S. Basu  · S. C. Mandal

# Impact of a torsional load on a penny-shaped crack sandwiched between two elastic layers embedded in an elastic medium

Received: 14 March 2017 / Revised: 11 September 2017 / Published online: 23 December 2017  
© Springer-Verlag GmbH Austria, part of Springer Nature 2017

**Abstract** The paper is focused on the effect of a sudden impact of a torsional load on a penny-shaped crack sandwiched between two elastic layers embedded in an elastic medium. The axisymmetric mixed boundary value problem is reduced to the problem of solving a pair of dual integral equations by using Hankel and Laplace transforms. Further, the integral equations are then reduced to a Fredholm integral equation of second kind which is solved numerically. Expression for the stress intensity factor at the tip of the crack is obtained and plotted for different parameters and materials.

## 1 Introduction

Composite materials are becoming an essential commodity in modern era as they offer advantages such as low weight to strength ratio, corrosion resistance, and high fatigue strength. Many composite materials are used in making aircraft structures to golf clubs, electronic packaging to medical equipment, and space vehicles to home building. It has been observed that applications of composite materials in the commercial market are also increasing day by day. Advanced composite materials are multi-phased non-homogeneous materials with anisotropic properties. This complicates the stress analysis for fracture, particularly if the loading is time dependent and the crack growth involves sharp edges.

The performance of engineered composite systems is affected by inhomogeneities such as cracks and inclusions which become the subject of investigations. The study of the fatigue crack growth models based on elastic–plastic stress–strain analysis at the crack tip region and strain–life damage has been discussed by Hadi Hafezi et al. [1]. In this paper, the authors assess the performance of the UniGrow model based on available experimental constant amplitude crack propagation data, derived for several metallic materials from Portuguese riveted metallic bridges. Recently, a number of new developments based on the theory of elasticity, fatigue crack growth models, and stress intensity factors for some practical crack geometries and their numerical analyses are discussed in the book of Kundu [2]. The solution to determine the transient stress intensity factor of an elliptical crack embedded in a thick plate, one side of which is subjected to a sudden temperature change under arbitrary normal loading, was given by Shah and Kobayashi [3]. An elliptical crack in a large beam in pure bending is also described in this paper. Transient dynamic stress intensity factors around a crack in a non-homogeneous interfacial layer between two dissimilar elastic half-planes have been considered by Itou [4].

The dynamic problem of torsional impact is one of the important parts in view of construction technology and fabrication process. The crack is mainly generated by the impact of a torsional load. The problem of a

---

S. Karan · S. Basu (✉)  
Department of Applied Sciences, Haldia Institute of Technology, Haldia, Purba Medinipur 721657, India  
E-mail: basu1982@gmail.com

S. C. Mandal  
Department of Mathematics, Jadavpur University, Kolkata 700032, India  
E-mail: scmandal.ju@gmail.com



sudden impact of torsional load in a half-space was investigated by Ghosh [5], Eason [6], and Shail [7]. Shibuya [8] analyzed the problem of torsional impact of a thick elastic plate.

An effective approach for finding dynamic stresses in a layered composite containing a crack has been performed by Sih and Chen [9]. Keer and Jabali [10] solved the problem of torsional oscillation of a layer bonded to an elastic half-space. The model of the penny-shaped crack has been first considered in 1970's by Arin and Erdogan [11,12], Kassir and Bregman [13], and Chen [14]. In these papers, some numerical examples are discussed to find stress intensity factors and the strain energy release rate at the edge of the crack with different material properties. The penny-shaped crack and the plane strain crack in an infinite body of power law material have been studied by He et al. [15]. Ueda et al. [16,17] also analyzed the problem of torsional impact of a penny-shaped interface crack. In both cases, Laplace and Hankel transforms are used to reduce the problem to the solution of a pair of dual integral equations which have been solved by using an integral transform technique, and the result is expressed in terms of a Fredholm integral equation of the second kind. A numerical Laplace inversion technique is also used to recover the time dependence of the solution, and the dynamic stress intensity factor is determined which is dependent on the time and material constants. But these are simple problems of diffraction of transient torsional shear waves by a penny-shaped crack at the interface of two bonded dissimilar elastic half-spaces. A penny-shaped interface crack of two bonded dissimilar transversely isotropic elastic half-spaces and dissimilar non-homogeneous elastic layers under axially symmetric torsion have been analyzed by Saxena et al. [18,19]. Das et al. [20] considered the problem of determining the stress intensity factors for an interfacial crack between an orthotropic half-plane bonded to a dissimilar orthotropic layer with a punch. In this paper, they reduced the problem to a system of simultaneous integral equations which have been solved by using Chebyshev polynomials. Li [21] solved the problem of dynamic fracture for a penny-shaped crack in an FGM interlaying between dissimilar half-spaces. The contact problem for an open penny-shaped crack under normally incident tension-compression wave has been developed by Menshykov et al. [22], and Mykhaskiv and Khay [23] discussed the problem of interaction between a rigid-disk inclusion and a penny-shaped crack under an elastic time-harmonic wave. Lee and Tran [24] considered the stress analysis for a penny-shaped crack interacting with inclusions and voids. Fracture of a half-space compressed along a penny-shaped crack located at a short distance from the surface has been discussed by Dovzhik [25]. Lee [26] considered the problem of a penny-shaped crack in a plate of finite thickness subjected to a uniform shearing stress. Recently Basu and Mandal [27] solved the problem of the impact of a torsional load on a penny-shaped crack in an elastic layer sandwiched between two similar elastic half-spaces.

In most of the above discussed papers, the problem involving the impact of torsional waves on a penny-shaped crack in a layer bonded to an elastic half-space, a non-homogeneous interfacial layer between two dissimilar elastic half-planes, in an unbounded thermo-elastic medium or in an elastic layer sandwiched between two similar elastic half-spaces has been considered. But the torsional problem of a penny-shaped crack sandwiched between two elastic layers embedded in another medium has not been treated yet. So, in this paper, the sudden impact of torsional load on a penny-shaped crack bonded by two dissimilar elastic layers embedded in an elastic medium has been analyzed. Using Hankel and Laplace transforms, the axisymmetric mixed boundary value problem has been reduced to a Fredholm integral equation of the second kind which has been solved numerically by the Fox and Goodwin method [28]. After taking numerical inversion of the Laplace Transform, the stress intensity factor (SIF) has been calculated at the tip of the crack and presented graphically for different parameters and different sets of materials to compare the bonded strength of the materials.

## 2 Formulation of the problem and method of solution

A study is made of torsional load on a penny-shaped crack of radius  $a$  which lies at the interface of two dissimilar elastic layers each of thickness  $b$  with material properties  $\mu_1, \nu_1, \rho_1$  (type-I) and  $\mu_2, \nu_2, \rho_2$  (type-II) with reference to the cylindrical polar coordinates  $(r, \theta, z)$ . These two layers are embedded in an infinite elastic medium with properties  $\mu_3, \nu_3, \rho_3$  (type-III) as shown in Fig. 1. Due to the symmetry of the problem, it is assumed that the magnitude of the load is  $\tau_0$  which is applied suddenly at time  $t = 0$  such that the upper and lower surfaces will move in opposite directions.

In this problem, the only nonzero component of displacement is the circumferential component  $u_\theta$ , and the only nonzero component of stress  $\sigma_{\theta z}$  is defined by the relation

$$\sigma_{\theta z} = \mu \frac{\partial u_\theta}{\partial z} \quad (1)$$

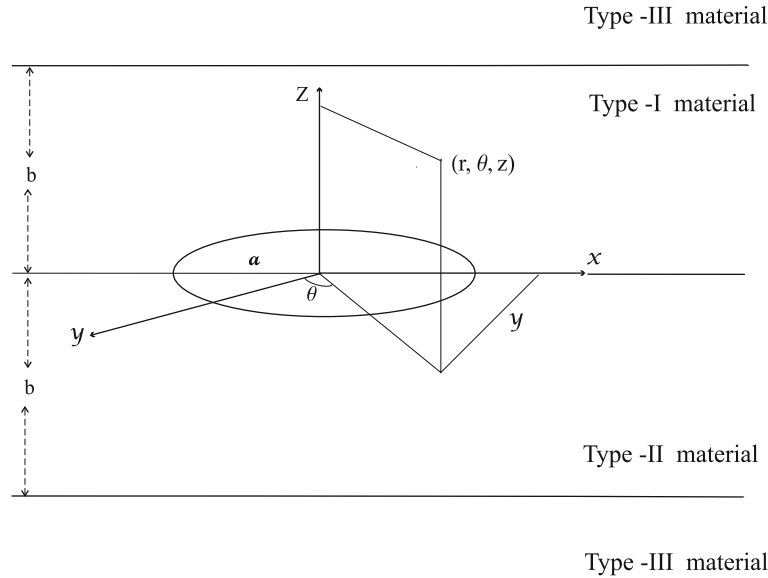


**Fig. 1** Geometry of the penny-shaped crack

where  $\mu$  is the shear modulus of the elastic material.

The displacement component  $u_\theta$  satisfies the partial differential equation [29]

$$\frac{\partial^2 u_\theta}{\partial r^2} + \frac{1}{r} \frac{\partial u_\theta}{\partial r} - \frac{u_\theta}{r^2} + \frac{\partial^2 u_\theta}{\partial z^2} = \frac{1}{c_j^2} \frac{\partial^2 u_\theta}{\partial t^2} \quad (j = 1, 2, 3) \tag{2}$$

where  $c_j = \left(\frac{\mu_j}{\rho_j}\right)^{\frac{1}{2}}$  is the shear wave velocity and  $\rho$  is the density of the material. In Eq. (2), subscripts “1,” “2”, and “3” have been used to refer to the materials of type-I, type-II, and type-III, respectively.

To eliminate the time variable from Eq. (2), a Laplace transform pair has been used which is defined by

$$\bar{f}(p) = \int_0^\infty f(t)e^{-pt} dt, \tag{3}$$

$$f(t) = \frac{1}{2\pi i} \int_{Br} \bar{f}(p)e^{pt} dp \tag{4}$$

where  $Br$  is the Bromwich path of integration (see the Appendix II).

By the use of Laplace transform, Eq. (2) is transformed to

$$\frac{\partial^2 \bar{u}_\theta}{\partial r^2} + \frac{1}{r} \frac{\partial \bar{u}_\theta}{\partial r} - \frac{\bar{u}_\theta}{r^2} + \frac{\partial^2 \bar{u}_\theta}{\partial z^2} = \frac{p^2}{c_j^2} \bar{u}_\theta \quad (j = 1, 2, 3). \tag{5}$$

The boundary conditions on the plane  $z = 0$  for  $r \leq a$  and  $r > a$  are

$$\tau_{\theta z}^{(1)}(r, 0, t) = \tau_{\theta z}^{(2)}(r, 0, t) = \tau_0 \left(\frac{r}{a}\right) H(t), \quad 0 \leq r \leq a, \tag{6}$$

$$u_\theta^{(1)}(r, 0, t) = u_\theta^{(2)}(r, 0, t), \quad r > a \tag{7}$$

where  $H(t)$  is the Heaviside unit step function.

Also, the interfaces of the layer  $z = \pm b$  are bonded perfectly to the elastic medium. The continuity conditions at the interface are given by

$$\tau_{\theta z}^{(1)}(r, b, t) = \tau_{\theta z}^{(3)}(r, b, t), \tag{8}$$

$$u_\theta^{(1)}(r, b, t) = u_\theta^{(3)}(r, b, t), \tag{9}$$

$$\tau_{\theta z}^{(2)}(r, -b, t) = \tau_{\theta z}^{(3)}(r, -b, t), \tag{10}$$

$$u_{\theta}^{(2)}(r, -b, t) = u_{\theta}^{(3)}(r, -b, t). \tag{11}$$

Applying the Laplace transform on the boundary and continuity conditions (6)–(11), it can be written as :

$$\bar{\tau}_{\theta z}^{(1)}(r, 0, p) = \bar{\tau}_{\theta z}^{(2)}(r, 0, p) = \frac{\tau_0\left(\frac{r}{a}\right)}{p}, \quad 0 \leq r \leq a, \tag{12}$$

$$\bar{u}_{\theta}^{(1)}(r, 0, p) = \bar{u}_{\theta}^{(2)}(r, 0, p), \quad r > a, \tag{13}$$

$$\bar{\tau}_{\theta z}^{(1)}(r, b, p) = \bar{\tau}_{\theta z}^{(3)}(r, b, p), \tag{14}$$

$$\bar{u}_{\theta}^{(1)}(r, b, p) = \bar{u}_{\theta}^{(3)}(r, b, p), \tag{15}$$

$$\bar{\tau}_{\theta z}^{(2)}(r, -b, p) = \bar{\tau}_{\theta z}^{(3)}(r, -b, p), \tag{16}$$

$$\bar{u}_{\theta}^{(2)}(r, -b, p) = \bar{u}_{\theta}^{(3)}(r, -b, p). \tag{17}$$

To solve Eq. (5), Hankel transform has been used to obtain the Laplace transform of the displacement component for the region *I* ( $0 < z < b$ ), and region *II* ( $-b < z < 0$ ), and region *III* ( $|z| \geq b$ ) in the following form:

$$\bar{u}_{\theta}^{(1)}(r, z, p) = \int_0^{\infty} [A_1(s, p) e^{-\gamma_1 z} + A_2(s, p) e^{\gamma_1 z}] J_1(sr) ds, \tag{18}$$

$$\bar{u}_{\theta}^{(2)}(r, z, p) = \int_0^{\infty} [A_3(s, p) e^{-\gamma_2 z} + A_4(s, p) e^{\gamma_2 z}] J_1(sr) ds, \tag{19}$$

$$\bar{u}_{\theta}^{(3)}(r, z, p) = \int_0^{\infty} A_5(s, p) e^{-\gamma_3(z-b)} J_1(sr) ds, \quad z \geq b, \tag{20}$$

$$\bar{u}_{\theta}^{(3)}(r, z, p) = \int_0^{\infty} A_6(s, p) e^{\gamma_3(z+b)} J_1(sr) ds, \quad z \leq -b \tag{21}$$

where

$$\begin{aligned} \gamma_1 &= (s^2 + k_1^2)^{\frac{1}{2}}, \quad \gamma_2 = (s^2 + k_2^2)^{\frac{1}{2}}, \quad \gamma_3 = (s^2 + k_3^2)^{\frac{1}{2}}, \\ k_1 &= p/c_1, \quad k_2 = p/c_2, \quad k_3 = p/c_3, \\ c_1 &= \sqrt{\frac{\mu_1}{\rho_1}}, \quad c_2 = \sqrt{\frac{\mu_2}{\rho_2}}, \quad c_3 = \sqrt{\frac{\mu_3}{\rho_3}} \end{aligned} \tag{22}$$

and  $J_1$  is the bessel function of the first kind of order one.

In Eqs. (18)–(21),  $A_i$  ( $i = 1, 2, \dots, 6$ ) are the constants which are to be determined later on. With the help of Eqs. (18)–(21), the expressions for  $\bar{\tau}_{\theta z}$  are

$$\bar{\tau}_{\theta z}^{(1)} = -\mu_1 \int_0^{\infty} \gamma_1 [A_1(s, p) e^{-\gamma_1 z} - A_2(s, p) e^{\gamma_1 z}] J_1(sr) ds, \tag{23}$$

$$\bar{\tau}_{\theta z}^{(2)} = -\mu_2 \int_0^{\infty} \gamma_2 [A_3(s, p) e^{-\gamma_2 z} - A_4(s, p) e^{\gamma_2 z}] J_1(sr) ds, \tag{24}$$

and

$$\bar{\tau}_{\theta z}^{(3)} = -\mu_3 \int_0^{\infty} \gamma_3 [A_5(s, p) e^{-\gamma_3(z-b)}] J_1(sr) ds, \quad z \geq b \tag{25}$$

$$= \mu_3 \int_0^{\infty} \gamma_3 [A_6(s, p) e^{\gamma_3(z+b)}] J_1(sr) ds, \quad z \leq -b. \tag{26}$$

Using the above expressions, the boundary conditions (12) and (13) yield

$$\mu_1 \int_0^{\infty} \gamma_1 [A_1(s, p) - A_2(s, p)] J_1(sr) ds = \mu_2 \int_0^{\infty} \gamma_2 [A_3(s, p) - A_4(s, p)] J_1(sr) ds, \tag{27}$$

$$\int_0^{\infty} [A_1(s, p) + A_2(s, p)] J_1(sr) ds = \int_0^{\infty} [A_3(s, p) + A_4(s, p)] J_1(sr) ds, \quad (28)$$

and from the continuity conditions (14)–(17) we obtain

$$\mu_1 \int_0^{\infty} \gamma_1 [A_1(s, p) e^{-\gamma_1 b} - A_2(s, p) e^{\gamma_1 b}] J_1(sr) ds = \mu_3 \int_0^{\infty} \gamma_3 A_5(s, p) J_1(sr) ds, \quad (29)$$

$$-\int_0^{\infty} [A_1(s, p) e^{-\gamma_1 b} + A_2(s, p) e^{\gamma_1 b}] J_1(sr) ds = \int_0^{\infty} A_5(s, p) J_1(sr) ds, \quad (30)$$

$$-\mu_2 \int_0^{\infty} \gamma_2 [A_3(s, p) e^{\gamma_2 b} - A_4(s, p) e^{-\gamma_2 b}] J_1(sr) ds = \mu_3 \int_0^{\infty} \gamma_3 A_6(s, p) J_1(sr) ds, \quad (31)$$

$$\int_0^{\infty} [A_3(s, p) e^{\gamma_2 b} + A_4(s, p) e^{-\gamma_2 b}] J_1(sr) ds = \int_0^{\infty} A_6(s, p) J_1(sr) ds. \quad (32)$$

Inverting Eqs. (27)–(32) by means of the Hankel inversion formula, we obtain the following relations:

$$\gamma_1 [A_1(s, p) - A_2(s, p)] = G_1 \gamma_2 [A_3(s, p) - A_4(s, p)], \quad (33)$$

$$A_1(s, p) + A_2(s, p) = A_3(s, p) + A_4(s, p), \quad (34)$$

$$\gamma_1 [A_1(s, p) e^{-\gamma_1 b} - A_2(s, p) e^{\gamma_1 b}] = G_2 \gamma_3 A_5(s, p), \quad (35)$$

$$A_1(s, p) e^{-\gamma_1 b} + A_2(s, p) e^{\gamma_1 b} = A_5(s, p), \quad (36)$$

$$-\gamma_2 [A_3(s, p) e^{\gamma_2 b} - A_4(s, p) e^{-\gamma_2 b}] = G_3 \gamma_3 A_6(s, p), \quad (37)$$

$$A_3(s, p) e^{\gamma_2 b} + A_4(s, p) e^{-\gamma_2 b} = A_6(s, p) \quad (38)$$

where  $G_1 = \mu_2/\mu_1$ ,  $G_2 = \mu_3/\mu_1$ , and  $G_3 = \mu_3/\mu_2$ .

After solving Eqs. (33)–(38) for  $A_2(s, p)$ ,  $A_3(s, p)$ ,  $A_4(s, p)$ ,  $A_5(s, p)$ , and  $A_6(s, p)$  in terms of  $A_1(s, p)$ , the expression for the constants can be written as

$$A_2(s, p) = \left( \frac{\gamma_1 - G_2 \gamma_3}{\gamma_1 + G_2 \gamma_3} \right) e^{-2\gamma_1 b} A_1(s, p), \quad (39)$$

$$A_3(s, p) = G A_1(s, p), \quad (40)$$

$$A_4(s, p) = \left( \frac{\gamma_2 + G_3 \gamma_3}{\gamma_2 - G_3 \gamma_3} \right) e^{2\gamma_2 b} G A_1(s, p), \quad (41)$$

$$A_5(s, p) = \frac{2\gamma_1}{(\gamma_1 + G_2 \gamma_3)} e^{-\gamma_1 b} A_1(s, p), \quad (42)$$

$$A_6(s, p) = \frac{2\gamma_2 e^{\gamma_2 b}}{(\gamma_2 - G_3 \gamma_3)} G A_1(s, p) \quad (43)$$

where

$$G = \left[ 1 - \left( \frac{\gamma_1 - G_2 \gamma_3}{\gamma_1 + G_2 \gamma_3} \right) e^{-2\gamma_1 b} \right] / \frac{G_1 \gamma_2}{\gamma_1} \left[ 1 - \left( \frac{\gamma_2 + G_3 \gamma_3}{\gamma_2 - G_3 \gamma_3} \right) e^{2\gamma_2 b} \right].$$

Applying (18), (19), and (23) in the boundary conditions (13) and (12), the following dual integral equations can be obtained involving the unknown function  $B(s, p)$ :

$$\int_0^{\infty} B(s, p) J_1(sr) ds = 0, \quad r > a, \quad (44)$$

$$\int_0^{\infty} s P_1(s, p) B(s, p) J_1(sr) ds = -\frac{\tau_0(r/a)}{p\mu_1}, \quad 0 \leq r \leq a \quad (45)$$

where

$$B(s, p) = \left[ \left\{ 1 + \left( \frac{\gamma_1 - G_2 \gamma_3}{\gamma_1 + G_2 \gamma_3} \right) e^{-2\gamma_1 b} \right\} - G \left\{ 1 + \left( \frac{\gamma_2 + G_3 \gamma_3}{\gamma_2 - G_3 \gamma_3} \right) e^{2\gamma_2 b} \right\} \right] A_1(s, p) \quad (46)$$

and

$$P(s, p) = \frac{\gamma_1 \left[ 1 - \left( \frac{\gamma_1 - G_2 \gamma_3}{\gamma_1 + G_2 \gamma_3} \right) e^{-2\gamma_1 b} \right]}{s \left[ \left\{ 1 + \left( \frac{\gamma_1 - G_2 \gamma_3}{\gamma_1 + G_2 \gamma_3} \right) e^{-2\gamma_1 b} \right\} - G \left\{ 1 + \frac{\gamma_2 + G_3 \gamma_3}{\gamma_2 - G_3 \gamma_3} e^{-2\gamma_2 b} \right\} \right]}. \quad (47)$$

To convert the dual integral Eqs. (44) and (45) to a single Fredholm integral equation of the second kind, the form of  $B(s, p)$  that satisfies Eq. (44) automatically can be considered as

$$B(s, p) = \frac{4 \tau_0 a^{\frac{5}{2}}}{3 \mu_1 p (2\pi)^{\frac{1}{2}}} \sqrt{s} \int_0^1 \sqrt{\xi} \Phi(\xi, p) J_{\frac{3}{2}}(sa\xi) d\xi \quad (48)$$

where  $\Phi(\xi, p)$  is an unknown function to be determined.

Using the formula

$$J_{\frac{3}{2}}(s_1 \xi) = -\frac{\sqrt{\xi}}{s_1} \frac{d}{d\xi} \left\{ \xi^{-\frac{1}{2}} J_{\frac{1}{2}}(s_1 \xi) \right\}, \quad s_1 = sa,$$

$B(s, p)$  can be written as

$$B\left(\frac{s_1}{a}, p\right) = \frac{4 \tau_0 a^2}{3 \mu_1 p (2\pi s_1)^{\frac{1}{2}}} \left[ \int_0^1 \Phi_1(\xi, p) J_{\frac{1}{2}}(s_1 \xi) d\xi - \Phi(1, p) J_{\frac{1}{2}}(s_1) \right] \quad (49)$$

where

$$\Phi_1(\xi, p) = \xi^{-\frac{1}{2}} \frac{d}{d\xi} [\xi \Phi(\xi, p)]. \quad (50)$$

The expression for  $P\left(\frac{s_1}{a}, p\right)$  approaches  $1/G_4$  for large values of  $s_1$ , so that

$$1 - G_4 P\left(\frac{s_1}{a}, p\right) \rightarrow 0 \quad \text{as } s_1 \rightarrow \infty$$

where  $G_4 = 1 + \frac{\mu_1}{\mu_2} = 1 + \frac{1}{G_1}$ .

Now Eq. (45) can be written in terms of dimensionless quantities as

$$\int_0^\infty s_1 B\left(\frac{s_1}{a}, p\right) J_1(R s_1) ds_1 = -\frac{\tau_0 a^2 G_4 R}{p \mu_1} + \int_0^\infty s_1 \left[ 1 - G_4 P\left(\frac{s_1}{a}, p\right) \right] B\left(\frac{s_1}{a}, p\right) J_1(R s_1) ds_1, \quad (R < 1)$$

where  $R = \frac{r}{a}$ .

With the help of Eq. (49) and using the result

$$\int_0^\infty t^{\frac{1}{2}} J_1(at) J_{\frac{1}{2}}(bt) dt = \begin{cases} 0, & 0 < a < b \\ \sqrt{\frac{2}{\pi}} \frac{\sqrt{b}}{a \sqrt{a^2 - b^2}}, & 0 < b < a \end{cases}$$

the above equation becomes

$$\begin{aligned} & \int_0^R \frac{\sqrt{\xi}}{\sqrt{R^2 - \xi^2}} \Phi_1(\xi, p) d\xi \\ &= -\frac{3\pi G_4 R^2}{4} + \sqrt{\frac{\pi}{2}} R \int_0^1 \sqrt{\xi} \Phi(\xi, p) d\xi \int_0^\infty s_1^{\frac{3}{2}} M\left(\frac{s_1}{a}, p\right) J_1(R s_1) J_{\frac{3}{2}}(\xi s_1) ds_1 \\ &= F(R) \end{aligned} \quad (51)$$

where  $M\left(\frac{s_1}{a}, p\right) = 1 - G_4 P\left(\frac{s_1}{a}, p\right)$

$$\text{and } F(R) = -\frac{3\pi G_4 R^2}{4} + \sqrt{\frac{\pi}{2}} R \int_0^1 \sqrt{\xi} \Phi(\xi, p) d\xi \int_0^\infty s_1^{\frac{3}{2}} M\left(\frac{s_1}{a}, p\right) J_1(R s_1) J_{\frac{3}{2}}(\xi s_1) ds_1.$$

By setting Abel's integral formula as

$$\sqrt{\xi} \Phi_1(\xi, p) = \frac{2}{\pi} \frac{d}{d\xi} \int_0^\xi \frac{R F(R)}{\sqrt{\xi^2 - R^2}} dR$$

and with the help of expression (50), Eq. (51) becomes

$$\begin{aligned} \xi \Phi(\xi, p) &= \frac{2}{\pi} \int_0^\xi \frac{R}{\sqrt{\xi^2 - R^2}} \left[ \frac{-3\pi G_4 R^2}{4} + \sqrt{\frac{\pi}{2}} R \int_0^1 \sqrt{u} \Phi(u, p) du \right. \\ &\quad \left. \times \int_0^\infty s_1^{\frac{3}{2}} M\left(\frac{s_1}{a}, p\right) J_1(R s_1) J_{\frac{3}{2}}(u s_1) ds_1 \right] dR \end{aligned} \quad (52)$$

which can be converted by using the Hankel transform into a Fredholm integral equation of the second kind as

$$\Phi(\xi, p) + \int_0^1 \Phi(u, p) L_3(\xi, u, p) du = -G_4 \xi^2 \quad (53)$$

$$\text{where } L_3(\xi, u, p) = -\sqrt{\xi u} \int_0^\infty s_1 \left[ 1 - G_4 P\left(\frac{s_1}{a}, p\right) \right] J_{\frac{3}{2}}(u s_1) J_{\frac{3}{2}}(\xi s_1) ds_1. \quad (54)$$

### 3 Stress intensity factor

For determining the stress intensity factor (SIF)  $K_1(t)$  from its Laplace transform  $K_1^*(p)$ , the stress components in the matrix layer are expanded in terms of the local coordinates  $r_1$  and  $\theta_1$  for small values of  $r_1$ . The local coordinates  $(r_1, \theta_1)$  are related to  $(r, \theta)$  as

$$\left. \begin{aligned} r &= a + r_1 \cos \theta_1 \\ z &= r_1 \sin \theta_1 \end{aligned} \right\} \quad (55)$$

where  $x = r \cos \theta$ ,  $y = r \sin \theta$ .

From Eq. (23), it is obtained that

$$\bar{\tau}_{\theta z}^{(1)}(r, 0, p) = -\mu_1 \int_0^\infty s P(s, p) B(s, p) J_1(sr) ds, \quad (r > a). \quad (56)$$

Now, letting  $P(s, p) \rightarrow 1/G_4$  as  $s \rightarrow \infty$ , Eq. (56) becomes

$$\begin{aligned} \bar{\tau}_{\theta z}^{(1)}(r, 0, p) &= \frac{4\tau_0}{3\pi p G_4} \left[ \frac{\phi(1, p)}{R\sqrt{R^2 - 1}} - \int_0^1 \frac{\sqrt{\xi}}{R\sqrt{R^2 - \xi^2}} \phi_1(\xi, p) d\xi \right] \\ &= \frac{4\tau_0}{3\pi p G_4} \frac{\phi(1, p)}{(R\sqrt{R^2 - 1})} + O(1), \quad (R > 1). \end{aligned} \quad (57)$$

To evaluate the singularity it is important to calculate the term  $|\bar{\tau}_{\theta z}^{(1)}(r, 0, p)|$ . Therefore,

$$\begin{aligned} |\bar{\tau}_{\theta z}^{(1)}(r, 0, p)| &= \frac{4\tau_0}{3\pi p G_4} \frac{\phi(1, p)}{(R\sqrt{R^2 - 1})} \quad (R > 1) \\ &= \frac{4\tau_0}{3\pi p G_4} \frac{\phi(1, p)}{\left(\frac{r}{a}\sqrt{\frac{r}{a}} - 1\sqrt{\frac{r}{a} + 1}\right)} \quad (r > a) \\ &= \frac{4\tau_0}{3\pi p G_4} \frac{\sqrt{a}\phi(1, p)}{\left(\frac{r}{a}\sqrt{r_1}\sqrt{\frac{r}{a} + 1}\right)} \quad (r > a) \end{aligned} \quad (58)$$

where  $r_1 = r - a$ .

**Table 1** Engineering elastic constants for elastic layer (Set-I)

Set-I	Name of the material	$\rho$ (Density, Mg/m <sup>3</sup> )	$\mu$ (shear modulus)
Layer I	Aluminum alloy (7075-T6)	2.7	28
Layer II	Brass (70Cu30Zn, annealed)	8.4	39
Layer III	Nickel alloys	8.5	70

**Table 2** Engineering elastic constants for elastic layer (Set-II)

Set-II	Name of the material	$\rho$ (Density, Mg/m <sup>3</sup> )	$\mu$ (shear modulus)
Layer I	Brass (70Cu30Zn, annealed)	8.4	39
Layer II	Aluminum alloy (7075-T6)	2.7	28
Layer III	Nickel alloys	8.5	70

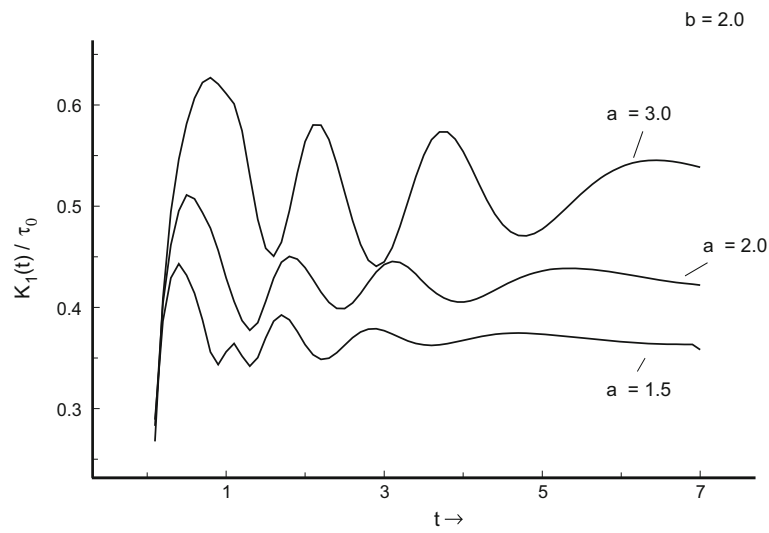


**Fig. 2** Normalized stress intensity factor against time  $t$  for set-I materials ( $b = 2.0$ )

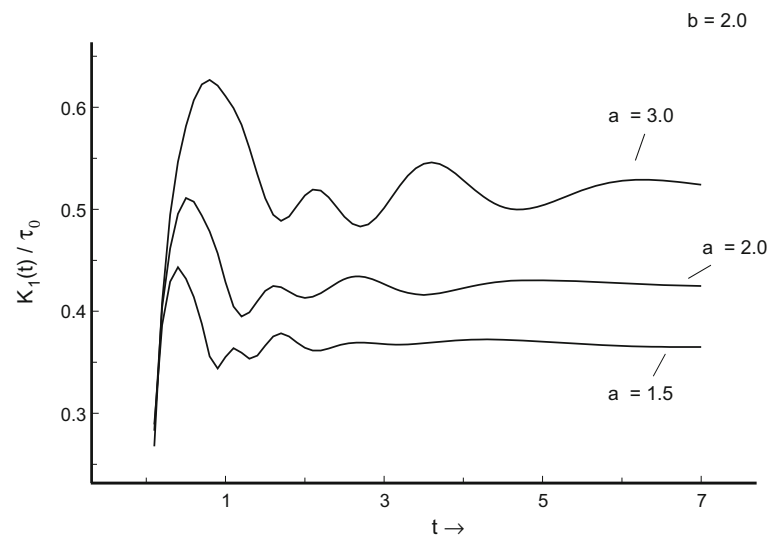


**Fig. 3** Normalized stress intensity factor against time  $t$  for set-II materials ( $b = 2.0$ )

The Laplace transform of the stress intensity factor is defined by

$$K_1^*(p) = \lim_{r \rightarrow a} \left[ |\bar{\tau}_{\theta z}^{(1)}(r, 0, p)| \sqrt{r-a} \right]. \quad (59)$$

With the help of Eq. (58), Eq. (59) becomes

$$K_1^*(p) = \frac{2\sqrt{2a} \tau_0}{3\pi G_4} \frac{\phi(1, p)}{p}. \quad (60)$$

Using the inverse Laplace transform, the stress intensity factor  $K_1(t)$  is obtained as

$$K_1(t) = \frac{2\sqrt{2a} \tau_0}{3\pi G_4} \frac{1}{2\pi i} \int_{Br} \frac{\phi(1, p)}{p} e^{pt} dp \quad (61)$$

where  $Br$  is the Bromwich path of integration. The values of the engineering elastic constants are given in Tables 1, 2 [30].

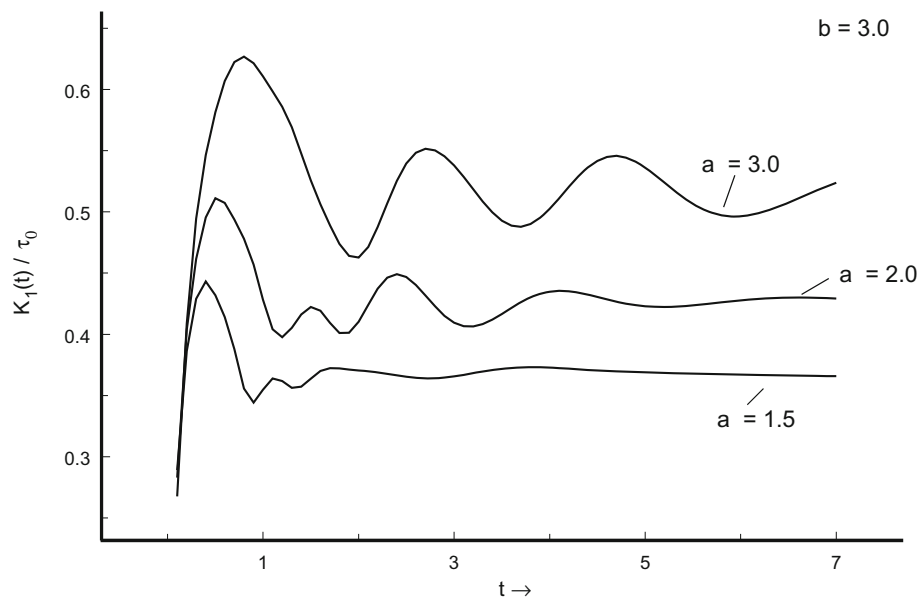


**Fig. 4** Normalized stress intensity factor against time  $t$  for set-I materials ( $b = 3.0$ )

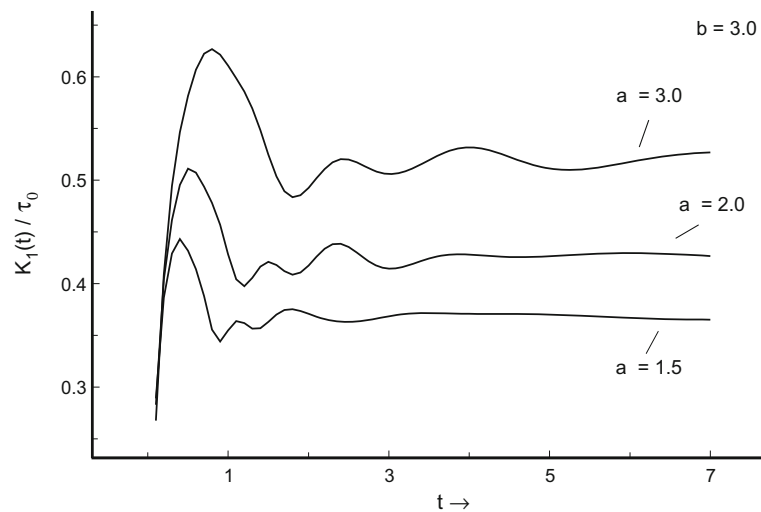


**Fig. 5** Normalized stress intensity factor against time  $t$  for set-II materials ( $b = 3.0$ )



#### 4 Numerical results and discussion

The method of Fox and Goodwin [28] has been used to solve the integral equation (53) numerically to obtain  $\phi(1, p)$ . The integral in (53) has been represented by a quadrature formula involving values of the desired function  $\phi$  at pivotal points in the range of integration which leads to a set of algebraic linear simultaneous equations. The solution of the set of linear algebraic equations gives a first approximation of the required pivotal values of  $\phi$  which has been improved by the use of difference correction technique.

After solving the integral equation (53), the Zakian Algorithm (see the Appendix II) has been used for the Laplace inversion of (61) to find the stress intensity factor  $K_1(t)$  at the tip of the crack for the engineering elastic constants of different types of material. Then, the value of  $K_1(t)/\tau_0$  has been plotted against the time  $t$  for different values of  $a$  and  $b$ .

In Figs. 2 and 4,  $K_1(t)/\tau_0$  has been plotted against  $t$  for set-I materials and in Figs. 3 and 5 for set-II materials for different values of crack radius  $a$  (1.5, 2.0, 3.0) with respect to different layer thicknesses  $b = 2.0$  and  $b = 3.0$ . Again,  $K_1(t)/\tau_0$  has been plotted against  $t$  in Figs. 6 and 8 for set-I materials and in Figs. 7 and 9 for set-II materials for different layer thicknesses  $b$  (1.5, 2.0, 3.0) for the crack radius  $a = 2.0$  and  $a = 3.0$ . In all cases it is observed that the SIF increases first and attains its maximum value near about  $t = 0.5$  and then decreases to its minimum value near  $t = 1.0$  and then shows wave like nature and finally

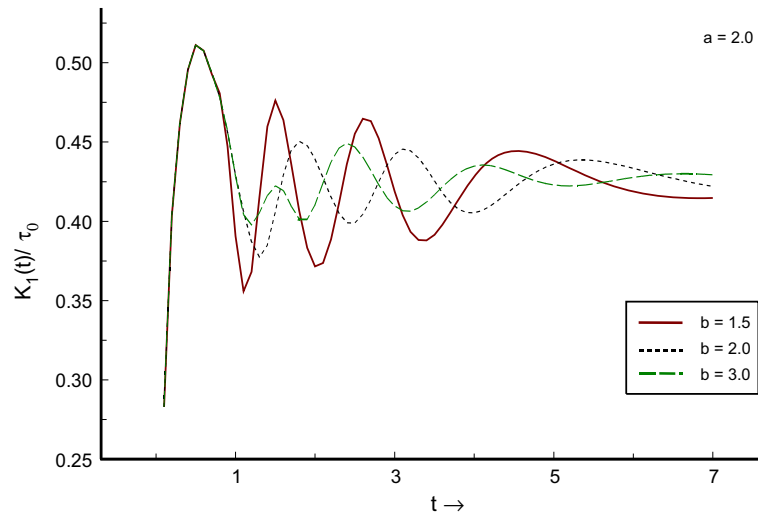


**Fig. 6** Normalized stress intensity factor against time  $t$  for set-I materials ( $a = 2.0$ )

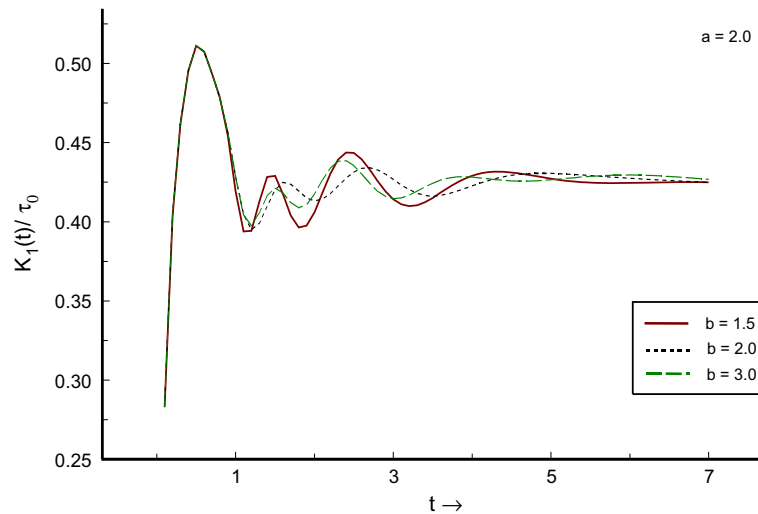


**Fig. 7** Normalized stress intensity factor against time  $t$  for set-II materials ( $a = 2.0$ )

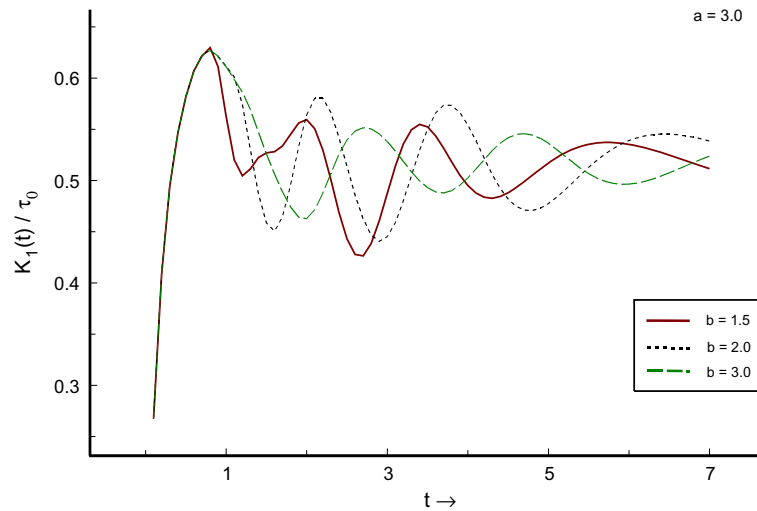


**Fig. 8** Normalized stress intensity factor against time  $t$  for set-I materials ( $a = 3.0$ )

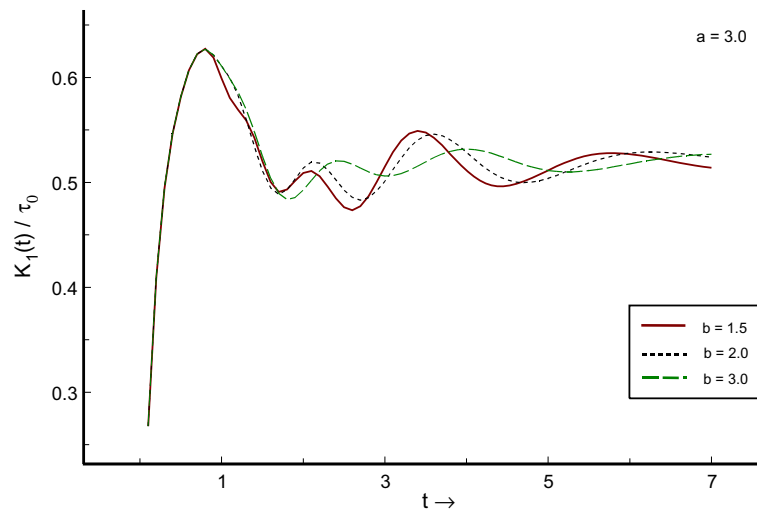


**Fig. 9** Normalized stress intensity factor against time  $t$  for set-II materials ( $a = 3.0$ )

decreases as  $t$  increases. In case of set-I materials, the SIF is found to be more wavy than in case of set-II materials. It is also seen that for fixed  $b$  the SIF is higher for a higher value of crack radius  $a$  (Figs. 2, 3, 4, 5).

If the system of equilibrium is disturbed by applying sudden torsion, then it reaches to maximum angular displacement with respect to the equilibrium position. At that moment, due to this displacement an internally developed reacting force acts on the material for which it moves in the opposite direction to that of the initial position, and then again it moves to the other extreme due to inertia. Here, it is clearly identified that the SIF initially increases and attains its maximum value, but after that it decreases showing damped oscillation for all the cases. This ensures the arrest of crack propagation or expansion of the crack. In the case of set-II materials, the elastic limit of those materials is higher than that of set-I materials. It can be concluded that set-II materials are elastically harder than the other.

## 5 Conclusions

The primary motivation of this investigation is to arrest the propagation of a penny-shaped crack sandwiched between two elastic layers embedded in an elastic medium when a sudden torsional load is applied, and this is analyzed to calculate the stress intensity factor (SIF) at the tip of the crack. The development of dynamic fracture

by the interaction of stress waves and crack is seriously impeded by experimental measurement techniques because of its inherent time dependency, and it is enormously difficult to measure the quantities of interest without interfering with the process being observed here. This model of experiment can be further used in the study of strength of these types of composite materials.

**Acknowledgements** We are thankful to the referee for valuable suggestions for the improvement of the paper.

## Appendix I

The Solution of the Integral Equation by Hankel Transform Technique:

Hankel transforms are integral transformations whose kernels are Bessel functions. They are sometimes referred to as Bessel transforms. When we are dealing with problems that show circular symmetry in cylindrical coordinates, Hankel transforms may be very useful. Laplace's partial differential equation in cylindrical coordinates can be transformed into an ordinary differential equation by using the Hankel transform. Let  $f(r)$  be a function defined for  $r \geq 0$ . The  $\nu$ th-order Hankel transform of  $f(r)$  is defined as

$$F_\nu(s) \equiv \int_0^\infty r f(r) J_\nu(sr) dr \quad (62)$$

where  $J_\nu(sr)$  is the Bessel function of the first kind of order  $\nu$ .  $r J_\nu(sr)$  is called the kernel of the transformation.

If  $\nu > -\frac{1}{2}$ , Hankel's repeated integral immediately gives the inversion formula

$$f(r) \equiv \int_0^\infty s F_\nu(s) J_\nu(sr) ds \quad (63)$$

The most important special cases of the Hankel transform correspond to  $\nu = 0$  and  $\nu = 1$ . Sufficient but not necessary conditions for the validity of (62) and (63) are

1.  $f(r) = o(r^{-k})$ ,  $r \rightarrow \infty$  where  $k > \frac{3}{2}$
2.  $f'(r)$  is piecewise continuous over each bounded subinterval of  $[0, \infty)$ .
3.  $f(r)$  is defined as  $\frac{[f(r+) + f(r-)]}{2}$ .

These conditions can be relaxed.

Hankel functions:

The two linearly independent solutions to Bessel's equation are the Hankel functions of the first and second kind,  $H_\nu^{(1)}$  and  $H_\nu^{(2)}$ , defined by

$$\begin{aligned} H_\nu^{(1)} &= J_\nu + iY_\nu, \\ H_\nu^{(2)} &= J_\nu - iY_\nu \end{aligned}$$

where  $i$  is the imaginary unit,  $J_\nu$  and  $Y_\nu$  are the Bessel functions of first and second kind, respectively. These linear combinations are also known as Bessel functions of the third kind.

The importance of Hankel functions of the first and second kind lies more in theoretical development than in application. These forms of linear combination satisfy numerous simple-looking properties like asymptotic formulae or integral representations. The Bessel function of the second kind can be thought to naturally appear as the imaginary part of the Hankel functions. The Hankel functions are used to express outward- and inward-propagating cylindrical wave solutions of the cylindrical wave equation, respectively (or vice versa, depending on the sign convention for the frequency).

**Appendix II**

Numerical inversion of the Laplace transform:

Let the Laplace transform  $F(p)$  of  $f(t)$  be given by

$$F(p) = \int_0^\infty e^{-pt} f(t) dt, \quad p \geq 0 \quad (p \text{ is transform parameter}).$$

The function  $F$  of the complex variable  $p$  is analytic throughout the finite  $p$  plane except for a finite number of isolated singularities. Then, let  $L_R$  denote a vertical line segment from  $s = \gamma - iR$  to  $s = \gamma + iR$  where the constant  $\gamma$  is positive and large enough that the singularities of  $F$  all lie to the left of that segment. A new function  $f$  of the real variable  $t$  is defined for positive values of  $t$  by means of the equation

$$\begin{aligned} f(t) &= \frac{1}{2\pi i} \lim_{R \rightarrow \infty} \int_{L_R} e^{pt} F(p) dp \quad (t > 0) \\ &= \frac{1}{2\pi i} P.V. \int_{\gamma-i\infty}^{\gamma+i\infty} e^{pt} F(p) dp \quad (t > 0), \end{aligned}$$

and such an integral is called a Bromwich integral [31]. For the Laplace inversion we use here Zakian’s Algorithm.

Zakian’s Algorithm:

This algorithm is one of a class of algorithms in which  $f(t)$  is computed as a sum of weighted evaluations of  $F(p)$ ,

$$f(t) = \sum_{i=1}^N K_i F(p_i),$$

where the values of  $K_i$ ,  $p_i$ , and  $N$  are dictated by a particular method. The development of Zakian’s algorithm is given in Rice and Do [32]. A significant feature of the derivation is the specification that the time function can be related to a finite series of exponential functions,

$$\sum_{i=1}^N K_i e^{\alpha_i t}.$$

The significance of this specification is that Zakian’s Algorithm is very accurate for overdamped and slightly underdamped systems. But it is not accurate for systems with prolonged oscillations:

Given  $F(p)$  and a value of time  $t$ , the following equation implements Zakian’s Algorithm and allows us to calculate the numerical value of  $f(t)$ :

$$f(t) = \frac{2}{t} \sum_{i=1}^5 REAL \left( K_i F \left( \frac{\alpha_i}{t} \right) \right).$$

Table 3 gives the set of five complex constants for  $\alpha_i$  and for  $K_i$  as in [33,34].

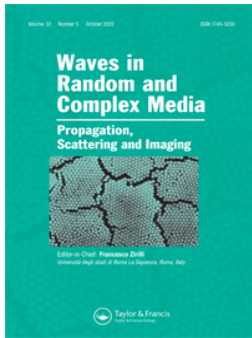
Zakian’s Algorithm is simple to implement and computes quickly. But note that the initial value,  $f(t)$  at  $t = 0$ , cannot be computed. Also, when there are oscillatory systems,  $f(t)$  becomes inaccurate after approximately the second cycle.

**Table 3** Set of five constants for  $\alpha_i$  and  $K_i$  for Zakian’s Method

i	$\alpha_i$	$K_i$
1	12.83767675 + i 1.666063445	- 36902.08210 + i 196990.4257
2	12.22613209 + i 5.012718792	61277.02524 - i 95408.62551
3	10.93430308 + i 8.409673116	- 28916.56288 + i 18169.18531
4	8.776434715 + i 11.92185389	4655.361138 - i 1.901528642
5	5.225453361 + i 15.72952905	- 118.7414011 - i 141.3036911

## References

1. Hadi Hafezi, M., Nik Abdullah, N., Correia, J.F., De Jesus, A.M.: An assessment of a strain-life approach for fatigue crack growth. *Int. J. Struct. Integr.* **3**(4), 344–376 (2012)
2. Kundu, T.: *Fundamentals of Fracture Mechanics*. CRC Press, Boca Raton (2008)
3. Shah, R.C., Kobayashi, A.S.: Stress intensity factor for an elliptical crack under arbitrary normal loading. *Eng. Fract. Mech.* **3**(1), 71–96 (1971)
4. Itou, S.: Transient dynamic stress intensity factors around a crack in a nonhomogeneous interfacial layer between two dissimilar elastic half-planes. *Int. J. Solids Struct.* **38**, 3631–3645 (2001)
5. Ghosh, M.L.: Disturbance in an elastic half space due to an impulsive twisting moment applied to an attached rigid circular disc. *Appl. Sci. Res.* **14**(1), 31–42 (1964)
6. Eason, G.: The displacements produced in an elastic half-space by a suddenly applied surface force. *J. Inst. Math. Appl.* **2**, 299–326 (1966)
7. Shail, R.: The impulsive Reissner–Sagocci problem. *J. Math. Mech.* **19**, 709–716 (1970)
8. Shibuya, T.: On the torsional impact of a thick elastic plate. *Int. J. Solids Struct.* **11**, 803–811 (1975)
9. Sih, G.C., Chen, E.P.: Normal and shear impact of layered composite with a crack: dynamic stress intensification. *J. Appl. Mech.* **47**, 351–358 (1980)
10. Keer, L.M., Jabali, H.H., Chantaramungkorn, K.: Torsional oscillation of a layer bonded to an elastic half-space. *Int. J. Solids Struct.* **10**, 1–13 (1974)
11. Arin, K., Erdogan, F.: Penny-shaped crack in an elastic layer bonded to dissimilar half spaces. *Int. J. Eng. Sci.* **9**(2), 213–232 (1971)
12. Erdogan, F., Arin, K.: Penny-shaped interface crack between an elastic layer and a half space. *Int. J. Eng. Sci.* **10**(2), 115–125 (1972)
13. Kassir, M.K., Bregman, A.M.: The stress-intensity factor for a penny-shaped crack between two dissimilar materials. *J. Appl. Mech.* **39**(1), 308–310 (1972)
14. Chen, E.P.: Elastodynamic response of a penny-shaped crack in a cylinder of a finite radius. *Int. J. Eng. Sci.* **17**(4), 379–385 (1979)
15. He, M.Y., Hutchinson, J.W.: The penny shaped crack and the plane strain crack in an infinite body of power law material. *J. Appl. Mech.* **48**, 830–840 (1981)
16. Ueda, S., Shindo, Y., Atsumi, A.: Torsional impact response of a penny-shaped crack lying on a bimaterial interface. *Eng. Fract. Mech.* **18**(5), 1059–1066 (1983)
17. Ueda, S., Shindo, Y., Atsumi, A.: Torsional impact response of a penny-shaped interface crack in a layered composite. *Eng. Fract. Mech.* **19**(6), 1095–1104 (1984)
18. Saxena, H.S., Dhaliwala, R.S.: A penny-shaped crack at the interface of two bonded dissimilar transversely isotropic elastic half-spaces. *Eng. Fract. Mech.* **37**(4), 891–899 (1990)
19. Saxena, H.S., Dhaliwala, R.S., He, W., Rokne, J.G.: Penny-shaped interface crack between dissimilar nonhomogeneous elastic layers under axially symmetric torsion. *Acta Mech.* **99**, 201–211 (1993)
20. Das, S., Patra, B., Debnath, L.: Stress intensity factors for an interfacial crack between an orthotropic half-plane bonded to a dissimilar orthotropic layer with a punch. *Comput. Math. Appl.* **35**(12), 27–40 (1998)
21. Li, C., Weng, G.J.: Dynamic fracture analysis for a penny-shaped crack in an FGM interlayer between dissimilar half spaces. *Math. Mech. Solids* **7**(2), 149–163 (2002)
22. Menshykov, O.V., Menshykov, V.A., Guz, I.A.: The contact problem for an open penny-shaped crack under normally incident tension–compression wave. *Eng. Fract. Mech.* **75**, 1114–1126 (2008)
23. Mykhaskiv, V.V., Khay, O.M.: Interaction between rigid-disc inclusion and penny-shaped crack under elastic time-harmonic wave incidence. *Int. J. Solids Struct.* **46**(3), 602–616 (2009)
24. Lee, H.K., Tran, X.H.: On stress analysis for a penny-shaped crack interacting with inclusions and voids. *Int. J. Solids Struct.* **47**, 549–558 (2010)
25. Dovzhik, M.V.: Fracture of a half-space compressed along a penny-shaped crack located at a short distance from the surface. *Int. Appl. Mech.* **48**(3), 294–304 (2012)
26. Lee, D.-S.: Penny-shaped crack in a plate of finite thickness subjected to a uniform shearing stress. *Z. Angew. Math. Phys.* **64**, 361–369 (2013)
27. Basu, S., Mandal, S.C.: Impact of torsional load on a penny-shaped crack in an elastic layer sandwiched between two elastic half-spaces. *Int. J. Appl. Comput. Math.* **2**, 533–543 (2016)
28. Fox, L., Goodwin, E.T.: The numerical solution of non-singular linear integral equations. *Philos. Trans.* **A.245**, 501–534 (1953)
29. Sih, G.C.: *Mechanics of Fracture*, vol. 4, p. 25. Noordhoff International Publishing, Leyden (1977)
30. Roylance, D.: *Mechanics of Materials*. Wiley, New York (1995)
31. Brown, J.W., Churchill, R.V.: *Complex Variables and Applications*, 8th edn, pp. 298–299. McGraw-Hill, New York (2009)
32. Rice, R.G., Do, D.D.: *Applied Mathematics and Modeling for Chemical Engineers*. Wiley, New York (1995)
33. Zakian, V.: Numerical inversions of Laplace transforms. *Electron. Lett.* **5**, 120–121 (1969)
34. Zakian, V.: Optimization of numerical inversion of Laplace transforms. *Electron. Lett.* **6**, 667–679 (1970)




## Torsional wave propagation on a penny-shaped crack in an orthotropic layer sandwiched between two rigid discs bonded by an orthotropic elastic half-space

Somashri Karan, Sourav Kumar Panja, Sanjoy Basu & S. C. Mandal

To cite this article: Somashri Karan, Sourav Kumar Panja, Sanjoy Basu & S. C. Mandal (2022): Torsional wave propagation on a penny-shaped crack in an orthotropic layer sandwiched between two rigid discs bonded by an orthotropic elastic half-space, *Waves in Random and Complex Media*, DOI: [10.1080/17455030.2022.2132315](https://doi.org/10.1080/17455030.2022.2132315)

To link to this article: <https://doi.org/10.1080/17455030.2022.2132315>

 Published online: 12 Oct 2022.

---

 Submit your article to this journal [↗](#)

---

 View related articles [↗](#)

---

 View Crossmark data [↗](#)

---



# Torsional wave propagation on a penny-shaped crack in an orthotropic layer sandwiched between two rigid discs bonded by an orthotropic elastic half-space

Somashri Karan <sup>a</sup>, Sourav Kumar Panja <sup>a</sup>, Sanjoy Basu <sup>b</sup> and S. C. Mandal<sup>a</sup>

<sup>a</sup>Department of Mathematics, Jadavpur University, Kolkata, India; <sup>b</sup>Department of Mathematics, Arignar Anna Government Arts and Science College, Karaikal, Puducherry, India

## ABSTRACT

The mechanical stability of the interface of two materials determines the stress behavior of the interface. So, observation of failure analysis in orthotropic composites with penny-shaped crack and circular disc in orthotropic materials due to the presence of torsional waves play a major role in structural design. The present article concerns the study of the torsional wave propagation of a penny-shaped crack in an orthotropic layer and two circular discs bonded between the layer and half-spaces. A general solution for the system is presented as a set of dual integral equations using the Hankel transform technique. Using Abel's transform method, the equations have been transformed into Fredholm integral equations of the second kind, which have been solved numerically to compute the stress intensity factors (SIFs) near the rims of crack and discs. Numerical results are obtained using material constants of two orthotropic mediums to demonstrate the impact of material non-homogeneity, normalized disc radius, and layer depth on SIFs and portrayed by virtue of graphs. The analysis of the physical quantity SIF in the present model leads to speculation about the stability of composites against the propagation of cracks in layered engineering solids by surveilling geometric parameters of orthotropic materials and layer depth.

## ARTICLE HISTORY

Received 1 May 2022  
Accepted 26 September 2022

## KEYWORDS

Penny-shaped crack; circular discs; orthotropic layer; dual integral equation; stress intensity factor

## 1. Introduction

In the field of material science and solid mechanics, orthotropic materials have material properties that differ from each other along three mutually orthogonal two-fold axes of rotational symmetry. High anisotropy of these materials with nine elastic constants are very useful in the fabrication process. Continued works [1–3] have been carried out upon modeling wave propagation through layered orthotropic materials for application in fields of non-destructive evaluation such as geophysics, aircraft engineering, aerospace engineering, acoustics, civil engineering, etc. In fracture analysis, the response of layered composites having cracks and inclusion is highly influenced by the orthotropic anisotropy. Our main objective is to resist the stress initiated by controlling a physical quantity named as stress

intensity factor. In this context, taking a look at orthotropic layered structures with the presence of cracks and inclusion reveals an emerging area of research in designing engineering structures and machines.

A wide variety of analytical and closed-form solutions for different wave propagation including torsion in various anisotropic layered systems have been discussed by many researchers [4–9]. The problem of multiple interfacial axisymmetric cracks in orthotropic layer with FGM orthotropic coating subjected to torsional impact loading was proposed by Bagherpoor et al. [10] using the distributed dislocation technique. The displacement field at a half-space surface caused by an internal crack under a twisting load was reported by Skalsky et al. [11] in the Fourier transform domain. An investigation of stresses associated with the torsional study of cracks in circular bars with a piezoelectric coating and for semi-elliptical surface cracks in a cylindrical bar under pure tension in closed form is presented in papers by Hassani et al. [12] and Ramezani et al. [13] respectively. Trivedi et al. [14] determined SIF for an edge crack influenced by time harmonic wave in orthotropic strip and orthotropic vertical semi-infinite strip utilizing Fourier transformation and Schmidh method.

Sih and Chen [15] gave a solution to the problem of a penny-shaped crack situated in a four-layered composite laminate of isotropic elastic media subject to torsion. Stress analysis was investigated by Rabieifar et al. [16] of functionally graded orthotropic medium with several axisymmetric cracks by the impact of torsional load, by Wu et al. [17] for multiple penny-shaped cracks in an infinite transversely isotropic magneto-electro-elastic space. The solution to torsional impact around a penny-shaped crack has been derived for an orthotropic FGM by Li et al. [18]. Craciun and Barbu [19] carried out the solution in compact closed form for prestressed orthotropic composite with an elliptical hole due to uniform tensile and uniform tangential shear loads using the conformal mapping technique. Selvadurai et al. [20] represented the axisymmetric problem of a penny-shaped crack in a poroelastic half-space based on Biot poroelasticity. He et al. [21] proposed the simulation model for penny-shaped cracks with the help of Lagrange interpolation polynomials and the boundary element method (BEM).

Among the problems related to multilayered anisotropic media, Wang et al. [22] studied the problem of an interface crack in the shape of a penny caused by the action of dynamic torsional load on different layers made of orthotropic media. Torsional impact near a penny-shaped crack has been considered in a transversely isotropic strip by Feng and Zou [23]. Here, the stress field near the crack tip has been derived by applying the asymptotic behavior of the Bessel function. The impact of a sudden torsional load on a penny-shaped crack in an elastic layer sandwiched between two elastic half-space has been considered by Basu et al. [24]. Erdogan and Arin [25] analyzed an axially symmetric elastostatic problem for a penny-shaped interface crack between an elastic layer and a half-space. Stress intensity factors have been determined for a penny-shaped crack located at the interface of two bonded dissimilar transversely isotropic half-spaces by Saxena and Dhaliwal [26]. In all the pieces of literature mentioned above, for the purpose of obtaining the solution, mainly with the aid of Hankel transforms, the mixed boundary value problem has been transformed into dual integral equations, which enables the reduction to second kind integral equations of Fredholm type. Stress analysis for a crack, shaped like a penny was evaluated by Lee and Tran [27], by Ueda et al. [28] in a layered composite under the torsional impact, by Li and Weng [29] within an FGM



interlayer between two different half-spaces subject to torsional impact load, by Saxena [30] for two dissimilar bonded elastic layers subjected to axially symmetric torsion.

Several studies were carried out to examine the effects of stresses on the fracture of composites weakened by subsurface disk-shaped torsion (mode-III) cracks by Bohdanov [31], around two coaxial cylindrical cracks by Itou [32]. Here, tensile stress is applied to cracks in the normal direction. Based on the interaction integral method, the SIFs for circular arc-shaped cracks in orthotropic nonhomogeneous media is derived by Yu et al. [33].

Recently, Madani and Kebli [34], first implemented the torsional wave propagation in a composite media with two rigid discs and a cracked isotropic layer. Based on the study above, in the context of applications of composite materials [35] such as orthotropic laminates, the above types of problems may provide a basis for designing layered composite structures. In many actual-world situations like impresser and turbine disks, various pipes where the geometry type and pressure are axially symmetric, composite materials have faced several types of waves and disturbances. Torsion is one kind of wave disturbance originating from pressure on the crack surface and disc surfaces leading to the onset of crack propagation and stress field around the circular discs within engineering solids. Propagation of torsional waves takes place in turbines, drillings, etc. Also, in the field of engineering foundation, various shapes of inclusion as circular, strip, rectangular, and other types have been used to make the desired foundation. To get a high level of mechanical performance like high-stiffness, lightweight phenomena, flexibility, durability, etc, orthotropic materials are designed as multi-directional laminates by combining two or more materials. So, orthotropic solids may be considered composite materials. In composite materials, crack-like flaws may be initiated during the manufacturing process. In light of this, the stress behavior of orthotropic composites influenced by torsional waves attains a significant field of research in geomechanics as well as applied mechanics. This communication aims to illustrate the nature of stress on geometric parameters of the assumed model for torsional wave propagation.

In what follows, the present article derives fracture analysis of a composite orthotropic medium with a penny-shaped crack and two circular discs subjected to the axisymmetric torsional response. The geometry of the orthotropic composite is modeled based on a layer of finite depth sandwiched between two half-spaces made of the dissimilar orthotropic medium. Hankel transform technique has been utilized to convert the problem to a set of dual integral equations. With the help of Abel's transform technique, the set of integral equations has been expressed in terms of Fredholm integral equations of the second kind. The integral equations are solved numerically by applying the Simpson quadrature formula to compute the stress intensity factors (SIFs) near the rims of the crack and discs. The numerical values of stress intensity factors (SIFs) have been computed considering material constants of two different orthotropic materials as the layer ( $L_1$ ) and the half-spaces ( $L_2$ ) and charted graphically. The graphs reveal that the material non-homogeneity, disc size, crack size, and layer depth have a significant influence on SIFs. The study can serve as a guideline in controlling failure mechanisms, failure propagation, fracture toughness, and the overall stress-strain behavior of composite materials. It is possible to use the conclusions obtained as a guide to engineering practice by comparing the fracture toughness of orthotropic materials.

## 2. Formulation of the elasticity problem

Schematic illustration (Figure 1) of a crack (radius  $h_1$ ) shaped like a penny is taken into account in an orthotropic layer ( $L_1$ ) of thickness  $2d$  where the media have a symmetry along the  $z$ -axis. The orthotropic layer ( $L_1$ ) and half-space ( $L_2$ ) are connected by two rigid discs. Two rigid discs having radius  $h_2$  are symmetrically placed between the layer ( $L_1$ ) and half-space ( $L_2$ ) in the planes  $z = \pm d$  and are twisted by the axisymmetric torsion. Cylindrical polar coordinates of  $(r, \theta, z)$  yield displacement components with a form similar to that below:

$$u_r = 0, \quad u_\theta = u_\theta(r, z), \quad u_z = 0.$$

The governing equation of motion for orthotropic material (Hassani et al. [36]) takes the form

$$\frac{\partial^2 u_\theta^{(j)}}{\partial r^2} + \frac{1}{r} \frac{\partial u_\theta^{(j)}}{\partial r} - \frac{u_\theta^{(j)}}{r^2} + C^{(j)} \frac{\partial^2 u_\theta^{(j)}}{\partial z^2} = 0 \quad (j = 1, 2), \quad (1)$$

where  $C^{(j)} = \frac{C_{44}^{(j)}}{C_{66}^{(j)}}$ , and  $C_{44}^{(j)}, C_{66}^{(j)}$  are orthotropic shear moduli in the radial and circumferential direction. Throughout the manuscript, superscripts '1', '2' have been used to refer to sandwiched orthotropic layer ( $L_1$ ), orthotropic half-space ( $L_2$ ), respectively. The nonzero component of stress tensor can be expressed as follows:

$$\sigma_{\theta r}^{(j)} = C_{66}^{(j)} \left( \frac{\partial u_\theta^{(j)}}{\partial r} - \frac{u_\theta^{(j)}}{r} \right),$$

$$\sigma_{\theta z}^{(j)} = C_{44}^{(j)} \left( \frac{\partial u_\theta^{(j)}}{\partial z} \right).$$

The regularity conditions at infinity are

$$\lim_{r, z \rightarrow \infty} u_\theta^{(j)}(r, z) = 0,$$

$$\lim_{r, z \rightarrow \infty} \sigma_{\theta z}^{(j)}(r, z) = 0. \quad (2)$$

The boundary conditions for the formulated problem are as follows:

$$\sigma_{\theta z}^{(1)}(r, 0^+) = 0, \quad 0 \leq r \leq h_1, \quad (3)$$

$$u_\theta^{(1)}(r, 0^+) = 0, \quad r > h_1, \quad (4)$$

$$u_\theta^{(1)}(r, d^-) = u_\theta^{(2)}(r, d^+) = \omega r, \quad 0 \leq r \leq h_2. \quad (5)$$

Also, the interfaces  $z = \pm d$  between the rigid discs and orthotropic half-spaces are bonded perfectly. So, at the interface  $z = \pm d$  we find the continuity conditions as

$$\sigma_{\theta z}^{(1)}(r, d^-) = \sigma_{\theta z}^{(2)}(r, d^+) = 0, \quad r > h_2, \quad (6)$$

$$u_\theta^{(1)}(r, d^-) = u_\theta^{(2)}(r, d^+) = 0, \quad r > h_2. \quad (7)$$

Application of the standard Hankel integral transform to the regularity condition given by Equation (2), the solution of Equation (1) for the orthotropic layer  $L_1$  ( $|z| \leq d$ ), and

orthotropic half-space  $L_2$  ( $|z| \geq d$ ) can be taken as

$$u_{\theta}^{(1)}(r, z) = \int_0^{\infty} \left[ E(\zeta) e^{-\frac{\zeta z}{\sqrt{C^{(1)}}}} + F(\zeta) e^{\frac{\zeta z}{\sqrt{C^{(1)}}}} \right] J_1(\zeta r) d\zeta, \quad (8)$$

and

$$u_{\theta}^{(2)}(r, z) = \int_0^{\infty} \left[ G(\zeta) e^{-\frac{\zeta z}{\sqrt{C^{(2)}}}} \right] J_1(\zeta r) d\zeta, \quad (9)$$

where  $J_1(\cdot)$  is the first kind of Bessel function of order one and  $C^{(1)} = \frac{C_{44}^{(1)}}{C_{66}^{(1)}}$ ,  $C^{(2)} = \frac{C_{44}^{(2)}}{C_{66}^{(2)}}$ . In Equations (8)–(9),  $E(\zeta)$ ,  $F(\zeta)$ ,  $G(\zeta)$  are unknown functions which are to be determined with the help of boundary conditions. The expressions for stresses  $\tau_{\theta z}$  now becomes

$$\sigma_{\theta z}^{(1)}(r, z) = P^{(1)} \int_0^{\infty} \zeta \left[ -E(\zeta) e^{-\frac{\zeta z}{\sqrt{C^{(1)}}}} + F(\zeta) e^{-\frac{\zeta z}{\sqrt{C^{(1)}}}} \right] J_1(\zeta r) d\zeta, \quad (10)$$

$$\sigma_{\theta z}^{(2)}(r, z) = -P^{(2)} \int_0^{\infty} \zeta \left[ G(\zeta) e^{-\frac{\zeta z}{\sqrt{C^{(2)}}}} \right] J_1(\zeta r) d\zeta, \quad (11)$$

where

$$P^{(1)} = \sqrt{C_{44}^{(1)} \cdot C_{66}^{(1)}}, \quad P^{(2)} = \sqrt{C_{44}^{(2)} \cdot C_{66}^{(2)}}.$$

### 3. Derivation of integral equation

Using the above expressions, the continuity condition (7) yields

$$G(\zeta) = E(\zeta) e^{\zeta d Q_3} + F(\zeta) e^{\zeta d Q_4}, \quad (12)$$

where

$$Q_3 = \frac{1}{\sqrt{C^{(2)}}} - \frac{1}{\sqrt{C^{(1)}}}, \quad Q_4 = \frac{1}{\sqrt{C^{(2)}}} + \frac{1}{\sqrt{C^{(1)}}},$$

and we derived the following set of dual integral equations utilizing boundary conditions (3)–(6)

$$\int_0^{\infty} \zeta [F(\zeta) - E(\zeta)] J_1(\zeta r) d\zeta = 0, \quad 0 \leq r \leq h_1, \quad (13)$$

$$\int_0^{\infty} [E(\zeta) + F(\zeta)] J_1(\zeta r) d\zeta = 0, \quad r > h_1, \quad (14)$$

$$\int_0^{\infty} \left[ E(\zeta) e^{-\frac{\zeta d}{\sqrt{C^{(1)}}}} + F(\zeta) e^{\frac{\zeta d}{\sqrt{C^{(1)}}}} \right] J_1(\zeta r) d\zeta = \omega r, \quad 0 \leq r \leq h_2, \quad (15)$$

$$\int_0^{\infty} \zeta \left[ F(\zeta) e^{\frac{\zeta d}{\sqrt{C^{(1)}}}} \right] J_1(\zeta r) d\zeta = 0, \quad r > h_2. \quad (16)$$

The above set of dual integral equations has been converted to a set of integral equations of Fredholm type by introducing two auxiliary functions  $m_1(x)$  and  $m_2(x)$  as follows:

$$E(\zeta) + F(\zeta) = \sqrt{\zeta} \int_0^{h_1} [\sqrt{x} m_1(x)] J_{\frac{3}{2}}(\zeta x) dx, \quad (17)$$

$$F(\zeta) e^{\frac{\zeta d}{\sqrt{C^{(1)}}}} = \sqrt{\zeta} \int_0^{h_2} [\sqrt{x} m_2(x)] J_{\frac{1}{2}}(\zeta x) dx. \quad (18)$$

After solving the unknown functions, we get

$$E(\zeta) = \sqrt{\zeta} \int_0^{h_1} [\sqrt{x}m_1(x)] J_{\frac{3}{2}}(\zeta x) dx - \sqrt{\zeta} e^{-\frac{\zeta d}{\sqrt{C(1)}}} \int_0^{h_2} [\sqrt{x}m_2(x)] J_{\frac{1}{2}}(\zeta x) dx, \quad (19)$$

$$F(\zeta) = \sqrt{\zeta} e^{-\frac{\zeta d}{\sqrt{C(1)}}} \int_0^{h_2} [\sqrt{x}m_2(x)] J_{\frac{1}{2}}(\zeta x) dx. \quad (20)$$

Now, Equations (13) and (15) become the following form

$$\begin{aligned} & \int_0^{h_1} \sqrt{x}m_1(x) dx \int_0^\infty \zeta^{\frac{3}{2}} g_1(\zeta) J_{\frac{3}{2}}(\zeta x) J_1(\zeta r) d\zeta \\ & + \int_0^{h_2} \sqrt{x}m_2(x) dx \int_0^\infty \zeta^{\frac{3}{2}} g_2(\zeta) J_{\frac{1}{2}}(\zeta x) J_1(\zeta r) d\zeta = 0, \quad r < h_1, \end{aligned} \quad (21)$$

and

$$\begin{aligned} & \int_0^{h_1} \sqrt{x}m_1(x) dx \int_0^\infty \zeta^{\frac{1}{2}} g_3(\zeta) J_{\frac{3}{2}}(\zeta x) J_1(\zeta r) d\zeta \\ & + \int_0^{h_2} \sqrt{x}m_2(x) dx \int_0^\infty \zeta^{\frac{1}{2}} g_4(\zeta) J_{\frac{1}{2}}(\zeta x) J_1(\zeta r) d\zeta = \omega r, \quad r < h_2, \end{aligned} \quad (22)$$

where

$$\begin{aligned} g_1(\zeta) &= 1, \quad g_2(\zeta) = -2e^{-\frac{\zeta d}{\sqrt{C(1)}}}, \\ g_3(\zeta) &= e^{-\frac{\zeta d}{\sqrt{C(1)}}}, \quad g_4(\zeta) = 1 - e^{-\frac{2\zeta d}{\sqrt{C(1)}}}. \end{aligned}$$

Using the following results

$$\int_0^\infty \zeta^{\frac{1}{2}} J_2(\zeta r) J_{\frac{3}{2}}(\zeta x) dx = \begin{cases} 0 & ; x > r, \\ \sqrt{\frac{2}{\pi}} \frac{x^{\frac{3}{2}}}{r^2 \sqrt{r^2 - x^2}} & ; x < r, \end{cases}$$

and

$$\zeta J_1(\zeta r) = \frac{1}{r^2} \frac{d}{dr} [r^2 J_2(\zeta r)],$$

Equation (21) converted to Abel equation as

$$\begin{aligned} & \sqrt{\frac{2}{\pi}} \int_0^r \frac{x^2 m_1(x)}{\sqrt{r^2 - x^2}} dx + r^2 \int_0^{h_1} \sqrt{x}m_1(x) dx \int_0^\infty \zeta^{\frac{1}{2}} (g_1(\zeta) - 1) J_{\frac{3}{2}}(\zeta x) J_2(\zeta r) d\zeta \\ & + r^2 \int_0^{h_2} \sqrt{x}m_2(x) dx \int_0^\infty \zeta^{\frac{1}{2}} g_2(\zeta) J_{\frac{1}{2}}(\zeta x) J_2(\zeta r) d\zeta = 0, \quad r < h_1, \end{aligned} \quad (23)$$

which can be inverted by using Abel transform as follows

$$\begin{aligned} x^2 m_1(x) &= \sqrt{\frac{2}{\pi}} \frac{d}{dx} \int_0^x \frac{r^3}{\sqrt{x^2 - r^2}} \left[ - \int_0^{h_1} \sqrt{\lambda} m_1(\lambda) d\lambda \int_0^\infty \zeta^{\frac{1}{2}} (g_1(\zeta) - 1) J_{\frac{3}{2}}(\zeta \lambda) J_2(\zeta r) d\zeta \right. \\ & \left. - \int_0^{h_2} \sqrt{\lambda} m_2(\lambda) d\lambda \int_0^\infty \zeta^{\frac{1}{2}} g_2(\zeta) J_{\frac{1}{2}}(\zeta \lambda) J_2(\zeta r) d\zeta \right] dr, \quad r < h_1. \end{aligned} \quad (24)$$

With the help of the formula

$$\sqrt{\frac{2}{\pi}} \frac{d}{dt} \int_0^x \frac{r^3}{\sqrt{x^2 - r^2}} J_2(\zeta r) dr = \sqrt{\zeta} x^{\frac{5}{2}} J_{\frac{3}{2}}(\zeta x),$$

Equation (24) is rewritten as a second kind of Fredholm integral equation in the following form

$$m_1(x) + x^{\frac{1}{2}} \int_0^{h_1} \lambda^{\frac{1}{2}} m_1(\lambda) P(x, \lambda) d\lambda + x^{\frac{1}{2}} \int_0^{h_2} \lambda^{\frac{1}{2}} m_2(\lambda) Q(x, \lambda) d\lambda = 0, \quad r < h_1, \quad (25)$$

where

$$P(x, \lambda) = \int_0^\infty \zeta (g_1(\zeta) - 1) J_{\frac{3}{2}}(\zeta x) J_{\frac{3}{2}}(\zeta \lambda) d\zeta,$$

$$Q(x, \lambda) = \int_0^\infty \zeta g_2(\zeta) J_{\frac{3}{2}}(\zeta x) J_{\frac{3}{2}}(\zeta \lambda) d\zeta.$$

Following a similar type of analysis, we get another Fredholm integral equation of the second kind from Equation (22) as

$$m_2(x) + x^{\frac{1}{2}} \int_0^{h_1} \lambda^{\frac{1}{2}} m_1(\lambda) R(x, \lambda) d\lambda + x^{\frac{1}{2}} \int_0^{h_2} \lambda^{\frac{1}{2}} m_2(\lambda) S(x, \lambda) d\lambda = \frac{4\omega}{\sqrt{2\pi}} x, \quad 0 < x < h_2, \quad (26)$$

where

$$R(x, \lambda) = \int_0^\infty \zeta g_3(\zeta) J_{\frac{1}{2}}(\zeta x) J_{\frac{3}{2}}(\zeta \lambda) d\zeta,$$

$$S(x, \lambda) = \int_0^\infty \zeta (g_4(\zeta) - 1) J_{\frac{1}{2}}(\zeta x) J_{\frac{1}{2}}(\zeta \lambda) d\zeta.$$

We then introduced dimensionless variables ( $\xi$  and  $\mu$ ) as:

$$\lambda = h_1 \xi, \quad 0 < \lambda < h_1; \quad x = h_1 \mu, \quad 0 < x < h_1;$$

$$\lambda = h_2 \xi, \quad 0 < \lambda < h_2; \quad x = h_2 \mu, \quad 0 < x < h_2.$$

Then, Equations (25) and (26) have been multiplied by  $\frac{\sqrt{2\pi} m_1(h_1 \mu)}{4h_1 \omega}$  and  $\frac{\sqrt{2\pi} m_2(h_2 \mu)}{4h_2 \omega}$  respectively and rewritten in terms of the dimensionless variables to obtain the non-dimensional form:

$$M_1(x) + a^2 \mu^{\frac{1}{2}} \int_0^1 \xi^{\frac{1}{2}} M_1(\xi) P(\mu, \xi) d\xi + \frac{\mu^{\frac{1}{2}}}{a^{\frac{1}{2}}} \int_0^1 \xi^{\frac{1}{2}} M_2(\xi) Q(\mu, \xi) d\xi = 0, \quad \mu < 1, \quad (27)$$

$$M_2(x) + a^{\frac{5}{2}} \mu^{\frac{1}{2}} \int_0^1 \xi^{\frac{1}{2}} M_1(\xi) R(\mu, \xi) d\xi + \mu^{\frac{1}{2}} \int_0^1 \xi^{\frac{1}{2}} M_2(\xi) S(\mu, \xi) d\xi = \mu, \quad \mu < 1, \quad (28)$$

where

$$P(\mu, \xi) = 0, \quad Q(\mu, \xi) = \int_0^\infty \eta g_2(\eta) J_{\frac{3}{2}}(\eta a \mu) J_{\frac{3}{2}}(\eta \xi) d\eta,$$

$$R(\mu, \xi) = \int_0^\infty \zeta g_3(\eta) J_{\frac{1}{2}}(\eta \mu) J_{\frac{3}{2}}(\eta a \xi) d\eta, \quad S(\mu, \xi) = \int_0^\infty \eta (g_4(\eta) - 1) J_{\frac{1}{2}}(\eta \mu) J_{\frac{1}{2}}(\eta \xi) d\eta.$$

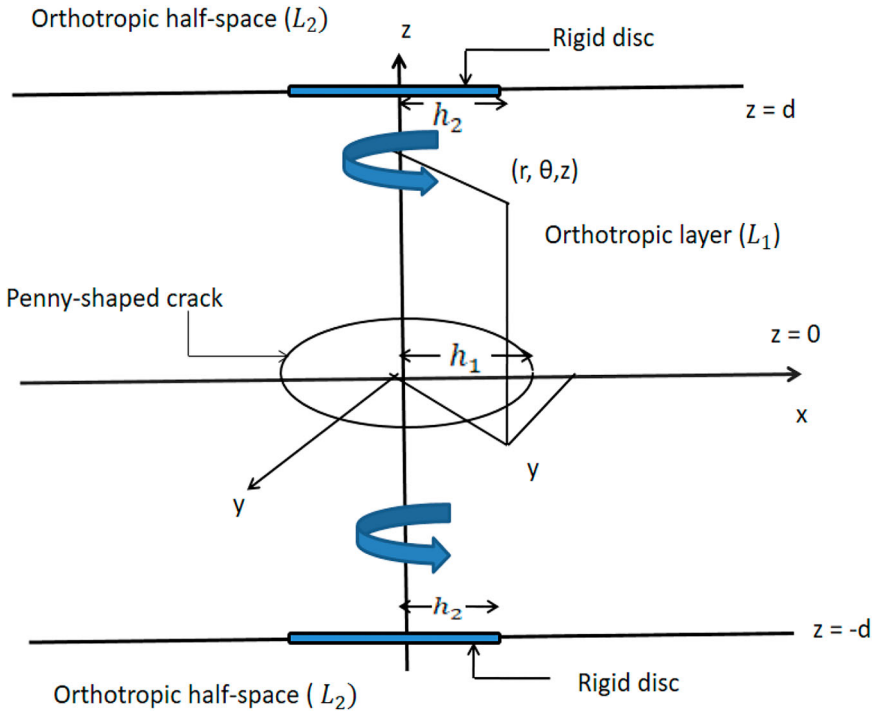


**Figure 1.** Geometry and notation of the problem.

In the above system, we have used the following transformations:

$$M_1(\mu) = \frac{\sqrt{2\pi}}{4h_1\omega} m_1(h_1\mu), \quad M_2(\mu) = \frac{\sqrt{2\pi}}{4h_2\omega} m_2(h_2\mu), \quad a = \frac{h_1}{h_2}, \quad \zeta = \frac{\eta}{h_2}, \quad D = \frac{d}{h_2}.$$

#### 4. The solution method of integral equations

The Fredholm integral Equations (27) and (28) have been solved by applying the Gaussian quadrature formula. Here the interval  $[0, 1]$  has been divided into  $T$  equal sub-interval each of length  $\frac{1}{T}$ . Next, Equations (27) and (28) can be written as:

$$M_{1\alpha} + \frac{1}{Ta^{\frac{1}{2}}} \mu_{\alpha}^{\frac{1}{2}} \sum_{\beta=1}^T (\mu_{\beta}^{\frac{1}{2}} M_{2\beta} Q_{\alpha\beta}) = 0, \quad \alpha, \beta = 1, 2, \dots, T$$

$$M_{2\alpha} + \frac{a^{\frac{5}{2}}}{T} \mu_{\alpha}^{\frac{1}{2}} \sum_{\beta=1}^T (\mu_{\beta}^{\frac{1}{2}} M_{1\beta} R_{\alpha\beta}) + \frac{1}{T} \mu_{\alpha}^{\frac{1}{2}} \sum_{\beta=1}^T (\mu_{\beta}^{\frac{1}{2}} M_{2\beta} S_{\alpha\beta}) = \mu_{\alpha}, \quad \alpha, \beta = 1, 2, \dots, T$$

with the following notations

$$\mu = \mu_{\alpha} = \frac{2\alpha - 1}{2T}, \quad \xi = \mu_{\beta} = \frac{2\beta - 1}{2T},$$

$$M_1(\mu_{\alpha}) = M_{1\alpha}, \quad M_2(\mu_{\alpha}) = M_{2\alpha}, \quad Q(\mu_{\alpha}, \mu_{\beta}) = Q_{\alpha\beta},$$

$$R(\mu_{\alpha}, \mu_{\beta}) = R_{\alpha\beta}, \quad S(\mu_{\alpha}, \mu_{\beta}) = S_{\alpha\beta},$$

$$\begin{aligned}
 Q_{\alpha\beta} &= \int_0^\infty \eta g_2(\eta) J_{\frac{3}{2}}(\eta a \mu_\alpha) J_{\frac{1}{2}}(\eta \mu_\beta) d\eta, \\
 R_{\alpha\beta} &= \int_0^\infty \eta g_3(\eta) J_{\frac{1}{2}}(\eta \mu_\alpha) J_{\frac{3}{2}}(\eta a \mu_\beta) d\eta, \\
 S_{\alpha\beta} &= \int_0^\infty \eta (g_4(\eta) - 1) J_{\frac{1}{2}}(\eta \mu_\alpha) J_{\frac{1}{2}}(\eta \mu_\beta) d\eta.
 \end{aligned}$$

Also, the unknown functions  $E(\zeta)$ ,  $F(\zeta)$ ,  $G(\zeta)$  can be approximated from Equations (12), (19) and (20) as follows for numerical computation:

$$\begin{aligned}
 G(\eta) &= E(\eta) e^{\eta D Q_3} + F(\eta) e^{\eta D Q_4}, \\
 E(\eta) &= \frac{4h_2^2 \omega}{\sqrt{2\pi T}} \eta^{\frac{1}{2}} \sum_{\alpha=1}^T \mu_\alpha^{\frac{1}{2}} \left[ a^{\frac{5}{2}} M_{1\alpha} J_{\frac{3}{2}}(\eta a \mu_\alpha) - e^{-\frac{\eta D}{\sqrt{c(1)}}} M_{2\alpha} J_{\frac{1}{2}}(\eta \mu_\alpha) \right], \\
 F(\eta) &= \frac{4h_2^2 \omega}{\sqrt{2\pi T}} \eta^{\frac{1}{2}} e^{-\frac{\eta D}{\sqrt{c(1)}}} \sum_{\alpha=1}^T \left[ \mu_\alpha^{\frac{1}{2}} M_{2\alpha} J_{\frac{1}{2}}(\eta \mu_\alpha) \right].
 \end{aligned}$$

## 5. Quantities of physical interest

The stress intensity factors (SIFs) at the edge of the crack and at the rim of the disc are as follows:

$$K_{h_1} = \lim_{r \rightarrow h_1^+} \sqrt{2\pi(r - h_1)} \sigma_{\theta z}^{(1)}(r, z)|_{z=0}, \quad (29)$$

$$K_{h_2} = \lim_{r \rightarrow h_2^-} \sqrt{2\pi(h_2 - r)} \sigma_{\theta z}^{(1)}(r, z)|_{z=d}. \quad (30)$$

From Equation (10), the stress on the plane  $z = 0$  for  $r \geq h_1$  and  $z = d$  becomes

$$\begin{aligned}
 \sigma_{\theta z}^{(1)}(r, 0) &= p^{(1)} \int_0^\infty \zeta^{\frac{3}{2}} \left[ - \int_0^{h_1} x^{\frac{1}{2}} m_1(x) J_{\frac{3}{2}}(\zeta x) dx \right. \\
 &\quad \left. + 2 e^{\frac{-\zeta d}{\sqrt{c(1)}}} \int_0^{h_2} x^{\frac{1}{2}} m_2(x) J_{\frac{1}{2}}(\zeta x) dx \right] J_1(\zeta r) d\zeta, \quad (31)
 \end{aligned}$$

$$\begin{aligned}
 \sigma_{\theta z}^{(1)}(r, d) &= p^{(1)} \int_0^\infty \zeta^{\frac{3}{2}} \left[ - e^{\frac{-\zeta d}{\sqrt{c(1)}}} \int_0^{h_1} x^{\frac{1}{2}} m_1(x) J_{\frac{3}{2}}(\zeta x) dx \right. \\
 &\quad \left. + (1 + e^{\frac{-2\zeta d}{\sqrt{c(1)}}}) \int_0^{h_2} x^{\frac{1}{2}} m_2(x) J_{\frac{1}{2}}(\zeta x) dx \right] J_1(\zeta r) d\zeta. \quad (32)
 \end{aligned}$$

Using the following relation,

$$J_1(\zeta r) = -\frac{1}{\zeta} \frac{d}{dr} J_0(\zeta r),$$

we obtain

$$\begin{aligned} \sigma_{\theta z}^{(1)}(r, 0) &= P^{(1)} \int_0^{h_1} x^{\frac{1}{2}} m_1(x) dx \int_0^\infty \zeta^{\frac{1}{2}} J_{\frac{3}{2}}(\zeta x) J_0(\zeta r) d\zeta \\ &+ 2P^{(1)} \int_0^{h_2} x^{\frac{1}{2}} m_2(x) dx \int_0^\infty \zeta^{\frac{3}{2}} e^{\frac{-\zeta d}{\sqrt{c^{(1)}}}} J_{\frac{1}{2}}(\zeta x) J_1(\zeta r) d\zeta, \end{aligned} \quad (33)$$

$$\begin{aligned} \sigma_{\theta z}^{(1)}(r, d) &= -P^{(1)} \int_0^{h_2} x^{\frac{1}{2}} m_2(x) dx \int_0^\infty \zeta^{\frac{1}{2}} J_{\frac{1}{2}}(\zeta x) J_0(\zeta r) d\zeta - P^{(1)} \int_0^{h_1} x^{\frac{1}{2}} m_1(x) dx \\ &\int_0^\infty \zeta^{\frac{3}{2}} e^{\frac{-\zeta d}{\sqrt{c^{(1)}}}} J_1(\zeta r) d\zeta + P^{(1)} \int_0^{h_2} x^{\frac{1}{2}} m_2(x) dx \int_0^\infty \zeta^{\frac{3}{2}} e^{\frac{-2\zeta d}{\sqrt{c^{(1)}}}} J_{\frac{1}{2}}(\zeta x) J_1(\zeta r) d\zeta. \end{aligned} \quad (34)$$

Based on the formula  $J_\nu(\zeta) \simeq \sqrt{\frac{2}{\pi\zeta}} \cos(\zeta - \frac{\pi\nu}{2} - \frac{\pi}{4})$  for asymptotic behavior of the first kind of Bessel function for large values of  $\zeta$ , we get the relations as

$$\begin{aligned} J_{\frac{3}{2}}(\zeta x) &\simeq \sqrt{\frac{2}{\pi\zeta x}} \cos(\zeta x - \pi) = -\sqrt{\frac{2}{\pi\zeta x}} \cos(\zeta x), \\ J_{\frac{1}{2}}(\zeta x) &\simeq \sqrt{\frac{2}{\pi\zeta x}} \cos\left(\zeta x - \frac{\pi}{2}\right) = -\sqrt{\frac{2}{\pi\zeta x}} \sin(\zeta x). \end{aligned}$$

Next, we use the following integral formula

$$\begin{aligned} \int_0^\infty \cos(\zeta x) J_0(\zeta r) d\zeta &= \begin{cases} 0 & ; r < x, \\ \frac{1}{\sqrt{r^2 - x^2}} & ; r > x. \end{cases} \quad \text{and} \\ \int_0^\infty \sin(\zeta x) J_0(\zeta r) d\zeta &= \begin{cases} 0 & ; r > x, \\ \frac{1}{\sqrt{x^2 - r^2}} & ; r < x, \end{cases} \end{aligned}$$

to get

$$\sigma_{\theta z}^{(1)}(r, 0) = -\sqrt{\frac{2}{\pi}} P^{(1)} \frac{d}{dr} \int_0^{h_1} \frac{m_1(x)}{\sqrt{r^2 - x^2}} dx + \chi_1(r), \quad (35)$$

$$\sigma_{\theta z}^{(1)}(r, d) = -\sqrt{\frac{2}{\pi}} P^{(1)} \frac{d}{dr} \int_0^{h_2} \frac{m_2(x)}{\sqrt{x^2 - r^2}} dx + \chi_2(r), \quad (36)$$

where

$$\begin{aligned} \chi_1(r) &= 2P^{(1)} \int_0^{h_2} x^{\frac{1}{2}} m_2(x) dx \int_0^\infty \zeta^{\frac{3}{2}} e^{\frac{-\zeta d}{\sqrt{c^{(1)}}}} J_{\frac{1}{2}}(\zeta x) J_1(\zeta r) d\zeta, \\ \chi_2(r) &= -P^{(1)} \int_0^{h_1} x^{\frac{1}{2}} m_1(x) dx \int_0^\infty \zeta^{\frac{3}{2}} e^{\frac{-\zeta d}{\sqrt{c^{(1)}}}} J_1(\zeta r) d\zeta \\ &+ P^{(1)} \int_0^{h_2} x^{\frac{1}{2}} m_2(x) dx \int_0^\infty \zeta^{\frac{3}{2}} e^{\frac{-2\zeta d}{\sqrt{c^{(1)}}}} J_{\frac{1}{2}}(\zeta x) J_1(\zeta r) d\zeta. \end{aligned}$$



**Table 1.** Elastic constants of layer ( $L_1$ ) and half-space ( $L_2$ ).

Elastic medium	$C_{44}$ (GPA unit)	$C_{66}$ (GPA unit)	$\rho$ (kg/m <sup>3</sup> )
Orthotropic layer ( $L_1$ )	5.35	6.47	3400
Orthotropic half-space ( $L_2$ )	4.35	5.0	9890

Then, we obtain by integrating

$$\sigma_{\theta z}^{(1)}(r, 0) = -\sqrt{\frac{2}{\pi}} P^{(1)} \left[ \frac{h_1 m_1(h_1)}{r\sqrt{r^2 - h_1^2}} - \int_0^{h_1} \frac{x m_1'(x)}{r\sqrt{r^2 - x^2}} dx \right] + \chi_1(r), \quad (37)$$

$$\sigma_{\theta z}^{(1)}(r, d) = -\sqrt{\frac{2}{\pi}} P^{(1)} \left[ \frac{h_2 m_2(h_2)}{r\sqrt{h_2^2 - r^2}} - \int_r^{h_2} \frac{x m_2'(x)}{r\sqrt{x^2 - r^2}} dx \right] + \chi_2(r). \quad (38)$$

So, SIFs at  $r = h_1$  and  $r = h_2$  can be written as

$$K_{h_1} = \lim_{r \rightarrow h_1^+} \sqrt{2\pi(r - h_1)} P^{(1)} \sqrt{\frac{2}{\pi}} \left( \frac{h_1 m_1(h_1)}{r\sqrt{r^2 - h_1^2}} \right), \quad (39)$$

$$K_{h_2} = \lim_{r \rightarrow h_2^+} \sqrt{2\pi(h_2 - r)} P^{(1)} \sqrt{\frac{2}{\pi}} \left( \frac{h_2 m_2(h_2)}{r\sqrt{h_2^2 - r^2}} \right). \quad (40)$$

Next, applying the transformations

$$m_1(h_1) = \frac{4h_1\omega}{\sqrt{2\pi}} M_{1T} \quad \text{and} \quad m_2(h_2) = \frac{4h_2\omega}{\sqrt{2\pi}} M_{2T},$$

we can write

$$K_{h_1} = \frac{4\omega P^{(1)} \sqrt{h_1}}{\sqrt{\pi}} M_{1T}, \quad (41)$$

$$K_{h_2} = \frac{4\omega P^{(1)} \sqrt{h_2}}{\sqrt{\pi}} M_{2T}. \quad (42)$$

## 6. Numerical and graphical demonstration

To explain the theoretical results graphically, numerical values of the SIFs are calculated at the edge of the penny-shaped crack and near the rim of circular disc from Equations (41) and (42) respectively. We use here Gaussian quadrature rule and the numerical computations are performed by using MATLAB software. We considered the numerical values of elastic constants and densities of the orthotropic layer and half-space as listed in Table 1 (Sourav et al. [37]).

In this section, numerical values of normalized SIFs along with the ratio of crack radius  $h_1$ , to radius  $h_2$  of disc (i.e.  $a = h_1/h_2$ ) are displayed through graphical demonstrations as shown in Figures 2–3. In order to explore the effect of normalized layer depth ( $D = d/h_2$ ) on SIFs, four values of layer depth, namely  $D = 0.25, 0.50, 0.75, 1.0$  has been considered.

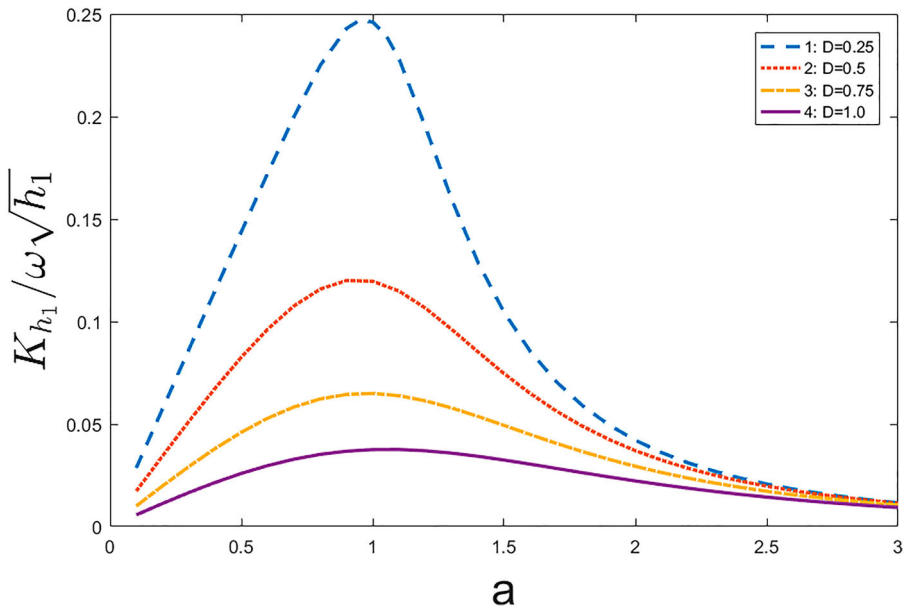


**Figure 2.** SIF as a function of the ratio of  $h_1/h_2 = a$  for crack.

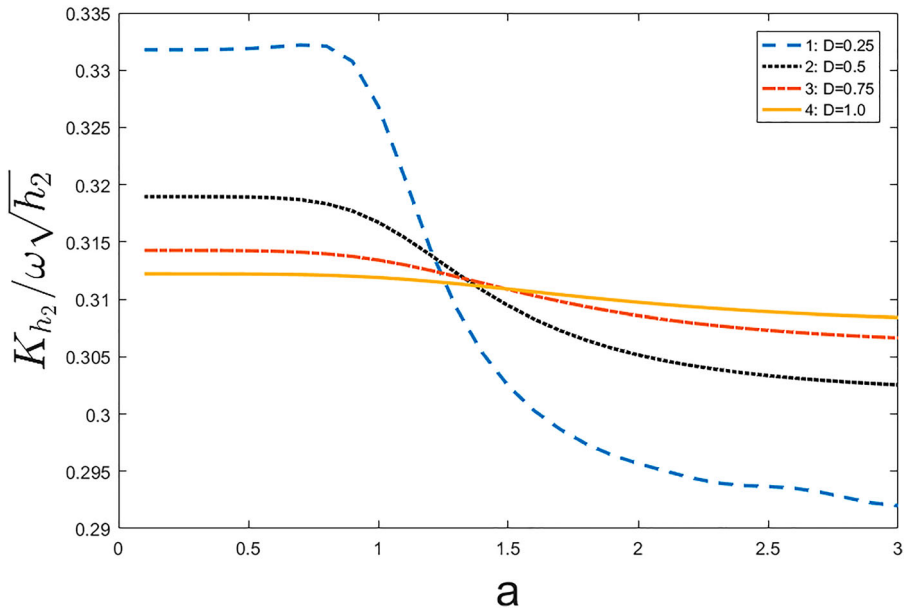


**Figure 3.** SIF as a function of the ratio of  $h_1/h_2 = a$  for circular disc.

From Figure 2, it can be observed that the depth of the orthotropic layer has significant effects on the normalized SIFs for the penny-shaped crack. For all values of the ratio 'a', it seems that with the decrease of layer depth (D), the peak SIFs will increase gradually. Also,

it is seen that the curve of SIFs gradually increases first, attains to peak value at  $a = 1.0$ , and then decreases with an increase of the ratio ' $a$ '.

In Figure 3, the SIFs at the rim of circular discs versus the ratio  $a$  of the crack radius with disc radius have been depicted. Here, the ratio  $a$  have a revealing influence on the values of SIFs, in which a rise in this ratio leads to a lower value of SIF. Furthermore, like Figure 2, this figure suggests that the peak value of SIF increases when layer depth  $D$  decreases.

Based on Figures 2–3, we may conclude that the values of SIFs variate in a large scale for large values of ' $a$ ' than those of the smaller values. Lastly, the peak value of SIFs can be raised or lowered by varying the layer depth (i.e. the width between the circular disc and penny-shaped crack). Within engineering solids, it has been seen that the onset of fracture occurs when the numerical values of SIFs cross a certain limit (depending on material anisotropy) named as critical SIFs. Our main objective in fracture analysis of composite medium is to prevent the crack propagation to avoid damage of solid structure by controlling the values of SIFs within a certain range called critical SIFs. In this regard, these results indicate that by modifying crack and disc size ( $a$ ) and layer depth ( $D$ ), the magnitude of SIFs can be controlled which is expected in fracture mechanics for safe structure. Therefore, the analysis can help us in studying the fracture toughness of composite orthotropic bodies with cracks and inclusion under stress.

Now, the results of our problem have been compared with existing literature [34] for isotropic material. Axisymmetric torsion of an internally cracked isotropic elastic medium by two embedded rigid discs has been investigated by Madani et al. [34]. The presented model was formulated for a cracked orthotropic layer with two rigid discs bonded between the layer and half-spaces under axially symmetric torsion. To verify our results with an isotropic case, we substitute  $C_{44} = C_{66} = \mu$  ( $\mu =$  shear modulus of the isotropic material) to convert the problem of orthotropic material to isotropic material. The following expressions of stress and governing partial differential equation have been obtained

$$\sigma_{\theta r}^{(j)} = \mu^{(j)} \left( \frac{\partial u_{\theta}^{(j)}}{\partial r} - \frac{u_{\theta}^{(j)}}{r} \right), \quad (43)$$

$$\sigma_{\theta z}^{(j)} = \mu^{(j)} \left( \frac{\partial u_{\theta}^{(j)}}{\partial z} \right).$$

$$\frac{\partial^2 u_{\theta}^{(j)}}{\partial r^2} + \frac{1}{r} \frac{\partial u_{\theta}^{(j)}}{\partial r} - \frac{u_{\theta}^{(j)}}{r^2} + C^{(j)} \frac{\partial^2 u_{\theta}^{(j)}}{\partial z^2} = 0 \quad (j = 1, 2). \quad (44)$$

In our paper, some terms have been converted to the following forms which are similar to the isotropic case.

$$C^{(j)} = \frac{C_{44}^{(j)}}{C_{66}^{(j)}} = \frac{\mu^{(j)}}{\mu^{(j)}} = 1, \quad P^{(1)} = \mu^{(1)}, \quad P^{(2)} = \mu^{(2)}.$$

Finally, the expressions of SIF at the rim of the crack and disc become

$$K_{h_1} = \frac{4\omega\mu^{(1)}\sqrt{h_1}}{\sqrt{\pi}} M_{1T}, \quad (45)$$

$$K_{h_2} = \frac{4\omega\mu^{(1)}\sqrt{h_2}}{\sqrt{\pi}} M_{2T}. \quad (46)$$

The expressions stated above and Equations (43), (44), (45), (46) are exactly the same as that expressions and Equations (1), (2), (56), (57) respectively of the work of Madani [34] for isotropic case. Similar terms can be found in all the other expressions. Therefore, according to Madani [34], our results are consistent.

## 7. Conclusion

In this research, the problem was formulated for a cracked orthotropic layer with two rigid discs bonded between the layer and half-spaces under axially symmetric torsion. Hankel transform is used to obtain the solution of mixed boundary value problem to a set of dual integral equation. Further, the set of dual integral equations has been converted into a pair of the second kind integral equations of Fredholm type by virtue of Abel's transforms and appropriate integral formula. Finally, to unfold the impact of layer depth and normalized disc size on SIFs, numerical implementations have been carried out using a quadrature rule and expressed through the graphical presentation.

It has been observed that the SIFs diminish with the increase of layer depth i.e. the distance between crack and disc. Also, the curve of SIFs shows a wave-like nature and decreases as the ratio disc radius to crack radius increases and gradually tends to a static value. So, we can conclude that the numerical values of SIFs at the vicinity of crack and disc can be arrested in a certain range varying the geometric parameters (layer depth, disc size and crack size). The technology of layered composites has experienced a significant development in the field of structural design, process engineering, macromechanics, material characterization, and optimization. The influence of torsional waves can not be avoided to prevent damage to solids by an earthquake and many more real situations. So the present study confirms the importance of stress analysis of orthotropic composites under a torsional wave. The proposed model can provide an analytical approach of characterizing structural behavior, stress analysis, non-destructive evaluation of material integrity, and comparing the resistance of composite anisotropic bodies with cracks and inclusion against crack growth.

## Disclosure statement

No potential conflict of interest was reported by the author(s).

## Funding

The research work is supported by Rashtriya Uchchar Shiksha Abhiyan (RUSA)-2.0, Jadavpur University, Kolkata-700032, West Bengal, India [grant number R-11/475/19].

## ORCID

Somashri Karan  <http://orcid.org/0000-0003-4396-1701>

Sourav Kumar Panja  <http://orcid.org/0000-0001-6710-3635>

Sanjoy Basu  <http://orcid.org/0000-0002-9436-1944>

## References

- [1] Lukyanov AA. Modeling shock waves in composite materials. *Mech Adv Mater Struct.* 2010;17(5):304–312.

- [2] Swain A, Baad S, Roy T. Modeling and analyses of thermo-elastic properties of radially grown carbon nanotubes-based woven fabric hybrid composite materials. *Mech Adv Mater Struct.* 2017;24(14):1206–1220.
- [3] Nath SD, Afsar A. Analysis of the effect of fiber orientation on the elastic field in a stiffened orthotropic panel under uniform tension using displacement potential approach. *Mech Adv Mater Struct.* 2009;16(4):300–307.
- [4] Kumari P, Sharma V. Propagation of torsional waves in a viscoelastic layer over an inhomogeneous half space. *Acta Mech.* 2014;225(6):1673–1684.
- [5] Chattopadhyay A, Gupta S, Kumari P, et al. Torsional wave propagation in non-homogeneous layer between non-homogeneous half-spaces. *Int J Numer Anal Methods Geomech.* 2013;37(10):1280–1291.
- [6] Guillén-Rujano R, Avilés F, Vidal-Lesso A, et al. Closed-form solution and analysis of the plate twist test in sandwich and laminated composites. *Mech Mater.* 2021;155:103753.
- [7] Kumari P, Sharma V, Modi C. Propagation of torsional waves in an inhomogeneous layer sandwiched between inhomogeneous semi-infinite strata. *J Eng Math.* 2015;90(1):1–11.
- [8] Alam P, Kundu S, Gupta S, et al. Study of torsional wave in a poroelastic medium sandwiched between a layer and a half-space of heterogeneous dry sandy media. *Waves Random Complex Media.* 2018;28(1):182–201.
- [9] Álvarez JG, Bisagni C. Closed-form solutions for thermomechanical buckling of orthotropic composite plates. *Compos Struct.* 2020;233:111622.
- [10] Bagherpoor F, Pourseifi M. Dynamic mode III stress intensity factors of multiple axisymmetric interfacial cracks in an FGM coated orthotropic layer. *Int J Comput Methods Eng.* 2022;1–17. <https://doi.org/10.1080/15502287.2022.2036869>.
- [11] Skalsky V, Stankevych O, Serhiyenko O. Wave displacement field at a half-space surface caused by an internal crack under twisting load. *Wave Motion.* 2013;50(2):326–333.
- [12] Hassani A, Faal R. Torsion analysis of cracked circular bars actuated by a piezoelectric coating. *Smart Mater Struct.* 2016;25(12):125030.
- [13] Ramezani M, Ramesh S, Purbolaksono J, et al. Closed-form solutions of stress intensity factors for semi-elliptical surface cracks in a cylindrical bar under pure tension. *Acta Mech Solida Sin.* 2022;35(2):344–356.
- [14] Trivedi N, Das S, Craciun E-M. The mathematical study of an edge crack in two different specified models under time-harmonic wave disturbance. *Mech Compos Mater.* 2022;58(1):1–14.
- [15] Sih G, Chen E. Torsion of a laminar composite debonded over a penny-shaped area. *J Franklin Inst.* 1972;293(4):251–261.
- [16] Rabieifar A, Pourseifi M, Derili H. Transient analysis for torsional impact of multiple axisymmetric cracks in the functionally graded orthotropic medium. *IMA J Appl Math.* 2018;83(1):131–147.
- [17] Wu T-H, Li X-Y, Tang H-P. Three-dimensional fields in an infinite transversely isotropic magneto-electro-elastic space with multiple coplanar penny-shaped cracks. *Int J Eng Sci.* 2021;159:103434.
- [18] Li C, Zou Z, Duan Z. Torsional impact of transversely isotropic solid with functionally graded shear moduli and a penny-shaped crack. *Theor Appl Fract Mech.* 1999;32(3):157–163.
- [19] Craciun E, Barbu L. Compact closed form solution of the incremental plane states in a pre-stressed elastic composite with an elliptical hole. *ZAMM-J Appl Math Mech.* 2015;95(2):193–199.
- [20] Selvadurai A, Samea P. Mechanics of a pressurized penny-shaped crack in a poroelastic halfspace. *Int J Eng Sci.* 2021;163:103472.
- [21] He D, Guo Z, Ma H. Penny-shaped crack simulation with a single high order smooth boundary element. *Eng Anal Bound Elem.* 2021;124:211–220.
- [22] Wang B, Han J, Du S. Fracture mechanics for multilayers with penny-shaped cracks subjected to dynamic torsional loading. *Int J Eng Sci.* 2000;38(8):893–901.
- [23] Feng W, Zou Z. Dynamic stress field for torsional impact of a penny-shaped crack in a transversely isotropic functional graded strip. *Int J Eng Sci.* 2003;41(15):1729–1739.
- [24] Basu S, Mandal S. Impact of torsional load on a penny-shaped crack in an elastic layer sandwiched between two elastic half-space. *Int J Appl Math.* 2016;2(4):533–543.
- [25] Erdogan F, Arin K. Penny-shaped interface crack between an elastic layer and a half-space. *Int J Eng Sci.* 1972;10(2):115–125.

- [26] Saxena H, Dhaliwal R. A penny-shaped crack at the interface of two bonded dissimilar transversely isotropic elastic half-spaces. *Eng Fract Mech.* **1990**;37(4):891–899.
- [27] Lee H-K, Tran X. On stress analysis for a penny-shaped crack interacting with inclusions and voids. *Int J Solids Struct.* **2010**;47(5):549–558.
- [28] Ueda S, Shindo Y, Atsumi A. Torsional impact response of a penny-shaped interface crack in a layered composite. *Eng Fract Mech.* **1984**;19(6):1095–1104.
- [29] Li C, Weng G. Dynamic fracture analysis for a penny-shaped crack in an FGM inter-layer between dissimilar half spaces. *Math Mech Solids.* **2002**;7(2):149–163.
- [30] Saxena H, Dhaliwal R, He W, et al. Penny-shaped interface crack between dissimilar nonhomogeneous elastic layers under axially symmetric torsion. *Acta Mech.* **1993**;99(1):201–211.
- [31] Bohdanov V. Influence of initial stresses on the fracture of composite material weakened by a subsurface mode III crack. *J Math Sci.* **2015**;205(5):621–634.
- [32] Itou S. Stress intensity factors around two coaxial cylindrical cracks in composite materials. *Mech Adv Mater Struct.* **2013**;20(9):721–729.
- [33] Yu H, Wang B. Stress intensity factor evaluations for a curved crack in orthotropic particulate composites using an interaction integral method. *Mech Adv Mater Struct.* **2019**;26(7):631–638.
- [34] Madani F, Kebli B. Axisymmetric torsion of an elastic layer sandwiched between two elastic half-spaces with two interfaced cracks. *Stud Geotech Mech.* **2019**;41(2):57–66.
- [35] Afsar A, Deb Nath S, Ahmed SR, et al. Displacement potential based finite difference solution to elastic field in a cantilever beam of orthotropic composite. *Mech Adv Mater Struct.* **2008**;15(5):386–399.
- [36] Hassani A, Hassani A, Monfared MM. Torsional analysis of an orthotropic long cylinder weakened by multiple axisymmetric cracks. *J Comput Appl Res Mech Eng.* **2018**;8(1):49–60.
- [37] Panja SK, Mandal SC. Propagation of love wave in multilayered viscoelastic orthotropic medium with initial stress. *Waves Random Complex Media.* **2022**;32(2):1000–1017.